Proposal for a Neutrino Facility at the Spallation Neutron Source

ν-SNS

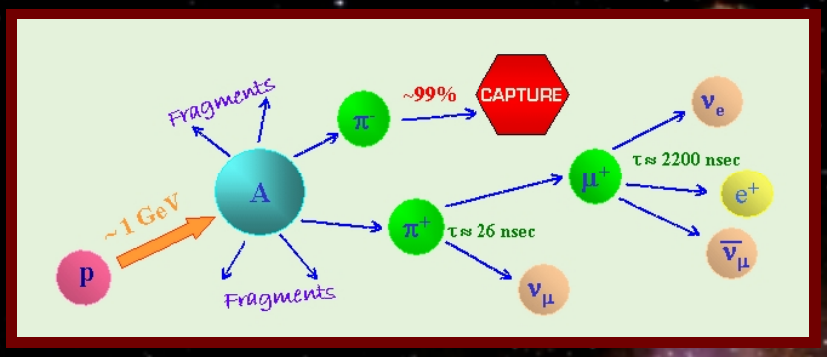

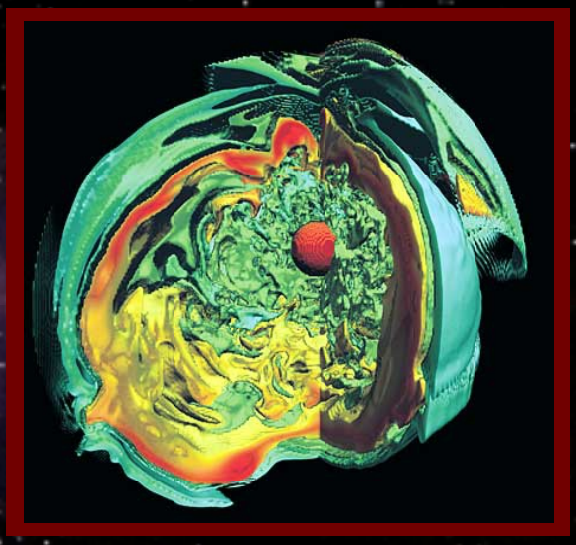

August, 2005

PROPOSAL FOR A NEUTRINO FACILITY AT THE SPALLATION NEUTRON SOURCE

Submitted to the
Department of Energy, Division of Nuclear Physics
by the
Physics Division of the Oak Ridge National Laboratory
on behalf of the
ν-SNS Instrument Development Team

August 2005

TABLE OF CONTENTS

LIST OF FIGURES

Figure **Page**

Figure **Page**

LIST OF TABLES

Table **Page**

ACRONYM LIST

ADC	-	Analog to Digital Converter
APD	-	Avalanche Photodiode
ASIC	-	Application Specific Integrated Circuit
BNL	-	Brookhaven National Laboratory
CCB	-	Change Control Board
DAC	-	Digital to Analog Converter
DAQ	-	Data Acquisition System
DOE	-	Department of Energy
DOE-NP	-	DOE Office of Nuclear Physics
EC	-	Executive Committee
ES&H	-	Environment, Safety and Health
FAIR	-	Facility for Antiproton and Ion Research
FFN	-	Fuller, Fowler and Newman
GT	-	Gamow-Teller
HV	-	High Voltage
IDT	-	Instrument Development Team
IPM	-	Independent Particle Model
ISMS	-	Integrated Safety Management System
LANSCE	-	Los Alamos Neutron Science Center
LMP	-	Langanke and Martinez-Pinedo
LMS	-	Langanke, Martinez-Pinedo, Sampaio, *et al*.
LMSH	-	Langanke, Martinez-Pinedo, Sampaio, Hix *et al*.
LOI	-	Letter of Intent
LSND	-	Liquid Scintillating Neutrino Detector
MoU	-	Memorandum of Understanding
MRI	-	Major Research Instrumentation
NAS	-	National Academy of Science
NRC	-	National Research Council
NSCL	-	National Superconducting Cyclotron Laboratory
NSF	-	National Science Foundation
OPC	-	Other Project Costs
ORNL	-	Oak Ridge National Laboratory
PAC	-	Program Advisory Committee
PE	-	Photoelectrons
PM	-	Project Manager
PMT	-	Photomultiplier Tube
PNS	-	Proto-neutron Star
QA	-	Quality Assurance
RIA	-	Rare Isotope Accelerator
RPA	-	Random Phase Approximation
RTBT	-	Ring to Target Beam Transport
SciDAC	-	Scientific Discovery Through Advanced Computing
SiPM	-	Silicon Photomultiplier

SMMC	-	Shell Model Monte Carlo
SNO	-	Sudbury Neutrino Observatory
SNS	-	Spallation Neutron Source
TDC	-	Time to Digital Converter
TEC	-	Total Estimated Cost
TPC	-	Total Project Cost
UT	-	University of Tennessee
WBS	-	Work Breakdown Structure
WLS	-	Wavelength Shifting
WW95	-	Woosley and Weaver, 1995

1 EXECUTIVE SUMMARY

Measurements during the last few decades have substantially improved our understanding of neutrino properties and reshaped the foundations of our understanding of nature. In spite of this remarkable progress several important questions still remain. Among these are the role that neutrino-nucleus interactions play in the supernova explosion process and subsequent nucleosynthesis. During these spectacular events 10^{46} joules of gravitational energy are released into space. The resulting flash of visible light is as bright as an entire galaxy, yet this represents only a tiny fraction of the total energy in the explosion: ~99% of the energy is carried away by neutrinos. Accurate knowledge of neutrino-nucleus cross sections is important to understanding these important events. However, the reliability of theoretical models used to predict such cross sections is highly uncertain, and almost no data exist. This lack of knowledge significantly limits our understanding of supernovae and of terrestrial observations of cosmic neutrinos to probe the deepest layer of these powerful explosions.

Broad agreement on the importance of neutrino measurements in general, and the relationship of neutrinos and supernovae in particular, are reflected in several recently published documents. These include the *DOE Office of Science Strategic Plan* [1], the National Academy of Science (NAS) Study *Connecting Quarks with the Cosmos* [2], and a report from the National Research Council (NRC) of the National Academies, *Neutrinos and Beyond—New Windows on Nature* [3]. Two of the seven highest priorities for the Office of Science listed in the Strategic Plan will impact our understanding of supernovae and heavy element nucleosynthesis where neutrinos play a key role. The NAS report lists eleven key questions that are of deep interest for science at the intersection of astronomy and physics, including *"How were the heavy elements from Iron to Uranium made?"* and *"How have neutrinos shaped the evolution of the Universe?"* That report notes *"More realistic simulations of supernova explosions and neutron star mergers are essential. …**In addition, better measurements are needed for both the inputs and outputs of these calculations."*** The NRC report lists several questions that the authors believe the nuclear physics community is now poised to answer. Among those questions are *"What causes the most powerful explosions in the universe?"* and *"What role do neutrinos play in the synthesis of the elements in the periodic table?"* The report also supports building large underground supernova neutrino detectors.

In response to the above studies and plans, and to the excitement over recent neutrino measurements, the American Physical Society Divisions of Particles and Fields, Nuclear Physics, Astrophysics, and the Physics of Beams, sponsored a year-long Study on the Physics of Neutrinos. The study lays the scientific groundwork for the choices for neutrino physics research to be made over the next few years. The Study Group recently published its final report, *The Neutrino Matrix* [4], which in *Section 4, Recommendations*, states:

> *"The precise determination of neutrino cross sections is an **essential ingredient** in the interpretation of neutrino experiments and is, in addition, capable of revealing exotic and unexpected phenomena, such as the existence of a neutrino magnetic dipole moment. Interpretation of atmospheric and long-baseline accelerator-based neutrino experiments, **understanding the role of neutrinos in supernova explosions, and predicting the abundances of events in those explosions all require knowledge of neutrino cross sections.***

*New facilities, such as the **Spallation Neutron Source**, and existing neutrino beams can be used to meet this essential need.*

Finally, the importance of these results and the unique opportunity provided by the construction of the Spallation Neutron Source (SNS) at the Oak Ridge National Laboratory was highlighted in the recent report of the Nuclear Science Advisory Council, "Guidance to Implementation of the 2002 Long Range Plan" [5], in which it was stated:

"Neutrino-nucleus interactions in a nascent supernova are an important but poorly understood influence on the synthesis of elements in the supernova and the reverse process of electron capture is a determining factor in the explosion dynamics. Once neutrinos from a supernova have reached the Earth, they are detected through neutrino-nucleus interactions. ***An experimental program to determined important unknown neutrino-nucleus cross sections is now possible using the copious flux from the SNS."***

The SNS will produce, as a by-product, the world's most intense intermediate energy neutrino flux. This allows a long-term program of high precision neutrino-nucleus cross section measurements on a variety of nuclear targets of interest to the astrophysics community. A unique and fortuitous property of the SNS neutrinos is that their energy range closely matches the energy of interest for nuclear astrophysics and supernovae dynamics. The intense flux and advantageous time structure of the SNS allows precise measurements (**~10% accuracy in one year for a given target**) to be performed using detectors of modest scale. Since neutrinos are highly penetrating, a truly non-intrusive facility to study neutrino reactions can be built at the SNS. We call the proposed facility **N**eutrinos at the **S**pallation **N**eutron **S**ource, or **ν-SNS**.

We propose to build a shielded neutrino detector enclosure at a distance of 20 meters from the SNS target [6], where the short-pulse neutrino flux will be more than 10 times greater than has been achieved at any previous facility. The enclosure will hold two independently operable detectors, designed so that measurements with several different targets can be performed with little modification to the detectors. The anticipated neutrino flux at the SNS facility will allow measurement of the charged-current neutrino-nucleus cross section for any selected nuclear target to a statistical accuracy of better then 10%. We anticipate that this will allow double-differential cross section measurements (vs. energy and angle), and that neutral current measurements may also be possible. Measurements with this level of precision will provide a unique test of fundamental questions in nuclear structure (allowing the resolution of the forbidden component of the strength distribution) and will validate the complex nuclear structure models required to compute these cross sections for nuclei that will not be measured. Armed with measured rates and improved nuclear structure theory, we will be able to improve our understanding of supernovae, important links in our cosmic chain of origins.

A multi-institutional collaboration with more than 30 scientists is actively involved in the proposal to build **ν-SNS** (see Appendix 1 for a full collaboration list and Appendix 2 for vitae of executive committee members). We have submitted a Letter of Intent (LOI) for our proposal to the SNS. Following favorable review of the LOI we have received preliminary approval for floor space in the SNS target building. As requested by SNS management we are submitting a copy of this proposal to them for consideration.

Our present cost estimate for the shielded enclosure with active veto system and two detectors is approximately $8.6 M. Institutional responsibilities for the major components of the proposed facility are shown in Table 1.1. As discussed in a meeting with DOE representatives in January, NSF has expressed an interest in receiving a proposal for one of the detectors (the segmented detector, appropriate for measurements on solid targets), as a Major Research Instrumentation (MRI) grant. The project cost without this second detector is approximately $7.0 M. Operation of and scientific output from the first detector are in no way contingent on the funding of the second detector – the two are completely independent. We estimate project construction could be complete within three years. There are no known or anticipated SNS schedule drivers.

Table 1.1 Institutional responsibilities for major **ν-SNS** components.

Subsystem	**Responsible Institution**
Bunker, Project Management	ORNL
Veto	Colorado School of Mines
Liquid Detector	University of Alabama
Segmented Detector	University of Tennessee, University of Houston

The initial scientific program funded by this proposal consists of measurements on carbon (with a liquid scintillator target) and oxygen (with a water target). The carbon measurement is necessary to calibrate the detector and understand the background environment and will significantly reduce systematic errors on the measurements of subsequent targets. The oxygen measurement is crucial to interpreting the wealth of data that would be collected by Super-Kamiokande and SNO for any nearby supernova explosion. The initial scientific program proposed for the second detector is a measurement on iron because of the great importance of the iron cross sections for understanding electron capture that drives core collapse at the onset of the supernova and for understanding the role that neutrino-nucleus interactions have in driving the supernova explosion.

The choice and ordering of subsequent targets is determined by many factors, both scientific and practical. Given the broad interest in neutrino cross section measurements and the wide array of potentially interesting targets and detectors, we envision that **ν-SNS** would be a user facility with a Program Advisory Committee to make recommendations as to priorities for the scientific program beyond the initial target suite.

In short, the **ν-SNS** facility will provide for a long-term program of high-precision neutrino-nucleus cross section measurements to address the needs of astrophysics and nuclear structure physics. Specifically, and as discussed more fully in the next two sections, **ν-SNS** measurements will directly address the areas of core collapse supernova dynamics, heavy element nucleosynthesis, and nuclear structure physics, and will provide calibration of future dedicated supernova detector techniques. **ν-SNS** measurements will be complementary to those which will be made at the Rare Isotope Accelerator (RIA) and which have been made by the astrophysics reaction community in a program long supported by the DOE. These measurements will leverage the significant DOE investment in the SNS to provide, for modest cost, data crucial to the DOE-sponsored Terascale Supernova Initiative (TSI).

The remainder of this document is organized as follows: In Section 2 we provide a comprehensive overview of the project, including discussion of the scientific motivation, the ideal timing and energy properties of neutrino production at the SNS, our technical approach and the expected cost. In Section 3 we more fully develop the scientific motivation for the measurements that can be made at **ν-SNS**. In Section 4 we present an overview of the project, including details on design considerations, design choices and cost for each of the major facility components. In Section 5 we present a rolled-up cost estimate, an ideal schedule and the resulting budget authority profile. In Section 6 we present an overview of our project management plan and initial thoughts for transitioning to an operating facility. Finally, there are appendices which contain the **ν-SNS** collaboration list, curriculum vitae for Executive Committee members, reviews of the LOI submitted to the SNS, an analysis of the SNS target hall floor loading capability, and a document detailing our R&D priorities.

References for Section 1:

1. Office of Science Strategic Plan, February, 2004 - http://www.science.doe.gov/sub/Mission/Strategic_Plan/Feb-2004-Strat-Plan-screen-res.pdf
2. "Connecting Quarks with the Cosmos, Eleven Questions for the New Century", Committee on the Physics of the Universe, M.S. Turner, Chair; Board on Physics and Astronomy, Division on Engineering and Physical Sciences, National Research Council of The National Academies, The National Academies Press, 2003, Washington, D.C.
3. "Neutrinos and Beyond, New Windows on Nature", Neutrino Facilities Assessment Committee, B.C. Barish, Chair; Board on Physics and Astronomy, Division of Engineering and Physical Sciences, National Research Council of the National Academies, The National Academies Press, 2003, Washington, D.C.
4. "The Neutrino Matrix: DNP/DPF/DAP/DPB Joint Study on the Future of Neutrino Physics", S. Freedman, B. Kayser *et al.*, Technical Report American Physical Society, 2004.
5. "Guidance to Implementation of the 2002 Long Range Plan", R. Tribble *et al.*, Report to the Nuclear Science Advisory Committee, 2005. http://www.sc.doe.gov/np/nsac/docs/nsac-report-final1_Tribble.pdf
6. "A Facility for Neutrino Nucleus Cross Section Measurements at the Spallation Neutron Source", Yu. Efremenko, Prepared for 8th International Workshop on Topics in Astroparticle and Underground Physics (TAUP 2003), Seattle, Washington, 5-9 Sep 2003. Published in *Nucl. Phys. Proc. Suppl.* **138**, 343, 2005

2 PROJECT OVERVIEW

2.1 Scientific Motivation

Experimental studies of neutrino-nucleus interactions (see Figure 2.1) will provide valuable information relevant both to the understanding of the structure of the atomic nucleus and to the understanding of our cosmic origins. With the knowledge gained from these experiments, improved astrophysical models will refine our understanding of fundamental puzzles. For example, such measurements will enable better answers to the questions "*How Have Neutrinos Shaped the Evolution of the Universe?"* and *"How Were the Elements from Iron to Uranium Made?"*, questions raised in the recent *Connecting Quarks with the Cosmos* study of the National Academy of Science [1].

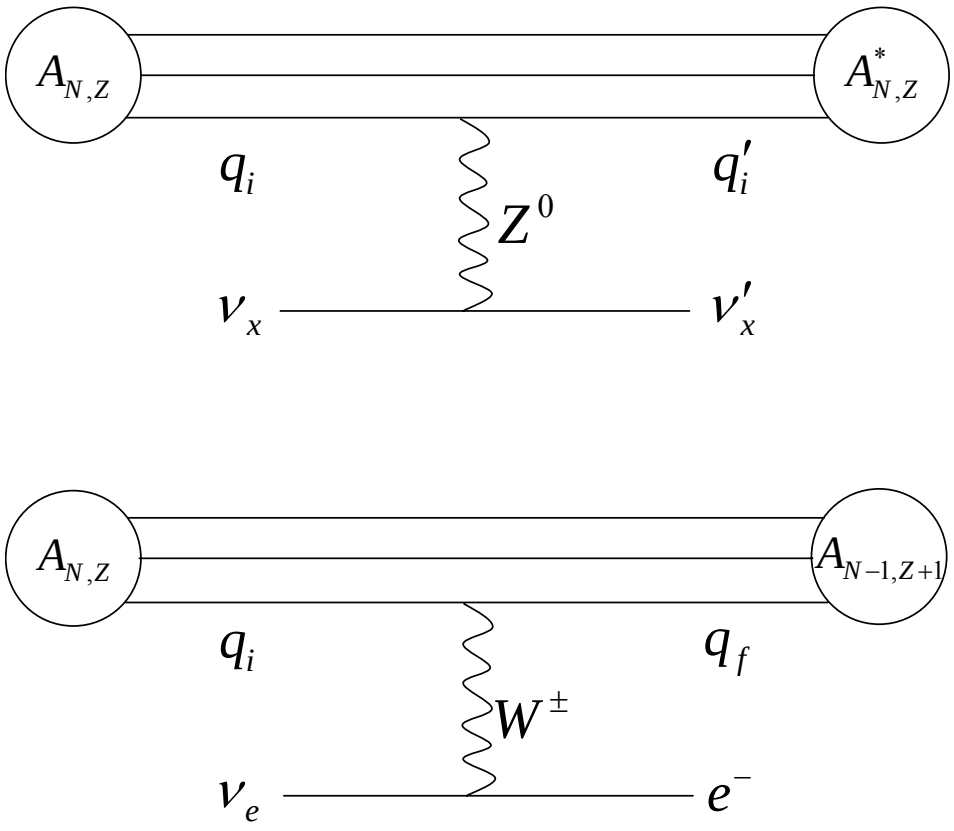

Figure 2.1 Diagrams for neutral-current (top) and charged-current (bottom) neutrino-nucleus interactions. At the SNS electron neutrinos (ν_e) can undergo both charged- and neutral-current interactions, but muon neutrinos (ν_μ) and anti-neutrinos ($\bar{\nu}_\mu$) are kinematically limited to neutral-current interactions. Other neutrino flavors are not present. Charged-current events are measured via the outgoing charged lepton. Neutral-current events, sometimes characterized as "nothing in, nothing out", can only be measured via the decay of the excited nucleus.

The life-cycles of massive stars naturally lead to luminous neutrino sources. Foremost among these are core collapse supernovae, which are among the most energetic explosions in our

universe, releasing 10^{46} Joules of energy in the form of neutrinos of all flavors at a staggering rate of 10^{57} neutrinos per second. Marking the death of a massive star (mass >8-10 solar masses) and the birth of a neutron star or black hole, core collapse supernovae serve as laboratories for physics beyond the Standard Model and for matter at extremes of density, temperature, and neutronization that cannot be produced in terrestrial laboratories. The kinetic energy and the rich mix of recently synthesized elements delivered into the interstellar medium by the ejecta of each supernova make core collapse supernovae a key link in our chain of origins from the Big Bang to the formation of life on Earth. **Currently, lack of data on neutrino-nucleus interactions limits our understanding of the mechanism by which core collapse supernovae explode, our understanding of the resulting nucleosynthesis, and our ability to interpret the results of neutrino astronomy.**

Recent studies have demonstrated unequivocally that electron and neutrino capture reactions on nuclei play a major role in dictating the dynamics of stellar core collapse, which set the stage for all of post-bounce dynamics and the formation of the supernova shock wave. Comparisons of results using modern prescriptions for electron and neutrino capture on nuclei with earlier calculations demonstrate quantitative and qualitative changes in the launch radius of the supernova shock wave after stellar core bounce and in the density, temperature, and compositional structure of the stellar core. Nucleosynthesis in core collapse supernovae falls into three basic categories: (1) explosive nucleosynthesis that occurs as the shock wave passes through the stellar layers and causes nuclear fusion through compression and heating of the material, (2) neutrino nucleosynthesis in the ejected layers that occurs as these layers are exposed to the intense neutrino flux emerging from the proto-neutron star, and (3) *r*-process nucleosynthesis that occurs in a neutrino-driven wind emanating from the proto-neutron star after the explosion is initiated. In all cases, the final elemental abundances produced and ejected are affected through nuclear transmutations by the neutrino-nucleus interactions that occur.

The ability to detect, understand, and ultimately use the detailed neutrino "light curve" from a future core collapse supernova in our galaxy is vital to better understanding supernovae and the use of supernova models, together with detailed astronomical observations, to constrain fundamental physics that is otherwise inaccessible in terrestrial experiments. To achieve this will require an accurate normalization of the neutrino flux in a supernova neutrino detector and knowledge of the cross sections and by-products of neutrino interactions in the detector material. From deuterium to lead, a number of nuclei have been proposed and, in some cases, used as supernova neutrino detector materials. In all cases, accurate neutrino-nucleus cross sections are essential. Only ν+Carbon has been measured to ~10% accuracy by LSND [2,3] and KARMEN [4]. With much lower accuracy (~40%) there are data for ν+Iron [5], ν+Iodine [6], and ν+Deuterium [7].

While it is impossible to experimentally measure all of the cross sections for the hundreds of weak interaction rates needed for realistic simulations of supernovae and supernova nucleosynthesis, a strategically chosen set of measurements will validate the fundamental nuclear structure and reaction models at the foundation of the hundreds of rate computations that are input for supernova models. Total neutrino-nucleus charged-current cross sections at low energy depend strongly on the charge number of the nucleus. For example the cross section in lead is predicted to be 300 times that of carbon. The charged-current reaction cross section induced by ν_e is thought to scale nearly as the square of the electron energy and is particularly sensitive to

the detailed structure of the induced nuclear excitation spectrum. It is therefore important to either obtain the cross sections directly from experiment and/or calibrate theoretical models so that systematic uncertainties can be estimated.

In addition to being crucially important to astrophysics, measurements of neutrino-nucleus cross sections provide an opportunity to study issues of vital interest to nuclear structure related to the weak interaction. One of these involves understanding of the axial-vector response in nuclei. That response is often characterized by a modification of the axial vector coupling constant, in comparison to its value for free nucleons. For the Gamow-Teller operator that arises as a leading term from the low-energy (long wavelength) expansion of the weak axial current, one finds empirically that the effective axial-vector coupling constant is modified (quenched) in the nuclear medium. It is unknown to what extent other operators, of higher multipolarity, arising from the other terms in the expansion of the weak axial current are analogously modified. Using neutrinos from the SNS to probe medium energy strength distributions in neutrino-nucleus scattering would open the possibility to investigate this fundamental problem. Such measurements could be performed on target materials for which low-energy charge-exchange experiments are available in order to compare low-energy excitations. Furthermore, a coordinated choice of SNS neutrino targets with those used for inelastic electron scattering at the FAIR facility in Darmstadt could yield simultaneous information on both neutral-current (via indirect measurements at FAIR) and charged-current (at the SNS) neutrino scattering in a similar energy range. This complementary information could be used to evaluate nuclear models that have been developed to predict total neutrino scattering cross sections.

For this wealth of reasons, measurements of neutrino-nucleus interactions are of utmost importance. With the dearth of experimental data, there is a clear need for a facility like **ν-SNS**.

2.2 Neutrino Production at the SNS

The Spallation Neutron Source (SNS), currently under construction at Oak Ridge National Laboratory, will be the world's premier facility for neutron-scattering research, producing pulsed neutron beams with intensities an order of magnitude larger than any currently operating facility. When full beam power is reached in 2009, 10^{14} 1 GeV protons will bombard the liquid mercury target in 700 ns wide bursts with a frequency of 60 Hz. Neutrons produced in spallation reactions with the mercury will thermalize in hydrogenous moderators surrounding the target and be delivered to neutron scattering instruments in the SNS experiment hall.

As a by-product, the SNS will also provide the world's most intense pulsed source of neutrinos in the energy regime of interest for nuclear astrophysics. Interactions of the proton beam in the mercury target will produce π-mesons in addition to neutrons. These will stop inside the dense mercury target and their subsequent decay chain, illustrated in Figure 2.2, will produce neutrinos with a flux of $\sim 2\times10^{7}$ ν/cm^2/s for all flavors at 20 m from the spallation target [8]. This exceeds the neutrino flux at ISIS (where the KARMEN experiment was located) by more than an order of magnitude.

Note: throughout this proposal we have assumed SNS power of 1 MW, but it is currently expected that higher power (1.4 MW) may be attained.

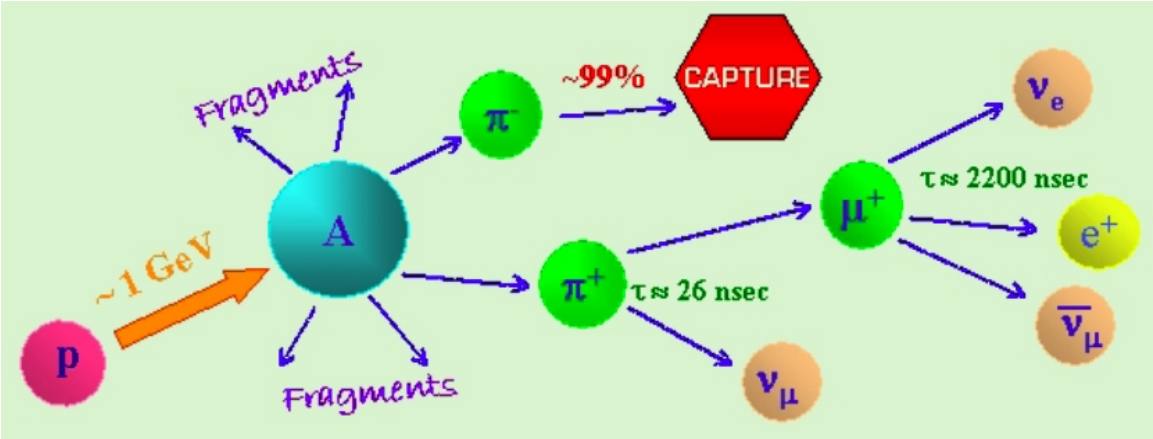

Figure 2.2 SNS neutrino production mechanism.

The time structure of the SNS beam is particularly advantageous for neutrino studies. Time correlations between candidate events and the SNS proton beam pulse will greatly reduce background rates and may provide sensitivity to neutral current events. As shown in the left panel of Figure 2.3, all neutrinos will arrive at the **ν-SNS** location within several microseconds of the 60 Hz proton beam pulses. As a result, background events resulting from cosmic rays will be suppressed by a factor of ~2000 by ignoring events which occur too long after a beam pulse. At the beginning of the beam spill the neutrino flux is dominated by muon neutrinos resulting from pion decay, perhaps making it possible to isolate pure neutral-current events. This exciting possibility is quite challenging due to the presence of a large number of high energy neutrons, the most important source of beam-induced background from the SNS. Investigations of the achievable time resolution and consultations with SNS operations staff about minimizing beam losses (both necessary to meet this challenge) will be a part of our proposed R&D effort in the next two years. However, charged-current measurements can be made essentially *background-free* because the neutron backgrounds are greatly suppressed for $t > \sim 1$ μs after the start of the beam spill while the neutrino production, governed by the muon lifetime ($\tau_\mu \sim 2.2$ μs), proceeds for several microseconds. This time structure presents a great advantage over a continuous-beam facility such as the Los Alamos Neutron Science Center (LANSCE), where the LSND experiment was located.

The energy spectra of SNS neutrinos are shown in the right hand panel of Figure 2.3. These spectra are known because almost all neutrinos come from decay-at-rest processes in which the kinematics are well defined. The decay of stopped pions produces monoenergetic muon neutrinos at 30 MeV. The subsequent 3-body muon decay produces a spectrum of electron neutrinos and muon antineutrinos with energies up to 52.6 MeV. This energy range overlaps extremely well with the range of neutrino energies in supernovae (see Figure 2.4). Cross sections for neutrino interactions at these energies are crucial for understanding supernova dynamics, nucleosynthesis, and the response of terrestrial supernova neutrino detectors, as discussed in the previous section.

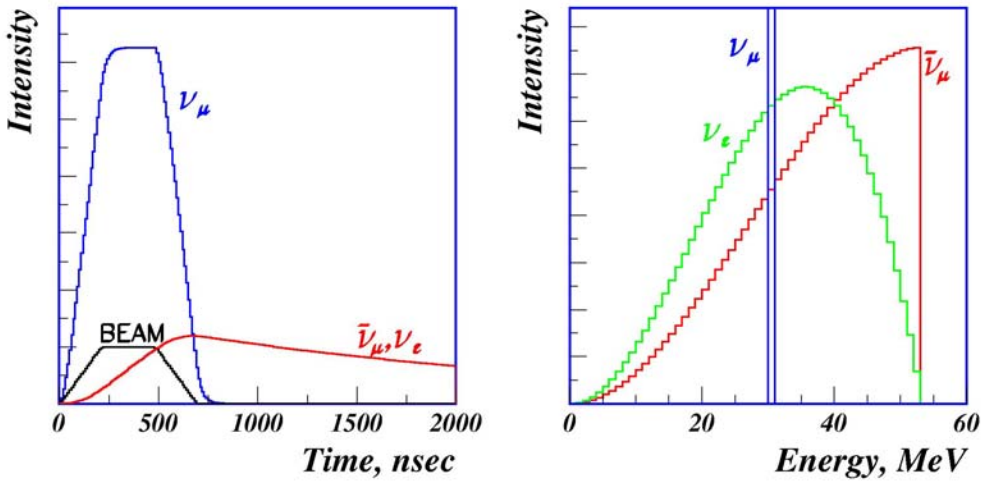

Figure 2.3 Time and energy distributions for different neutrino flavors produced at the SNS.

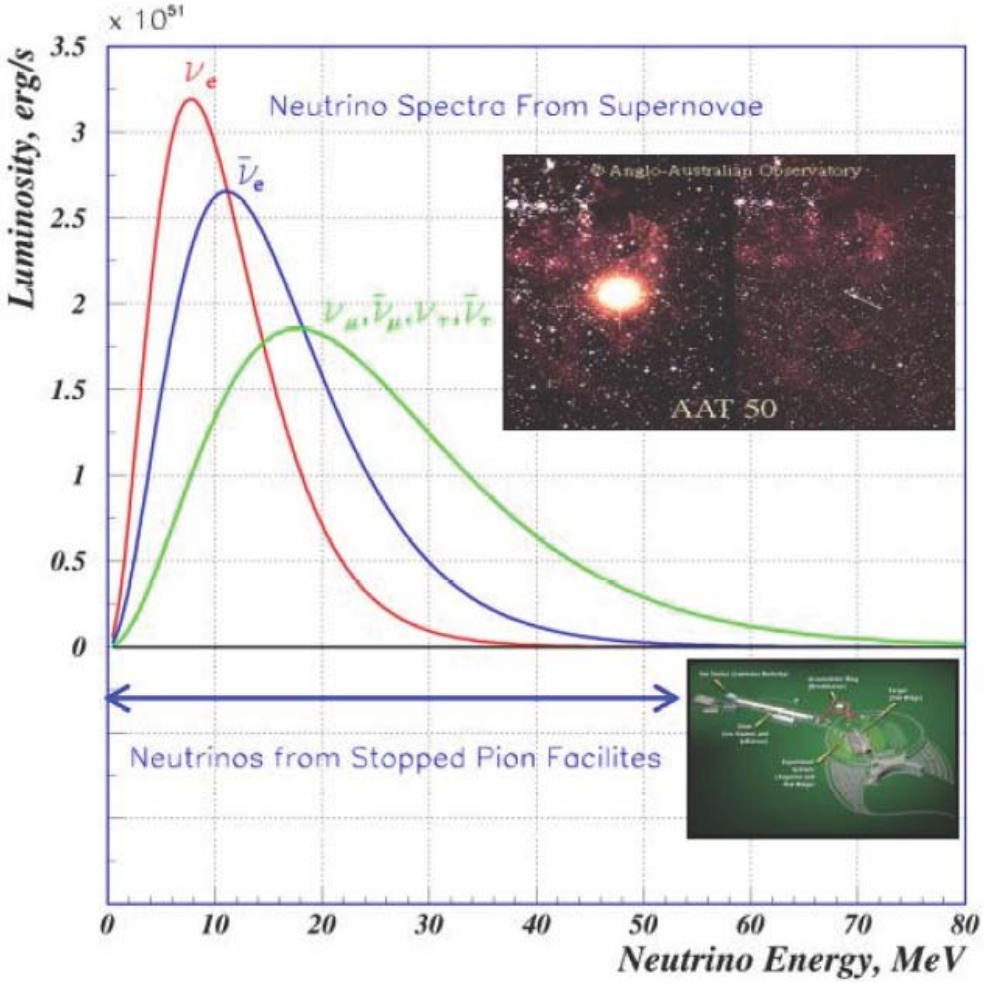

Figure 2.4 Supernova neutrino spectra compared to the neutrino energy range at stopped-pion facilities.

2.3 ν-SNS Facility Overview

A location in the SNS target hall (see Figures 2.5 and 2.6) has been identified that is well suited for measurements of neutrino-nucleus cross sections and which does not interfere with SNS operations. Minimizing the distance to the SNS target is crucial to reduce the required detector mass and cost. The location we have identified is only ~20 m from the SNS target, as close as possible to the target given the constraints imposed by planned beamlines and shielding in the target hall. A letter-of-intent was submitted to the SNS management to use this location for a facility for neutrino measurements and was favorably reviewed (see Appendix 3). An area 4.5 × 4.5 m^2 (with a clear height of 6.5m) is currently being reserved for the **ν-SNS** facility.

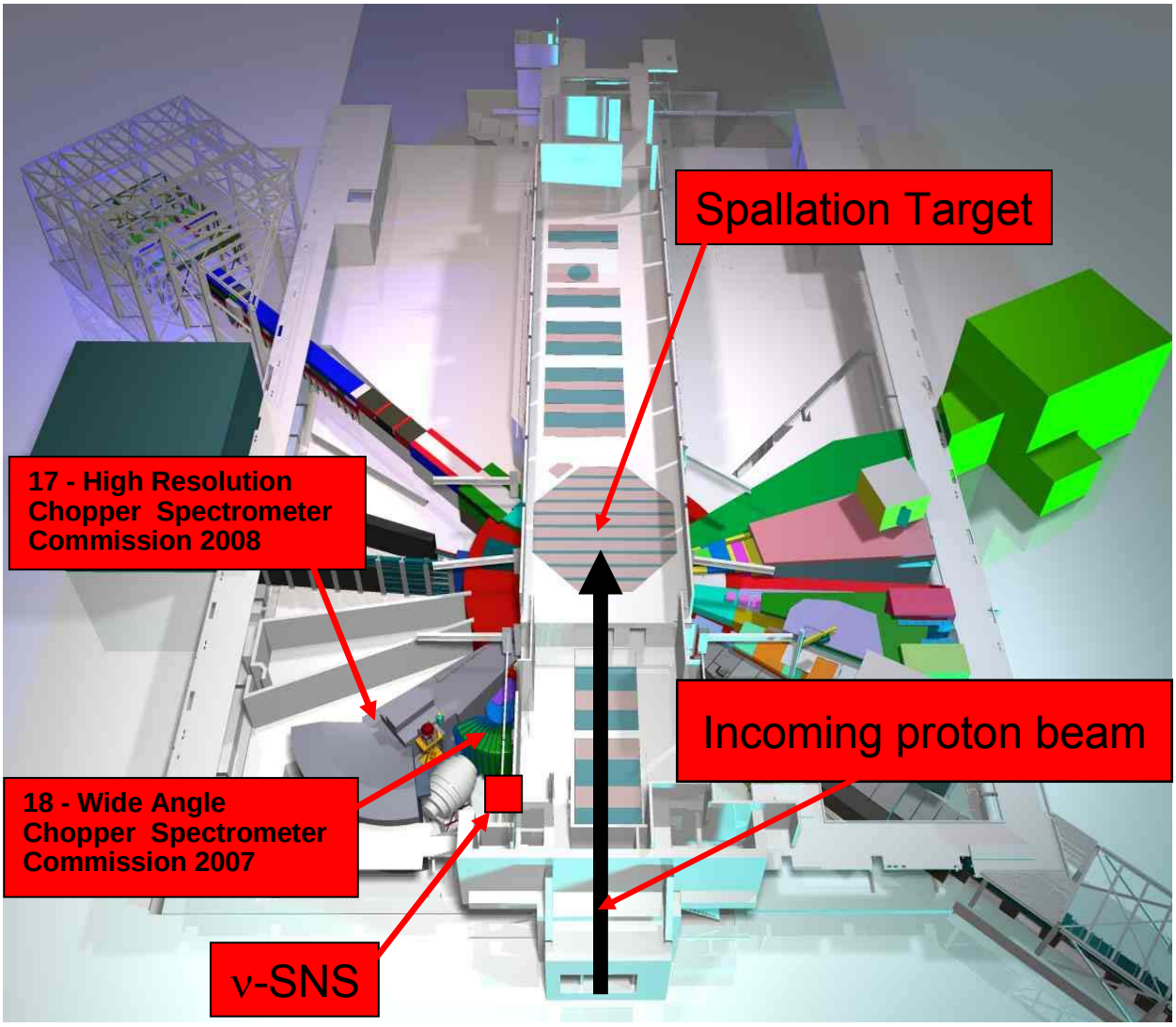

Figure 2.5 ν-SNS location in the SNS target hall.

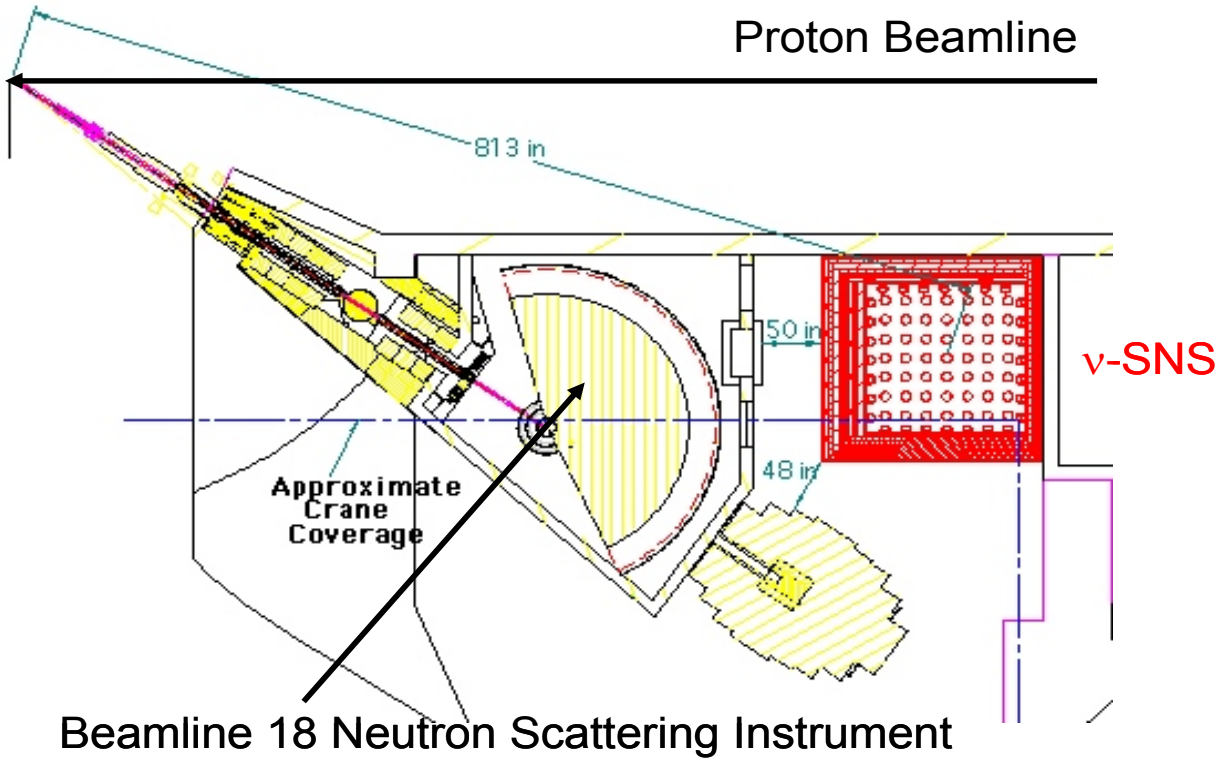

Figure 2.6 Close-up of the **ν-SNS** location in the SNS target hall (red area). This $4.5 \times 4.5 \times 6.5$ m^3 volume is 20 meters from the target at an angle of 165^o relative to the incoming proton beam. The instrument and beam dump for the neighboring neutron scattering beamline are also shown.

While the SNS pulse structure substantially reduces background rates, passive shielding and an efficient active veto are also required to reduce background rates to an acceptable level. Integrating over only the time windows of peak neutrino flux, an effective cosmic-ray muon (neutron) flux through the detector volume of 1.5×10^5 (3000) per day is still expected. In addition, in spite of heavy shielding around the spallation target, incoming beamline and nearby neutron scattering instruments, ~10^9 SNS neutrons pass through the detector volume each day.

Passive shielding is critical for reducing the backgrounds due to neutrons from cosmic rays and from the SNS target. We propose to construct a steel enclosure surrounding the neutrino instruments. A ceiling consisting of 1 m thick steel is required in order to reduce the cosmic-ray neutron flux by a factor of 100, putting it on the same level as the neutron flux that will be created from cosmic-ray muon interactions in the shielding. It is desirable to use as much shielding as possible for the walls in order to suppress beam-induced background sources. However, the total shielding is essentially limited by the maximum floor loading allowed at the **ν-SNS** location. An analysis by SNS target building engineers indicates that a mass of about 550 tons is allowed at the **ν-SNS** location. This is sufficient to hold a steel enclosure ($4.5 \times 4.5 \times 6.5$ m^3) with a 1 m thick ceiling and 0.5 m thick sides (~490 tons) plus a cosmic-ray veto system and two ten-ton fiducial mass neutrino targets/detectors (mass dominated by the target material). Monte Carlo simulations of neutron production and transport from SNS proton beam loses, from the mercury target, and from the closest neutron scattering beamlines (BL17/18) are being

conducted. Preliminary calculations show that with this amount of shielding the facility backgrounds are manageable within 1 microsecond of the start of the proton pulse. However additional calculations are needed, especially for neutrons scattered from BL17/18, which are still under design. Future background simulations will allow us to optimize the bunker thickness on each side so as to minimize background rates.

We propose to surround the bunker with an active veto system consisting of four layers of extruded scintillator (1 cm thickness) with absorber plates in between each layer. This active veto will reject ~99% of the charged component of the cosmic-ray flux. Most of the remaining 1500 muons/day can be rejected based upon the characteristic track in the neutrino detectors. However, ~30 events/day are generated by high energy muons that do not fire the veto and produce a neutron in the last interaction length of shielding. This background source, which is essentially independent of the amount of passive shielding, drives the veto's cosmic-ray efficiency requirement. We also require simultaneous veto *inefficiency* (~0.1%) for neutrons and gammas so that it is not blinded by the large flux of these particles inherent to the SNS.

We propose to build two instruments for neutrino cross section measurements that would operate simultaneously inside the **ν-SNS** bunker. The available volume inside the shielded enclosure (3.5 × 3.5 × 5.5 m^3) is sufficient for two instruments with a mass of ~20 tons each. Each will be designed to allow for reuse of the detectors with different target material, an important feature reducing long-term program costs and systematic errors.

One of the instruments would be a homogeneous scintillation detector filling the bottom half of the **ν-SNS** enclosure. A 43 m^3 steel tank would be viewed by 600 8-inch PMTs, resulting in a fiducial volume of about 15 m^3. This detector would be used to measure neutrino-nucleus cross sections on liquid target materials like carbon (mineral oil), oxygen (water) or deuterium (heavy water). Monte Carlo simulations indicate a rate of ~1300 events/year for charged-current interactions on carbon. This approach has been well established in solar neutrino detectors, but flat photosensor alternatives (for instance, avalanche photodiodes) would result in a fiducial volume more than two times larger.

The second detector is based on gas proportional counters interleaved with thin sheets of solid target materials. This detector would be mounted above the homogeneous detector and would be slightly smaller in size. (Easy access to the top of homogenous detector would still be available.) Development is focused primarily on strawtubes (independent single-channel position-sensitive proportional cells) in a design where individual tubes are completely surrounded by target material formed into corrugated sheets. This design has several cost and performance advantages. The detector would be comprised of about 15,000 strawtubes with 3 m length and 8 mm radius. Charged particles can be tracked through the segmented detector in three dimensions based upon the strawtubes that fire and the ADC signal that is read from each end of the struck tubes. Particle identification and energy can also be determined based upon the track characteristics (length and energy deposited). For a fiducial mass of 10 tons, 3500 events per year are expected with iron as a target material. Target materials like iron, aluminum, and lead can be easily interchanged.

Simultaneous operation of the two detectors is desirable since it allows a reduction in background (and resulting increase in sensitivity) since true neutrino events will not fire both

detectors. Simultaneous operation also allows each detector to serve as an independent source of relative normalization. However, each detector can also operate independently, so one detector may still continue to operate while the second is undergoing changes (*e.g.*, of target) or development. Access to the detectors will be available at any time during normal SNS operation.

2.4 R&D Program

Detectors similar to those proposed for **ν-SNS** have been deployed in nuclear and particle physics experiments, so R&D for new technology development is not required. However, a modest, focused R&D program prior to the construction project would allow optimization of the shielding and detector designs for cost, performance, and simplicity of installation and target changes. The key R&D areas are:

- **Backgrounds**: We propose to measure the background levels at the SNS after the start of operations. We will use this information to benchmark model calculations which can then be used to optimize our shielding package and provide feedback to the SNS on background source reduction.
- **Cosmic-ray Veto**: Our current design satisfies our criteria for cosmic-ray muon efficiency and low-energy neutron inefficiency. However, R&D is necessary to verify detector simulations and may lead to optimizations that reduce price, improve performance and simplify assembly.
- **Segmented Detector**: This detector must be designed in such a way that it can be easily taken apart and rebuilt with a new target material. In addition it must be designed to optimize timing and energy resolution. The large number of channels requires adaptation of custom-made readout electronics that are being developed for the MECO experiment and any necessary modifications need to be identified, tested and incorporated into the chosen solution.
- **Homogeneous Detector**: The primary question for this detector is whether use of a flat photosensor would be possible. This development would be important since it would increase the detector's fiducial volume by more than a factor of two.

More details on the proposed R&D program can be found in Appendix 5.

2.5 Scientific Program

We propose that the first neutrino cross section measurement be made with iron as the target material in the segmented detector due to the great importance of the iron cross sections for understanding the electron capture that drives core collapse at the onset of the supernova and for understanding the role that neutrino-nucleus interactions have in driving the supernova explosion. We propose to measure the iron cross section in parallel with a cross section measurement on carbon, using mineral oil in the liquid detector. Since carbon is the only nucleus that has been previously measured, an accurate initial measurement of this cross section will allow us to understand the neutrino flux normalization, calibrate the detector, and understand the background environment. Cross sections on iron and carbon with an accuracy of about ~10% should be achievable within the first full year of operation. Accuracy of total cross section measurements will be limited by absolute knowledge of neutrino production rate, as discussed in Section 4.7.

A program of neutrino cross section measurements that are important for understanding nucleosynthesis as well as supernova dynamics would follow these initial measurements on iron and carbon. This program is extremely cost effective since the sensitive components can be reused with new target materials. For example, a measurement of the neutrino cross section on ^{16}O could be performed in the liquid detector by exchanging the mineral oil with water with minimal added expense. Measurements of the neutrino cross section on lead, which is important for understanding how neutrinos may effect the synthesis of heavy elements and for understanding the response of terrestrial supernova neutrino detectors, could be performed with only the added cost of the lead target material. Accurate neutrino cross section measurements on such relatively simple nuclei spanning a wide mass range (A = 16, 58, and 208) would be a crucial first step toward assessing and eventually improving the reliability of neutrino-nucleus cross section calculations. Measurements on lighter, odd-Z nuclei (such as aluminum in the segmented detector) and a very precise measurement of the neutrino cross section on deuterium (using heavy water in the liquid detector) would be excellent candidates for the next set of measurements. There is also strong interest in testing supernova neutrino detector prototypes at the **ν-SNS** facility.

The choice and ordering of targets is determined by many factors, both scientific and practical. Given the broad interest in neutrino cross section measurements and the wide array of potentially interesting targets and detectors, we envision that **ν-SNS** would be a user facility with a Program Advisory Committee to make recommendations as to priorities for the scientific program beyond the initial set of measurements on iron, water and mineral oil targets.

2.6 High Level Cost and Schedule

Table 2.1 shows the estimated unescalated costs for top-level project components in FY05 $K. The total comes to $8,575K, with $2,022K (31%) contingency. We estimate an additional $440K in Other Project Costs (preparation of a conceptual design report, R&D and pre-ops). With a Total Project Cost (TPC) exceeding $5M, **ν-SNS** must adhere to DOE Order 4.13.3. We believe the construction project can be completed in a period of three years. The profile resulting from these considerations in as-spent dollars (including escalation) is shown in Figure 2.7. From this we can derive the **ν-SNS** TPC of $9,934K.

Table 2.1 Unescalated **ν-SNS** cost summary for top-level work breakdown structure elements (in FY05 $K).

WBS #	Title	Cost w/o Contingency	Contingency	Total	Contingency Fraction
1.1	Bunker	2,256	564	2,819	25%
1.2	Veto	1,059	377	1,436	36%
1.3	Segmented Detector	1,155	427	1,582	37%
1.4	Homogeneous Detector	1,189	452	1,641	38%
1.5	Utilities	229	62	291	27%
1.6	Safety System	63	17	80	27%
1.7	DAQ	258	64	323	25%
1.8	Project Management	344	59	403	17%
	Total	**6,553**	**2,022**	**8,575**	**31%**

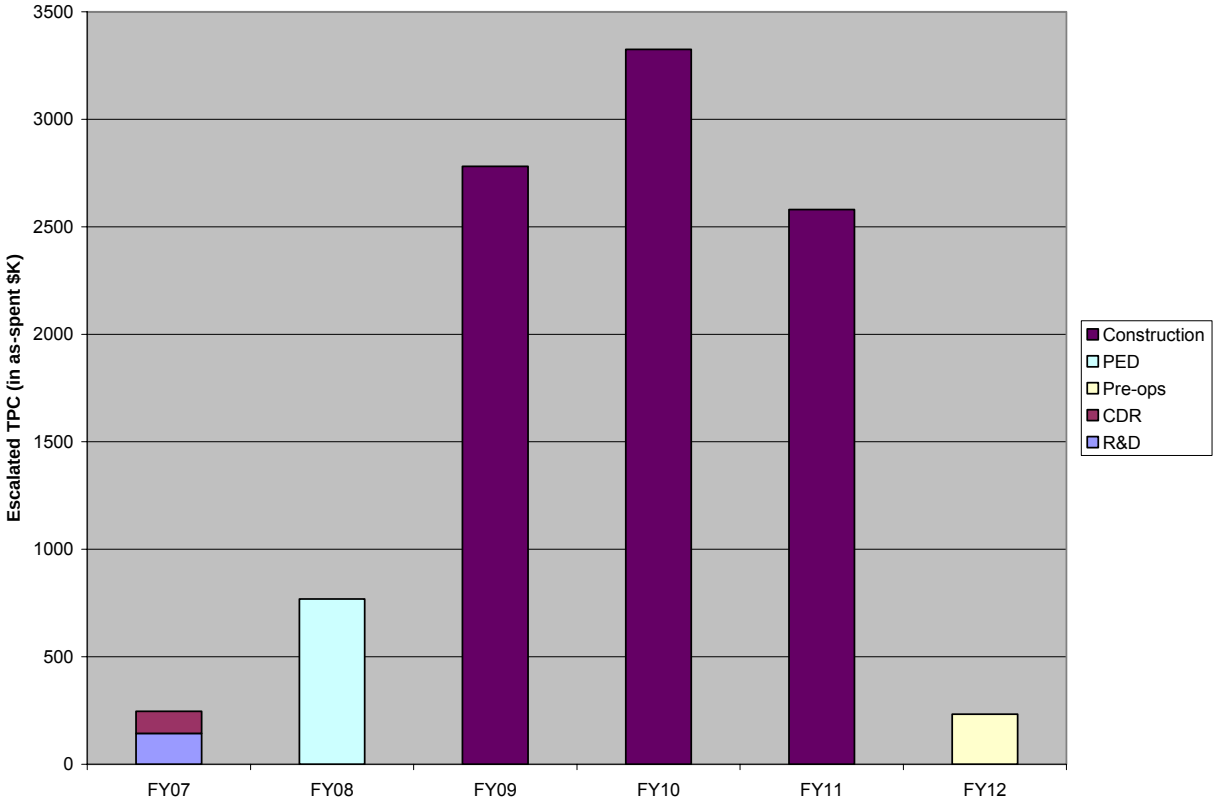

Figure 2.7 ν-SNS suggested budget profile, including contingency and escalation, in as-spent dollars.

2.7 Summary

The **ν-SNS** facility will initiate an era of systematic, high precision neutrino-nucleus cross section measurements. In only the first full year of operation we will more than double our experimental knowledge of medium energy neutrino-nucleus cross sections. In the long term we will be able to make measurements that span the periodic table and address the needs of astrophysics and nuclear structure physics. Such measurements have been well supported by recent planning efforts within the nuclear physics community because they help provide the answers to some of the most fundamental questions we can ask: *"How were the heavy elements from Iron to Uranium made?"*, *"What causes the most powerful explosions in the universe?"*, and *"What role do neutrinos play in the synthesis of the elements in the periodic table?"*

References for Section 2:

1. "Connecting Quarks with the Cosmos, Eleven Questions for the New Century", Committee on the Physics of the Universe, Michael S. Turner, Chair; Board on Physics and Astronomy, Division on Engineering and Physical Sciences, National Research Council of The National Academies, The National Academies Press, 2003, Washington, D.C.
2. C. Athanassopoulos *et al*., *Phys. Rev. C* **55**, 2078, 1997.
3. L.B. Auerbach *et al*., *Phys. Rev. C* **64**, 065501, 2001.
4. B. Bodmann *et al*., *Phys. Lett. B* **280**, 198, 1992.
5. R. Maschuw, *Prog. Part. Phys.* **40**, 183, 1998.
6. J.R. Distel *et al., Phys. Rev. C* **68**, 054613, 2003.
7. S.E. Willis *et al., Phys. Rev. Lett.* **44**, 522, 1980.
8. F.T. Avignone, Yu. Efremenko, *J. Phys. G* **29**, 2615, 2003.

3 SCIENTIFIC MOTIVATION

There are many ways in which interactions between neutrinos and nuclei are important in nuclear astrophysics and in the unique information they can provide about the structure of nuclei. In this section we discuss how this proposed facility to measure neutrino interactions with nuclei will help answer several of the eleven questions raised in *Connecting Quarks with the Cosmos* [1], the recent study by the Committee on the Physics of the Universe of the National Academy of Science. The life-cycles of massive stars lead naturally to bright neutrino sources where interactions between the neutrinos and nuclei are common. The leading examples of this are core collapse supernovae, although two related scenarios - accretion induced collapse, where a white dwarf collapses to form a neutron star (without launching a supernova); and collapsars, where a failed supernova results in a black hole surrounded by a massive accretion disk - may produce similar conditions. We begin this section by briefly reviewing the core collapse supernova mechanism and the current state of its modeling. We then discuss the importance of neutrino-nucleus interaction measurements to the supernova mechanism, supernova nucleosynthesis, neutrino astronomy, and our knowledge of the structure of nuclei.

3.1 The Mechanism of Core Collapse Supernovae

Core Collapse Supernovae are thought to be neutrino powered events.

Core collapse supernovae are among the most energetic explosions in the Universe, releasing 10^{46} Joules of energy in the form of 10^{58} neutrinos of all flavors released over ~10 seconds. Marking the death of a massive star (mass >8-10 solar masses) and the birth of a neutron star or black hole, core collapse supernovae serve as laboratories for physics beyond the Standard Model and for matter at extremes of density, temperature, and neutronization that cannot be produced in terrestrial laboratories. The ejecta of each supernova delivers 10^{44} Joules of kinetic energy and a rich mix of recently synthesized elements into the interstellar medium (ISM), providing a major source of heat in the ISM as well as a potential trigger for star formation. This enrichment in heavy elements make core collapse supernovae a key link in our chain of origins from the Big Bang to the formation of life on Earth. Understanding how (and which) heavy elements are produced in supernovae is therefore an important subject for investigation. Of particular interest to this proposed facility is the role of neutrinos in the nucleosynthesis process.

As it nears its demise, the center of a massive star is composed of iron, nickel, and similar elements, the end products of stellar nucleosynthesis. Above this *iron core* lie concentric layers of successively lighter elements, recapitulating the sequence of nuclear burning that occurred in the core during the star's lifetime. Unlike prior burning stages, where the ash of one stage became the fuel for its successor, no additional nuclear energy can be released by further fusion of the maximally bound iron peak nuclei. Nuclear energy production can no longer stave off the inexorable force of gravity. When the iron core grows too massive to be supported by electron degeneracy pressure, the core collapses. This collapse continues until the core reaches or exceeds the density of nucleons in a nucleus, whereupon the strongly repulsive short range nuclear interaction renders the core incompressible, halting the collapse. Collision of the supersonically falling overlying layers with this stiffened core produces the *bounce shock*, which drives these layers outward. However, this bounce shock is sapped of energy by the escape of neutrinos and by nuclear dissociation and stalls before it can drive off the envelope of the star (see, *e.g.*, [2]).

The failure of this *prompt* supernova mechanism sets the stage for a *delayed* mechanism, wherein the intense neutrino flux, which is carrying off the binding energy of the proto-neutron star (PNS), heats matter above the neutrinospheres and re-energizes the shock [3,4]. The heating is mediated primarily by the absorption of electron neutrinos and antineutrinos on the dissociation-liberated free nucleons behind the shock. Figure 3.1 illustrates the geography of the neutrino reheating mechanism. Although four decades of supernova modeling have established this textbook explanation, models of this mechanism frequently fail to produce explosions, thus fundamental questions about the explosion mechanism remain.

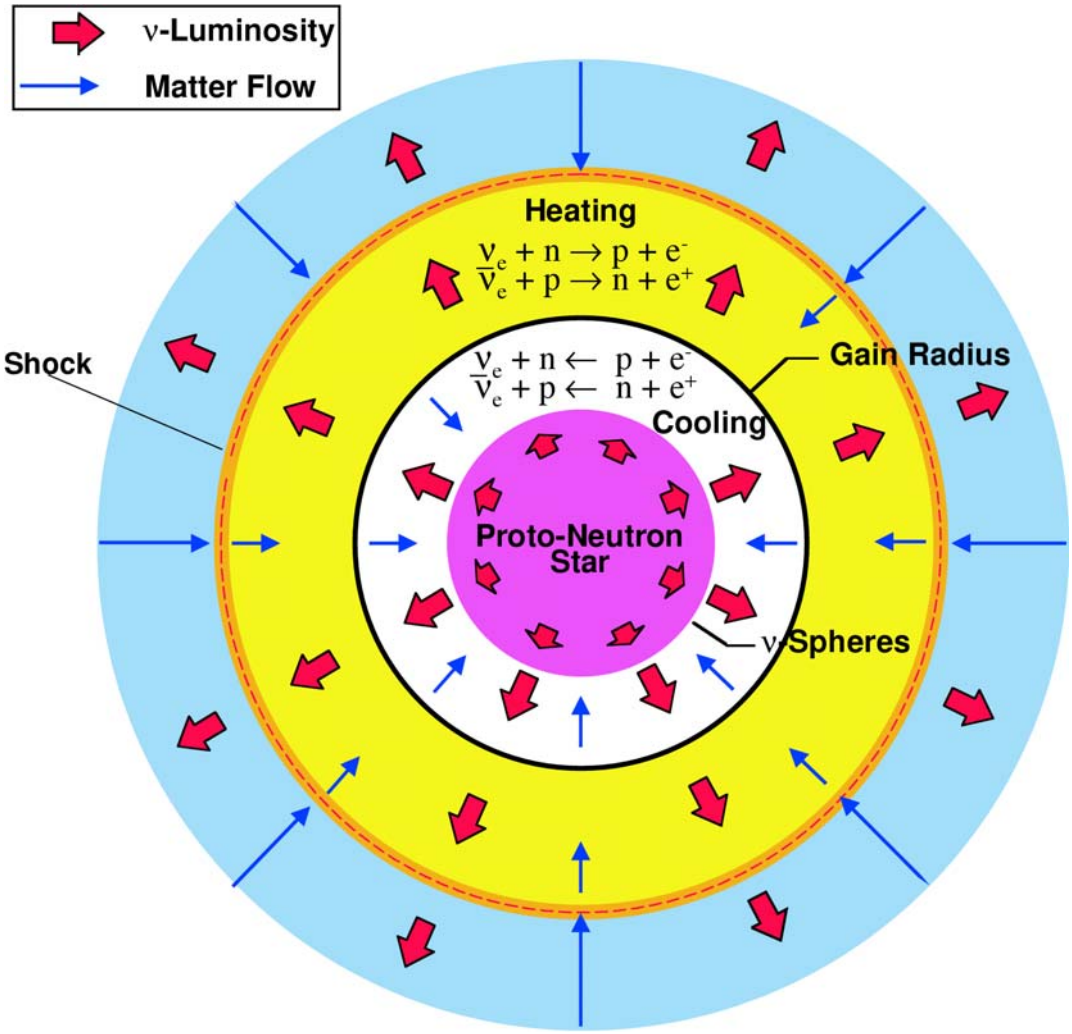

Figure 3.1 Geography of the neutrino reheating mechanism. The neutrinospheres (the effective neutrino radiating surfaces) lie at the PNS surface. The stalled shock sits far above, separating rapidly infalling matter in the envelope from the matter slowly settling on the PNS. This settling matter between the neutrinospheres and the shock is divided into cooling and heating regions, where the matter is respectively losing and gaining energy from the neutrino field. The gain radius separates these regions.

The neutrino energy deposition behind the shock depends sensitively on the neutrino luminosities, spectra, and angular distributions in the post-shock region. Ten percent variations in any of these quantities can make the difference between explosion and failure in supernova models [5,6]. Thus, accurate multi-group (spectrally resolved) Boltzmann neutrino transport must be considered in supernova models. Past spherically symmetric simulations have implemented increasingly sophisticated approximations to Boltzmann transport: simple leakage schemes, two-fluid models, and multi-group flux-limited diffusion [7-10]. A generic feature of this last, most sophisticated approximation is that it underestimates the isotropy of the neutrino angular distributions in the heating region and, thus, the heating rate [11,12]. With these limited transport approximations came the possibility that failure to produce explosions in the past may have resulted from incomplete neutrino transport. To address this possibility, complete Boltzmann neutrino transport models have been constructed in recent years [13-16]. As a class, these models have failed to produce explosions for a range of progenitor masses from 13-40 solar masses. Though the neutrino heating rate is large, because of the stratified temperature structure imposed by spherical symmetry, the heating region is small and the total deposited energy is insufficient to eject the envelope. These models make it clear that the failure of prior supernova models was not the result of inadequate transport approximations.

Models that break the assumption of spherical symmetry have achieved some success, either by enhancement of the neutrino luminosity due to fluid instabilities within the PNS [10] or by enhanced efficiency of the neutrino heating due to large scale convection behind the shock [17-19]. The PNS instabilities are driven by lepton and entropy gradients, and to date simulations in this regime have been highly dependent on the assumptions made in constructing the models [20-24]. Convection behind the shock originates from gradients in entropy that result from the stalling of the shock and grow as the matter is heated from below. However, even with such convective enhancements explosions are not guaranteed [5,20,22,25]. One potential cause of the failure to produce explosions in numerical models is incomplete (or inaccurate) treatment of the wide variety of nuclear and weak interaction physics that is important to the supernova mechanism.

Given the approximations made necessary by present day computational capabilities, next-generation simulations will be necessary to fully explore convection, rotation and magnetic fields in the context of three-dimensional hydrodynamics coupled to more realistic multi-group three-dimensional neutrino transport. **However, the improvement made by such simulations must be complimented by improvements in our understanding of the neutrino-matter interactions on which they depend.**

3.2 Neutrino-Nucleus Interactions and Core Collapse Dynamics

Electron/neutrino capture on heavy nuclei is vitally important during core collapse.

While neutrino interactions with shock-heated nucleons are the major source of the neutrino heating which drives the delayed shock, neutrino interactions with nuclei are important in unshocked regions, particularly the collapsing core. As Bethe *et al.* [26] pointed out, due to the low entropy of the stellar core and resulting dominance of heavy nuclei over free nucleons, electron capture processes on heavy nuclei dominate the evolution of the electron fraction during the late stages of stellar evolution up to the onset of stellar core collapse. In the iron core, this predominantly occurs via Gamow-Teller (GT) transitions changing protons in the $1f_{7/2}$ level into

neutrons in the $1f_{5/2}$ level. Improved weak interaction rates for electron/positron capture and β decays on nuclei relevant for stellar evolution (nuclear mass between 45 and 65) have become available in recent years using shell model diagonalization [27,28]. Heger *et al.* [29] utilized these new weak reaction rates to improve upon the stellar evolution simulations of Woosley & Weaver [30] (WW95). The WW95 models used the electron capture rates of Fuller, Fowler, & Newman [31] (FFN), which estimated the GT contributions based on an independent particle model parameterization, and older sets of β decay rates [32,33]. The most noticeable effect of these improvements is a marked increase in the electron fraction (Y_e) throughout the iron core before collapse.

It was suggested that the persistence of these initial differences in Y_e throughout collapse should have a discernible (positive) effect on the shock energetics, because the final size of the homologous core is proportional to the square of the trapped lepton fraction at core bounce [34]. However, the electron/lepton fraction is greatly modified during the collapse of the stellar core. The increasing density, and concomitant increase in the electron chemical potential, accelerates the capture of electrons on heavy nuclei and free protons in the core, producing electron neutrinos that initially escape, thus deleptonizing the core. Thus the location at which the shock forms in the stellar core at bounce and the initial strength of the shock are largely set by the amount of deleptonization during collapse. Figure 3.2 summarizes the thermodynamic conditions throughout the core at bounce and displays the temperature, electron fraction (Y_e), electron chemical potential (μ_e), and mean electron neutrino energy ($E_{\nu e}$) in MeV as functions of the matter density. Also shown is the representative nuclear mass (A). The kinks near 3×10^7 g/cm^3 mark the transition to the silicon shell. Deleptonization would be complete (Y_e~0) if electron capture continued without competition, but at densities of order $10^{11\text{-}12}$ g/cm^3, the electron neutrinos become "trapped" in the core, and inverse neutrino capture reactions begin to compete with electron capture until the reactions are in weak equilibrium and the net deleptonization of the core ceases on the core collapse time scale. The equilibration of electron neutrinos with matter occurs at densities between $10^{12\text{-}13}$ g/cm^3.

As the densities increase, the characteristic nuclei in the core increase in mass, owing to a competition between Coulomb contributions to the nuclear free energy and nuclear surface tension, until heavy nuclei are replaced by nuclear matter for mass densities near that of the nucleons in the nucleus (~10^{14} g/cm^3). For densities of order 10^{13} g/cm^3, nuclei with mass ~100 dominate. Figure 3.3 demonstrates that the nuclear composition during stellar collapse shows a wide spread in mass (species with significant concentrations have masses that differ by 40 mass units) and that the abundances of nuclei with mass greater than 100 are significant as early as 10^{11} g/cm^3. Fuller [36] realized that electron capture on heavy nuclei would soon be quenched in the picture of Bethe *et al.* [26], as neutron numbers approach 40, filling the neutron $1f_{5/2}$ orbital. Calculations using the independent particle model (IPM) showed that neither thermal excitations nor forbidden transitions substantially alleviated this blocking [36,37]. For many years, this prescription was widely adopted in core collapse simulations (see *e.g.* [8]), leading to a higher rate of electron capture on protons than on heavy nuclei during collapse.

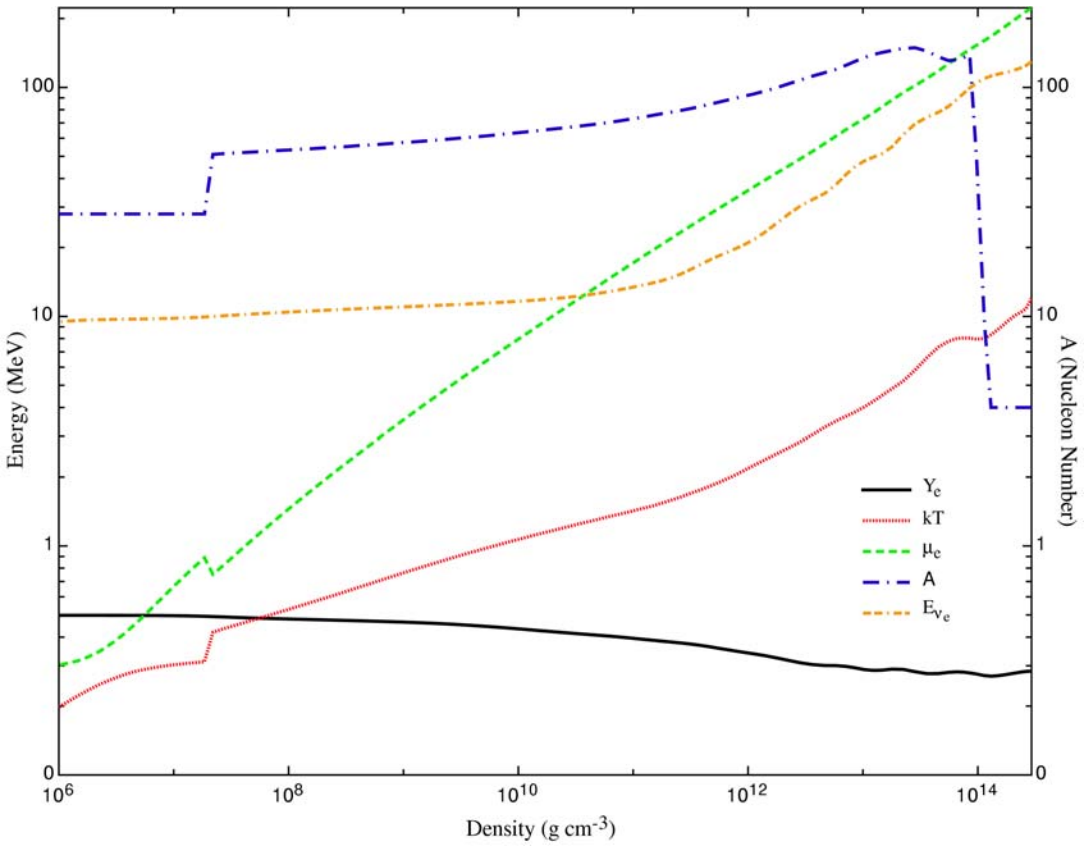

Figure 3.2 Energy scales and composition as a function of density in the collapsed stellar core at bounce for a 15 $M_{\odot}$ progenitor [29].

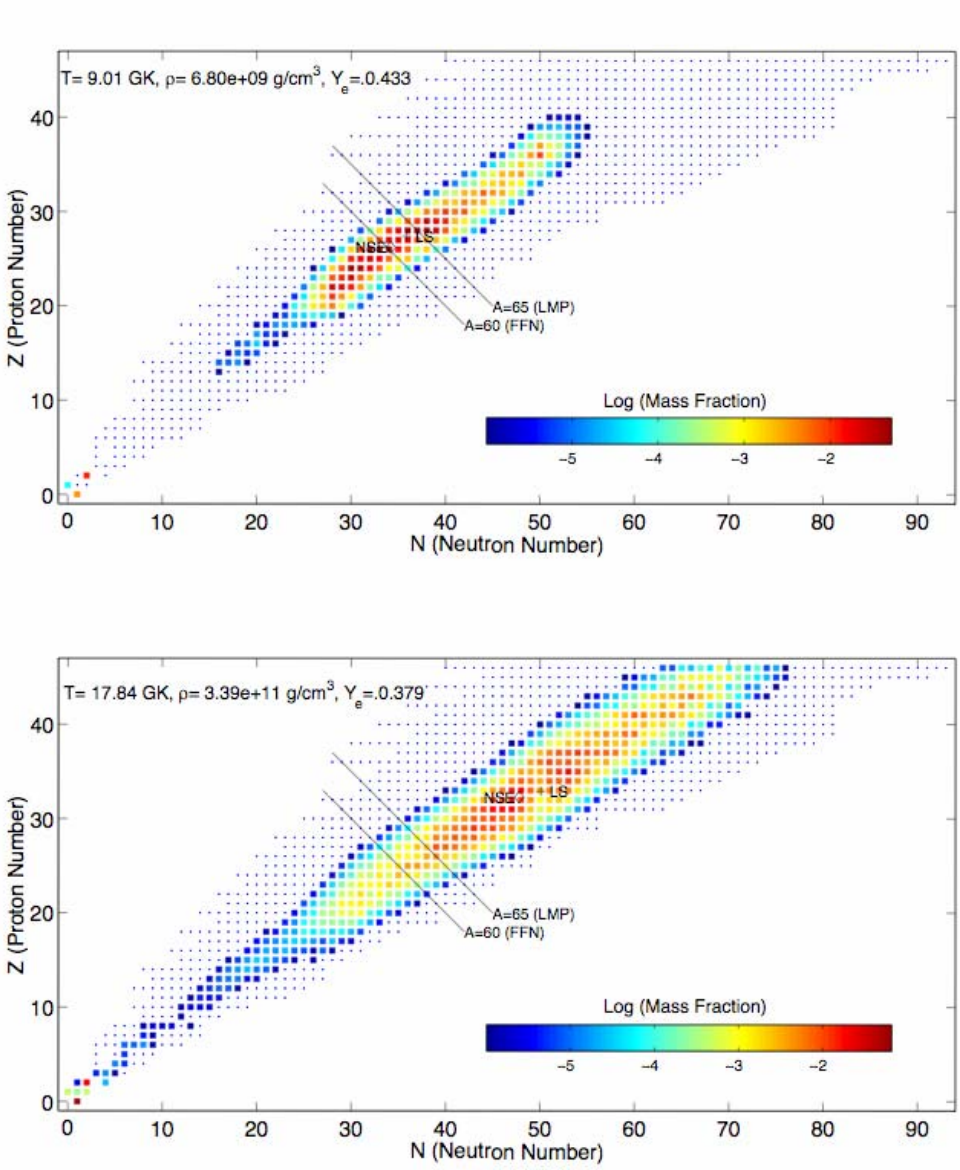

Figure 3.3 Composition details at two points during stellar core collapse [35].

However, it is well known that the residual nuclear interaction (beyond the IPM) mixes the *fp* and *gds* shells, for example, making the closed $1g_{9/2}$ shell a magic number in stable nuclei (N=50) rather than the closed *fp* shell (N=40). **To examine the possibility that nuclear electron capture is not quenched at N=40, cross sections for charged-current electron and electron-neutrino capture on many nuclei up to at least A=100 are needed to accurately simulate core deleptonization.** Full shell model diagonalization calculations remain impossible in this regime due to the large number of available levels in the combined *fp*+*gds* system [27]. Langanke *et al.* [38] developed a "hybrid" scheme, employing Shell Model Monte Carlo (SMMC) calculations of the temperature-dependent occupation of the various single-particle orbitals to serve as input to Random Phase Approximation (RPA) calculations for allowed and forbidden transitions to calculate the capture rate. With this approach, Langanke *et al.* [39]

(LMS) calculated electron capture rates for a sample of nuclei with A=66-112. As Figure 3.4 demonstrates, though the electron capture rates for individual heavy nuclei are smaller than that on protons, they are large enough that capture on the much more abundant heavy nuclei dominates the capture on protons throughout core collapse.

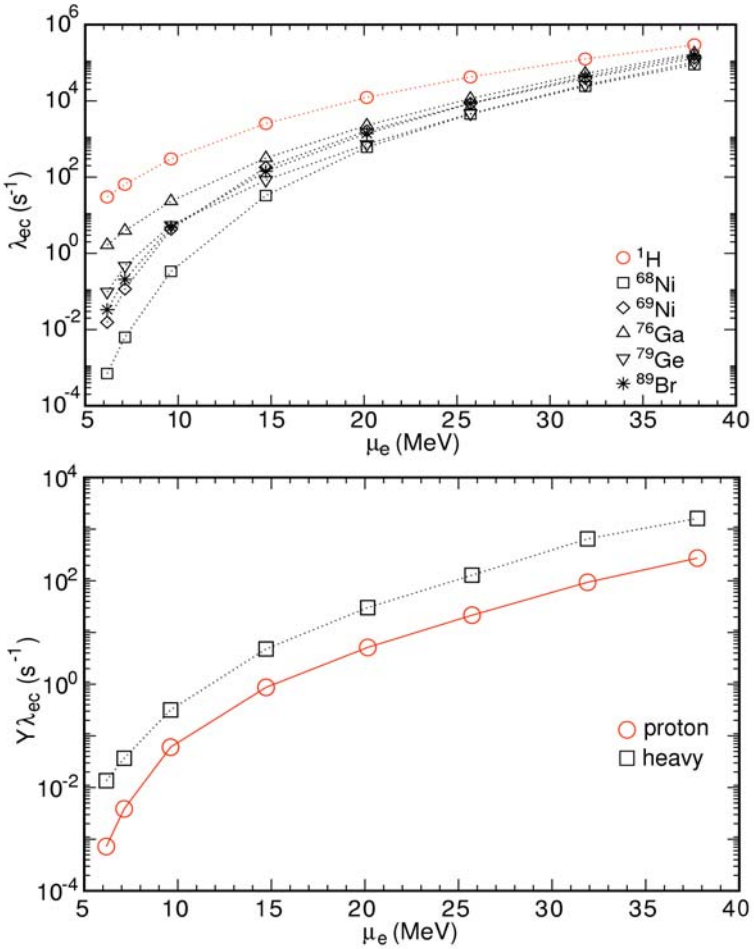

Figure 3.4 Comparison between the electron capture rate on heavy nuclei to that on protons versus the electron chemical potential over the range found in a collapsing stellar core [38]. The upper panel shows the rates for individual species, the lower panel folds in the relative abundance of the protons and heavy nuclei.

Hix *et al.* [40] used these rates, along with the shell model diagonalization rates of Langanke & Martinez-Pinedo [27] (LMP) for lighter nuclei, to develop a greatly improved treatment of nuclear electron capture. To calculate the needed abundances of the heavy nuclei, a Saha-like Nuclear Statistical Equilibrium expression was used, including Coulomb corrections to the nuclear binding energy [41,42], but neglecting the effects of degenerate nucleons [43]. Comparison between the long standard Bruenn prescription [8] (shown below in Equation 1) and the improved treatment of nuclear electron capture used by Hix *et al.*, which we will term the LMSH prescription, reveals two competing effects. In lower density regions, where the average nucleus is well below N=40 and the cutoff of electron capture on heavy nuclei due to filling the neutron $1f_{5/2}$ orbital, the Bruenn parameterization results in more electron capture than the

LMSH case. This is similar to the reduction in the amount of electron capture seen in stellar evolution models [29] and thermonuclear supernova [44] models when the FFN rates are replaced by shell model calculations. In denser regions, the continuation of electron capture on heavy nuclei alongside electron capture on protons results in more electron capture in the LMSH case. Hix *et al.* [40] demonstrated that for a 15 $M_\odot$ progenitor this produces a marked reduction (11%) in the electron fraction in the interior of the PNS, resulting in a nearly 20% reduction in the mass of the homologous core. As can be seen in Figure 3.5, this manifests itself at bounce as a reduction in the mass interior to the formation of the shock from 0.67 $M_\odot$ to 0.57 $M_\odot$ in the LMSH case for models using Newtonian gravity. A shift of this size is very significant dynamically because the dissociation of 0.1 solar mass of heavy nuclei by the shock costs 10^{51} erg, the equivalent of the explosion energy. There is also a 10% reduction in the central density and entropy at bounce, as well as a 10% smaller velocity difference across the shock and quite different lepton and entropy gradients throughout the core. Thus, the LMSH prescription results in the launch of a weaker shock with more of the iron core overlying it, inhibiting a successful explosion.

Messer *et al.* [45] have examined the sensitivity of the models to uncertainties in the nuclear electron capture rates. For simplicity (and reproducibility by others), the Bruenn prescription [8] was taken as a starting point. In this prescription, the neutrino emissivity due to electron capture on heavy nuclei is given by:

$$j_{nuclear} = \frac{2[2\pi]^4 G_F^2}{7\pi h^4 c^4} g_A^2 \frac{\rho X_H}{m_B A} N_p(Z) N_h(N) [E + Q']^2 [1 - [\frac{M_e}{E + Q'}]^2]^{1/2} F_e(E + Q') \qquad (1)$$

where $F_e(E)$ is the Fermi-Dirac occupation function for electrons and the functions $N_p(Z)$ and $N_h(N)$, defined as:

$$N_p(Z) = \left\{ \begin{array}{ccc} 0 & : & Z < 20 \\ Z - 20 & : & 20 < Z < 28 \\ 8 & : & Z > 28 \end{array} \right\} \quad \text{and} \quad N_h(N) = \left\{ \begin{array}{ccc} 6 & : & N < 34 \\ 40 - N & : & 34 < N < 40 \\ 0 & : & N > 40 \end{array} \right\}, \qquad (2)$$

respectively, indicate the number of protons in the $1f_{7/2}$ level and the number of holes in the $1f_{5/2}$ level of the average nucleus. The product $N_p N_h$ approaches zero as N approaches 40, quenching electron capture on heavy nuclei and allowing electron capture on protons to dominate in this prescription. Instead of letting the product $N_p N_h$ in Equation 1 vary as determined by the equation of state, Messer *et al.* [45] set this product to several constant values in Newtonian collapse simulations. Figure 3.5 shows the effect of this variation on the velocity distribution at bounce, in comparison to the results of Newtonian models using the LMSH and Bruenn prescriptions. This clearly demonstrates that a reduction in the total electron capture rate by a factor of ten from those predicted by Langanke *et al.* [39] would erase the changes demonstrated by Hix *et al.* [40]. Likewise, a systematic increase by a factor of ten would further reduce the initial PNS mass by at least 10%. Even changes intermediate to these would significantly alter the location of shock formation. Further efforts to verify the electron and neutrino capture rates, both theoretical and experimental, are clearly required.

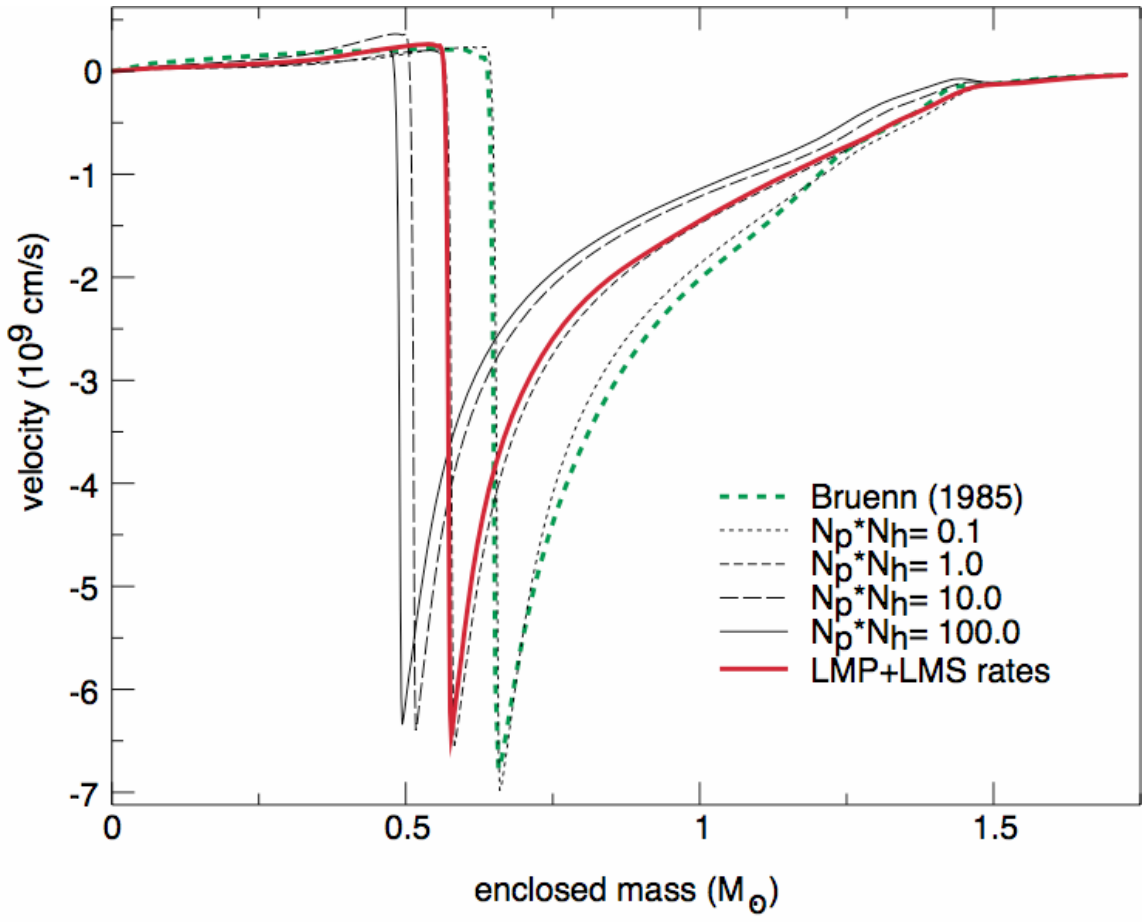

Figure 3.5 Comparison of the core velocity structure of a 15 $M_\odot$ star at bounce. Green and red lines indicate models using the Bruenn and LMSH prescriptions. Dotted lines show results of a range of simulations using a modification of the Bruenn prescription where the product of the number of protons in the $1f_{7/2}$ level and the number of holes in the $1f_{5/2}$ level is held constant throughout the simulation.

These differences in the behavior of collapsing stellar cores illustrate the importance of weak interactions with nuclei. At the onset of collapse, the nuclei of interest are clustered in mass between 50 and 70 along the neutron-rich edge of stability. Throughout collapse, decreasing electron fraction and increasing density pushes the composition to heavier and more neutron-rich nuclei, including nuclei 4-6 decays away from stability and with masses greater than 100. The KARMEN collaboration pioneered work in this regime, measuring the cross section for $Fe(\nu_e, e^-)Co$ [46], which is one of the nuclei of interest early in collapse. However, this measurement has a 40% uncertainty. The sheer number of potentially important species, and the fact that they are unstable, makes direct measurements of all needed rates an impossibility. Nonetheless, measurements of representative neutrino-nucleus interactions are crucial since they provide the most relevant constraints on nuclear structure and reaction models. The technique which we propose in subsequent sections can be used in a very cost effective manner to measure the electron-neutrino capture cross section on any of a wide range of nuclei which are affordable in ton quantities. Several such nuclei are in the critical nuclear mass range: Mn, Fe, Co, Y, Nb, Rh and In.

In addition to their effects prior to the formation of the supernova shock, charged-current neutrino capture (and neutral-current inelastic neutrino scattering [47]) on heavy nuclei above the shock can alter the entropy and neutronization of this infalling matter prior to its arrival at the shock. It has been suggested that if sufficient energy is transferred to this matter to melt a fraction of the nuclei, then the shock dynamics can be altered. Though this "pre-heating" of the shock could help the shock, it could also hinder the shock because the melted nuclei produce a higher pressure, reducing the Mach number of the shock. Potentially, these changes in the pre-shock matter affect not only the shock propagation but also the thermodynamic conditions in the post-shock convective region. **Only with accurate neutrino-nucleus cross sections can we gauge the full impact of these interactions on the supernova mechanism and begin to answer the corresponding questions raised by *Connecting Quarks with the Cosmos*.**

3.3 Supernova Nucleosynthesis

Neutrinos impact all phases of supernova nucleosysnthesis.

Supernova nucleosynthesis is commonly divided into several "processes", each of which is impacted by neutrino-nucleus interactions. (1) Explosive nucleosynthesis occurs as a result of compressional heating by the supernova shock wave as it passes through the stellar layers. In the inner layers of the ejecta, where iron group nuclei result from α-rich freezeout, interactions with neutrinos alter the neutronization, changing the ultimate composition. (2) Neutrino nucleosynthesis or the "ν" process occurs due to neutrino-induced nuclear transmutations in the outer stellar layers followed by shock heating. (3) The rapid neutron capture or "*r*" process may occur in the neutrino-driven wind that emanates from the proto-neutron star after the explosion is initiated. The neutrinos both drive the wind and interact with the nuclei in it. Early phases of this wind have also been suggested as the source of light *p*-process nuclei [48]. Thus, neutrino-nucleus interactions are important to all core collapse supernova nucleosynthesis processes.

3.3.1 Neutrinos and the α-Rich Freezeout

Neutrino interactions help determine the isotopic composition of the iron group ejecta.

One common property exhibited by recent spherically symmetric Boltzmann simulations [13,14] is a decrease in the neutronization (which is equivalent to an increase in the electron fraction Y_e) of the inner layers of the ejecta due to neutrino interactions. This is a feature that current parameterized nucleosynthesis models cannot replicate because they ignore the neutrino interactions. The neutronization of the ejecta is important because galactic chemical evolution calculations and the relative neutron-poverty of terrestrial iron and neighboring elements strongly limits the amount of neutronized material that may be ejected into the interstellar medium by core collapse supernovae [49]. Those previous multidimensional models for core collapse supernovae that did produce explosions tended to greatly exceed these limits (see, *e.g.*, [5,17,50]). To compensate, modelers have been forced to assume the fallback of a considerable amount of matter onto the neutron star, occurring on a timescale longer than was simulated. While the decreased neutronization seen in Boltzmann models reduces the need to invoke fallback, it also makes any fallback scenario more complicated, since the most neutron-rich material may no longer be the innermost.

As a result of neutrino-nucleus interactions, the nucleosynthesis products from future explosion simulations (utilizing multi-group neutrino transport) will be qualitatively different, both in

composition and spatial distribution, from either parameterized bomb [51] or piston [30] nucleosynthesis models or the present generation of models of the core collapse mechanism. This has been demonstrated in exploratory calculations by McLauglin, Fuller & Wilson [52], Frölich *et al.* [53] and Pruet *et al.* [54]. In the innermost ejecta, the shock fully dissociates the matter, so neutrino interactions with free nucleons dominate, producing a marked increase in the electron fraction. In more distant regions, cooler peak temperatures cause more poorly known neutrino and electron/positron interactions with heavy nuclei to contribute significantly. Recent models [53,54] that include the impact of neutrinos on the nucleosynthesis have shown abundances for ^{45}Sc, ^{49}Ti, and ^{64}Zn in much better agreement with observations of metal-poor stars. Neutrino captures, as well as neutral-current inelastic neutrino scattering off these nuclei [47], are also important to the thermal balance, affecting the α-richness of the ejecta and, thereby, the abundance of important products of α-rich freezeout like ^{44}Ti, ^{57}Fe, ^{58}Ni and ^{60}Zn [30]. In addition to these global effects on the neutronization and entropy of the matter, Frölich *et al.* [53], using neutrino capture rates from Zinner & Langanke [55], find that neutrino capture reactions on heavy nuclei have direct impact on the abundances of species like ^{53,54}Fe, ^{55,56,57}Co, ^{59}Ni and ^{59}Cu. **Thus, there is a clear need for improved neutrino-nucleus interaction rates in order to accurately calculate the iron-peak nucleosynthesis from core collapse supernovae.** Because the degree of neutronization is much less than in deeper layers of the star, several important nuclei are directly measurable in the proposed facility: Ca, Sc, V, Mn and Co. However, these measurements will need to be supplemented by calibrated nuclear structure calculations to provide full coverage of the many species present in significant concentrations.

3.3.2 Neutrino Nucleosynthesis

Neutrino interactions may be responsible for producing some of Nature's rarest isotopes.

Neutrino nucleosynthesis is driven by the spallation of protons, neutrons, and alpha particles from nuclei in the overlying stellar layers by the intense neutrino flux that is emanating from the central proto-neutron star powering the supernova [56]. Moreover, neutrino nucleosynthesis continues after the initial inelastic scattering reactions and the formation of their spallation products. The neutrons, protons, and alpha particles that are released continue the nucleosynthesis through further reactions with other abundant nuclei in the high-temperature supernova environment, generating new rare species. The suggestion has been made [56] that neutrino nucleosynthesis is responsible for the production of two of Nature's rarest isotopes, ^{138}La and ^{180}Ta, as well as two lighter species, ^{11}B and ^{19}F, for which stellar sources may not fully account.

That the rare isotopes ^{138}La and ^{180}Ta can be produced via neutrino nucleosynthesis in supernovae is compelling, and may serve as an important fingerprint of the neutrino process. If so, these nuclei may provide powerful diagnostics of the physics of supernovae outer layers. ^{138}La and ^{180}Ta are produced through the following charged and neutral-current channels:

$$^{138}Ba(\nu_e, e^-)^{138}La$$
$$^{139}La(\nu_x, \nu_x' n)^{138}La$$
$$^{180}Hf(\nu_e, e^-)^{180}Ta$$
$$^{181}Ta(\nu_x, \nu_x' n)^{180}Ta$$

Recent models [57] show significantly increased production of these isotopes (with charged-current reactions dominating for ^{138}La) enhancing the possibility that these isotopes originate in

supernovae. Measurements on Ba and Ta are possible and would provide meaningful constraints on the theoretical rates used in models thus far.

Observations of the abundance of boron in stars as a function of metallicity do not show the strictly quadratic dependence that is expected from secondary production mechanisms, like cosmic-ray spallation, that operate after the galaxy has been enriched with metals. This implies [58] that primary mechanisms that operate early in the history of our galaxy, such as neutrino nucleosynthesis, also contribute significantly. According to current supernova nucleosynthesis models, neutrino nucleosynthesis in supernovae favors the production of ^{11}B over ^{10}B. These two isotopes are produced through the following spallation channels:

$$^{12}C(\nu_x,\nu_x' p)^{11}B$$
$$^{12}C(\nu_x,\nu_x' n)^{11}C(e^+\nu_e)^{11}B$$
$$^{12}C(\nu_x,\nu_x' d)^{10}B$$
$$^{12}C(\nu_x,\nu_x' pn)^{10}B,$$

which need laboratory calibration. Neutrino spallation measurements, used in conjunction with future Hubble Space Telescope observations discriminating between ^{10}B and ^{11}B, would be invaluable in resolving this controversy and supporting (or refuting) the suggestion that neutrino nucleosynthesis in supernovae is an important source of ^{11}B in the galaxy [59].

It has been suggested [60] that the final abundance of ^{19}F produced in a supernova can serve as a "supernova thermometer" because the ratio of $[^{19}\text{F}/^{20}\text{Ne}]/[^{19}\text{F}/^{20}\text{Ne}]_\odot$ (the denominator is the measured ratio in our sun) is a measure of the μ and τ neutrinosphere temperatures (provided the abundance of ^{19}F produced in the supernova is due to neutrino nucleosynthesis). ^{19}F is produced through the following spallation channels:

$$^{20}Ne(\nu_x,\nu_x' n)^{19}Ne(e^+,\nu_e)^{19}F$$
$$^{20}Ne(\nu_x,\nu_x' p)^{19}F.$$

Recent models [57], using improved neutrino nucleus reaction rates, show marked decreases in the production of ^{19}F, casting some doubt on the possibility that ^{19}F is made in supernovae. Laboratory measurements of the relevant rates are clearly necessary to resolve this.

Experiments to directly measure the cross sections for these reactions are extremely challenging and are not the goal of the initial suite of experiments at the ν-SNS facility. However, they are worthy of future consideration, since they provide direct insight into the productions sites of these rare isotopes and shed light on the conditions within these sites.

3.3.3 Nucleosynthesis in the Neutrino-Driven Wind

Neutrino interactions may aid or prevent the *r*-process in a neutrino driven wind.

The astrophysical *r*-process is responsible for roughly half of the Solar System's supply of elements heavier than iron, with the remainder originating from the *s*-process occurring in Asymptotic Giant Branch stars. While the nuclear conditions necessary to produce the *r*-process are well established (see, *e.g.*, [61]), the astrophysical site remains uncertain. The leading candidate is the neutrino-driven wind emanating from the proto-neutron star after a core collapse

supernova is initiated [62]. Other plausible sites have been suggested [63,64], however all should result in neutrino-rich outflows. In all of these cases, as the ejecta expands rapidly and cools, the nuclear composition is dominated by α-particles and free neutrons with a small concentration of iron group nuclei. As temperatures continue to drop, charged particle reactions "freeze out" while neutron capture reactions continue on the "seed" heavy nuclei present at freeze-out. Neutron capture (n,γ) reactions are balanced by their inverse photodisintegration (γ,n) reactions, establishing an equilibrium between free neutrons and nuclei in the wind. Because of the high concentration of free nucleons, this (n,γ)-(γ,n) equilibrium among isotopes of the same element produces nuclei that are quite neutron rich. β-decays of nuclei with short half-lives compared to the time scale for the *r*-process link these (n,γ)-(γ,n) clusters, producing nuclei with higher Z and leading to the synthesis of heavier elements [65].

Qian *et al.* [66] have demonstrated that neutrino-induced reactions can significantly alter the *r*-process path and its yields in both the (n,γ)-(γ,n) equilibrium phase and the "postprocessing phase" that occurs once these reactions fall out of equilibrium. In the presence of a strong neutrino flux charged-current reactions on the waiting point nuclei at the magic neutron numbers N=50,82,126 might compete with β-decays and speed up passage through these bottlenecks. Also, neutrinos can inelastically scatter on *r*-process nuclei via charged and neutral-current reactions, leaving the nuclei in excited states that subsequently decay via the emission of one or more neutrons. This processing may for example shift the abundance peak at A=195 to smaller mass. Extending this, Haxton *et al.* [67] pointed out that neutrino postprocessing effects would provide a fingerprint of a supernova *r*-process. Eight abundances on the low mass side of the A~130 and A~195 peaks are particularly sensitive to the neutrino postprocessing: ^{124}Sn, ^{125}Te, ^{126}Te, ^{183}W, ^{184}W, ^{185}Re, ^{186}W, and ^{187}Re. Observed abundances of these elements are consistent with the postprocessing of an *r*-process abundance pattern in a neutrino fluence consistent with current supernova models. If the neutrino interaction leaves the daughter in a sufficiently excited state fission may result [68,69] essentially linking the mass 195 peak to the mass 130 peak. Some such correlation is suggested by observations of ultra-metal poor stars (see, *e.g.*, [70]).

On a more pessimistic note, Meyer, McLaughlin, and Fuller [71] have investigated the impact of neutrino-nucleus interactions on the *r*-process yields and have discovered that electron neutrino capture on free neutrons and heavy nuclei (in the presence of a strong enough neutrino flux) can actually hinder the *r*-process by driving the neutrino-driven wind proton rich, posing a severe challenge to theoretical models. However, this push to lower neutronization makes the early phases of the neutrino-driven wind a candidate for production of the light *p*-process nuclei like ^{74}Se, ^{78}Kr, ^{84}Sr and ^{92}Mo [48]. Fröhlich et al. [53] see similar behavior in the late stages of the convective bubble. The abundances of these species are likely highly sensitive to neutrino-nucleus interactions. Simulations by Meyer [72] showed that significant amounts of ^{92,94}Mo are only produced when neutrino-nucleus interactions are included, with neutrino-nucleus interactions on nuclei with Z≥40 (particular ^{92}Zr) most responsible for the enhancement of the production of ^{92,94}Mo.

While the neutrino-nucleus reactions of interest for the *p*-process nuclei are accessible, during the *r*-process and subsequent postprocessing in the supernova neutrino fluence, neutrinos interact with extremely neutron-rich, radioactive nuclei. Thus, neutrino-nucleus measurements cannot be made on the nuclei of interest. **However, measurements of charged- and neutral-current**

neutrino-nucleus interactions on nearby heavy stable nuclei would be invaluable as a gauge of the accuracy of nuclear structure and reaction predictions.

3.4 Supernova Neutrino Astronomy

Observations of supernova neutrino luminosities are only as accurate as knowledge of neutrino interaction rates.

The twenty neutrino events detected by IMB and Kamiokande from SN1987A confirmed a central tenant of supernova theory—that core collapse supernovae mark the formation of a proto-neutron star and release of the liberated binding energy in the form of neutrinos—and signaled the birth of extra-Solar-System neutrino astronomy. For a Galactic supernova, thousands of events will be seen by Super-Kamiokande [73], SNO [74], and KamLAND, which for the first time will give us detailed neutrino "light curves" and provide volumes of information about the deepest regions in the explosion. In turn, these light curves can be used to test and improve supernova models, thereby improving predictions about the explosion and resultant nucleosynthesis as well as the behavior of matter at super-nuclear densities. Moreover, from these detailed neutrino light curves and an understanding of the effects of neutrino oscillations, interesting insight could be gained about the density structure of the supernova progenitor. To achieve this will require an accurate normalization of the neutrino flux in a supernova neutrino detector and knowledge of the cross sections and by-products of neutrino interactions in the detector material. For a galactic supernova, variants of the Baade-Wesselink method will likely provide distances to the supernova with uncertainties of 10% or less [86,87], making 10% or smaller uncertainties for the neutrino-nucleus cross sections desirable. From deuterium to lead, a number of nuclei have been proposed and, in some cases, used as supernova detector materials. **In all cases, accurate neutrino-nucleus cross sections are essential and currently not available. Among the neutrino-nucleus interactions most relevant for supernova neutrino detection are neutrino interactions on ^{2}H, C, O, Fe and Pb.**

While the occurrence of a Galactic supernova is a rare event, Beacom and Vagins [75] have recently suggested a modification of Super-Kamiokande that would allow detection of the diffuse supernova neutrino background, *i.e.*, the flux from all supernovae that have occurred in the history of the universe, at the rate of 2-6 events per year. In just a few years, the yield from SN 1987A could be exceeded, allowing improved tests of numerical supernova models through the measured flux and spectral shape. In addition, this modification should also allow neutrino observations of pre-supernova massive stars within 1 kpc [76]. These possibilities open the opportunity to expand our knowledge of supernovae (and their progenitors) on an ongoing basis while we await a nearby event.

3.4.1 Oxygen

In water Cherenkov detectors like the Sudbury Neutrino Observatory (SNO) and Super-Kamiokande, the charged-current reaction $^{16}O(\nu_e,e^-)^{16}F$ is the principal channel for electron neutrino interactions for thermal sources in the range $T_\nu \geq$ 4-5 MeV. Its rate exceeds that of neutrino-electron scattering by an order of magnitude for $T_\nu \geq$ 7-9 MeV [77]. Moreover, the electron angular distribution is strongly correlated with the electron neutrino energy [78], providing a way to measure the incident neutrino energy.

In addition, the appearance of back-angle electron emission from this reaction in, for example, Super-Kamiokande would result from energetic electron neutrinos, more energetic than predicted by supernova models, providing further evidence for flavor oscillations and thereby information about the μ and τ neutrino spectra emanating from supernovae [78]. μ and τ neutrinos in the stellar core couple to the core material only via neutral currents, whereas electron neutrinos and antineutrinos couple via both neutral and charged currents. As a result, the former decouple at higher density and, therefore, temperature, and have harder spectra. Utilizing reactions on ^{16}O, Langanke, Vogel, and Kolbe [79] have suggested a novel way of also unambiguously identifying μ and τ neutrino signatures in Super-Kamiokande. The larger average energies for these neutrino flavors may be sufficient to excite giant resonances via the neutral-current reactions $^{16}O(\nu_{\mu,\tau},\nu'_{\mu,\tau})^{16}O^*$. These resonances are above particle threshold and subsequently decay via the emission of protons, neutrons, and γ rays. The γ rays would provide the μ and τ neutrino signatures. The two decay channels are: $^{16}O^*(\gamma n)^{15}O$ and $^{16}O^*(\gamma p)^{15}N$. However, potential channels for observing the μ and τ neutrinos from supernovae must be re-examined in light of recent work (see, *e.g.*, [80-82]), which indicates that nucleon-nucleon bremsstrahlung and the effects of nuclear recoil in neutrino-nucleon scattering significantly soften the μ and τ neutrino spectra, lessening their energy excess over electron neutrinos.

Thus, accurate measurements of both charged- and neutral-current neutrino cross sections on Oxygen would serve as a foundation for interpreting neutrino data from the next core collapse supernova in our galaxy and for using the data to potentially observe μ and τ neutrino spectra as they are emitted from the proto-neutron star. An experiment to measure the cross section for:

$$^{16}O(\nu_e,e^-)^{16}F$$

is a high priority. Further useful experiments could focus on the cross sections for:

$$^{16}O(\nu_\mu,\nu'_\mu n\gamma)^{15}O$$
$$^{16}O(\nu_\mu,\nu'_\mu p\gamma)^{15}N$$

3.4.2 Iron and Lead

The use of iron and lead in supernova neutrino detectors like the proposed ADONIS detectors would provide another way of detecting the μ and τ neutrino spectra in core collapse supernovae [83]. Iron has a sufficiently high threshold for neutron production via charged-current neutrino interactions that such production is negligible, whereas in lead neutrons are produced by both charged- and neutral-current interactions. Oscillations between the more energetic μ and τ neutrinos and the electron neutrinos would boost the charged-current event rate while leaving the neutral-current rate roughly unchanged. Thus, the ratio of the event rate in lead to that in iron would serve as a further constraint on the extent of neutrino oscillations and the emitted μ/τ neutrino spectra, provided the reaction rates in iron and lead are well known. **To further the development of a detector like ADONIS, experiments to measure the neutrino-iron and neutrino-lead cross sections are critical.**

For iron, the neutral-current reaction:

$$^{56}Fe(\nu_x,\nu_x' n)^{55}Fe$$

dominates.

For lead, cross sections for the following neutral- and charged-current channels are desirable:

$$^{A}Pb(\nu_x,\nu_x' n)^{A-1}Pb$$
$$^{A}Pb(\nu_x,\nu_x' 2n)^{A-2}Pb$$
$$^{A}Pb(\nu_e,e^- n)^{A-1}Bi$$

Since they are a both a necessary calibration for future supernova neutrino experiments and are important to nucleosynthesis simulations, iron and lead cross section measurements are a very high priority.

3.4.3 Deuterium

Neutrino experiments that use heavy water, like SNO, can detect supernova neutrinos via four main channels:

$$e^-(\nu_x,\nu_x')e^-$$
$$d(\nu_x,\nu_x' n)p$$
$$d(\nu_e,e^- p)p$$
$$d(\bar{\nu}_e,e^+ n)n$$

Measurement of the reaction $d(\nu_e,e^- p)p$, which has been suggested as a calibration for the reaction $p(e^+,\nu_e)d$ (part of the *pp* chain of reactions powering the Sun), would also provide a calibration for heavy water neutrino detectors. **Monte Carlo studies suggest that for the source brightness predicted for the SNS, two years of data in approximately fifteen fiducial tons of D_2O would yield a cross section measurement with an accuracy of a few percent [84], which in turn may enable a more accurate interpretation of SNO data.** This measurement would also serve as an important test case for the effective field theory approach to neutrino-nucleus interactions (see [85] and references therein).

3.4.4 Carbon

Large neutrino detectors that use liquid scintillator, such as KamLAND and MiniBoone, are ideally suited to detect antineutrinos from a supernova collapse via $\bar{\nu}_e + p \rightarrow e^+ + n$. In addition, a significant number of neutral- and charged-current interactions could be detected [88] via:

$$^{12}C(\nu_e,e^-)^{12}N_{gs}$$
$$^{12}C(\nu_e,e^-)^{12}N^*$$
$$^{12}C(\nu_x,\nu_x')^{12}C^*$$

It is clear that every recorded neutrino interaction from the next galactic supernova will be extremely important. Detailed measurements of neutrino interactions in multiple channels will help untangle intensities and temperature of individual neutrino species. Although ν+Carbon interactions have been measured by LSND and KARMEN, **ν-SNS** measurements of double

differential cross sections can provide powerful additional information to assist the interpretation of supernova neutrino signals.

3.5 Nuclear Structure

ν-SNS will make definitive measurements of nuclear excitations that would be difficult to generate or analyze with any other type of experiment. When combined with reliable nuclear theory, this will enable a more quantitative understanding of neutrino cross sections throughout the periodic table.

Nuclei are correlated quantum-many body systems that can be excited by neutrinos through a variety of channels. For example neutrinos with energies less than 15 MeV excite nuclei mainly through the Gamow-Teller resonance, while higher energy neutrinos will also excite first and second forbidden transitions. Experimental information obtained from **ν-SNS** will place strong constraints on nuclear structure calculations of neutrino cross sections for three reasons. First, the neutrino spectra in astrophysical systems are quite similar to those at **ν-SNS**, so the **ν-SNS** measurements provide the desired information directly. Second, the neutrino reactions at **ν-SNS** energies and below proceed largely through a few multipoles of the weak interaction with spin $J \leq 3$. Thus a limited number of nuclear operators determine the cross sections, and some information about their matrix elements can be extracted from other kinds of experiments in which kinematics are better controlled. Finally, the strength in the few important multipoles is often concentrated in collective nuclear resonances, which usually have relatively simple structure, are subject to sum rules, and can be modeled effectively through, *e.g.*, the random phase approximation or the shell model. The important resonances in charged-current reactions are the allowed $J = 1^+$ Gamow-Teller mode, and the forbidden 1^- dipole and 0^-, 1^-, 2^- spin-dipole modes. In neutral-current reactions, the analogs of these resonances are the most important.

Measurements of neutrino-nucleus cross sections will allow study of interesting nuclear structure issues related to the weak interaction. One of these is improving our understanding of the ratio of the axial to vector coupling constants. For the Gamow-Teller operator that arises from the low-energy expansion of the weak interaction, one finds that this ratio is modified by the nuclear medium. It is unknown whether other operators in the weak interaction are similarly modified. Using **ν-SNS** to probe medium energy strength distributions in neutrino-nucleus scattering (by binning the cross section with respect to the outgoing electron energy) will open the possibility to investigate this fundamental problem. This measurement could be performed on any target material for which low-energy (p,n)-reaction experiments are available in order to compare low-energy excitations. These excitations can be obtained within the shell-model. Furthermore, a judicious choice of SNS targets that can also be developed for inelastic electron scattering at facilities like FAIR in Darmstadt, could yield information on both neutral-current (via indirect measurements at FAIR or other facilities) and charged-current (at the SNS) neutrino scattering in similar excitation energy windows. This complementary information could be used to evaluate nuclear models that have been developed to predict total neutrino scattering cross sections.

As detailed in the proceeding sections an additional motivation for constraining nuclear structure theory comes from the needs of astrophysics. It would, of course, be impossible to measure all of the cross sections that enter the hundreds of weak interaction rates needed in realistic simulations of supernovae and supernova nucleosynthesis. This is especially true given the unstable nature of many of the nuclei of interest. Nonetheless, a strategically chosen set of measurements will help

validate the fundamental nuclear structure models at the foundation of the rate computations that are input for supernova models. Examination of the *N*-*Z* chart of nuclei (Figure 3.6) helps to illustrate this point. Superimposed on the figure are circles of radius eight nucleons centered on the nuclear target. Reliable extrapolations from experimental data could be made within these circles up to lines where major shell closures are crossed. With just seven of the 36 affordable nuclear targets, we obtain the ability to calibrate relevant calculations for neutrino cross sections throughout the periodic table and particularly in the regions of interest to supernova science. The selected target materials for this plot are: ^{40}Ca, ^{56}Fe, ^{75}As, ^{89}Y, ^{127}I, ^{165}Ho, and ^{208}Pb.

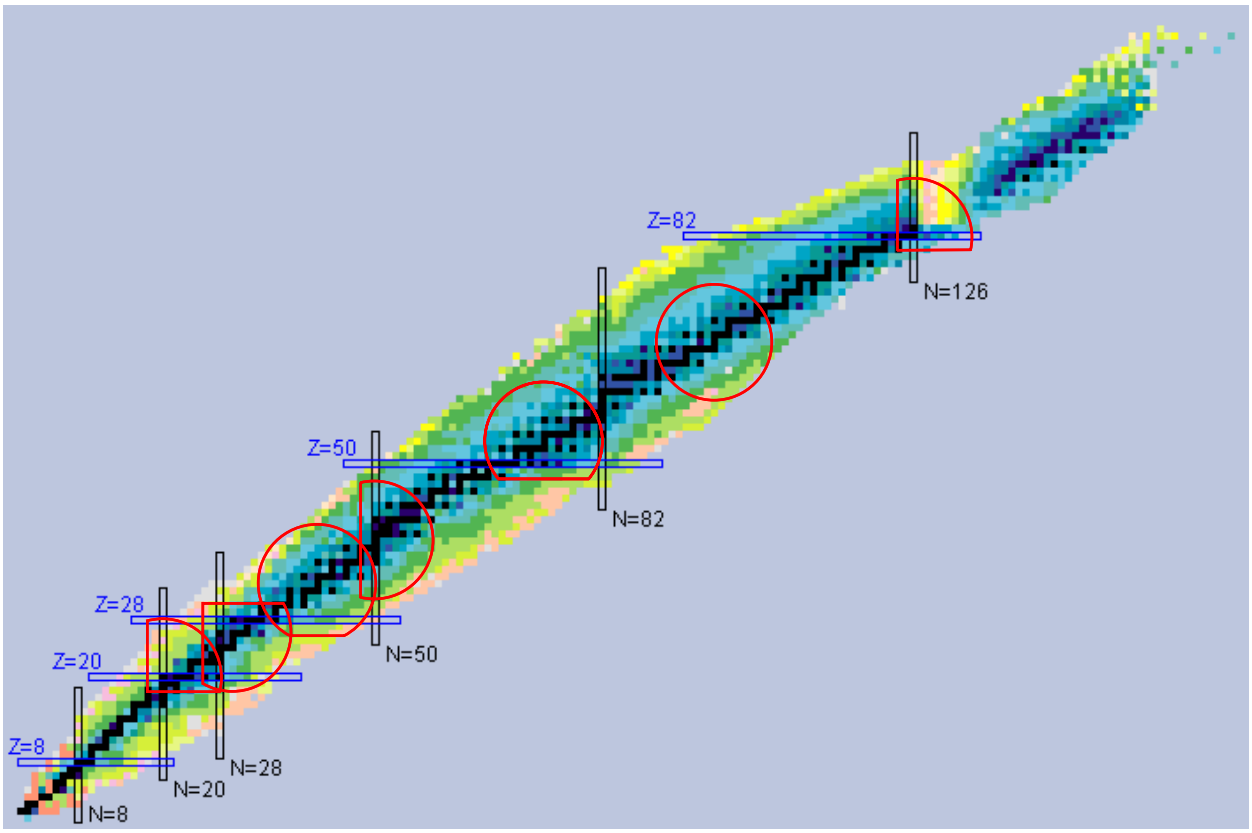

Figure 3.6 ν-SNS coverage of the nuclear *N*-*Z* plane with seven selected targets. See text for details.

If the nuclear theory that reproduces known experimental data (nuclear structure information such as masses, decay half-lives, low-lying spectra, and giant-resonance states) on unstable systems also reproduces neutrino-nucleus cross section measurements on stable nuclei, then we will have reasonably trustworthy estimates of neutrino-nucleus cross sections for unstable systems. For lighter systems (through mass 65) various shell model approaches could be employed, while for heavier systems modern mean-field theories combined with RPA could be used. It is important to note that for unstable nuclei a number of new approaches are being developed today (ranging from mean-field theories to shell models that include continuum effects) that could also be utilized to calculate cross sections. Most of these developments are targeted at understanding masses, β decay, and spectroscopy of nuclear systems. The experiments at **ν-SNS** could be used to validate our theoretical understanding of higher-energy nuclear excitations within the same models, which is important in the astrophysical environment.

Another example of the impact that **ν-SNS** will have on nuclear theory and its relationship with astrophysics arises from supernova detection. If neutrinos did not oscillate, supernova ν_e spectra would be dominantly at energies insufficient to strongly excite the forbidden spin-dipole resonances (of order 10 MeV). In that case existing (*p,n*) measurements in ^{54}Fe and ^{208}Pb, from which the GT strength distributions can be extracted, would largely determine the cross section. However, oscillations will tend to harden the ν_e spectrum since some will have left the proto-neutron star as μ/τ neutrinos with higher energies (see Figure 2.4). For 25 MeV neutrinos allowed transitions will contribute only about half of the cross section, the other half coming from forbidden transitions. Our ability to measure the hardening of supernova ν_e spectra (which would provide crucial information about the supernova structure and, possibly, about non-MSW oscillation mechanisms) is limited by our lack of knowledge of the strength of the forbidden transitions. Although (*p,n*) experiments have identified these transitions in lead, they could not completely untangle the various multipoles, making it impossible to extract the nuclear matrix elements necessary to compute neutrino cross sections. While these data may improve in the future, and are important checks on any calculation of neutrino cross sections, at these energies the most important check by far will come from the **ν-SNS** measurements themselves.

For the *r*-process, the most important nuclear physics inputs are the binding energies and lifetimes of nuclei along the *r*-process path, especially at the so-called waiting points where the flow stagnates, thus producing the major abundances. These waiting points occur in nuclei with 50, 82, and 126 neutrons. An important set of secondary inputs are neutrino-nucleus interactions on the waiting point nuclei. Unfortunately, neutrino-nucleus measurements on such unstable targets are impossible. However, measurements of neutrino interactions on stable nickel nuclei can calibrate nuclear theory in this region, even though the waiting point nuclei are over ten neutrons away from stability. In addition, charged-current information on stable Kr, Rb, and Sr, which are relatively close to the top of the *N*=50 *r*-process path waiting point, may prove very useful for both *r*-process nucleosynthesis studies and for constraining nuclear models in this somewhat heavier mass region. It is doubtful that the *N*=126 waiting point nuclei could be addressed in any predictive way even with data from SNS neutrinos on stable nuclei in the region due to their distance from nuclear stability.

3.6 Standard Model Tests

The opportunity to deploy detectors next to the world most powerful intermediate energy pulsed neutrino source will open interesting possibilities for precise tests of the Standard Model of electroweak interactions in the neutrino sector. Such tests would only require a different analysis of the same datasets collected for the neutrino-nucleus interaction measurements that form the bulk of this proposal. We are briefly list here a few opportunites that we believe can be explored with the proposed intial set of targets/detectors.

3.6.1 Lepton Flavor Number Violation in Muon Decay

Lepton flavor number violation has been clearly demonstrated in the neutrino sector in the form of neutrino flavor oscillations [91]. Many extensions to the standard model, e.g. grand unified theories [92] and left-right symmetric models [93], violate lepton flavor number and predict exotic decays of the muon, e.g. $\mu^+ \to e^+ + \bar{\nu}_e + \nu_\mu$, which may be present at branching ratios as high as 10^{-4}. (See [94] for a review.) Spallation sources like the SNS provide a special

opportunity to search for lepton flavor number violating processes due to the small flux of electron antineutrinos produced; nearly all π^- and μ^- are captured in the target. Electron antineutrinos are readily observed by the $\bar{\nu}_e + p \rightarrow e^+ + n$ reaction correlated with the subsequent neutron capture, and the observation of $\bar{\nu}_e$ events in excess of the small flux expected from μ^- decay and other sources provides a sensitive signature for lepton flavor number violation.

The LSND experiment has provided positive results for the appearance of $\bar{\nu}_e$ at LANSCE using a 167 ton detector of liquid scintillator at a distance of 30 m from the LANSCE beam stop. An excess of $\bar{\nu}_e$ events of $(2.64\pm0.67\pm0.45)\times10^{-3}$ $\bar{\nu}_e/\mu^+$ was reported and interpreted as evidence for neutrino flavor oscillations, specifically $\bar{\nu}_\mu \rightarrow \bar{\nu}_e$ [95]. The LSND results, when combined with solar and atmospheric neutrino data, are not consistent with mixing between three neutrino flavors and require extensions such as sterile neutrino flavors. However, other lepton flavor violating processes, like a weak branch for the muon decay $\mu^+ \rightarrow e^+ + \bar{\nu}_e + \nu_\mu$, could explain some or all of the LSND excess without invoking more exotic solutions like sterile neutrinos.

Thus far there have been no observations that contradict the V-A theory of weak interactions in muon decay. The most sensitive limit comes from the KARMEN experiment at ISIS which reported an upper limit (90% confidence level) of 5 $\bar{\nu}_e$ events from a combined 4 years of data, implying a branching ratio for $\bar{\nu}_e$ emission in μ^+ decay of $< (0.9 \times 10^{-3})$ $\bar{\nu}_e/\mu^+$ [96]. While the KARMEN limit is inconsistent with the full signal observed by LSND, $(2.64\pm0.67\pm0.45)\times10^{-3}$, more stringent limits on the $\bar{\nu}_e$ branching ratio are highly desired to rule out any substantial contribution to the LSND signal from exotic muon decay and to test extensions to the Standard Model.

The high proton beam power of the SNS will provide the opportunity to achieve significantly improved sensitivity for lepton flavor number violating decays of the muon. Table 3.1 shows the number of events expected per year in the homogeneous detector assuming a branching ratio of 1 for the decay $\mu^+ \rightarrow e^+ + \bar{\nu}_e + \nu_\mu$. The net event rates are also shown with fiducial cuts and with the expected efficiency for e^+ and correlated neutron detection of about 25%. While the background event rate is somewhat more difficult to quantify, we estimate that the background rate could be improved over that observed by KARMEN. The largest single background source in the KARMEN experiment, due to $^{12}C(\nu_e,e^-)^{12}N$ reactions, can be determined with high accuracy and will be eliminated during operations with water. Simulations also show that the intrinsic background from $\bar{\nu}_e$ production in the SNS target will be reduced, relative to the corresponding background for KARMEN, by at least a factor of two. The reduced time for data collection will also reduce backgrounds that are independent of the μ^+ production rate, e.g. cosmic-ray induced backgrounds. We estimate the background from a combined analysis of two years of operation with the **ν–SNS** homogeneous detector (one year with water and one year with mineral oil) to be about 40% less than that obtained in four years of operation at KARMEN. With these rates, **ν–SNS** would be sensitive to a branching ratio of 5×10^{-4} on $\bar{\nu}_e$ production in μ^+ decay after only two years of operation. There are several factors that may provide **ν–SNS** with substantially improved sensitivity to $\bar{\nu}_e$. The planned upgrade of the SNS proton beam energy to 1.3 GeV would improve the rate by about a factor of two. Operations with mineral oil or water in the homogeneous detector may continue for longer than two years, e.g. to provide an accurate calibration for measurements in the segmented detector, and would provide proportionally improved statistics. With these improvements, there is a possibility that the

sensitivity achieved by **ν–SNS** for $\bar{\nu}_e$ production in μ^+ decay would reach a sufficient level to provide an interesting test of Standard Model extensions.

Table 3.1 Expected event rates in the homogeneous detector from the $\bar{\nu}_e + p \rightarrow e^+ + n$ reaction assuming a branching ratio of 1.0 for $\bar{\nu}_e$ production in μ^+ decay.

Target material:	**Mineral oil**	**Water**
$\bar{\nu}_e$ events/year	31400	32300
with fiducial cut	12900	13200
and combined efficiency	3200	3300

3.6.2 High Precision Measurement of Neutrino Spectra from Muon Decay

The electron spectrum from the reaction $^{12}C(\nu_e,e^-)^{12}N_{gs}$ can be used to derive the original ν_e spectrum from muon decay, taking into account $E_\nu = E_e + Q$ (17.8 MeV), the detector response function, and the $(E_{\nu e} - Q)^2$ dependence of the differential cross section. It is well known that a measurement of Michel parameters in muon decay is a direct test of the Standard Model and is a method to search for manifestations of new physics since these parameters are sensitive to the Lorentz structure of the Hamiltonian of weak interactions. The Michel parameters are related to electron spectrum shape in muon decay. The neutrino spectrum from this decay can be described in terms of similar parameters. In this manner the neutrino spectrum can provide complimentary information to the set of Michel parameters, increasing the accuracy and reliability in the search for new physics in the lepton sector.

As pointed out in [89], the shape of the ν_e spectrum from μ^+ decay at rest is sensitive to scalar and tensor admixtures to pure V-A interactions due to the parameter ω_L which is analogous to the Michel parameter ρ, which determines the shape of the electron spectrum in muon decay. The ν_e spectrum can be written as:

$$dN_{\nu_e} / dx = \frac{G_F^2 m_\mu^5}{16\pi^3} Q_L^\nu (G_{0(x)} + G_1(x) + \omega_L G_2(x))$$

where m_μ is the muon mass, $x = 2E_\nu / m_\mu$ is the reduced neutrino energy, Q^ν_L is the probability for emission of a left-handed electron neutrino, G_0 describes pure V-A interactions, G_1 takes into account radiative corrections, and $\omega_L G_2$ includes effects of scalar and tensor components. G_1 is very small and can be neglected.

In the Standard Model, ω_L is exactly zero. The KARMEN experiment [90] determined an upper limit for ω_L: $\omega_L \leq 0.113$ (90% CL). Figure 3.7 shows the calculated **ν-SNS** electron spectra for the reaction $^{12}C(\nu_e,e^-)^{12}N_{gs}$ for $\omega_L = 0$ ($\omega_L = 0.113$) with a black (blue) line. The largest difference between the two distributions is at the high energy end of the spectra where the detector resolution is very good and the absolute energy scale will be very accurately calibrated using Michel electrons from stopped cosmic muons. The expected statistical accuracy for a one year measurement with the **ν-SNS** homogeneous detector is shown by the red points. We should be able to significantly improve the KARMEN limit on scalar and tensor admixtures to V-A interactions in the lepton sector.

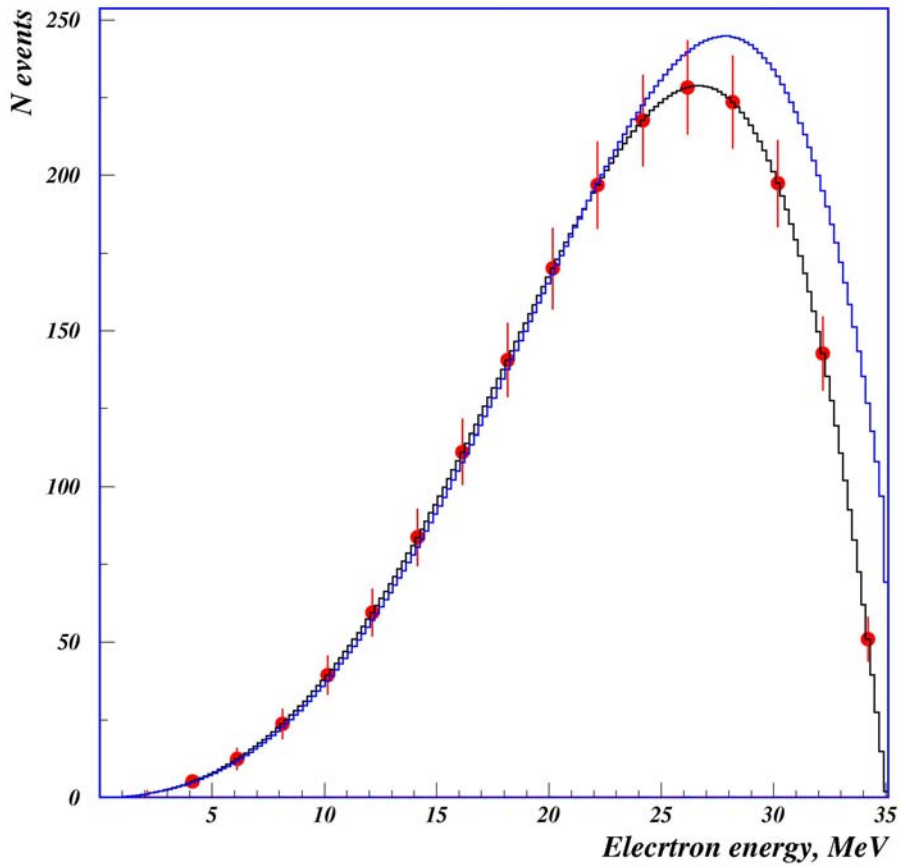

Figure 3.7 Electron spectrum from the reaction $^{12}C(\nu_e,e^-)^{12}N_{gs}$ caused by neutrinos from muon decay at rest calculated in the framework of the Standard Model is shown with the black line. The blue line shows the upper limit, measured in the KARMEN experiment [90], on the distortion of the spectra caused by scalar and tensor admixtures to pure V-A interactions. Red points represent the statistical accuracy of a one-year measurement at **ν-SNS** with liquid scintillator in the homogeneous detector.

3.7 Conclusion

Charged- and neutral-current neutrino-nucleus interactions in the stellar core play a central role in supernova dynamics and nucleosynthesis and are important for supernova neutrino detection. The Spallation Neutron Source is a pulsed source of neutrinos with unprecedented intensity and a fortuitous overlap with supernova neutrino spectra. This presents us with a unique opportunity to build an experimental foundation for the many neutrino-nucleus weak interaction rates needed in supernova models and with which to calibrate supernova neutrino detectors. Measurements of these reactions on strategically chosen targets will provide an invaluable test of the complex theoretical models used to compute neutrino-nucleus cross sections. This would enable more realistic supernova models and allow us to cull fundamental physics from these models with greater confidence when their predictions are compared with detailed observations. In addition, the proposed facility could open new windows into exciting studies of Standard Model extensions.

References for Section 3:

1. "Connecting Quarks with the Cosmos, Eleven Questions for the New Century", Committee on the Physics of the Universe, Michael S. Turner, Chair; Board on Physics and Astronomy, Division on Engineering and Physical Sciences, National Research Council of The National Academies, The National Academies Press, 2003, Washington, D.C.
2. A. Burrows and J.M. Lattimer, *ApJ* **299**, L19, 1985.
3. J.R. Wilson, Numerical Astrophysics (Boston) (ed. J.M. Centrella, J.M. LeBlanc and R.L. Bowers) Jones and Bartlett, 422, 1985.
4. H.A. Bethe and J.R. Wilson, *ApJ* **295**, 14, 1985.
5. H.-T. Janka and E. Müller, *A&A* **306**, 167, 1996.
6. A. Burrows and J. Goshy, *ApJ* **416**, L75, 1993.
7. W.D. Arnett, *ApJ* **218**, 815, 1977.
8. S.W. Bruenn, *ApJS* **58**, 771, 1985.
9. E.S. Myra *et al.*, *ApJ* **318**, 744, 1987.
10. J.R. Wilson and R.W. Mayle, *Phys. Rep.* **227**, 97, 1993.
11. H.-T. Janka, *A&A* **256**, 452, 1992.
12. O.E.B. Messer *et al.*, *ApJ* **507**, 353, 1998.
13. M. Rampp and H.-T. Janka, *ApJ* **539**, L33, 2000.
14. A. Mezzacappa *et al.*, *Phys. Rev. Lett.* **86**, 1935, 2001.
15. M. Liebendörfer *et al.*, *Phys. Rev. D* **63,** 103004, 2001.
16. T.A. Thompson, A. Burrows and P.A. Pinto, *ApJ* **592**, 434, 2003.
17. M. Herant *et al.*, *ApJ* **435**, 339, 1994.
18. A. Burrows, J. Hayes, and B.A. Fryxell, *ApJ* **450**, 830, 1995.
19. C.L. Fryer and M.S. Warren, *ApJ* **574**, L65, 2002.
20. A. Mezzacappa *et al.*, *ApJ* **493**, 848, 1998.
21. W. Keil, H.-T. Janka and E. Müller, *ApJ* **473**, L111, 1996.
22. R. Buras, *et al.*, *Phys. Rev. Lett.* **90,** 241101, 2003.
23. S.W. Bruenn and T. Dineva, *ApJ* **458**, L71, 1996.
24. S.W. Bruenn, E. Raley and A. Mezzacappa, *ApJ* submitted (2005).
25. A. Mezzacappa *et al.*, *ApJ* **495**, 911, 1998.
26. H.A. Bethe *et al.*, *Nucl. Phys. A* **324**, 487, 1979.
27. K. Langanke and G. Martínez-Pinedo, *Nucl. Phys. A* **673**, 481, 2000.
28. T. Oda *et al.*, *Atomic Data and Nuclear Data Tables* **56**, 231, 1994.

29. A. Heger *et al.*, *Phys. Rev. Lett.* **86**, 1678, 2001.
30. S.E. Woosley and T.A. Weaver, *ApJS* **101**, 181, 1995.
31. G.M. Fuller, W.A. Fowler and M.J. Newman, *ApJ* **293**, 1, 1985.
32. T.J. Mazurek, Ph.D. thesis Yeshiva University, 1973.
33. C.J. Hansen, Ph.D. thesis Yale University, 1966.
34. A.Yahil, *ApJ* **265**, 1047, 1983.
35. M. Liebendörfer *et al.*, Proceedings of the 20th Texas Symposium on Relativistic Astrophysics (Melville) (ed. Wheeler J. and Martel H.) AIP, 472, 2001.
36. G.M. Fuller, *ApJ* **252**, 741, 1982.
37. J. Cooperstein and J. Wambach, *Nucl. Phys. A* **420,** 591, 1984.
38. K. Langanke, E. Kolbe and D.J. Dean, *Phys. Rev. C* **63,** 32801, 2001.
39. K. Langanke *et al.*, *Phys. Rev. Lett.* **90,** 241102, 2003.
40. W.R. Hix *et al.*, *Phys. Rev. Lett.* **91**, 201102, 2003.
41. W.R. Hix and F.-K. Thielemann, *ApJ* **460**, 869, 1996.
42. E. Bravo and D. García-Senz, *MNRAS* **307**, 984, 1999.
43. M.F. El Eid and W. Hillebrandt, *A&AS* **42**, 215, 1980.
44. F. Brachwitz *et al.*, *ApJ* **536**, 934, 2000.
45. O. Messer *et al.*, *ApJ* (2005).
46. R. Maschuw, *Prog. Part. Phys.* **40**, 183, 1998.
47. S.W. Bruenn and W.C. Haxton, *ApJ* **376**, 678, 1991.
48. R.D. Hoffman *et al.*, *ApJ* **460**, 478, 1996.
49. V. Trimble, *A&AR* **3**, 1, 1991.
50. K. Kifonidis *et al.*, *ApJ* **531**, L123, 2000.
51. F.-K. Thielemann, K. Nomoto and M. Hashimoto, *ApJ* **460**, 408, 1996.
52. G.C. McLaughlin, G.M. Fuller and J.R. Wilson, *ApJ* **472**, 440, 1996.
53. C. Fröhlich *et al.*, *ApJ* submitted (2005).
54. J. Pruet *et al.*, *ApJ* (2005).
55. N.T. Zinner and K. Langanke, private communication.
56. S.E. Woosley *et al.*, *ApJ* **356,** 272, 1990.
57. A. Heger *et al.*, *Phys. Lett. B* **606**, 258, 2005.
58. B.D. Fields *et al.*, *ApJ* **540**, 930, 2000.
59. D. Hartmann *et al.*, ASP Conf. Ser. 171: LiBeB Cosmic Rays, and Related X- and Gamma-Rays, 235, 1999.

60. W.C. Haxton, Neutrinos In Physics And Astrophysics From 10^{-33} to 10^{28} cm (TASI 98) (Singapore) (ed. Langacker P.) World Scientific, 432, 1999.
61. K.-L Kratz *et al.*, *ApJ* **403**, 216, 1993.
62. S.E. Woosley *et al.*, *ApJ* **433,** 229, 1994.
63. J.C. Wheeler, J.J. Cowan and W. Hillebrandt, *ApJ* **493**, L101, 1998.
64. C. Freiburghaus, S. Rosswog and F.-K. Thielemann, *ApJ* **525**, L121, 1999.
65. B.S. Meyer, *ARA&A* **32**, 153, 1994.
66. Y.-Z. Qian *et al.*, *Phys. Rev. C* **55**, 1532, 1997.
67. W.C. Haxton *et al.*, *Phys. Rev. Lett.* **78**, 2694, 1997.
68. Y.-Z. Qian, *ApJ* **569**, L103, 2002.
69. E. Kolbe, K. Langanke and G.M. Fuller, *Phys. Rev. Lett.* **92**, 111101, 2004.
70. C. Sneden *et al.*, *ApJ* **591**, 936, 2003.
71. B.S. Meyer, G.C. McLaughlin and G.M. Fuller, *Phys. Rev. C* **58**, 3696, 1998.
72. B.S. Meyer, *Nucl. Phys. A* **719**, 13, 2003.
73. J.F. Beacom and P. Vogel, *Phys. Rev. D* **58**, 053010, 1998.
74. J.F. Beacom and P. Vogel, *Phys. Rev. D* **58**, 093012, 1998.
75. J.F. Beacom and M.R. Vagins, *Phys. Rev. Lett.* **93**, 171101, 2004.
76. A. Odrzywolek, M. Misiaszek and M. Kutschera, *Astroparticle Phys.* **21**, 303, 2004.
77. W.C. Haxton, *Phys. Rev. D* **36**, 2283, 1987.
78. E. Kolbe *et al.*, *J. Phys. G* **29** 2569, 2003.
79. K. Langanke, P. Vogel and E. Kolbe, *Phys. Rev. Lett.* **76**, 2629, 1996.
80. T.A. Thompson, A. Burrows and J.E. Horvath, *Phys. Rev. C* **62**, 035802, 2000.
81. G.G. Raffelt, *ApJ* **561**, 890, 2001.
82. S.W. Bruenn, *ApJ* in preparation.
83. R.N. Boyd *et al.* (OMNIS Collaboration), *Nucl. Phys. A* **688**, 386, 2001.
84. F.T. Avignone and Y.V. Efremenko, *J. Phys. G* **29**, 2615, 2003.
85. V. Gudkov and K. Kubodera, *J. Phys. G* **29**, 2597, 2003.
86. B.P. Schmidt, R.P. Kirshner, and R.G. Eastman, ApJ, 395, 366, 1992.
87. E. Baron, P.E. Nugent, D. Branch, and P.H. Hauschildt, *ApJ*, 616, L91, 2004.
88. M. Sharp, *et al. Phys Rev* **D** 66, 013012, 2002.
89. W. Fetshcher, *Phys. Rev. Lett.* **69**, 2758, 1992.
90. B. Armbruster *at al., Phys. Rev. Lett.* **81**, 520, 1998.
91. Y. Ashie *et al.*, *Phys. Rev. D* **71**, 112005, 2005.

92. H. Fujii *et al*., *Phys. Rev. D* **49**, 559, 1994.
93. P. Herczeg and R.N. Mohapatra, *Phys. Rev. Lett.* **69**, 2475, 1992.
94. P. Herczeg, *Los Alamos Science* **25**, 28, 1997.
95. A. Aguilar *et al*., *Phys. Rev. D* **64**, 112007, 2001.
96. B. Armbruster *et al.*, *Phys. Rev. Lett.* **90**, 181804, 2003.

4 PROJECT DESCRIPTION

The Spallation Neutron Source (SNS) at Oak Ridge National Laboratory will provide the world's most intense flux of neutrinos in the energy regime of interest for nuclear astrophysics. We propose to build two instruments that will be installed inside a single shielded enclosure in the target hall of the SNS for a program of precision measurements of neutrino-nucleus cross sections that are important for supernova science.

In this section, we first describe background sources (some inherent to the spallation process and some of cosmic origin) and their impact on the design of the **ν-SNS** facility. Then we present technical and cost details of the major components of the **ν-SNS** facility (shielded bunker, veto, detectors and common data acquisition system). Finally we discuss the measurement precision that we expect to obtain.

4.1 Backgrounds

For neutrino measurements, understanding and reducing backgrounds is of vital importance. The facility-related backgrounds of most concern to neutrino measurements are high-energy neutrons that can penetrate significant amounts of shielding and which can, occasionally, mimic a neutrino interaction in the detectors. To estimate neutron fluxes at the neutrino bunker location we evaluated the target building topology and identified three sources of high-energy neutrons (see Figure 4.1):

- Neutrons originating from the spallation target (blue arrow).
- Neutrons originating from the proton beam tunnel, either resulting from proton beam losses in the RTBT (Ring to Target Beam Transport) or from the interaction of albedo hadrons from the spallation target (red arrow).
- Neutrons originating from beamlines 17 and 18 (green arrow).

Cosmic ray muons (both the soft component - which can stop in the detector and decay, and the hard component - which can miss the veto, interact in the shielding and produce a high-energy neutron), and cosmic-ray neutrons can also mimic a neutrino signal in the detectors.

Potential backgrounds from each of these sources are considered in the following subsections.

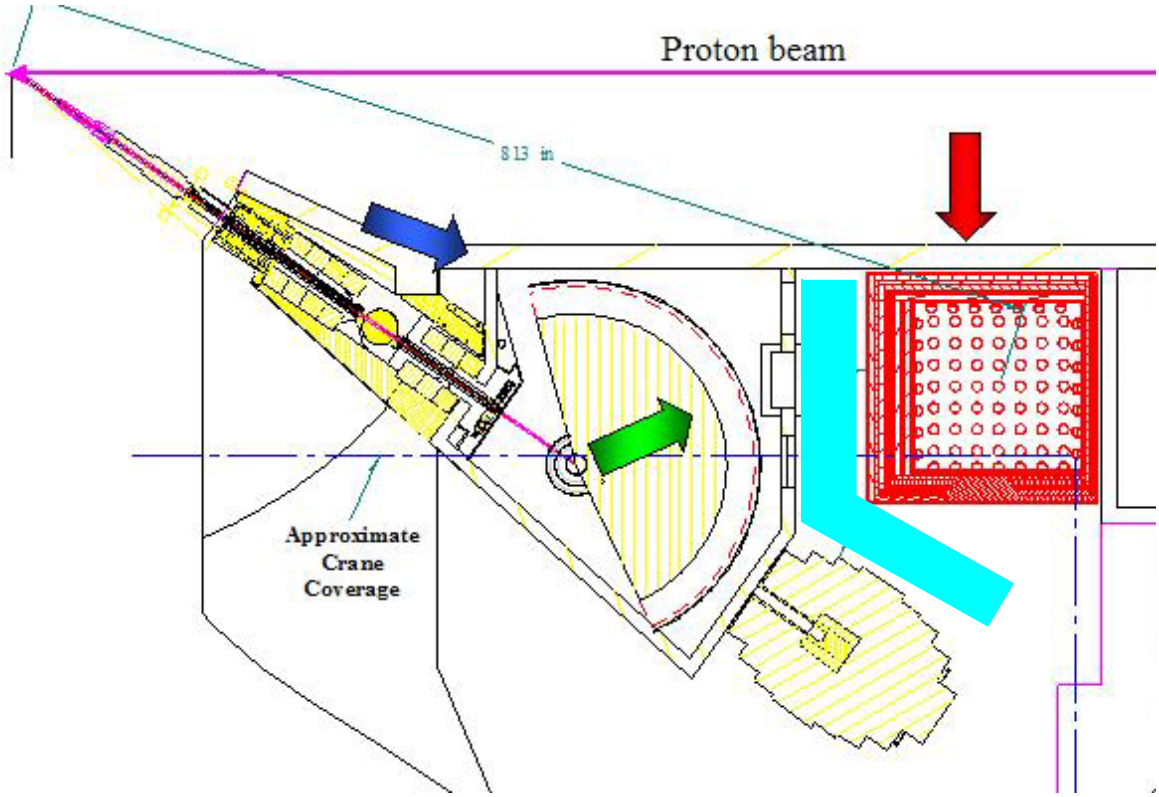

Figure 4.1 Major sources of neutron background at the SNS, see text for details. **ν-SNS** is the red square. The keep-clear area between **ν-SNS** and beamline 18 is the blue shaded region.

4.1.1 Neutrons Escaping from the Spallation Target

The SNS neutronics group performed coupled Monte Carlo/discrete ordinates calculations to investigate the neutron leakage through the target monolith in the direction of the neutrino bunker. In the first step, neutron production and transport were simulated with the Monte Carlo code MCNPX [1] applying the full 3D target station model depicted in Figure 4.2. Neutron trajectories intersecting the outer edge of the so-called outer plug (a cylindrical surface with 1 m radius and 2 m height centered at the intersection of the target monolith axis and the target mid-plane) were stored in a data file.

A boundary source was generated from these trajectories using the coupling tool MTD [2] scoring only those trajectories in two wedges; one to study backscattered neutrons (extending from 140 to 220 degrees relative to the proton beam direction) and one to study forward scattered neutrons (extending from -40 to +40 degrees). The boundary source was then picked up by the two-dimensional cylinder-symmetrical discrete ordinates code DORT [3] that generates neutron/gamma flux distributions throughout its model extensions.

For the DORT analyses, a modified version of the SNS target monolith shielding model [4] was applied. The model describes the SNS target monolith axially from 4.5 m below to 8 m above the target center, and radially to the outer edge of the steel monolith at a radius of ~5 m. In this model the target is located at the origin of the cylindrical coordinate system. Various void areas in the upper part of the monolith are also included in the model. The bulk beamline shielding, a high-density concrete structure, extends outward from the target monolith to a radius of 10 m and to a height of 2 m above the target center. The instrument pit, with the floor level of 4.5 meters below the target center, was modeled to extend to a radius of 30 m.

The HILO2k cross section library [5] was used to describe the interactions of the radiation with material, and the P5 Legendre polynomials together with the S12 symmetric quadrature set was used for the angular representation.

The time averaged neutron flux results are summarized in six broad energy groups. An example of one energy group (from 10 to 100 MeV) is shown in Figure 4.3. The approximate position of the neutrino bunker is shown by a red rectangle. Significant ray effects are visible in the air zones of the instrument hall, which are inherent to the discrete ordinates method. Although these rays falsely indicate local elevated flux values, the flux averages over large axial areas at a fixed radius give reasonable results because of the particle conservation algorithms built into the code. At the **ν-SNS** bunker location the neutron flux levels due to neutrons escaping the target monolith are very low, $\sim 10^{-4}$ n/cm^2/s.

Figure 4.4 shows the neutron flux spectra originating from the spallation target at the approximate radius of the neutrino bunker in the forward and backward direction relative to the proton beamline. It quantitatively demonstrates the benefit of the backward-angle location of the **ν-SNS** bunker. This results in background estimates that are orders of magnitude below calculations presented in the original study report "Neutrino Program at the Spallation Neutron Source - **ν-SNS**" [6] which conservatively assumed isotropic production of high-energy neutrons from the target.

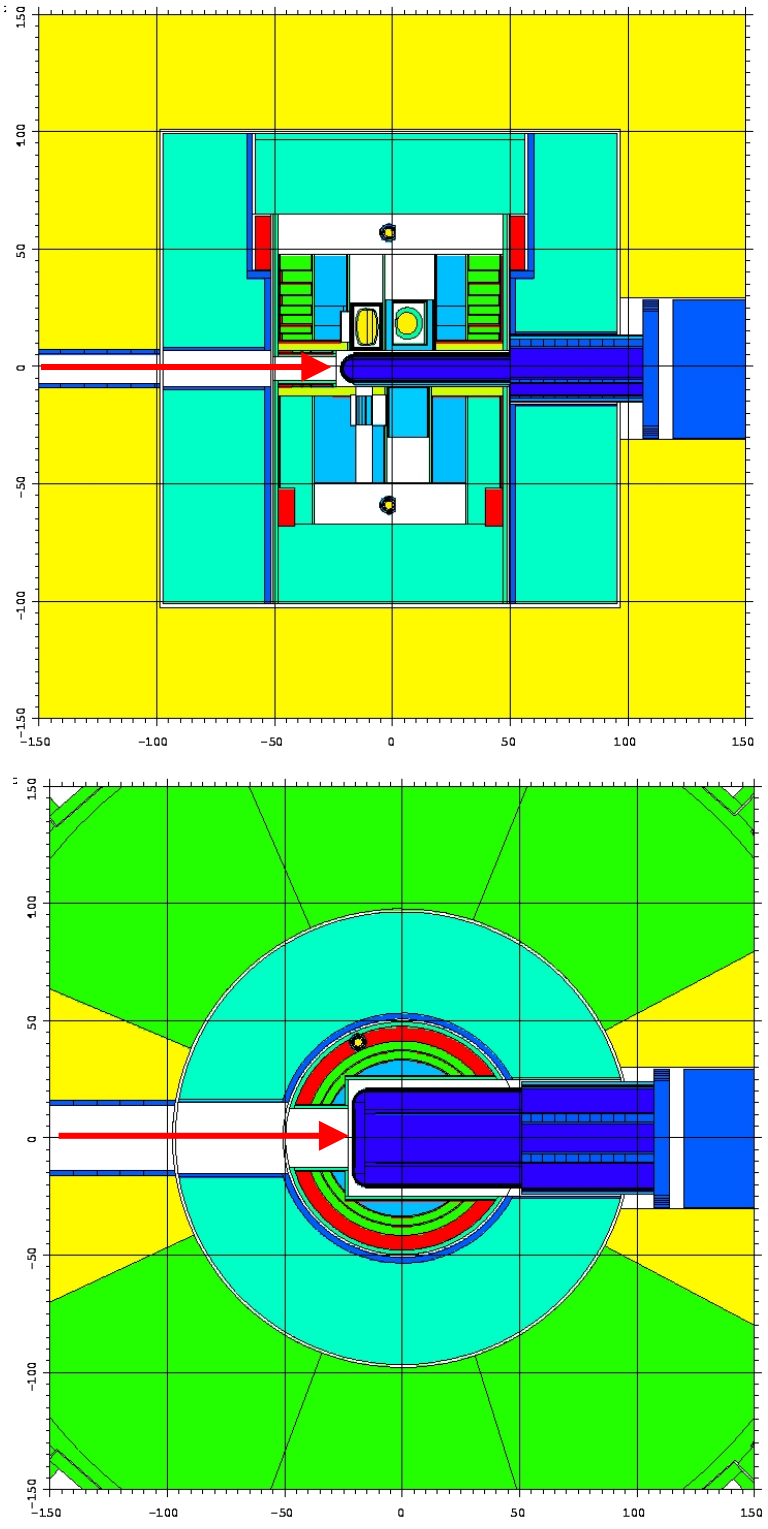

Figure 4.2 Vertical (top) and horizontal (bottom) cuts through the MCNPX target station model at the proton beam centerline. In both panels the proton beam enters from the left (red arrow) and the outer plug is the turquoise volume with 1 m radius.

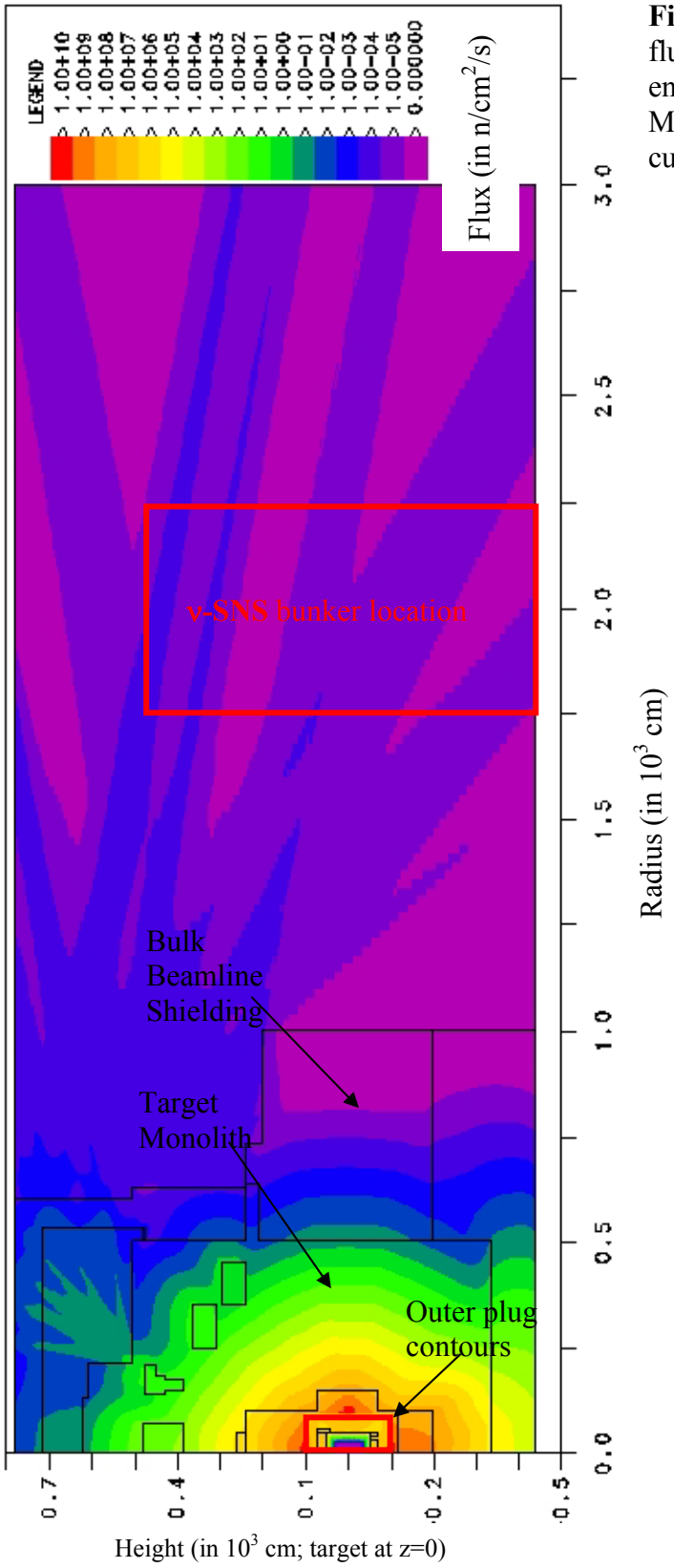

Figure 4.3 Backscattered neutron flux from the spallation target for an energy slice between 10 and 100 MeV. The figure shows a horizontal cut through the SNS target hall.

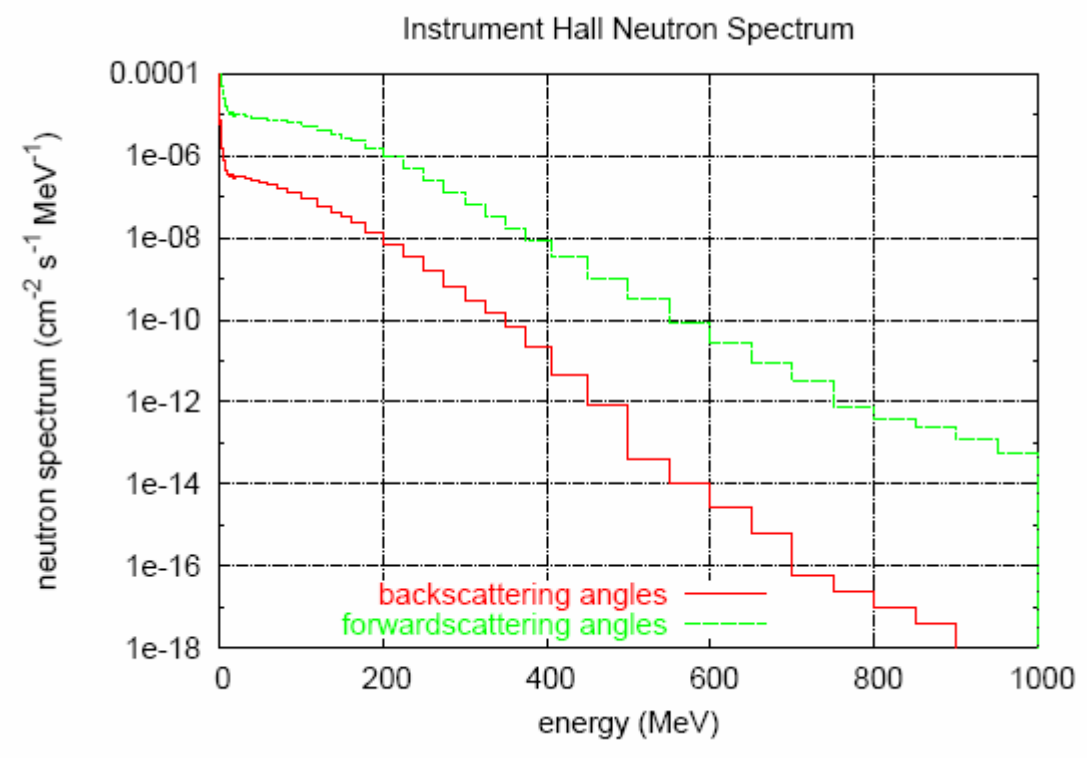

Figure 4.4 Forward and backscattered neutron flux spectra at the approximate **ν-SNS** bunker distance from the spallation target.

4.1.2 NEUTRONS ENTERING FROM THE RTBT

The SNS neutronics group also performed calculations for the two sources for neutrons entering the **ν-SNS** bunker from the RTBT:

- Loss of the primary proton beam in various beamline elements.
- Hadrons backscattering from the target followed by interactions in the tunnel walls.

Figures 4.5 and 4.6 show the calculation geometry for the dose rates outside the RTBT. Horizontally from the beamline, in the direction of the **ν-SNS** bunker location, the RTBT shielding model consists of 0.12 m of high-density concrete, followed by 2.6 m of Duratek (junk steel), followed by 0.5 m of regular concrete. In the simulation the shielding was split into thin (10 cm) layers. In order to register neutrons, a set of virtual detectors 10 cm thick was created 10 cm outside of the RTBT shielding. The inside set of detectors is 36 cm high, centered on the proton beamline. The outside set of detectors is above and below the first set, extending to ± 95.5 cm relative to the proton beamline. Both sets of detectors are 15 m long.

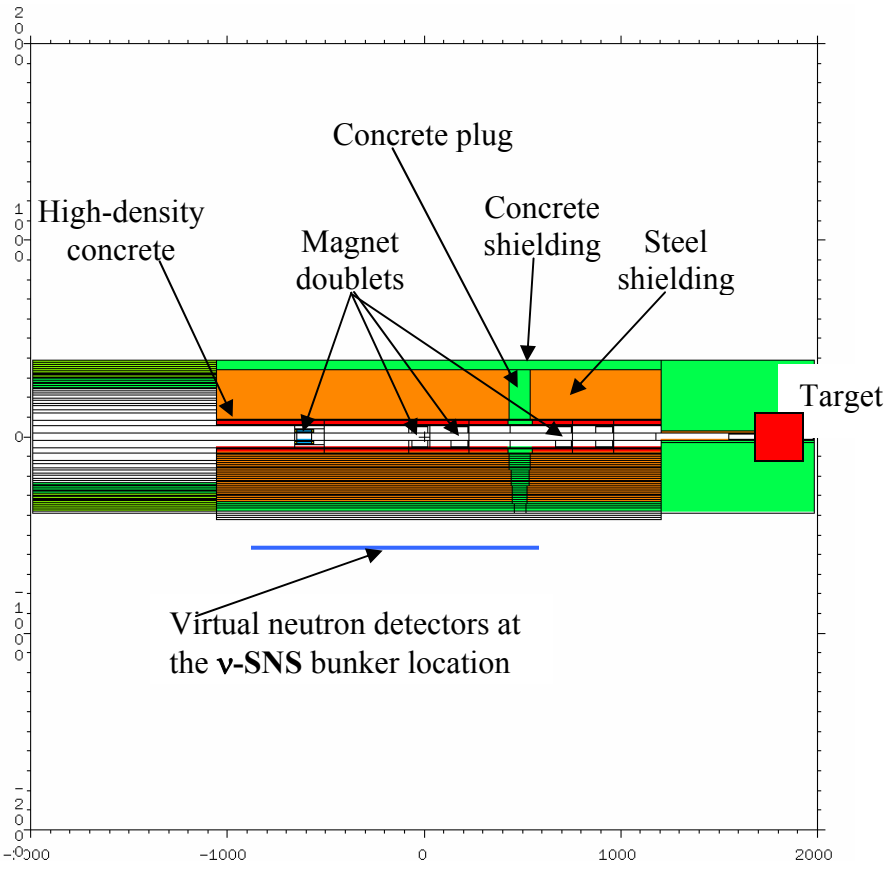

Figure 4.5 Horizontal section of the RTBT through the proton beam centerline.

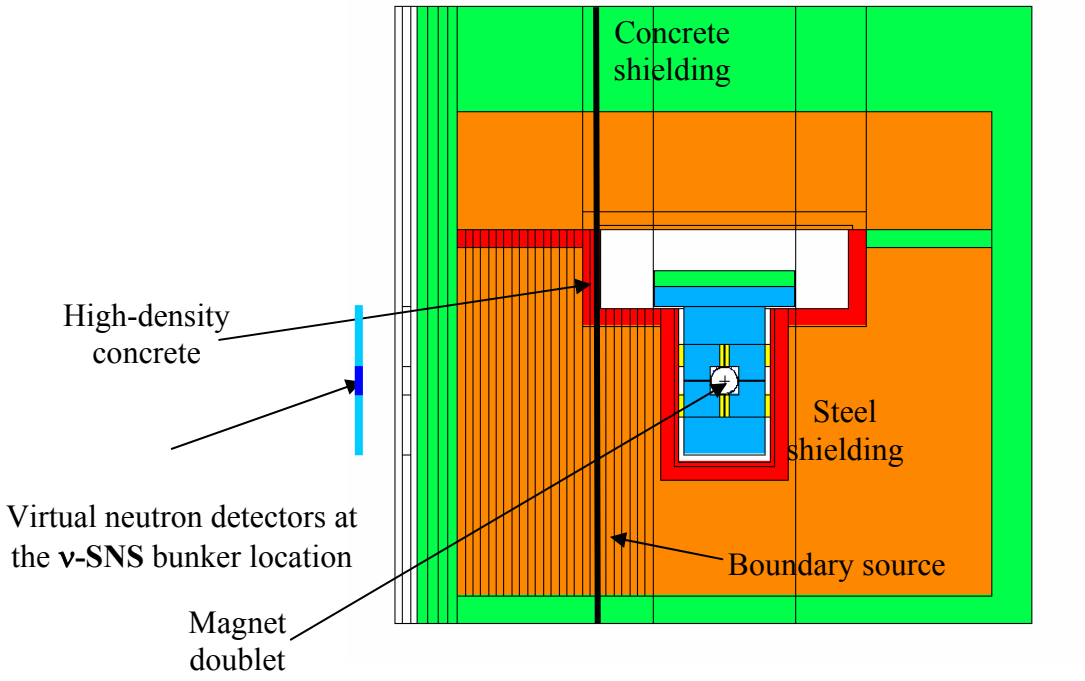

Figure 4.6 Vertical section of the RTBT perpendicular to the beamline.

The Monte Carlo code MCNPX [1] was used to perform transport analyses for both RTBT sources (proton beam losses and hadrons backscattered from the spallation target). The calculation for the proton beam loss source assumed the SNS design basis of 1W/m proton beam loss (6.2×10^9 protons/m) with a proton energy of 1 GeV. The calculation for backscattered hadrons used the same boundary source created in the previous subsection located 0.55 m upstream from the target. Simple geometry splitting to force neutron transport was applied for both analyses as well.

Fluxes due to neutrons backscattering are calculated to be slightly higher at 90 cm from the beam centerline, but they attenuate faster in the shielding because their spectrum is softer. Consequently, at the **ν-SNS** bunker location the dominant RTBT source is proton beam loss, as shown in Figure 4.7.

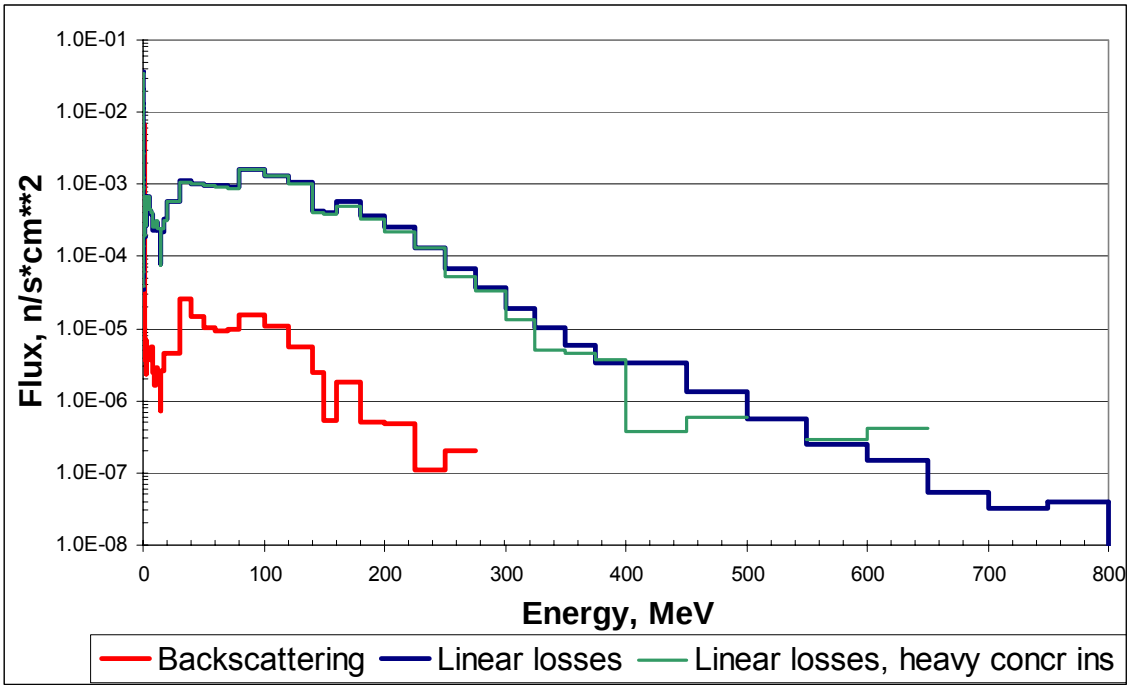

Figure 4.7 Neutron spectrum outside the RTBT in the outside set of virtual detectors. The red curve shows the flux of neutrons through the RTBT shield wall due to backscattering off the spallation target. The green (blue) curve shows the neutron flux due to primary proton beam scattering off RTBT elements with (without) inclusion of a heavy concrete plug at $z = -15$ m.

The map of neutron fluxes due to proton beam loss is shown in Figure 4.8, where the approximate location of the neutrino bunker is shown by a red line. The neutron field attenuates significantly in the tunnel shielding and becomes less than 10^{-2} n/cm^2/s at the neutrino bunker location. The elevated flux of neutrons escaping the tunnel shielding due to the concrete plug (at $z = -15$ m) misses the **ν-SNS** bunker location.

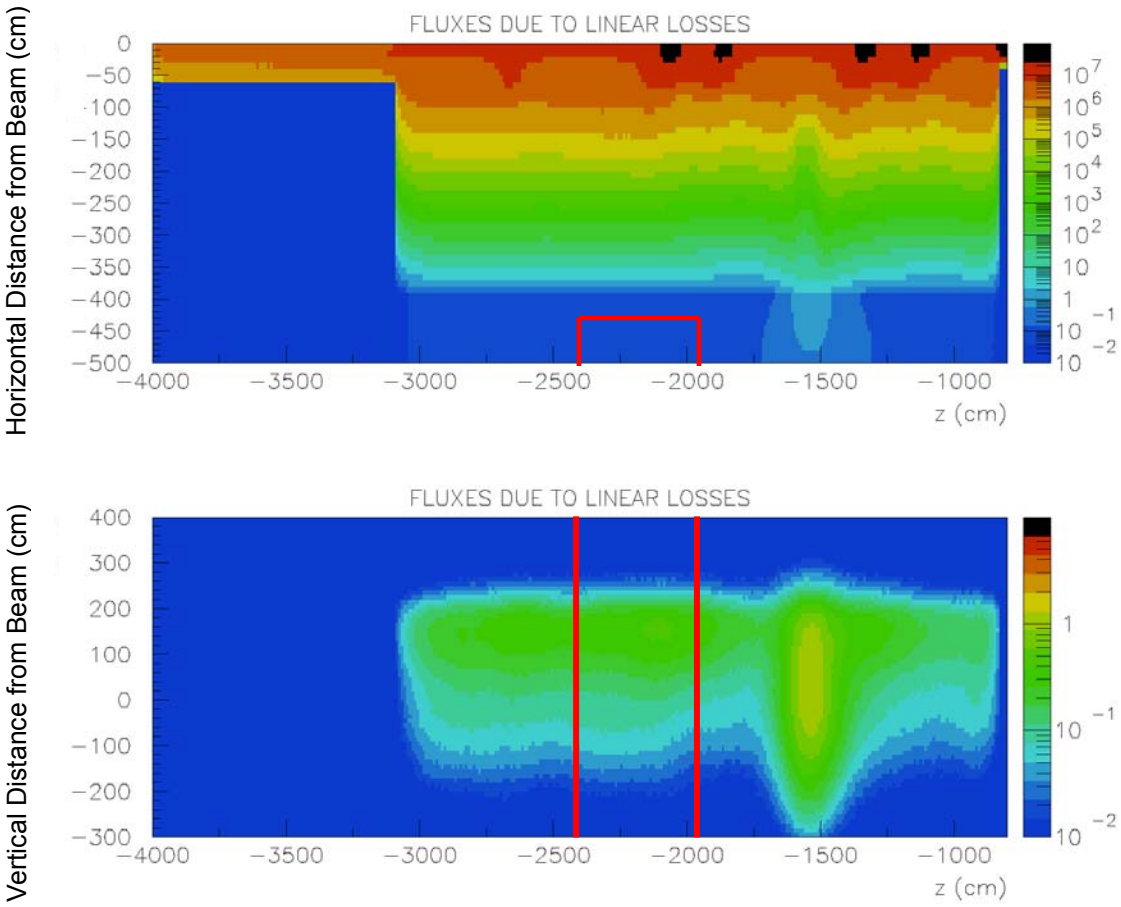

Figure 4.8 Flux maps (n/s/cm^2), due to proton beam loss, through the RTBT shielding. The upper panel shows a horizontal cut through the proton beamline. The bottom panel shows a vertical cut 4.0 meters from beamline (note the change in the color scale). The approximate location of the **ν-SNS** bunker is shown with red lines.

4.1.3 Neutrons from Beamlines 17 and 18

Detailed calculations for neutrons originating from the neutron scattering beamlines, in particular beamlines 17 and 18 (BL17/18), those closest to the **ν-SNS** bunker location, have not been completed. At present it is not practical to conduct detailed simulations because the shielding for those beamlines is still under optimization, and significant changes are foreseen.

In the original "Neutrino at SNS Study Document" [6], we made initial estimates for all three background sources. The more detailed studies presented in this proposal for the first two sources show that our initial estimates for those sources were overestimated by a factor of 50-1000. This is primarily a result of our initial assumption (common to estimates from all three sources) that the high-energy neutron flux from the spallation target was isotropic. The neighboring neutron-scattering beamlines are also at backward angles relative to the proton beamline and are therefore illuminated by a similarly reduced high-energy neutron flux. As a result, it is safe to assume that we can lower our initial estimate of the backgrounds from this third source by at least a factor of fifty.

4.1.4 SNS Backgrounds Summary

The resulting neutron fluxes (with SNS at full power; in n/cm^2/s/MeV) from all three SNS sources are shown in Figure 4.9. The target (blue) and RTBT (red) sources have been realistically modeled by the SNS neutronics group, using state-of-the-art, well-documented, well-tested codes. Neutron instrument sources (green; BL17/18) have been scaled from previous overly-conservative estimates as described above. Precise calculations for this last source require further definition of the BL17/18 shielding packages. The consequences of these background rates are detector-specific and are addressed in the subsections on different detectors below. As will be seen, SNS-related backgrounds which can fake a neutrino signal are reduced to negligible levels within ~1 μs of the proton beam hitting the spallation target. With a time cut so that the detectors are only active after this point charged-current measurements can be made essentially background-free.

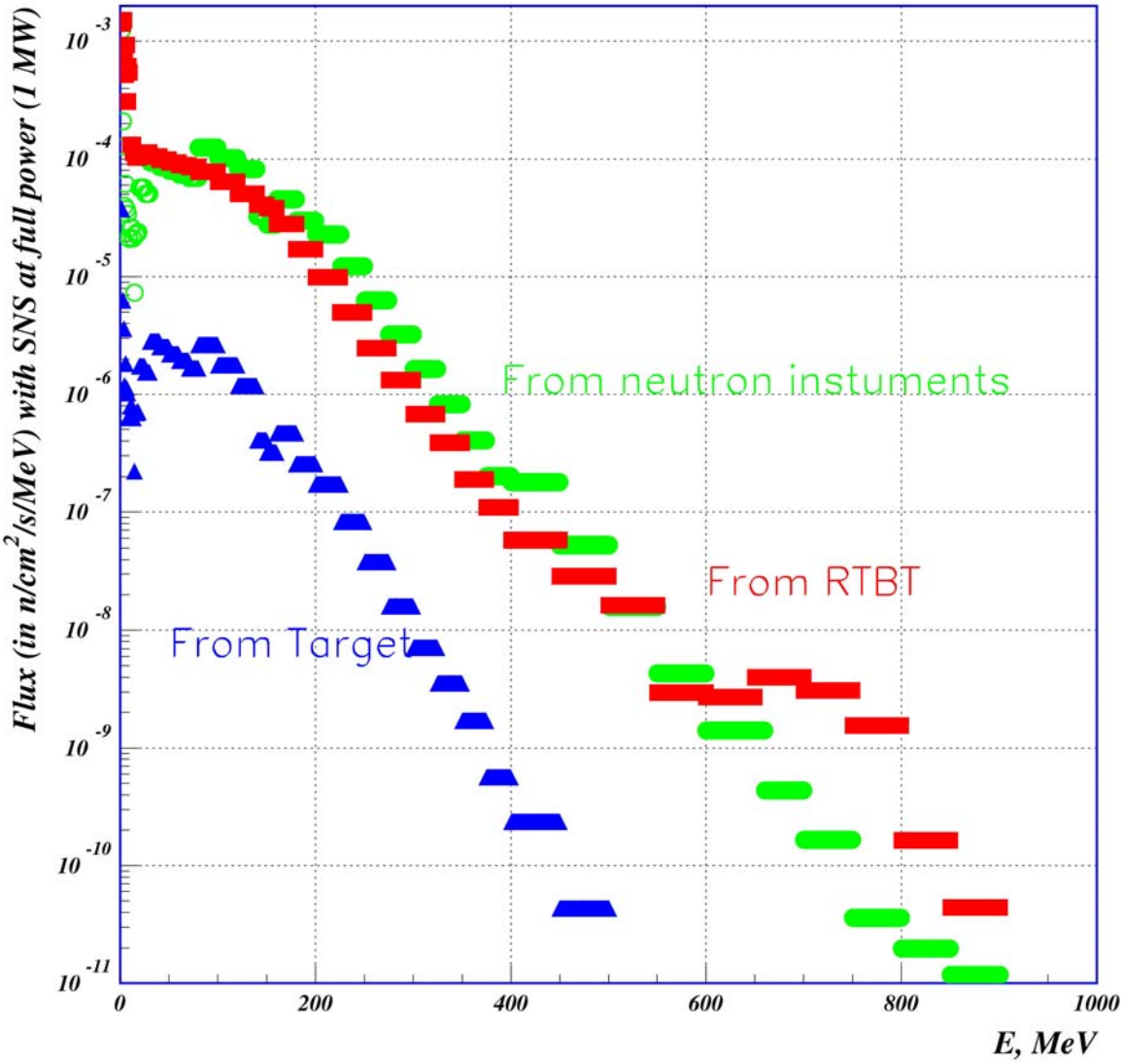

Fgure 4.9 Flux (n/s/cm^2/MeV) from SNS sources of high-energy neutrons.

4.1.5 Cosmic Ray Backgrounds

The cosmic ray background flux is well-known. At sea-level the flux of penetrating particles (primarily muons) through a horizontal area from above is 130 Hz/m^2 [7]. The muon flux has a mean energy of 2 GeV (range = 130 cm in iron) and a spectrum falling as E^{-2}. The flux is peaked in the vertical direction with an angular distribution of $\cos^2(\theta)$. In addition there is a hadron component (pessimistically assumed to be exclusively neutrons) of ~2.6 Hz/m^2 [7-9].

4.1.6 Background Reduction Strategy

At full power a target with ten ton fiducial mass will have tens of neutrino-nucleus interactions per day. This must be compared with the cosmic-ray muon (neutron) flux through the target volume of $\sim 2.5\times10^8$ (5.0×10^6) events per day and machine-related backgrounds which contribute an additional $\sim 3\times10^9$ events per day. These background sources must be suppressed through a combination of the SNS time structure, shielding (see Section 4.2), an active veto system (see Section 4.3), and particle identification (see Sections 4.4 and 4.5).

Cosmic-Ray Muons

The SNS time structure (~700 ns proton pulses at 60 Hz) allows us to eliminate a large amount of this type of background by turning off the detector except for the small fraction of time during which neutrinos can come from the target. Target neutrinos, which result from the $\pi\rightarrow\mu\rightarrow\nu$ decay chain, will all arrive within ~10 μs due to the muon decay lifetime (τ_μ = 2.2 μs). This results in an active time of only 6×10^{-4} seconds for every second of machine operation, thus reducing the effective cosmic-ray muon flux through the detector volume to 1.5×10^5/day. Two more orders of magnitude reduction are provided by the active veto (99% efficiency), leaving ~1500/day untagged cosmic ray muon events. The level of cosmic-ray muon background is essentially independent of how thick the bunker is because any realistic bunker will only range out a small fraction of the total flux.

Most of the untagged muons can be rejected based upon the characteristic track in the neutrino detectors. However, occasionally a high energy untagged muon will interact in the shielding, producing a high-energy neutron (to first order we are only concerned with those produced in the last interaction length of the shielding). The observed $\mu \rightarrow n + X$ yield is 4×10^{-5} n/μ/(g/cm^2), giving ~30 neutrons/day generated in the shielding enclosure by untagged muons. Most of these events are eliminated with particle identification measures in the detectors themselves (Cherenkov light in the homogeneous detector; track linearity and density of energy deposition in the segmented detector).

Cosmic-Ray Neutrons

Cosmic-ray neutrons are similarly reduced by the SNS time structure to ~3000/day. The active veto does not help with this background source, but shielding does. In order to reduce this source by ~two orders of magnitude (making it approximately equal to the irreducible neutron background from untagged cosmic-ray muons) a meter of steel shielding is required for the enclosure roof. The cosmic ray flux is lower through the enclosure sides, and only ~half-meter walls are required. As with other background sources, this one is further reduced by applying particle identification techniques.

Spallation Products

Cosmic-ray muons can generate long-lived radioactive isotopes like ^{12}B in liquid scintillator or ^{16}N in water. Those isotopes have lifetimes long enough that it is impractical to use information from the parent muon to tag them. The estimated rate of those events is ~10/day. Although the *Q*-value of their decay products is in the range of 10-15 MeV, which is below the average lepton energy from neutrino interactions, this is still a dangerous background that can affect cross section measurements. The strategy to eliminate their contribution is to accurately measure their rate during periods when the SNS beam is off and statistically subtract them.

Machine-related Backgrounds

Machine-related background is primarily neutrons, whose energy spectrum is shown in Figure 4.9. As with cosmic-ray neutrons, the active veto does not help with this background source. In fact, as discussed in Section 4.3, the veto system must be carefully designed to be *inefficient* for neutrons to avoid excessive deadtime. The shielding does help reduce this background source, but, as summarized here and discussed at length in Section 4.4, the SNS time structure is the real key to eliminating it.

For ν_e (charged-current) and $\bar{\nu}_\mu$ (neutral-current) induced events backgrounds from all machine-related sources can be effectively mitigated with a simple time cut relative to the start of the proton pulse ($\tau > \sim 1100$ ns) since the neutron flux dissipates in time much faster than the neutrinos (whose time spectrum is defined by the muon half-life; $\tau_\mu = 2.2$ μs). There is a very attractive possibility to measure *pure* neutral-current events while beam is on target, since during this time pure neutral-current events (induced by ν_μ's and defined by the pion lifetime, $\tau_\pi = 26$ ns) dominate over charged current events. The fastest neutrons from the spallation target and neighboring beamlines don't arrive until ~50 ns after the pulse, whereas the neutrinos arrive within ~20 ns. In this time window the backgrounds are dominated by neutrons coming from the RTBT which can actually arrive *before* the neutrinos since they have a shorter path length; directly *through* the RTBT shield wall. Our current calculations indicate that this background source is too high to allow pure neutral-current measurements. However, these calculations are based on the maximum amount of beam loss that the SNS is allowed to have, and very conservatively assumes a line source (in reality the losses will likely originate primarily at the downstream quadrupole defocusing magnets). These neutral-current measurements are important, so further calculations to improve the RTBT background rate predictions, measurements once SNS operations begin to verify these calculations, and discussions with SNS personnel about possible background reduction strategies will be pursued as a part of our R&D program.

To summarize, we eliminate:

- Cosmic-ray muons by tagging them in the veto.
- Neutrons from cosmic-rays and from the SNS through shielding.
- All backgrounds by utilizing the SNS time structure (looking only in a small time window close enough to the spallation pulse for neutrino interactions to be present and far enough from the spallation pulse for machine backgrounds to have died down.

- All backgrounds by utilizing particle identification capabilities of the detectors. These capabilities are detector specific and must be explored with a full simulation incorporating the shielding, the veto and the detector. In Section 4.4 we present a detailed analysis of the background rejection capabilities of the Segmented Detector.
- All beam unrelated backgrounds which will pass neutrino identification cuts will be accurately measured while the SNS beam is off and statistically subtracted.

4.2 Shielded Bunker

4.2.1 Design

The basic parameters of the bunker shielding (volume and thickness) are determined by the detector size required to obtain the signal of interest, the required rejection of backgrounds from cosmic and machine sources, and the allowable floor loading in the SNS target hall.

As discussed above, the bunker thickness requirements are driven by the cosmic neutron flux. A ceiling thickness of 1 m and wall thickness of 0.5 m is sufficient to reduce backgrounds from this source to the same level as irreducible neutron backgrounds resulting from neutron production inside the shielding by untagged cosmic-ray muons. The bunker volume identified on the SNS target hall floor is ~$4.5 \times 4.5 \times 6.5$ m^3. The required shielding thickness leaves an instrumentable volume of ~$3.5 \times 3.5 \times 5.5$ m^3, sufficient to house the active veto system and the two neutrino target/detector systems.

The weight of the shielding is ~490 tons. The detectors and the veto system are ~50 tons. This is more than the floor capacity calculated under the most conservative possible assumption that the entire floor near the bunker is loaded to the maximum rated floor capacity (1500 PSF). (See Appendix 4 for calculations performed by the engineering firm **m+w zander** (SNS Target Building designers).) However, the engineering report goes on to examine the consequences of an aisleway that will run between **ν-SNS** and beamline 18 (BL18) which is needed to allow access to the BL18 neutron-scattering instrument (a top view of the **ν-SNS** bunker, the aisleway and BL18 is shown in Figure 4.1). Since the thick concrete floor of the target building is a very effective load spreader, the report finds that we can take credit for the area of the aisleway when calculating the floor loading capacity *if there are administrative controls in place to enforce a ban on large static loads in the aisleway*. This represents sufficient additional capacity for the proposed bunker and detector suite. We note that the aisleway could presumably be used as a staging area for shielding blocks going in or out of the local beamlines; since the floor spreads the load it does not matter much if a shield block is in the aisleway as opposed to being in its normal location. Furthermore, when the BL17 and BL18 shielding packages are finalized they may well be lighter than the floor loading capacity. If so, it may be possible to take credit for some of the unused load capacity.

The detailed shielding design will be constrained by requirements on seismic stability, detector accessibility, installation constraints and the necessity to provide a secondary containment vessel for the homogeneous detector target material. The detailed design must also take into consideration the fact that much of the area allocated for **ν-SNS** is not accessible to the SNS target hall crane (as shown in Figure 4.1).

These considerations have led us to develop the concept shown in Figure 4.10. The bottom of the bunker will host the liquid detector. It will be made of plates that can be rigged into place with the help of a rail system that will extend into the region accessible to the crane. The plates will be welded in place to form a containment vessel. Two sides will be secured to the wall to provide seismic stability. A roof over this lower section will be the floor for the segmented detector. Access to the liquid detector, which will be underneath this floor, will be required. The walls of the top bunker section will be made of plates and rigged into place with a rail system and secured to the wall similar to the bottom section. The side of the bunker facing away from the proton

beamline will be removable, with the help of a rail-mounted crane on the bunker roof, to allow access to the segmented detector for target replacement.

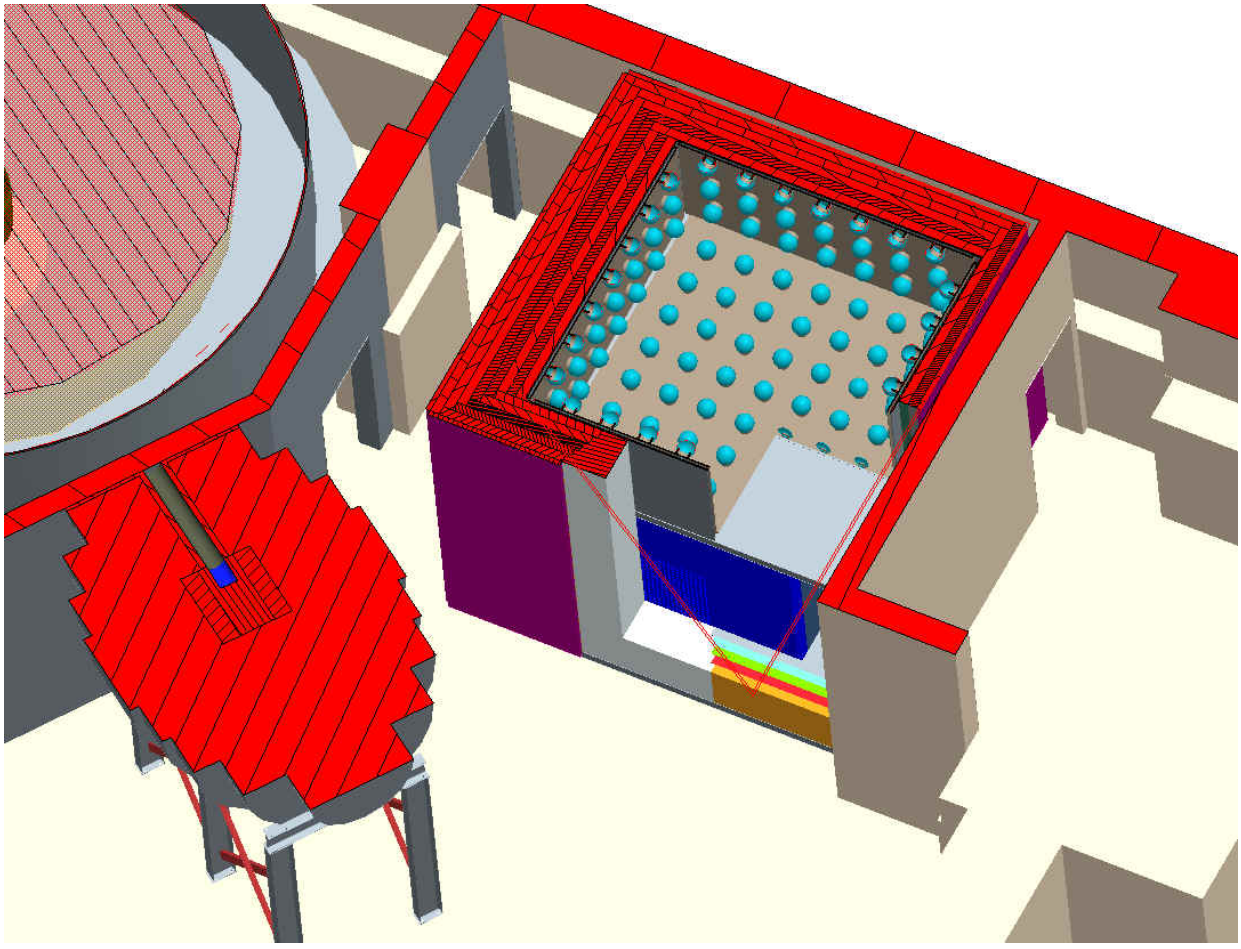

Figure 4.10 Schematic drawing of the **ν-SNS** shielded bunker with the two detectors inside.

4.2.2 Interface with Beamlines 17 and 18

Our goal is zero interference with the neighboring neutron-scattering beamlines, BL17/18. In order to realize this goal we have been working closely with BL17/18 staff members to understand their operational needs, identify possible areas of concern, and find solutions that will eliminate any impact on operations. Three issues that have been raised are access requirements for the beamlines, floor loading restrictions, and the impact of beamline shielding decisions on **ν-SNS** background levels. These issues are being addressed in the following manner:

- Sufficient clearance between our bunker and BL18 to allow forklift access to the BL18 instrument is required. We anticipate very little equipment outside the bunker volume itself. Readout and control electronics will be located on the SNS mezzanine and gas (segmented detector) and liquid (liquid detector) will be stored outside the SNS target building.
- Floor loading will remain a concern until the shielding packages for the neighboring beamlines are finalized. As discussed above, based on extremely conservative assumptions we expect there will be sufficient capacity for the required **ν-SNS** shielding.
- Current calculations indicate that a significant contributor to machine-related backgrounds is scattering off the BL18 frame-overlap choppers. It is possible that the BL18 shielding package can be optimized to reduce this background.

4.2.3 Cost Estimate

Design considerations described in Section 4.2.1 push us towards a bunker design which is built up from thin (6") machined steel plates with relatively tight geometrical tolerances. In addition, we anticipate a significant amount of design, engineering and installation effort, including the development of special fixtures and rail systems for mounting the plates where the crane access is limited.

The raw material for the bunker is assumed to be off-spec steel, currently priced at $0.38/pound. Steel prices are currently stable but they have risen significantly over the last few years. Presently steel futures are very uncertain with price decreases predicted as often as further price increases. This uncertainty makes it very difficult to assign a reasonable contingency to this item. Consequently, we are exploring means to reduce our exposure to this risk, such as using poured plates of low-activity steel (potentially available from Duratek, Inc.).

Costs, (including overheads and contingency) and estimated labor hours are shown in Table 4.1.

Table 4.1 Cost breakdown for the shielded bunker.

WBS #	Title	Cost w/o Contingency	Contingency	Total	Contingency Fraction	Labor Hours
1.1	**Bunker**	**$2,255,487**	**$563,872**	**$2,819,359**	**25%**	**7,420**
1.1.1	**Design Bunker**	**$276,787**	**$69,197**	**$345,984**	**25%**	**1920**
	Design	$122,112	$30,528	$152,640	25%	960
	Engineering	$154,675	$38,669	$193,344	25%	960
1.1.2	**Procure Bunker**	**$1,231,800**	**$307,950**	**$1,539,750**	**25%**	**0**
	Steel	$434,000	$108,500	$542,500	25%	0
	Machining/Shipping	$707,800	$176,950	$884,750	25%	0
	Misc components	$90,000	$22,500	$112,500	25%	0
1.1.3	**Install Bunker**	**$746,900**	**$186,725**	**$933,625**	**25%**	**5500**
	Site Prep	$50,000	$12,500	$62,500	25%	700
	Rigging Hardware	$352,500	$88,125	$440,625	25%	0
	Assembly Labor	$344,400	$86,100	$430,500	25%	4800

4.3 Active Cosmic-Ray Veto System

4.3.1 Requirements

There are two basic requirements for the Active Cosmic-Ray Veto system. First it must eliminate, with an efficiency of ~99%, background caused by cosmic rays. Second, low energy particles (mostly gammas from (n,γ) captures, and low energy neutrons that cannot penetrate the bunker) should not introduce significant deadtime into the measurement: any SNS pulse in which the veto fires is unusable. Based on the facility backgrounds calculated in Section 4.1, achieving an efficiency below 0.1% for such events allows the use of 90% of the pulses.

4.3.2 Approach

To achieve similar requirements (98% efficiency) the KARMEN [10] collaboration used 2 inch thick, high-quality scintillator, in which cosmic-ray muons deposit more then 10 MeV of energy, more then the maximum photon energy from (n,γ) capture on iron (8 MeV). However, in our case this approach is cost prohibitive (~ $2.4 M for the cast scintillator material alone).

We propose to use relatively inexpensive extruded scintillator bars with wavelength shifting (WLS) fiber readout. We are planning to use three layers of such scintillators and require coincident signals from each of them. This is the same scheme used by the MINOS [11] collaboration and adopted for the proposed veto system of the MECO [12] experiment at BNL. The MECO collaboration plans to use extruded scintillator bars ($10 \times 1 \times 450$ cm^3); see cross section in Figure 4.11. The production method for the bars is limited to about 1 cm thickness, so we will need to use multiple layers.

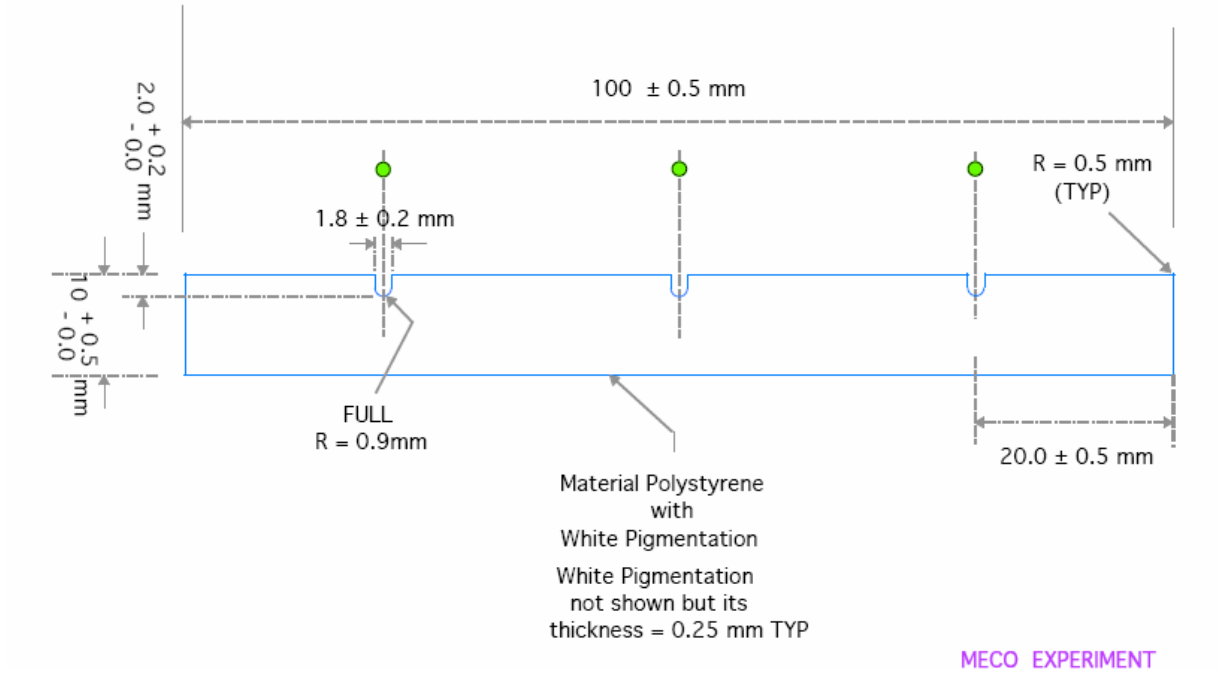

Figure 4.11 Cross section of the extruded scintillation bars for the MECO experiment.

4.3.3 Simulated Performance

In order to study the feasibility of our approach simulations were run on simple scintillator setups. Figure 4.12 shows a GEANT simulation of the effect of muons, gammas and neutrons on a three-layer scintillator stack. (The normalization was arbitrarily chosen such that ten times more neutrons and gammas were generated than muons.) Each scintillator layer is 1 cm thick and read out from one end via a 1 mm diameter wavelength shifting fiber of 6 m length.

The top panel of Figure 4.12 shows the energy deposited in all three layers, indicating modest separation of the muon signal from others. The middle panel shows the actual light output in number of photoelectrons (assuming light collection in the fiber of 10 photoelectrons/MeV, corresponding to the quantum efficiency of avalanche photodiodes (APDs), a possible photosensor technology). This displays the effects of fluctuation in light attenuation and photon statistics resulting in a significant overlap of the different distributions. The bottom panel shows the actual light output for events in which we require at least two photoelectrons be collected per layer. It can be clearly seen that this coincidence requirement leads to a significant suppression in unwanted backgrounds (only 0.13% detection efficiency for neutrons and 1.5% for gammas) but also leads to a cosmic-ray efficiency of only 96% (assuming 100% geometric efficiency).

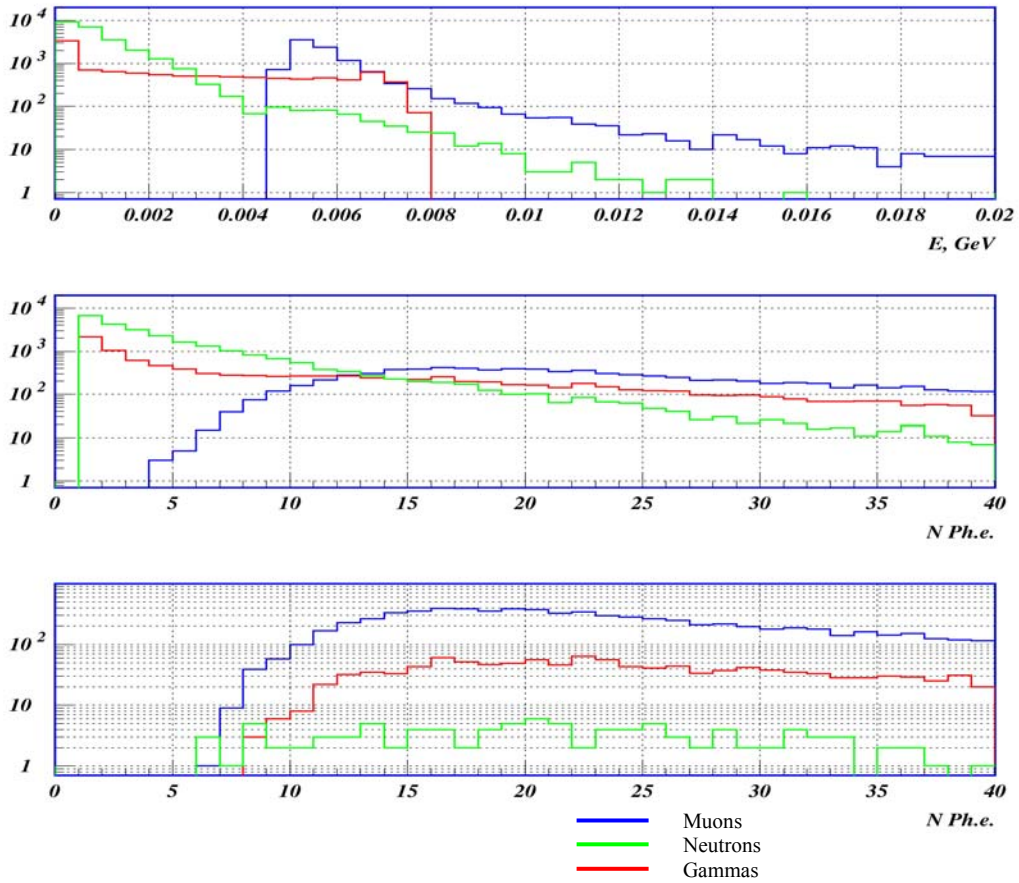

Figure 4.12 Simulated response of a three-layer scintillator stack to muons (blue), neutrons (green), and gammas (red). Top: total energy deposited in the scintillator. Middle: total photoelectron production at the photosensor. Bottom: total photoelectron production at the photosensor for events in which at least two photoelectrons were detected in each layer.

In order to increase the efficiency for muons we can increase the number of layers and/or allow for a missed layer. However, this increases our (unwanted) efficiency for gammas from neutron capture. We can retain our muon efficiency and significantly reduce our gamma efficiency by placing thick absorber plates between the scintillators. Figure 4.13 shows the effect in introducing 1.5 cm iron plates between the scintillator layers.

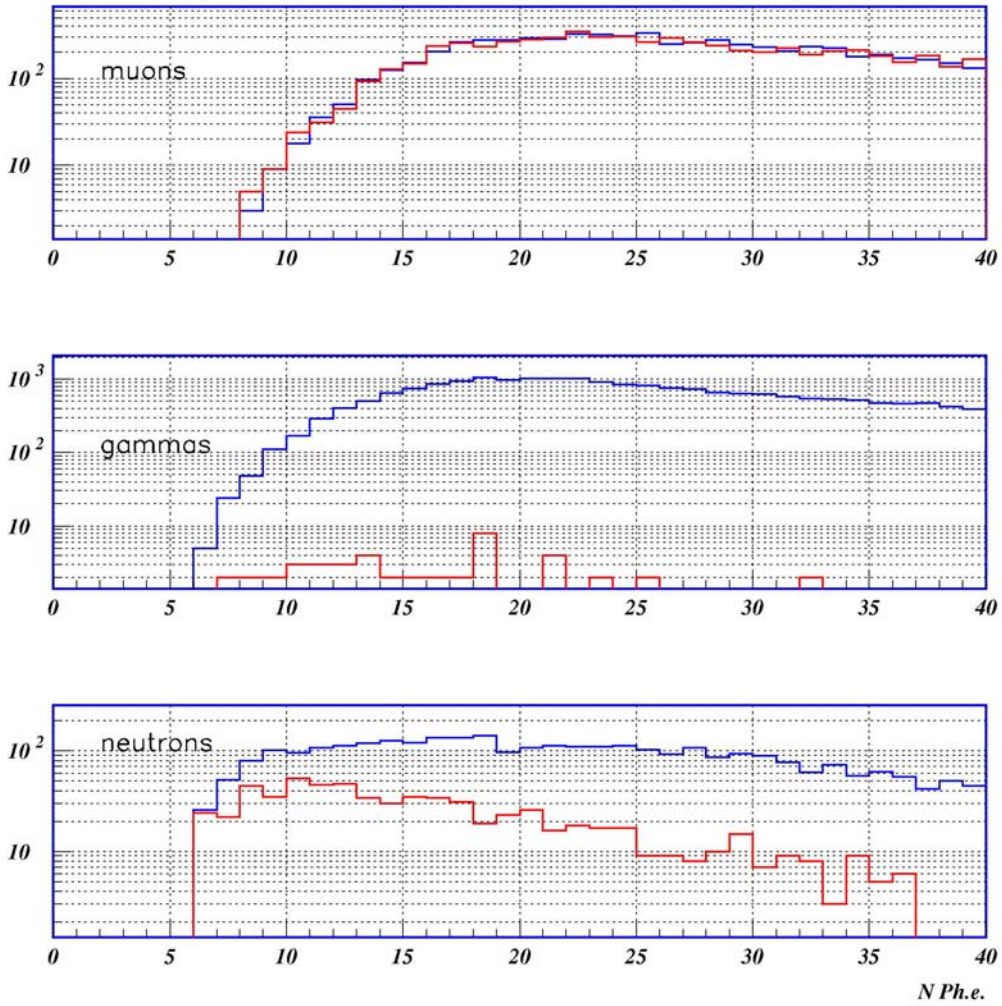

Figure 4.13 Background suppression with 1.5 cm iron absorber plates between scintillator layers. The total number of photoelectrons detected in all scintillator layers are shown without (blue) and with (red) the iron plates. Muons (top panel) show almost no suppression; gammas (middle panel) are reduced by an additional factor of 500, for a total efficiency of 0.005%; neutrons (bottom panel) are suppressed by an additional factor of 6, for a total efficiency of 0.07%.

The following configuration was found to satisfy our requirements: four 1 cm scintillator layers with 1.5 cm iron plates between each layer; a two photoelectron threshold on each layer and a requirement that three of the four layers be hit. This yields a 99.5% efficiency for cosmic rays (assuming 100% geometric efficiency) and an efficiency for neutrons (gammas) of only 0.07%

(0.005%). Using current neutron flux assumptions this will cause a false veto for a little more than 10% of the SNS pulses.

Additional design optimization (that may reduce cost, improve performance and simplify construction) may be possible. For instance: the use of larger diameter wavelength shifting fiber, the use of clear fiber for the routing between scintillator end and photosensor, and two-sided readout. Note: two-sided readout is impossible for phototube readout due to space limitations, but may be possible with flat readout such as avalanche photodiodes (APDs [13]) or silicon photomultipliers (SiPMs [14]), technologies which are developing rapidly at the moment. A vertical mounting scheme may greatly simplify installation, but at the price of longer fibers. Tradeoffs between the different approaches need to be explored in more detail in simulations and confirmed in our R&D program.

In order to design the cosmic ray veto in more detail, we are currently performing GEANT simulations on different veto options that also include the properties/geometries of the two main detectors. Current simulations include a bunker with a homogenous detector; segmented detector and various outer and inner veto system configurations (see Figure 4.14). These configurations also include relevant structure of the SNS facility (structural beam, wall, and ceiling) in addition to a concrete floor in order to be able to avoid possible leaks in our veto from below the bunker.

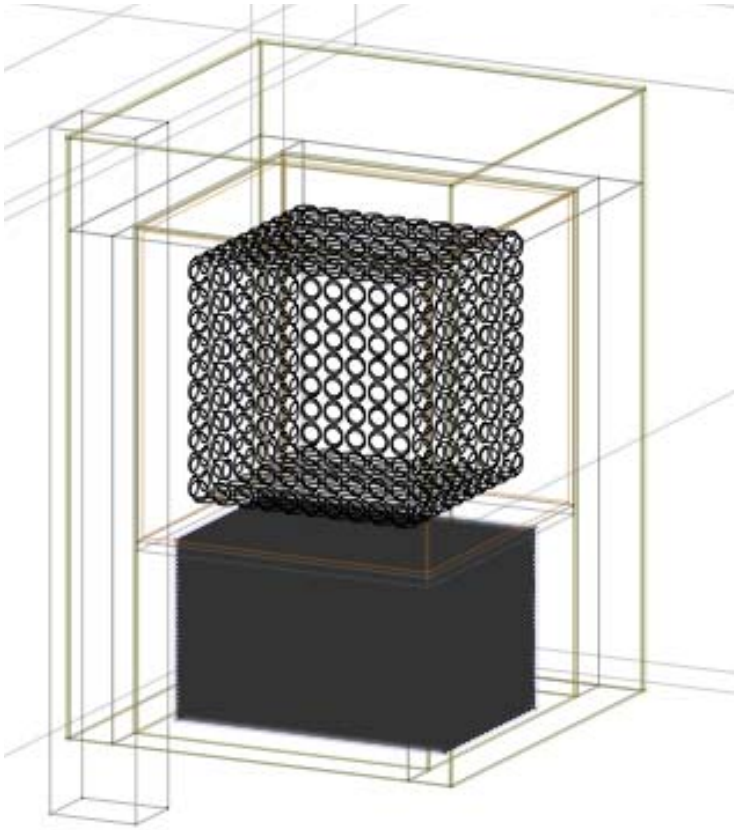

Figure 4.14 GEANT model of the **ν-SNS** facility including homogenous liquid scintillator detector, segmented iron tube/strawtube detector, and veto panels.

4.3.4 Assembly and Construction

The present design of the veto system is shown on Figures 4.15 and 4.16. The veto system will consist of extruded scintillator planks (active length ~ 4.5m) mounted in panels consisting of four layers (glued with 1.5 cm thick iron absorbers in between). Six panels will be assembled inside a light-tight box to form a module. Each plank will be read out by three wavelength shifting fibers that connect to clear fiber at the end of the plank. The clear fiber connects to one segment of a 2×2 multianode PMT. Each PMT segment can accommodate the 18 fibers from one of the layers of a module, so a complete panel is read out by an individual PMT. The PMT bases are read out via an amplifier/discriminator combination, which produces timing signals for time to amplitude converters.

The current configuration for the veto requires the production of ~1300 MECO-type 4.5 m long scintillator planks, which will be combined into ~52 modules of 24 planks. Currently we anticipate the production of two different module lengths (determined by the available space at the SNS) for horizontal installation. Additionally, narrower modules will be used for corner veto shielding.

Individual modules will be assembled at the Colorado School of Mines and delivered for installation to the SNS site. The PMTs will be mounted with their bases in light tight cases ready for the attachment of connectors. Each module will be tested before shipping to ORNL. The weight of a module is determined mostly by the absorber thickness (~1300 kg for the simulated 1.5 cm iron sheets). Modules will be mounted on a support structure outside of the bunker.

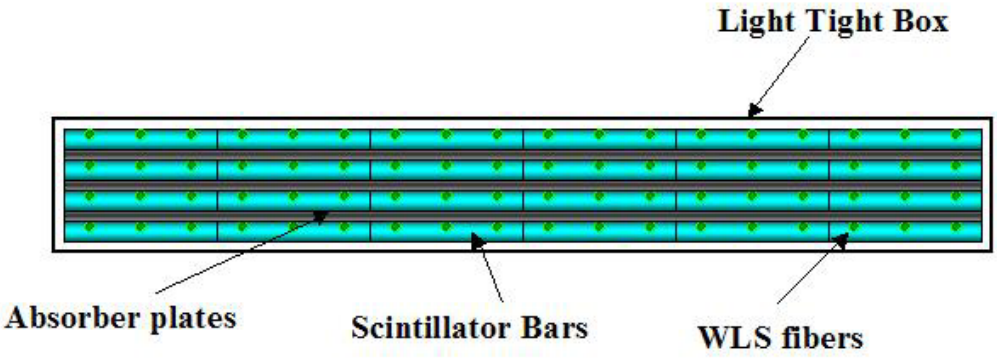

Figure 4.15 Conceptual design of one veto panel. It is 60 cm wide and consists of 24 scintillator bars organized in four layers with absorber plates in between. The layers will be staggered slightly to reduce leakage. Light readout is from one end via WLS fibers.

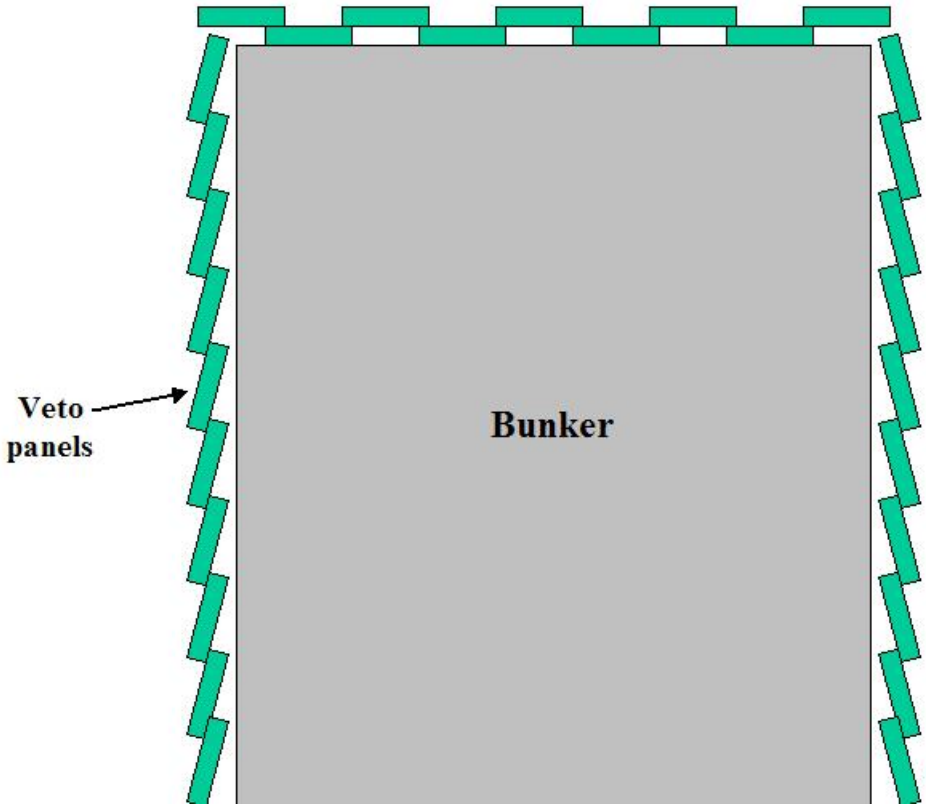

Figure 4.16 Conceptual design of the veto panel arrangement. To achieve high geometric efficiency, individual panels are overlapped either "siding" style (shown on the sides) or "brick" style (shown on the top).

4.3.5 Cost Estimate

The cost for the veto system is dominated by the costs for the scintillator, electronics, and equipment for mounting and readout. We obtained cost estimates from Hamamatsu for PMTs and bases; from Wiener Plein & Baus for electronics; from Bicron on WLS fiber; and from Industrial Fiber Optics for clear fiber. All other prices were estimated based on engineering judgment. We have included the cost of the test benches, quality control, the support structure shipping and travel for commissioning. Note: joining with the MECO group for scintillator production may allow us to reduce production costs below our current estimates.

We have incorporated appropriate contingency to account for the uncertainty in our design and other project risks:

- The prices for scintillation planks are based on recent discussions with ITASCA Plastics. This company also did the extrusions for the MINOS project but will use for the production/development for **ν-SNS** a different price structure, which leaves nearly all the risk in the production with us.
- There is risk associated with the price and quality of the raw polystyrene.
- R&D is necessary to verify the performance of the extruded scintillator (which varies with batches), fiber readout, the different connectors, and photomultiplier tubes. Note: current estimates are based on experience by the MINOS collaboration.
- We may be required to use non-PMT photosensor technology (for example APDs or SiPMs) if high magnetic fields are present on neighboring neutron-scattering beamlines.

Costs, (including overheads and contingency) and estimated labor hours are shown in Table 4.2.

Table 4.2 Cost breakdown for the cosmic-ray veto system.

WBS #	Title	Cost w/o Contingency	Contingency	Total	Contingency Fraction	Labor Hours
1.2	**Active Cosmic Veto System**	**$1,058,835**	**$376,961**	**$1,435,796**	**36%**	**6,400**
1.2.1	**Design Veto**	**$76,785**	**$19,964**	**$96,749**	**26%**	**710**
	Monte Carlo Simulation (Physicist)	$0	$0	$0	0%	100
	Design drawings (Engineer)	$31,995	$8,319	$40,314	26%	270
	Equipment Specs. (Engineer)	$21,330	$5,546	$26,876	26%	180
	QC Process (Engineer)	$18,960	$4,930	$23,890	26%	160
	Travel	$4,500	$1,170	$5,670	26%	0
	Monte Carlo Simulation (Grad. Stud.)	$0	$0	$0	0%	300
1.2.2	**Procure Veto Parts**	**$647,170**	**$258,868**	**$906,038**	**40%**	**550**
	Quality Control at ITASCA (Tech)	$29,160	$11,664	$40,824	40%	360
	Quality Control PMT/Bases (Tech)	$4,860	$1,944	$6,804	40%	60
	Quality Control WLS Fibers (Tech)	$4,050	$1,620	$5,670	40%	50
	Quality Control Setup	$5,000	$2,000	$7,000	40%	0
	Travel cost for Quality Control	$22,500	$9,000	$31,500	40%	0
	Shipping Costs	$37,500	$15,000	$52,500	40%	0
	Electronics and Cables	$173,000	$69,200	$242,200	40%	0
	Scintillator	$126,100	$50,440	$176,540	40%	0
	Mounting and Readout equipment	$245,000	$98,000	$343,000	40%	0
	Quality Control (Physicist)	$0	$0	$0	0%	80
1.2.3	**Assemble and Test Veto**	**$224,280**	**$58,313**	**$282,593**	**26%**	**3,840**
	Assembly Benches	$10,000	$2,600	$12,600	26%	0
	Module Assembly (Tech)	$142,560	$37,066	$179,626	26%	1,760
	Quality Control Setup	$5,000	$1,300	$6,300	26%	0
	Quality Control (Tech)	$17,820	$4,633	$22,453	26%	220
	Module Shipping	$22,500	$5,850	$28,350	26%	0
	Supervision (Physicist)	$0	$0	$0	0%	100
	Undergraduate Student Help	$26,400	$6,864	$33,264	26%	1,760

WBS #	Title	Cost w/o Contingency	Contingency	Total	Contingency Fraction	Labor Hours
1.2.4	**Install Veto**	**$110,600**	**$39,816**	**$150,416**	**36%**	**1,300**
	Mounting Materials for Shelving	$20,000	$7,200	$27,200	36%	0
	Aluminum Sheets	$12,000	$4,320	$16,320	36%	0
	Mounting (Tech)	$48,600	$17,496	$66,096	36%	600
	Travel Mounting	$30,000	$10,800	$40,800	36%	0
	Supervision (Physicist)	$0	$0	$0	0%	100
	Graduate Student Mounting	$0	$0	$0	0%	600

4.4 Segmented Detector

4.4.1 Requirements

The segmented detector will be a flexible universal detector in which neutrino interactions with a variety of targets can be studied. To achieve this, the detector must:

- Contain ten fiducial tons of target material and fit inside the fixed shielding volume.
- Minimize the mass of non-target material.
- Have the capability to easily replace targets without rebuilding the sensitive part of the detector.
- Have relatively good time resolution (few ns) to facilitate operation in the SNS background environment.
- Have particle identification capability and allow 3-dimensional track reconstruction for further background discrimination.
- Have good energy resolution to allow differential cross section measurements.
- Be affordable (minimize channel count).

4.4.2 Approach

To satisfy these requirements we propose to build a highly segmented detector with strawtubes separated by thin-walled corrugated sheets of the target material. Signals will be read from both sides of each strawtube's anode wire in order to provide time information and three-dimensional position information by charge division. A similar concept was used by the 1000 ton Soudan-II proton decay experiment [15]. However, the **ν-SNS** project requires a detector with much finer segmentation and significantly improved time resolution.

The energy of detected particles will be determined by the number of strawtubes hit, which is closely related to the particle's range. For electrons in the energy range of a few tens of MeV the energy resolution obtained by a measurement of the track length is comparable to that obtained by energy sampling [16].

Gas-based detectors have a number of advantages over other detector technologies for this application because they are less expensive than other detectors (*e.g.*, scintillator) and do not require an expensive readout system. In addition, the low detector mass eliminates the necessity to statistically separate interactions in the target from interactions in the detector.

4.4.3 Simulated Performance

We simulated the detector response to the neutrino signal together with the response to the three major sources of background; 1) neutrons from the SNS, 2) cosmic-ray muons, and 3) cosmic-ray neutrons. Although cosmic-ray neutrons are usually neglected in background simulations, we include them here, as floor-loading limitations preclude a bunker overburden sufficiently thick to completely eliminate the hadronic component of cosmic rays. A complete model of the detector, bunker shielding, and veto system was implemented in the GEANT simulation package. The geometric efficiency for the veto system was assumed to be 98%. The sensitive volume of the segmented detector was $2 \times 2 \times 3$ m^3. In the actual detector the target will be constructed from

thin corrugated plates, as shown Figure 4.17. For these simulations the target material was assumed to have a cylindrical geometry (pipes), to simplify the GEANT code. Results for the actual detector geometry are expected to be close to those simulated here.

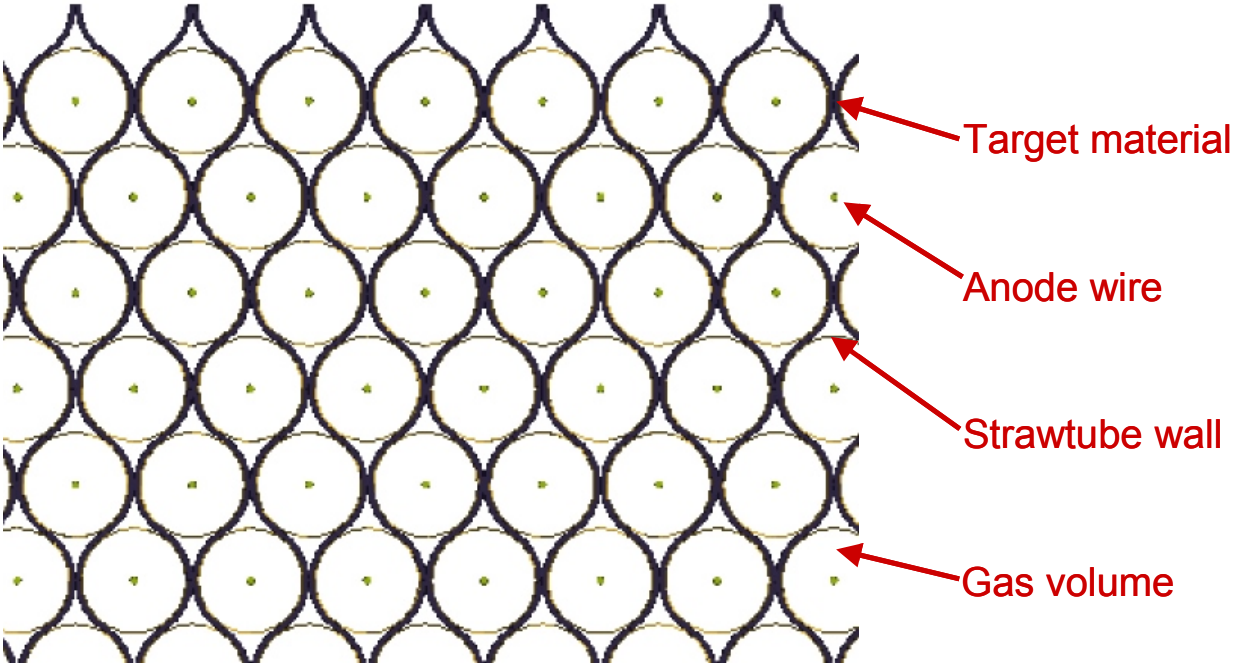

Figure 4.17 Schematic cross cut view of the segmented detector.

All simulations assume iron targets since this is the highest priority target for the segmented detector. The KARMEN experiment extracted a cross section of 2.5 ± 0.83 (stat.) ± 0.42 (syst.) for ν_e + Fe from interactions in their shield [17]. Neutrino-iron interactions have also been extensively studied theoretically [18,19], giving a similar cross sections and a prediction for the electron spectrum (see Figure 4.18). For the signal input of our simulation we used electrons with this spectrum and assumed isotropic emission at a random point within the target volume.

The first simulation task was to optimize the cell radius and target thickness in order to satisfy requirements on energy resolution, detector size and affordability. Thinner cell walls result in lower energy loss during the crossing of an individual cell wall, and thus offer superior energy resolution and better particle identification capability. However, this also results in a larger detector volume and a larger number of channels for a fixed target mass. Smaller cell radii result in better energy resolution and a smaller overall detector, but at the cost of a larger number of channels, and thus greater cost, for a fixed target mass. Table 4.3 shows the required number of individual cells for an iron detector with a fiducial mass of 10 tons, built from 3 m long tubes. Calculations for various cell sizes and target thickness are presented; combinations that will fit inside the shielding volume are indicated in red.

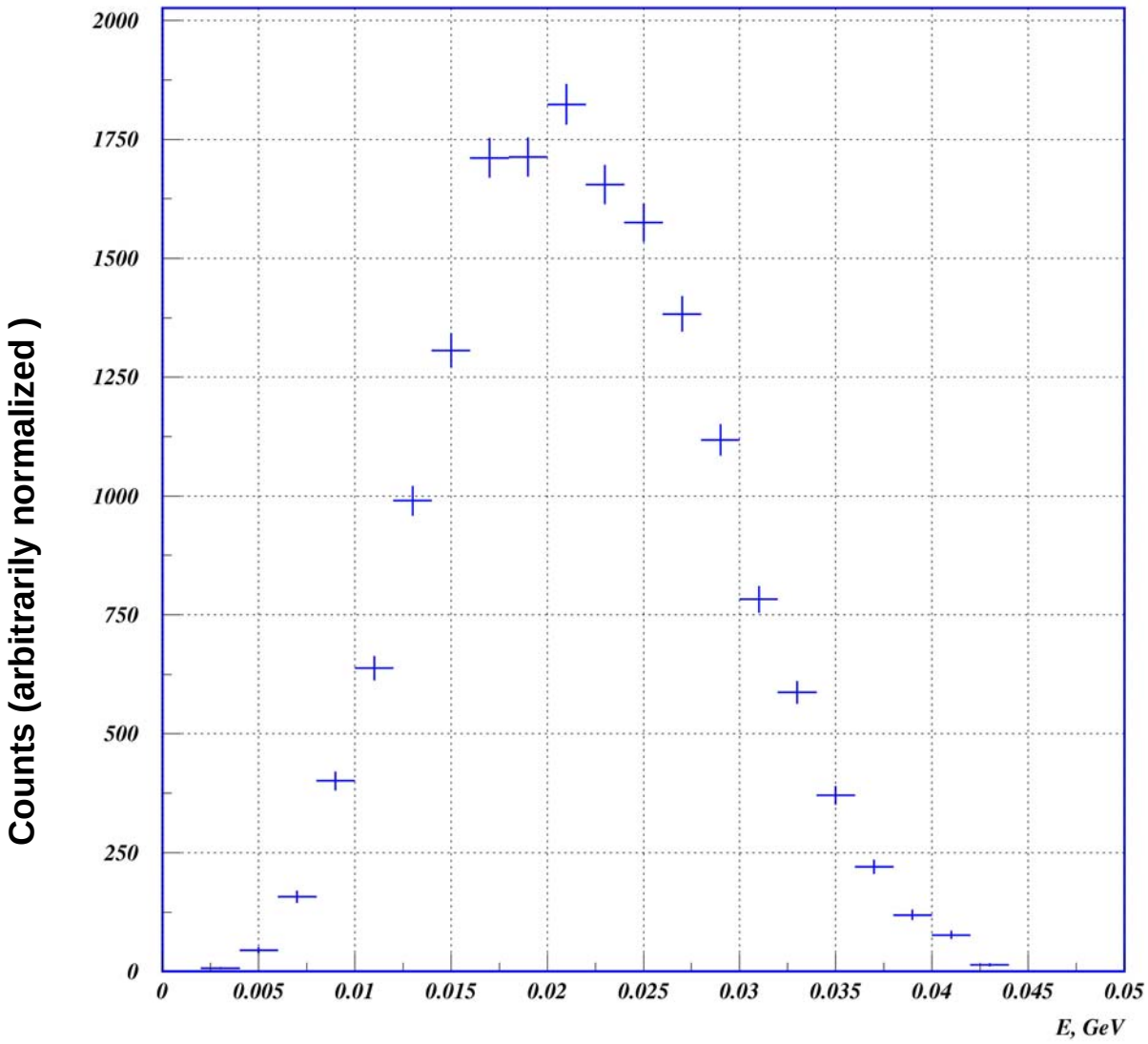

Figure 4.18 The electron spectrum assumed for the reaction ν+Fe→e+X [18].

Table 4.3 Required number of tubes (in thousands) for a ten ton fiducial mass iron target. Tube length is fixed at 3 meters. Combinations of radius and wall thickness that will fit inside the proposed neutrino bunker are shown in red

Cell radius\ Target thickness, mm	1.0	0.75	0.5
5	19.8	24.7	34.5
6	15.8	19.9	27.9
7	13.1	16.6	23.4
8	11.2	14.2	20.2
9	9.7	12.4	17.6
10	8.6	11.0	15.7

In Figure 4.19 simulated hit distributions are shown for three different target thicknesses. In all cases, the cell radius is 8 mm. The response of the detector to Michel electrons is shown as well. Michel electrons are abundantly produced in the detector as a result of the decay of stopped cosmic-ray muons. They can easily be tagged by tracking the incoming muon, and will serve as an excellent calibration reference. The number of neutrino interactions (10K) corresponds to one nominal year of data acquisition. The number of Michel electrons is arbitrary, and selected to be equal to the number of neutrino interactions.

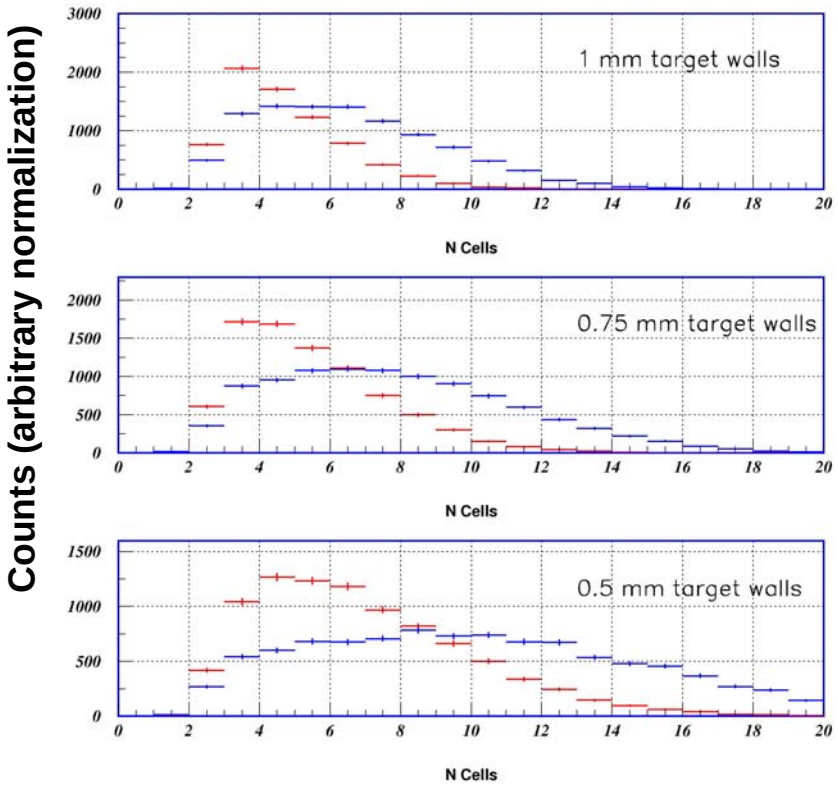

Figure 4.19 Number of cells hit in the segmented detector by neutrino interactions and by muon decays. The neutrino signal is shown in red, and the Michel electron signal in blue. Three target wall thicknesses are shown. The cell radius is 8 mm.

As expected, thinner targets allow more detector cells to be hit. In order to eliminate random coincidences we believe it will be necessary to require at least three hits in close proximity. For 1 mm target walls, this requirement alone reduces the overall efficiency to 66%. Thinner walls yield better signal strength and efficiency; 0.75 mm and 0.5 mm walls give 77% and 86% efficiency respectively. However a detector with 0.5 mm walls, 8mm radius and 10 ton fiducial mass requires ~40K channels, and becomes prohibitively expensive. A reasonable compromise (0.75 mm walls) provides a detector that has good energy resolution, fits inside the allocated volume, and has ~15K readout channels.

The next simulation task was to demonstrate required signal efficiency and background rejection. We explain the results by the following approach. First, in Figures 4.20 – 4.25, we show signal and background distributions for a number of parameters that can be measured by the detector and veto system:

- **Figure 4.20**: Number of detector cells hit. This distribution is relatively flat for cosmic ray muons and peaked at low values for neutrino interactions.
- **Figure 4.21**: Event vertex. Neutrino interactions are geometrically uniform while cosmic ray muons have a high probability of being near the detector edges and events due to SNS neutrons decrease with distance from the SNS target.
- **Figure 4.22**: Three-dimensional RMS separation of hits (the "compactness" of the track). Neutrino events are more compact than events caused by neutrons showering in the detector or the surrounding shielding.
- **Figure 4.23**: Energy deposition in the veto scintillator panels. Nearly all cosmic ray muons will deposit observable energy in the veto scintillators. However, a significant number of neutrons (from the SNS and from cosmic-rays) pass through the veto without large energy deposition.
- **Figure 4.24**: Average energy deposition per segmented detector cell. Neutrino and cosmic ray muon events give primarily minimum ionizing particles. Low-energy, recoil protons from neutron interactions typically have much larger energy deposition per cell.
- **Figure 4.25**: A fiducial cut eliminates events which have activity within 8 cm (5 cells) of the detector edges. This requirement reduces neutrino efficiency by ~30%, but eliminates ~99.5% of the cosmic ray muon background.

In all cases the different components (neutrino interactions, SNS neutrons, cosmic-ray muons, and cosmic-ray hadrons) are arbitrarily normalized so that all can be visualized on the same scale. One can see from these parameter distributions that neutrino and background events have very different detector responses and can be cleanly separated with appropriate choice of cuts. In Figures 4.26 and 4.27 we show the cumulative effect of these cuts for signal and background distributions, properly normalized for one year of operation at full SNS power.

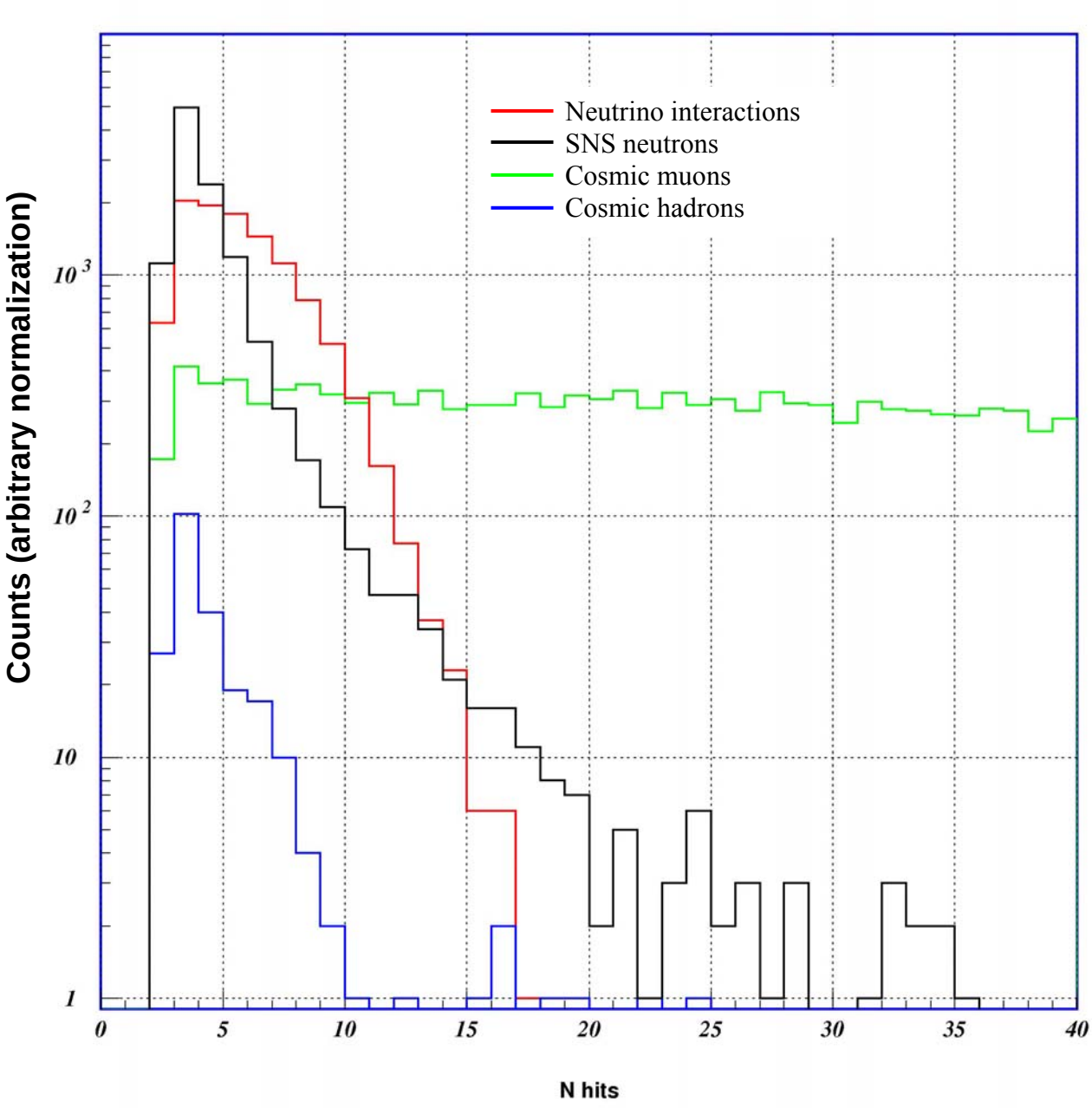

Figure 4.20 Distribution of the number of hits in the segmented detector for neutrino interactions and background sources. One can see the relatively flat distribution for cosmic-ray muons.

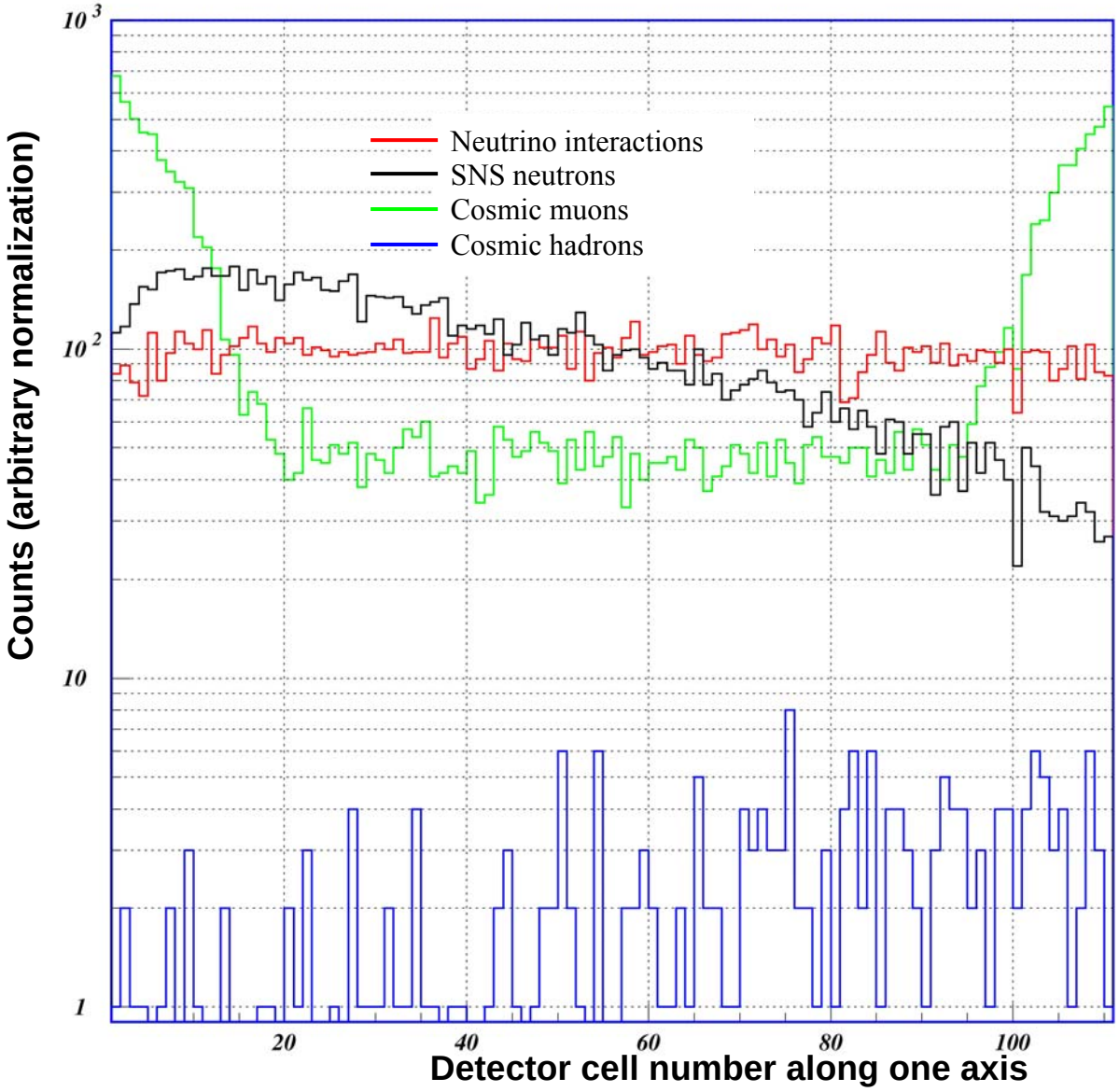

Figure 4.21 Event vertex distribution along one axis of the segmented detector for neutrino interactions and background sources. One can see that cosmic muons have a higher probability of being near the detector edges. SNS neutron hits decrease with distance from the SNS target.

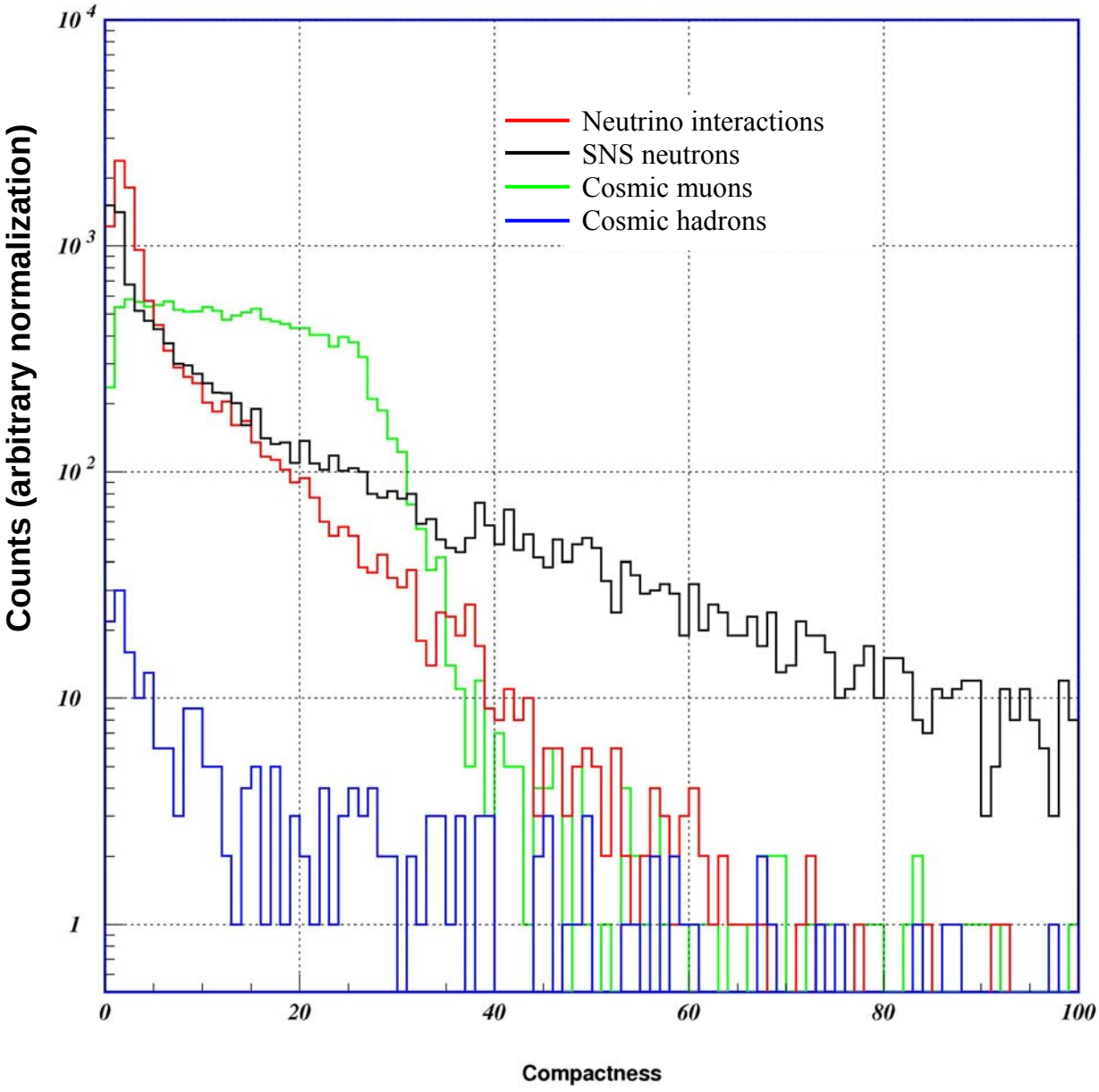

Figure 4.22 Distribution of the three-dimensional RMS separation of hits within the segmented detector (the "compactness" of the track) for neutrino interactions and background sources. One can see that isolated neutrino events are more compact than events caused by neutrons showering in the detector or the surrounding shielding.

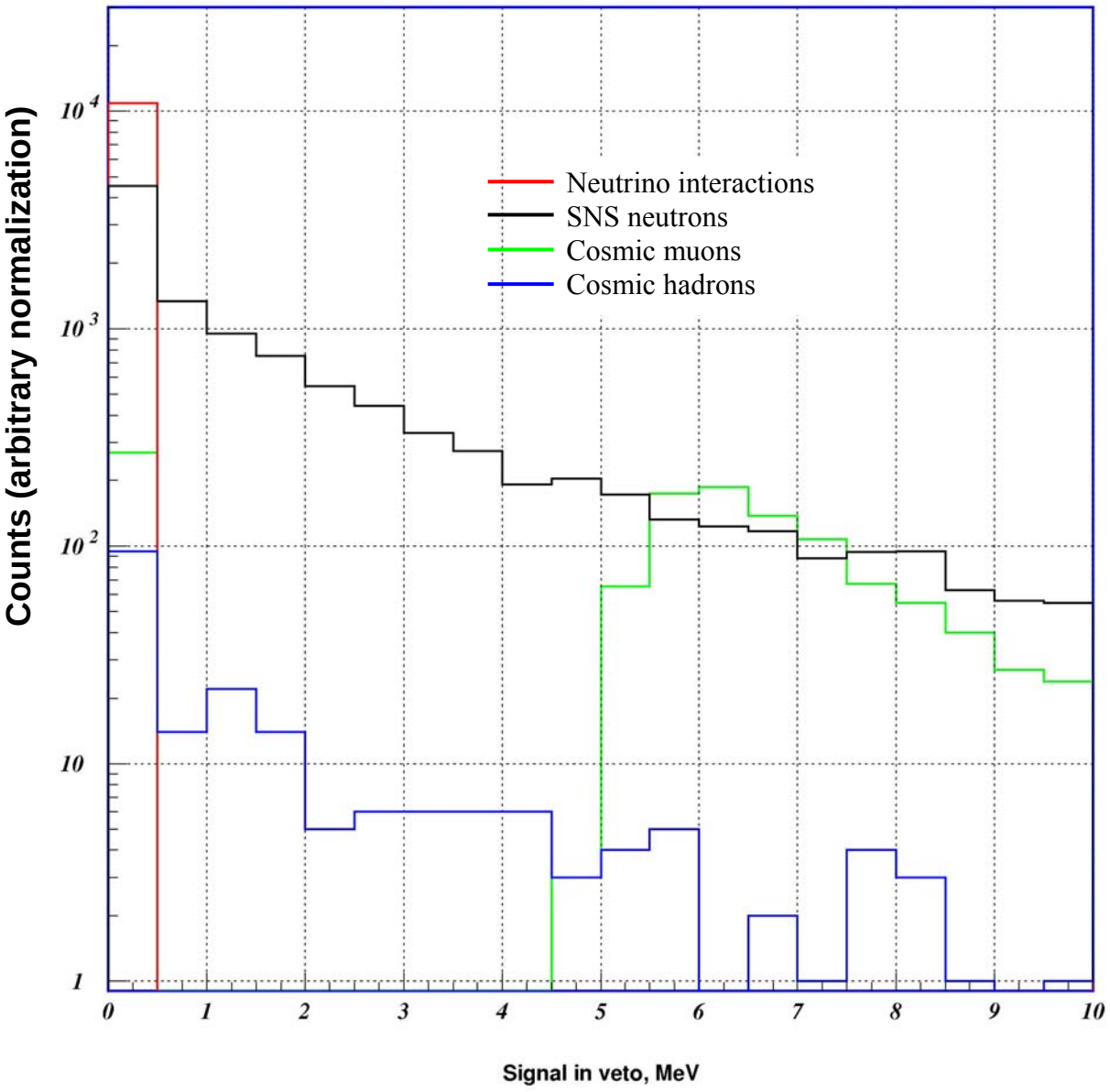

Figure 4.23 Energy deposition in the veto scintillator panels. A significant fraction of the neutrons (from the SNS and from cosmic rays) pass through the veto without large energy deposition. Note: this shows the energy deposition calculated by GEANT; light collection fluctuations are not included. The veto efficiency is assumed to be 98%.

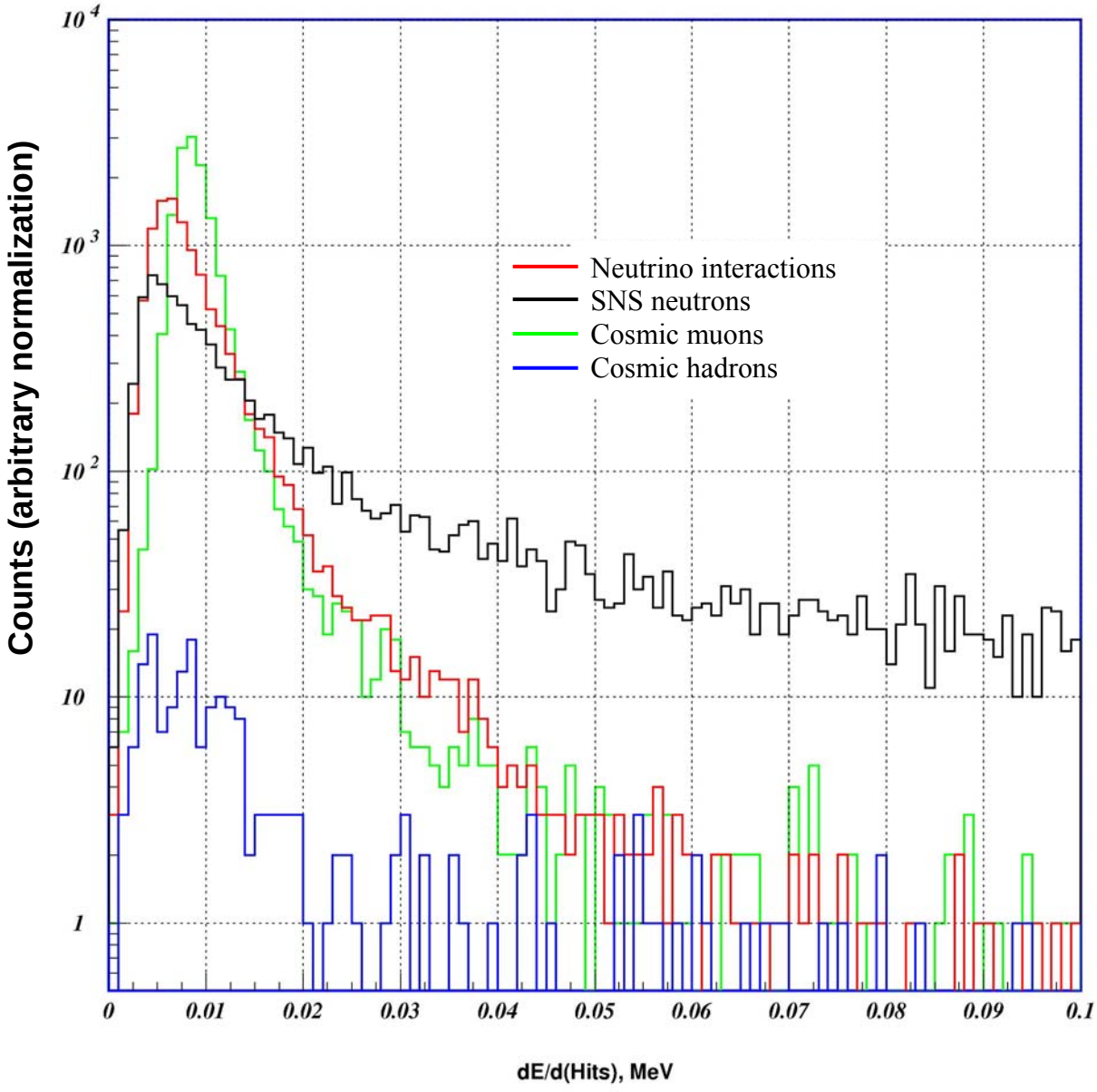

Figure 4.24 Average energy deposition per segmented detector cell in MeV for neutrino interactions and background sources. Neutrino and cosmic ray muon events give primarily minimum ionizing particles. However, low-energy, recoil protons from neutron interactions typically have much larger energy deposition per cell.

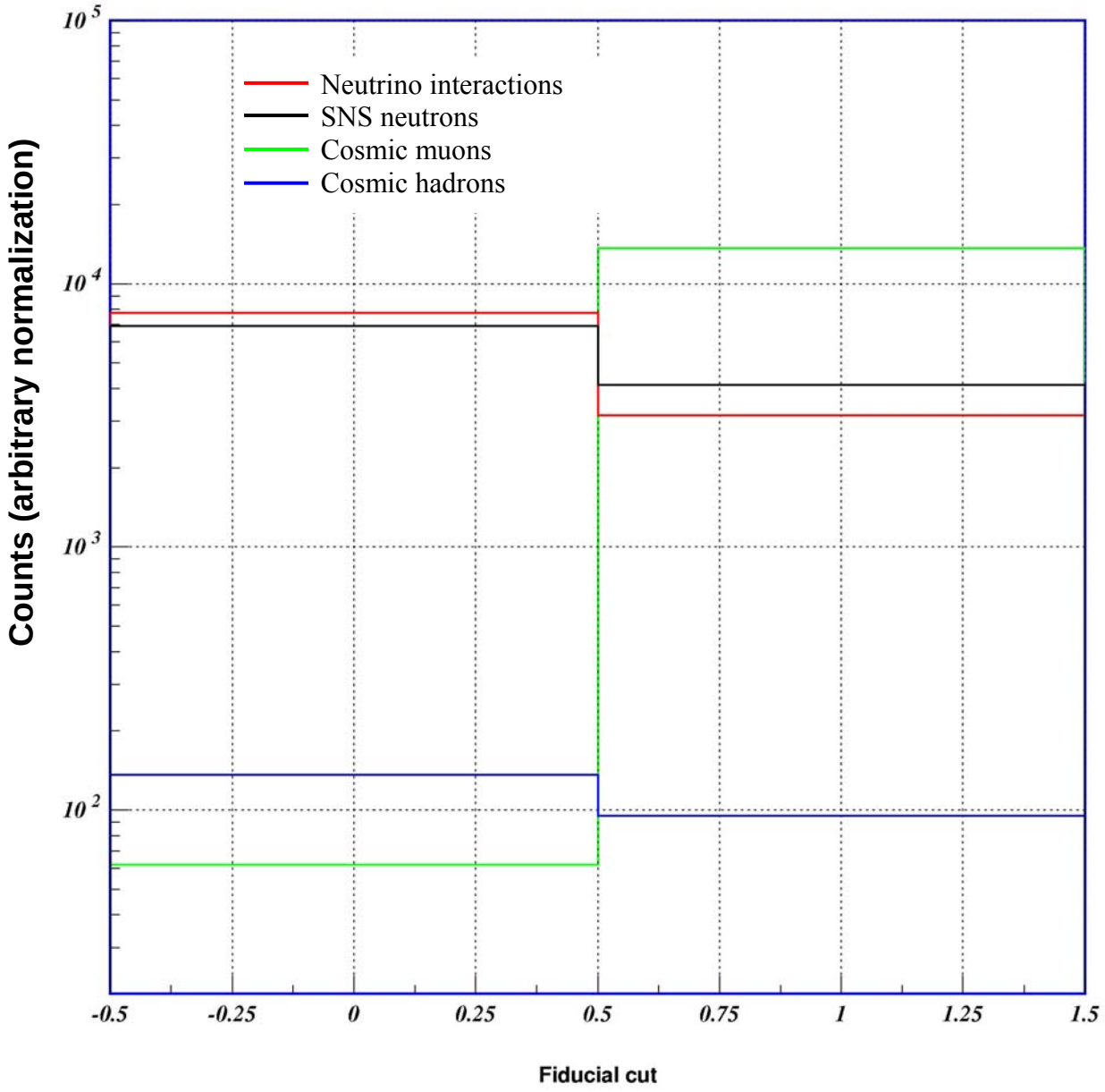

Figure 4.25 The fiducial flag distribution in the segmented detector for neutrino interactions and background sources. The fiducial flag equals 0 when there is no activity in the detector within 8 cm (5 cells) of the detector edges. This requirement reduces neutrino efficiency by ~30%, but eliminates ~99.5% of the cosmic ray muon background.

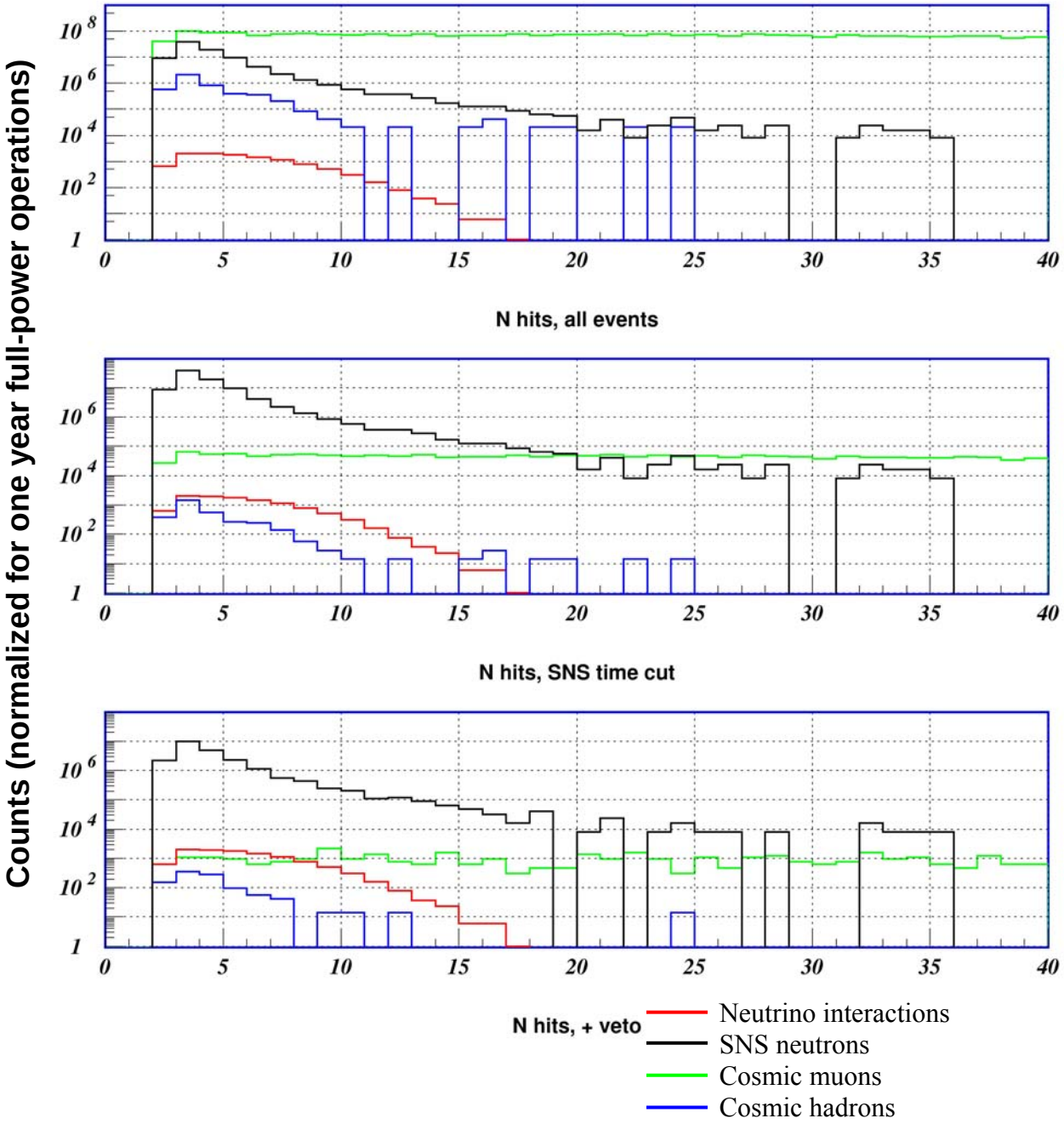

Figure 4.26 Distribution of the number of hits in the segmented detector for neutrino interactions and background sources after successive background cuts are applied. All panels show properly normalized number of events in the detector from neutrino and background interactions for one year of operation at full SNS power. In the upper panel no cuts are made. In the middle panel only events within 10 μs of the proton hitting the spallation target are shown. In the lower panel only events with no activity in the veto are allowed.

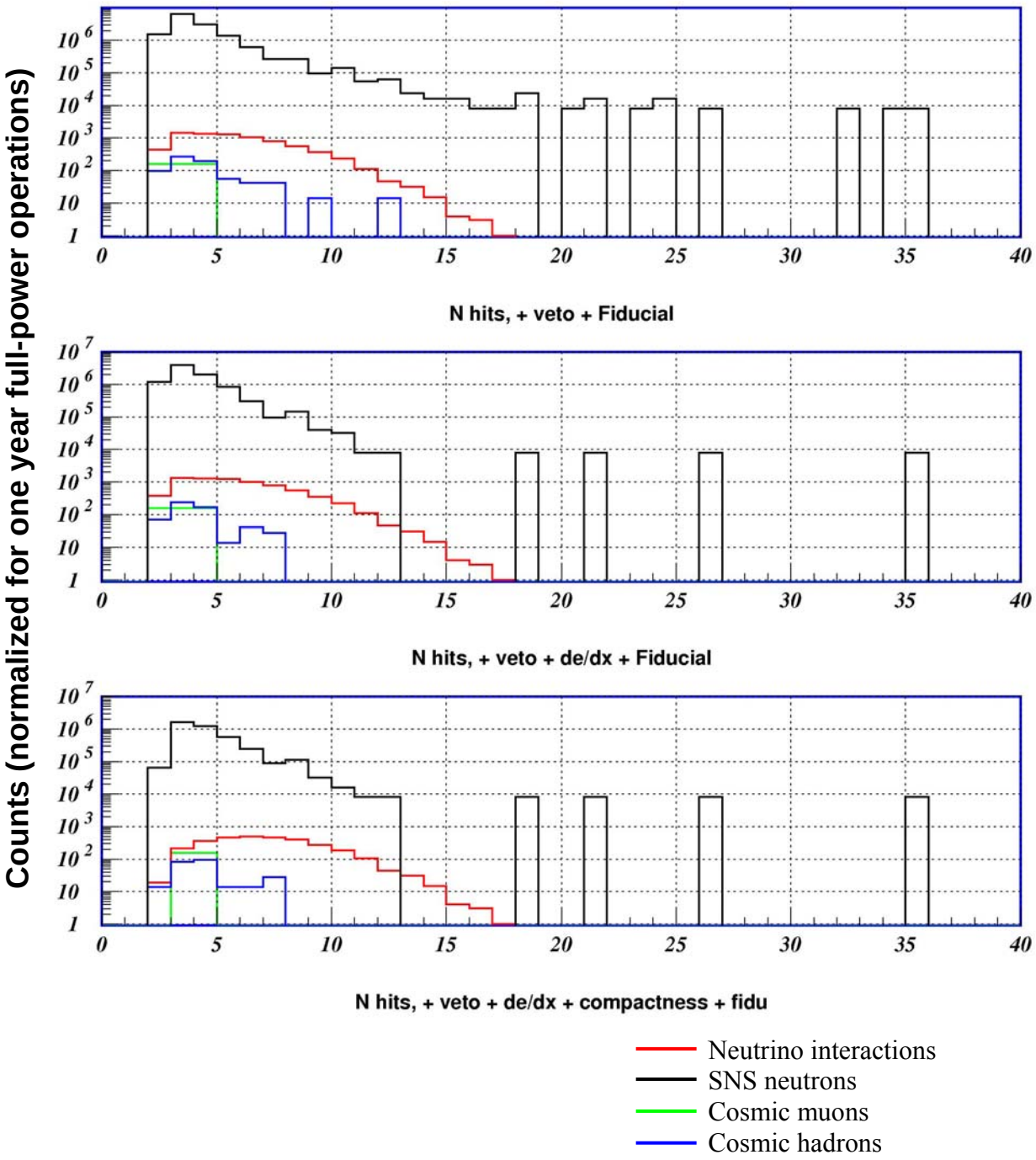

Figure 4.27 Distribution of number of hits in the detector after successive background cuts are applied (in addition to those in Figure 4.26). All panels show properly normalized number of events in the detector from neutrino and background interactions for one year of operations at full SNS power. In the upper panel the fiducial flag is required to be 0. The middle panel includes a cut requiring the average energy deposition per cell be less then 10 keV. The bottom panel includes an additional cut on the track compactness (< 50). The neutrino efficiency after these cuts is 57%.

The lower panel in Figure 4.27 shows the number of hits in the detector after all cuts have been made. One can see that after applying these cuts, SNS neutrons are the only remaining appreciable background source. We note here that this is an initial investigation of the detector response, and we expect to achieve better background rejection when more sophisticated algorithms are developed.

Figure 4.28 shows the energy spectrum of the SNS neutrons which survive the background cuts applied above. One can see that neutrons near 100 MeV are the most significant, and these are slow to arrive at the detector relative to the neutrinos. To further reduce potentially dangerous neutron background, more accurate time information from the detector together with SNS beam time structure is crucial. In Figure 4.29 the expected time distribution of the SNS neutron events is compared to that of neutrino events from pion decay and muon decay. The neutron background becomes negligible about 1100 ns after the beginning of the beam spill, thus making an essentially background-free window in which to study neutrino interactions caused by sum of neutral- and charged-current interactions. In Figure 4.30 the final hit number distribution after time cut has been applied is shown. No background from neutrons can be seen.

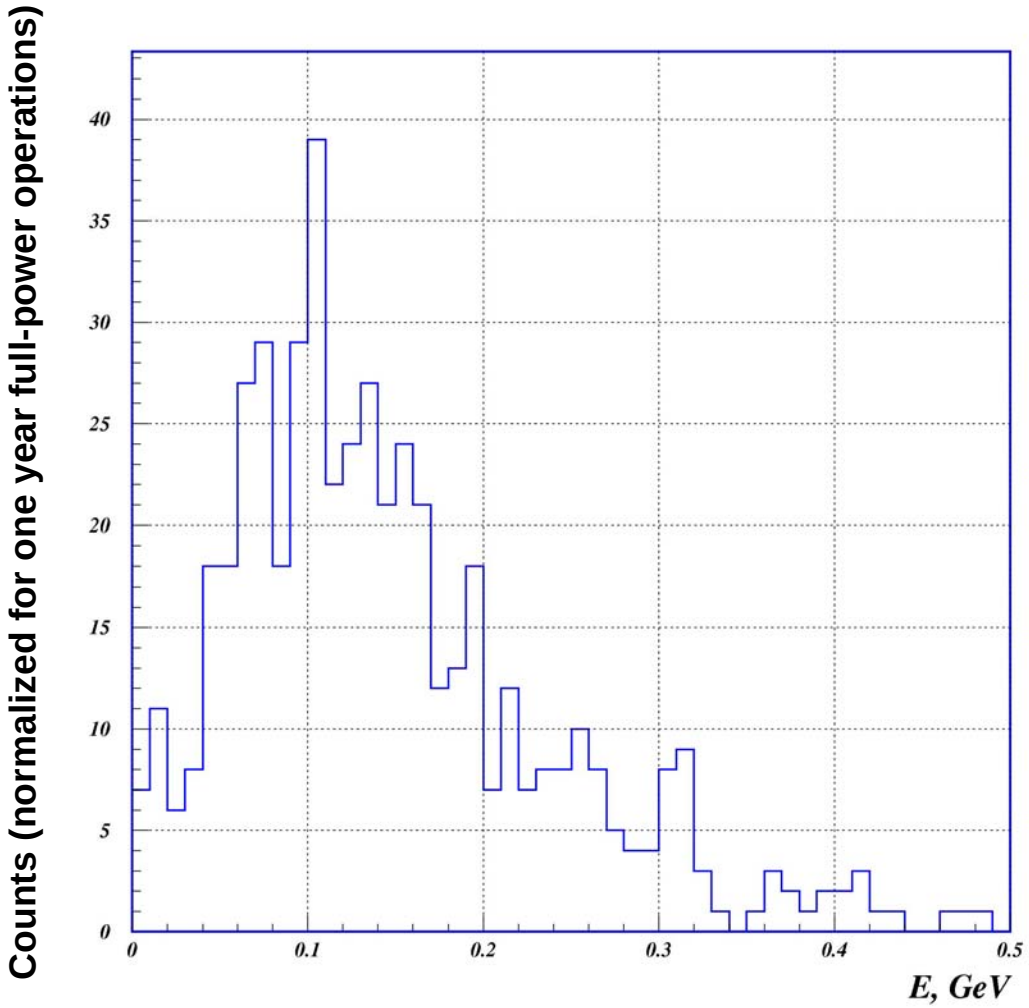

Figure 4.28 Energy spectrum (in GeV) of SNS neutrons that survive all cuts and appear in the segmented detector as a neutrino signal.

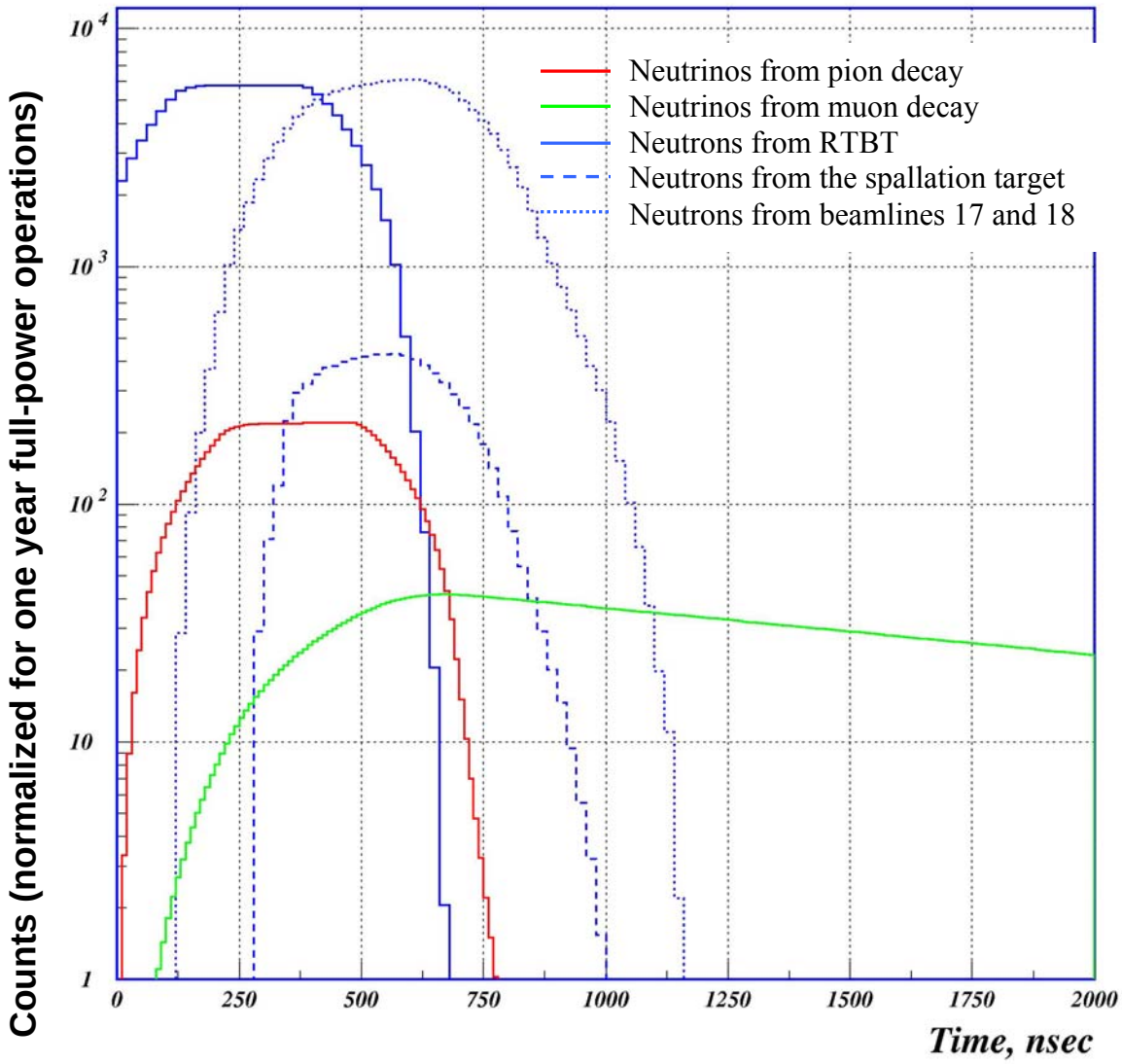

Figure 4.29 Arrival time relative to the proton pulse for neutrino signals from pion decay (red), muon decay (green) and the three sources of SNS neutrino backgrounds (blue, three linestyles).

Furthermore, the neutron background flux originating in the spallation target and in beamlines 17 and 18 is negligible until several tens of nanoseconds after the spallation pulse, perhaps allowing pure neutral-current interactions to be studied at the very beginning of the spill when pion-decay neutrinos dominate muon-decay neutrinos. Unfortunately, the present estimate for neutron background due to the beam losses (which can arrive earlier than the spallation pulse) is too high to permit this. The contribution from these neutrons is shown in Figure 4.29 by the solid blue contour. Future improvements in the SNS facility operation by reduction of proton beam losses in the RTBT could significantly reduce this background, making pure neutral-current measurements possible for a detector with a time resolution of 10-20 ns. Future R&D and better understanding of real backgrounds at SNS will allow us to determine the feasibility of this unique opportunity to study pure neutral-current interactions.

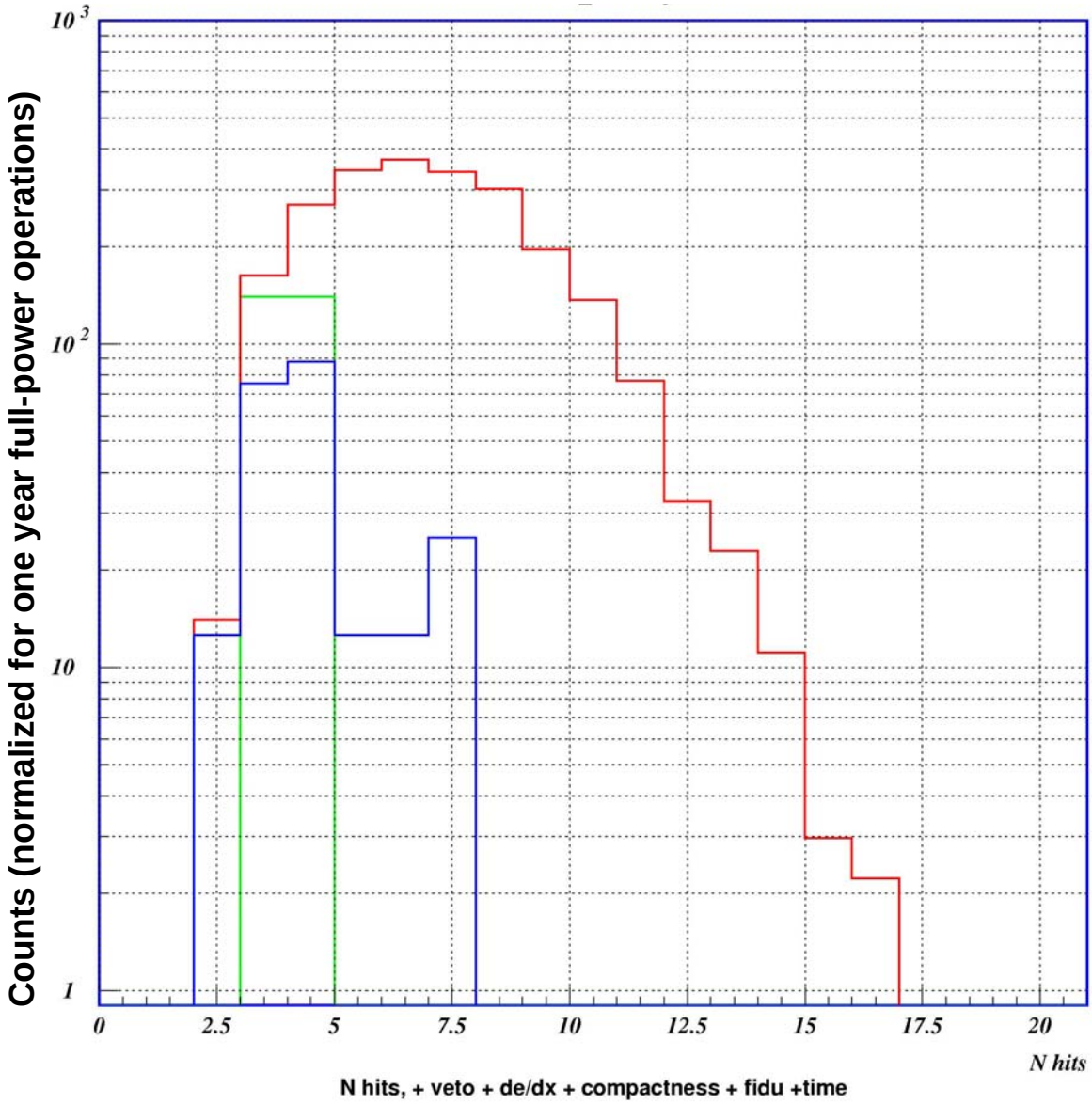

Figure 4.30 Distribution of number of hits in the detector after all background cuts are applied. This is the same as Figure 4.27 with the addition of a cut on the arrival time of the event, $\tau > 1.2$ μs. Neutrino efficiency after all cuts is 43%.

In conclusion, Monte Carlo studies show that a reasonable design of the target geometry would consist of 8 mm diameter cells with a target wall thickness of 0.75 mm. An iron target with a 10 ton fiducial mass would be 1.84 × 1.84 × 2.84 m^3. The total target/detector volume should include an additional 8 cm beyond this fiducial volume to ensure that accepted events are totally contained. This results in a size of 2.0 × 2.0 × 3.0 m^3 and a total of 14,200 3.0 m long detector tubes. For an iron target with 10 ton fiducial mass, at a mean distance of 20 m from the SNS spallation target, and assuming an expected cross section of ~2.5 × 10^{-40} cm^2, the neutrino interaction rate is 46 per day. We estimate a detector efficiency of ~30% (including all detector-specific cuts and also allowing for 10% deadtime in the cosmic veto system) leading to a signal rate of ~15 events per day or about 3000 events per year. For neutrinos from muon decay (a mixture of charged- and neutral-current events) a variety of data selection criteria can be applied, yielding a sample with good efficiency that is effectively background-free.

4.4.4 Assembly and Construction

We envision a detector assembled out of sequential layers of sensitive gas volumes and corrugated target plates.

The straws will be purchased from a commercial vendor. They are made of metallized mylar with walls 50-100 μm thick, 15 mm in diameter, and 150 cm in length. The straws are double layers of over-wound material to seal the seams, as shown in Figure 4.31.

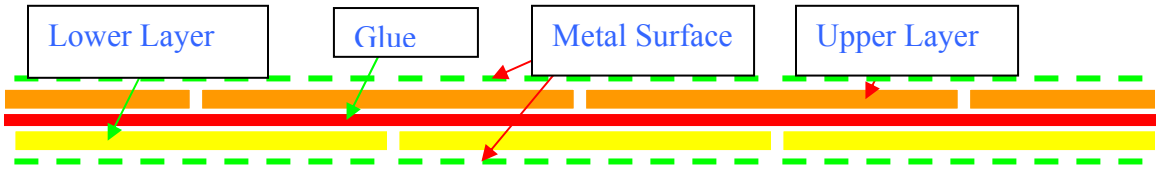

Figure 4.31 This shows the construction of a strawtube wall. A ribbon of this material is helically wound into a tube to form the cathode and the gas volume for individual detector cells.

Collaboration members will be responsible for strawtube assembly, see the cut-away view of the end of a straw shown in Figure 4.32. Two straws are joined with a wire support; end-plugs and feed-throughs are installed into the ends of the straws; and wires are strung and tensioned. Wires are held in place with a retaining pin and a sleeve over the straw (the sleeve is not shown). Gas input and output are through holes in the feedthrough.

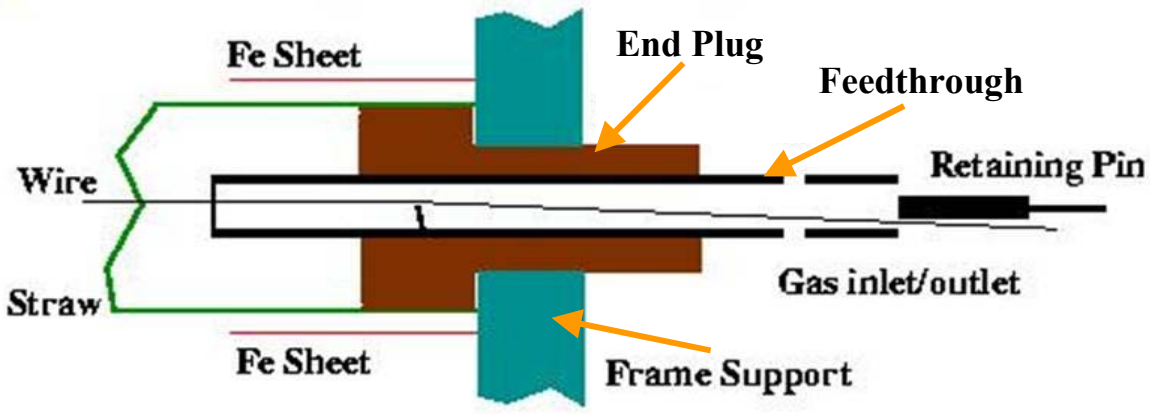

Figure 4.32 Cut-away view of a strawtube end. End plugs (brown) and feed-throughs are inserted into the commercially available straw. After being strung and tensioned the wire is held in place with a retaining pin. A sleeve around the straw (not shown) adds further tension between the straw and the retaining pin. The completed assembly is then installed inside a steel frame (teal) which relieves the wire tension and holds together each independent detector layer.

One layer's strawtubes (~150) will be inserted into a steel frame that serves to position the strawtubes, relieve the wire tension, and hold the target material. See the end view of the detector shown in Figure 4.33. A total of ~150 frames are required. Front-end electronics (pre-amplifiers and high-voltage distribution) are mounted directly on the frames to make each layer an independent unit. The layers are stacked and the entire detector is then placed inside a gas-tight volume, thus eliminating gas connections for individual tubes and gas leakage concerns. This arrangement also greatly simplifies re-assembly for a change in target material.

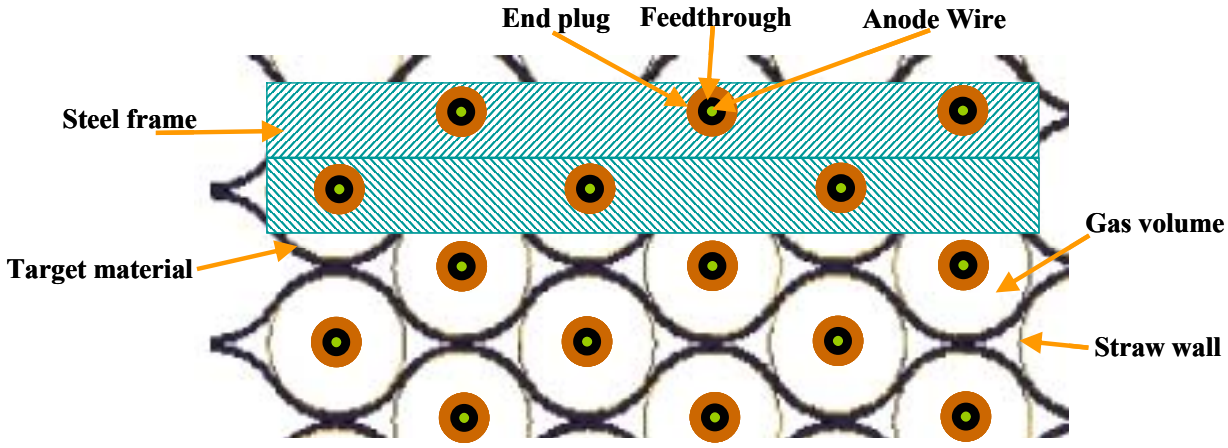

Figure 4.33 A schematic cross section of the segmented detector showing the straws, feedthroughs, corrugated sheets, and two layers of the detector frame.

Sense wires are held at high voltage and cathode planes at ground potential. Although this requires a blocking capacitor for each readout channel, operating the wires at voltage prevents large current discharge through a sense wire if a spark occurs. We assume charge division in order to obtain 3-dimensional information for each hit. We intend to use a fast gas such as CF_4, which has a drift velocity of ~9.5 cm/μs, giving a maximum drift time of 79 ns for a 15 mm diameter straw.

The readout from each strawtube must have amplitude and timing information from both ends, giving ~30,000 channels of ADC and TDC information. Thus we need to minimize the per-channel costs of our front-end electronics. Commercial solutions would be prohibitively expensive, but the relatively small scale of the project makes development of specially designed electronics unfeasible. Thus we intend to benefit from electronic developments in strawtube readout by the BTeV and MECO collaborations. In particular, MECO will have designed pre-amplifier and digitizing ASICs which will be applicable to our needs, and these should be available to us for a few dollars per channel.

Table 4.4 shows the expected data rates for the segmented detector at full SNS power, assuming that the data acquisition is live only for a 20 μs window centered on the spallation pulse and is triggered by events having more than two contiguous hits. The result is a total data flow of 0.6 Gbytes/day, and is quite modest by modern standards.

Table 4.4 Expected data rates for the segmented detector at full SNS power. These numbers assume 10 bytes per cell (two bytes of cell location and two bytes/side each of ADC and TDC information).

Source	Events/sec	Avg. # of cells	Bytes/sec
Neutrinos	0.0005	5.8	0.029
SNS neutrons	147.0	4.7	6909
Cosmic muons	0.14	20.3	28.4
Cosmic neutrons	0.001	4.5	0.005
Total			~7000

There are several possibilities for improving the performance and cost-effectiveness of the segmented detector that we propose to study in our R&D program.

Fast gases, such as CF4, are expensive. It is possible to insert 3 sense wires and 4 field wires within each straw to reduce the system drift time and improve time resolution as shown in Figure 4.34. In this design, all three sensitive wires are connected to the one preamplifier. Signal processing techniques (such as development of a trailing edge detection circuit) may also allow us to achieve the necessary timing resolution without using a fast gas.

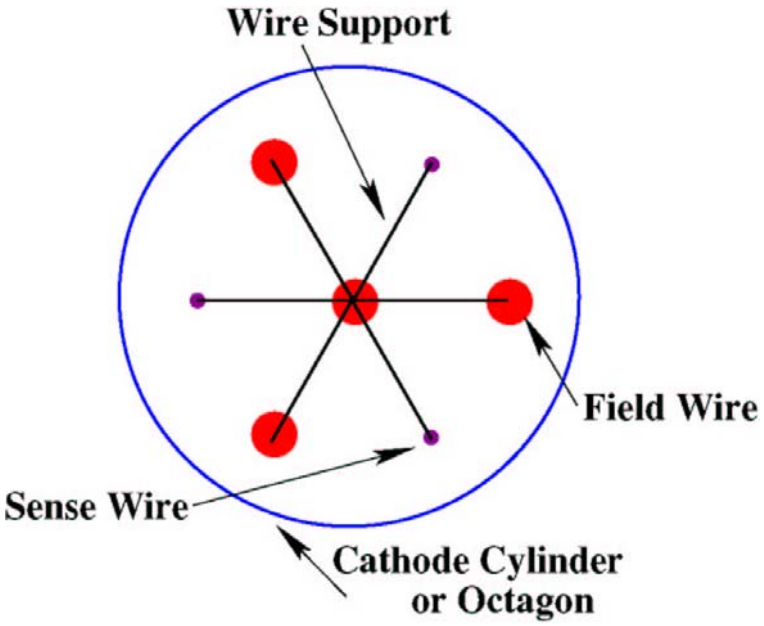

Figure 4.34 Cross section of a multi-anode strawtube design to improve detector timing resolution.

Another possibility for cost savings is multiplexing the data. Data rates are so low that reduction in the number of readout channels by a factor of four is entirely feasible.

Finally, there are other possible geometries for the sensitive detectors and target material; including the possibility of using the target material itself as the cathode (and eliminating the need for straws) and using planar arrays of target and drift chambers. These need to be examined for ease of assembly, disassembly, and performance (timing and energy resolution).

4.4.5 Cost Estimate

The cost drivers for the segmented detector are the straw tube assemblies and the readout electronics. We obtained a cost estimate for the strawtubes from Lamina Dielectrics, Ltd. The electronics estimate is based on experience with the MECO electronics that we will adapt for **ν-SNS.** We include sufficient spare quantities, the initial iron target sheets, high-voltage and gas systems, and incorporate appropriate contingency.

Costs, (including overheads and contingency) and estimated labor hours are shown in Table 4.5.

Table 4.5 Cost breakdown for the segmented detector.

WBS #	Title	Cost w/o Contingency	Contingency	Total	Contingency Fraction	Labor Hours
1.3	**Segmented Detector**	**$1,154,859**	**$426,785**	**$1,581,644**	**37%**	**10,930**
1.3.1	**Design SD**	**$106,775**	**$27,762**	**$134,537**	**26%**	**3,290**
	Simulation + prototyping - Physicist	$0	$0	$0	0%	400
	Design drawings - Engineer	$18,225	$4,739	$22,964	26%	270
	Equipment Specs. - Engineer	$12,150	$3,159	$15,309	26%	180
	QC Process - Engineer	$2,700	$702	$3,402	26%	40
	Travel	$4,500	$1,170	$5,670	26%	0
	Simulation + prototyping - Grad.Stud.	$0	$0	$0	0%	2,000
	Prototyping - Tech	$19,200	$4,992	$24,192	26%	400
	Prototyping materials	$50,000	$13,000	$63,000	26%	0
1.3.2	**Procure SD**	**$882,584**	**$353,034**	**$1,235,618**	**40%**	**80**
	Travel and cost for Quality Control	$7,500	$3,000	$10,500	40%	0
	Shipping Costs	$22,500	$9,000	$31,500	40%	0
	Electronics and Cables	$350,000	$140,000	$490,000	40%	0
	Straw tubes	$163,584	$65,434	$229,018	40%	0
	Gas and HV system	$44,000	$17,600	$61,600	40%	0
	Mounting and Readout equipment	$228,000	$91,200	$319,200	40%	0
	Wires	$67,000	$26,800	$93,800	40%	0
	Quality control - Physicist	$0	$0	$0	0%	80
1.3.3	**Assemble and Test SD**	**$135,900**	**$35,334**	**$171,234**	**26%**	**6,000**
	Assembly Benches	$10,000	$2,600	$12,600	26%	0
	Assembly - Technician	$38,400	$9,984	$48,384	26%	800
	Quality Control Setup	$5,000	$1,300	$6,300	26%	0
	Quality Control - Graduate student	$0	$0	$0	0%	1,000
	Module Shipping	$22,500	$5,850	$28,350	26%	0
	Supervision - Physicist	$0	$0	$0	0%	200
	Undergraduate Student Help	$60,000	$15,600	$75,600	26%	4,000

WBS #	Title	Cost w/o Contingency	Contingency	Total	Contingency Fraction	Labor Hours
1.3.4	**Install SD**	**$29,600**	**$10,656**	**$40,256**	**36%**	**1,560**
	Mounting Materials	$20,000	$7,200	$27,200	36%	0
	Mounting - Technician	$9,600	$3,456	$13,056	36%	200
	Supervision - Physicist	$0	$0	$0	0%	360
	Grad. Stud.	$0	$0	$0	0%	1,000

4.5 Homogeneous Detector

4.5.1 Requirements

The homogeneous detector will be a flexible universal detector in which neutrino interactions with a variety of liquid targets can be studied. To achieve this, the detector must:

- Contain at least ten fiducial tons of liquid target material and fit inside the fixed shielding volume.
- Have the capability to easily replace targets without rebuilding the sensitive part of the detector.
- Have relatively good time resolution (few ns) to facilitate operation in the SNS background environment.
- Have good energy and angular resolution, even with non-scintillating target materials, in order to allow differential cross section measurements.
- Have sufficient pixellation to allow for electron identification through detection of the Cherenkov ring in the presence of scintillating light.
- Be affordable.

4.5.2 Approach

The homogeneous detector consists of a $3.5 \times 3.5 \times 3.5$ m^3 steel vessel with 600 8" photomultiplier tubes (PMTs) mounted on the inner walls, to provide approximately 41% photocathode coverage. A schematic drawing of the detector is shown in Figure 4.35 below. The actual distribution and orientation of the PMTs will be optimized using Monte Carlo simulations. It is expected that at least the edge and corner PMTs should be angled such that the light collection efficiency is maximized. The 41% surface coverage allows the detector to have good event reconstruction and particle identification when operating with a variety of fluids as active media (*e.g.*, mineral oil, water, heavy water) independent of the amount of scintillator doping (*i.e.*, operation as a pure Cherenkov imaging detector).

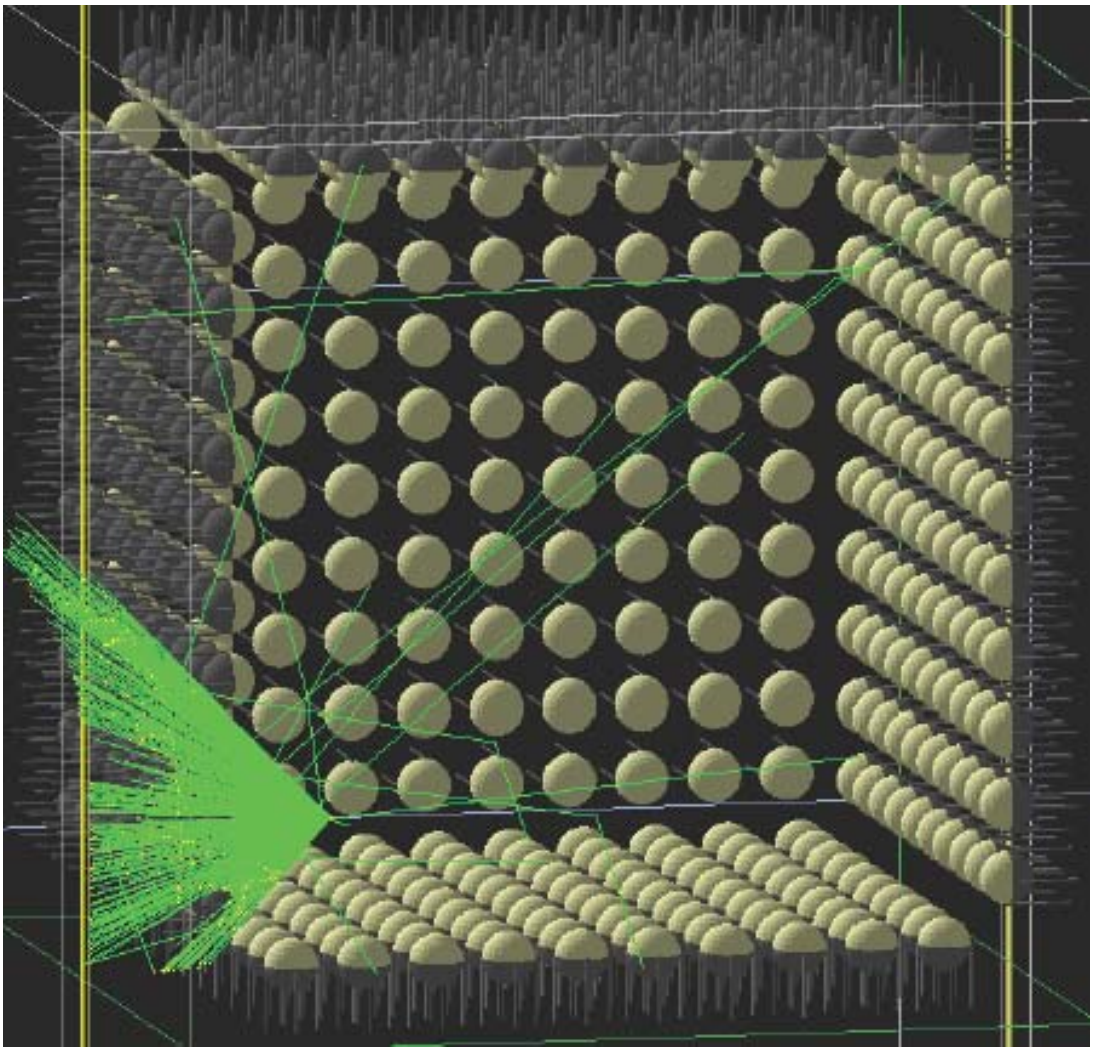

Figure 4.35 Schematic view (GEANT) of the **ν-SNS** homogeneous detector showing response to a 1.5 MeV electron. The beige surfaces show the active area of the photocathodes. The front wall and its PMTs, have been removed for clarity.

A candidate for the PMTs to be used in this detector is the Hamamatsu R5912, which is currently successfully used in a variety of experiments, such as the MiniBooNE experiment (E-889) at Fermilab. This PMT has reasonably good single photoelectron (PE) charge and time response resolutions ($\sigma_q \approx 0.6$ PE and $\sigma_t \approx 1.2$ ns respectively), as we illustrate in Figure 4.36, below. These distributions have been obtained *in situ* from the low-intensity laser calibration runs in MiniBooNE.

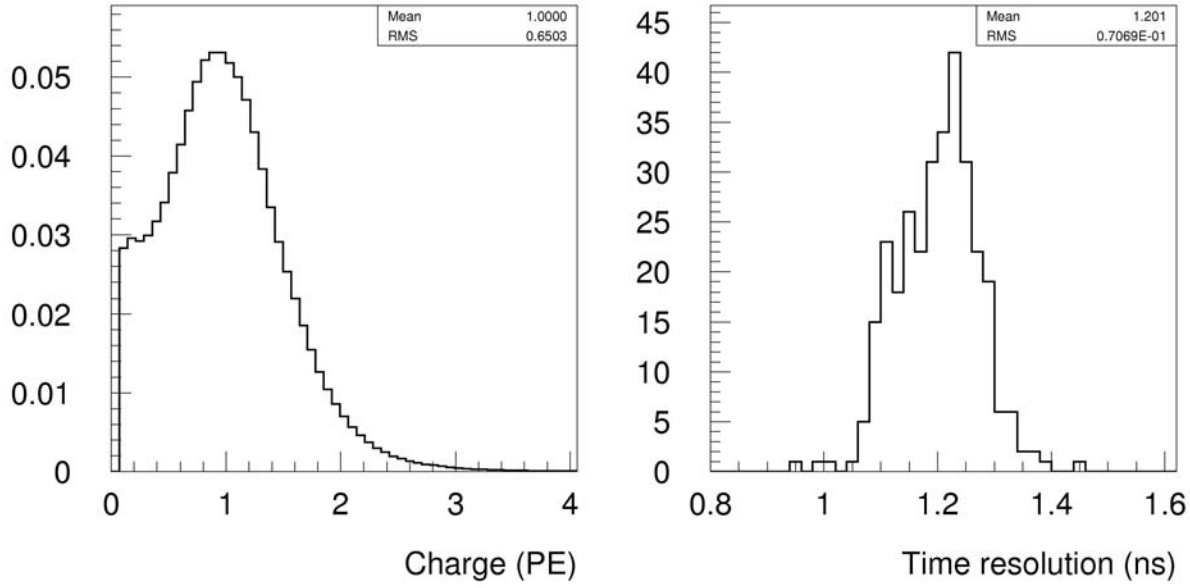

Figure 4.36 Single PE charge response (left) and time resolution distribution (right) for the 340 MiniBooNE Hamamatsu R5912 PMTs.

The *in situ* calibration of the PMTs (gains, time offsets and slewing) will be performed using a system similar to that used in MiniBooNE and its precursor, the Liquid Scintillator Neutrino Detector (LSND). An external laser of tunable wavelength delivers short light pulses through an optical fiber to a flask inside the tank, which scatters light isotropically. In contrast to LSND and MiniBooNE which used 3 and 4 flasks, respectively, at fixed positions in the detector, we will use a single flask, movable in a controlled manner throughout the active region of the tank. The energy calibration of the detector is easily performed using Michel electrons from the decays of stopped cosmic-ray muons, with an endpoint energy of 52.8 MeV. In addition, provision will be made for deployment of radioactive sources in the tank for calibration at lower energies, and for testing the accuracy of the reconstruction algorithms.

The data acquisition (DAQ) for the homogeneous detector is based on the robust and well-tested design used in LSND and MiniBooNE, running at 10 MHz. While this rate is too slow to record PMT anode pulses directly, a "QT board" converts these pulses into slower varying signals which still contain the necessary charge and time information. The anode signal feeds an integrating capacitor with a time constant of ~1200 ns. The voltage V_q across the capacitor is digitized every 100 ns, in step with the 10 MHz clock. If the pulse is large enough to fire an on-board discriminator (set typically to about 0.10-0.25 PE), a separate voltage V_t begins ramping linearly away from the baseline. The ramp continues until two clock ticks have passed, at which point it is rapidly reset to the baseline. V_t is also digitized every 100 ns. The DAQ software looks

continuously at the stream of digitized V_q and V_t numbers coming from each channel and, if the discriminator has fired, it records a set of four V_q and V_t values: one before the discriminator fired and three after. This process is illustrated schematically in Figure 4.37. The actual charge and time reconstruction of the hit is performed at a higher level in the software, using the recorded V_q and V_t "quads".

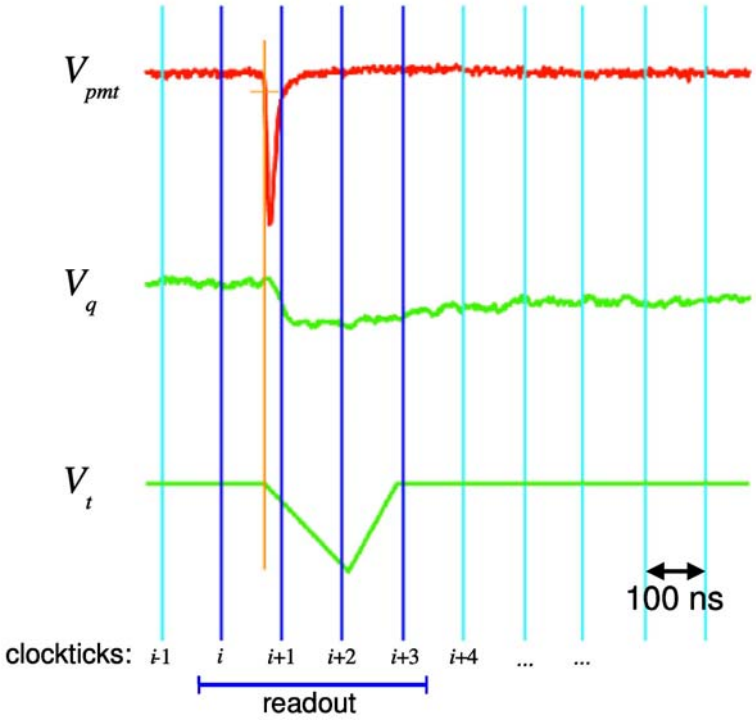

Figure 4.37 Schematic pulses in the MiniBooNE front-end electronics: V_{pmt} is the incoming anode signal and V_q is its integral convoluted with an exponential decay. The vertical orange line indicates the firing of the discriminator which starts the time ramp V_t and is reset after two clock ticks. For this hit the DAQ records the four V_q and V_t values digitized at i, i+1, i+2, and i+3.

Considering the low duty factor of the SNS beam, the DAQ system is triggered simply by a precursor signal from the accelerator. The circular buffers are large enough to hold and write all detector data in a time window of greater than 20 μs around the 0.6 μs beam spill. During this time window we record sufficient beam-off data for both detector studies and for beam on/off subtraction. In addition, special purpose triggers will be used for control data sample recording (*e.g.*, laser calibration, Michel electrons, etc.).

4.5.3 Simulated Detector Performance

From experience with the LSND and MiniBooNE detectors and the configuration of this apparatus, we expect an energy resolution of approximately 5-7% at 53 MeV (depending on the light per MeV collected in a particular active medium), a spatial position resolution of about 15-20 cm, and an angular resolution of approximately 3-5°. Event reconstruction and particle identification will be based on the maximum likelihood techniques developed for the final LSND and MiniBooNE analyses. The parameters necessary for these techniques (such as charge and time likelihoods, attenuation lengths, PMT quantum efficiencies, etc.) can be determined directly

from control samples recorded during the beam off periods, such as Michel electrons from stopped cosmic-ray muon decays, cosmic-ray neutrons, etc. These samples provide excellent checks of the reconstruction and particle identification performance, largely independent of the Monte Carlo simulations.

Preliminary GEANT simulations of the homogeneous detector with the standard PMT configuration and pure mineral oil as active medium yield the hit multiplicity and total visible charge distributions as shown in Figure 4.38 below. The electron events used in this study, similar to those from the $\nu_e + C \rightarrow e^- + X$ charged current reaction in mineral oil, have been generated within the fiducial volume, and give rise to an average recorded signal of 28 PE/MeV and an energy resolution of 6.3% at 50 MeV, see Figure 4.39. This result, consistent with our initial estimates, was obtained using the Hamamatsu R5912 single PE charge response function illustrated in Figure 4.36, as measured in MiniBooNE.

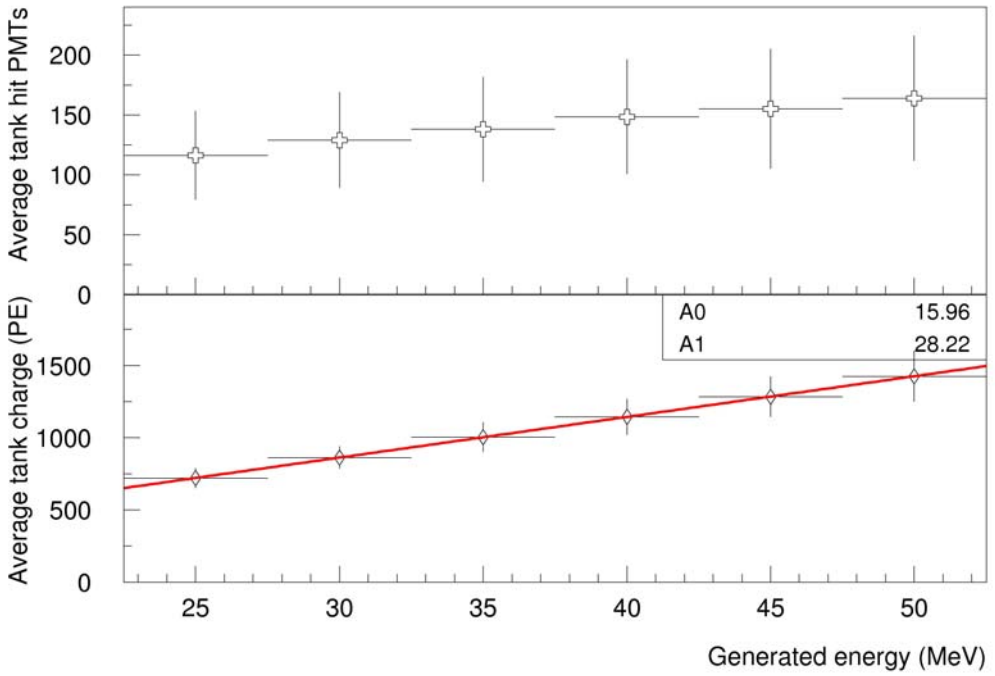

Figure 4.38 Average hit multiplicity and total visible charge as a function of the generated energy for electrons in mineral oil.

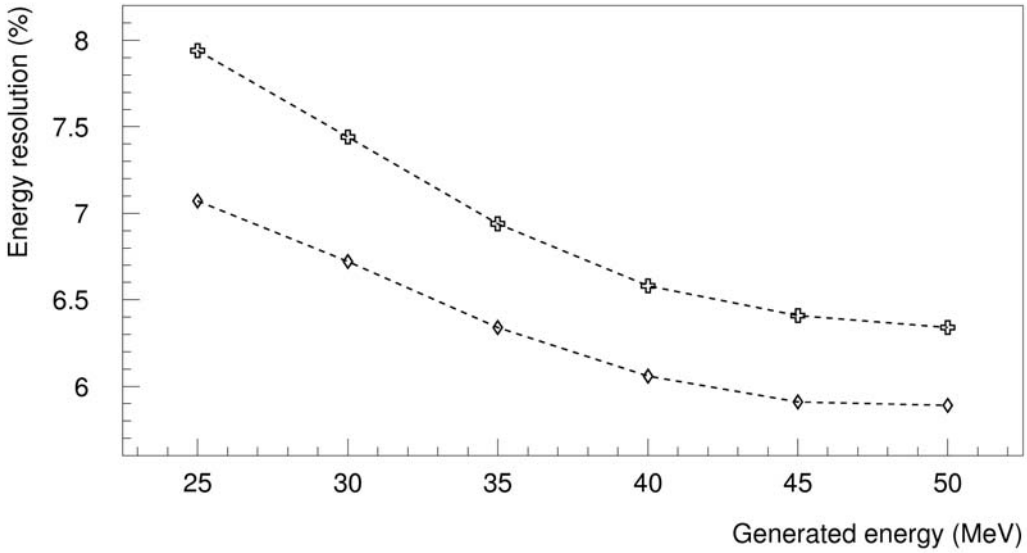

Figure 4.39 Energy resolution as a function of the generated energy for electrons in mineral oil. The lower curve represents the energy resolution obtained after position corrections, as described in the text.

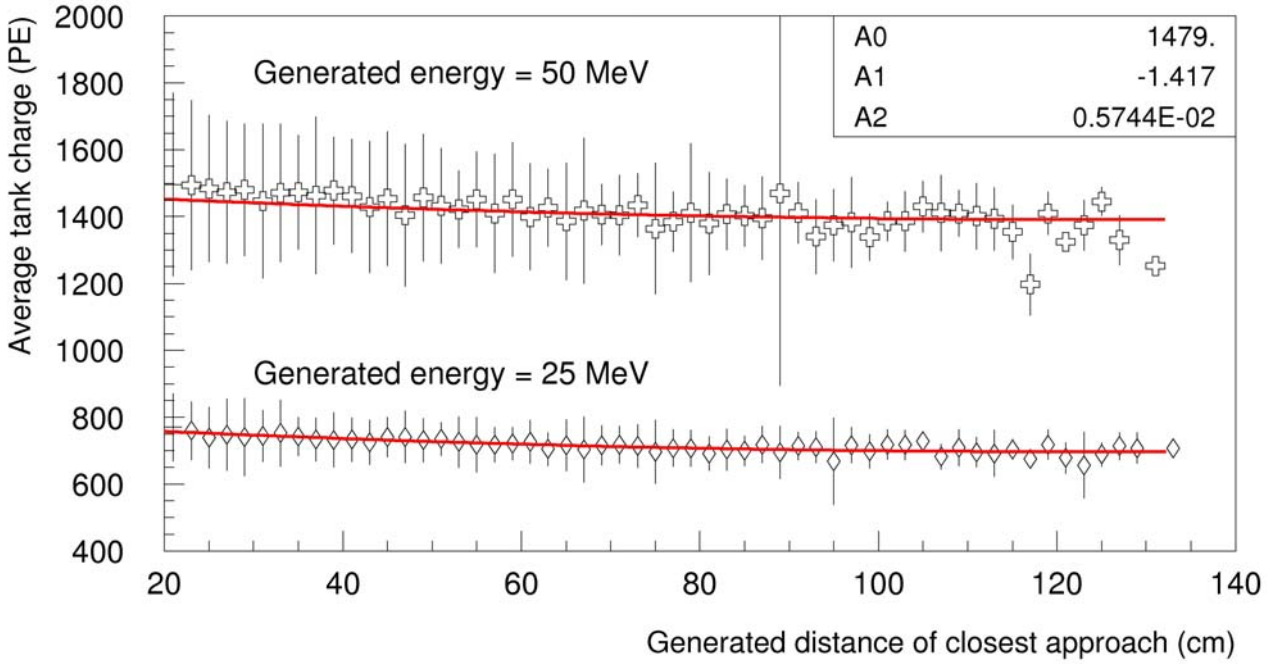

Figure 4.40 Average total charge versus distance of closest approach to the surface of the PMTs for two generated electron energies.

The visible light signal recorded in the homogeneous detector is dependent on the location and direction of the event. This is due to the fact that the light detected in a particular event is proportional to the total solid angle spanned by the PMTs as viewed from that particular location, folded with attenuation length and angular response function. To illustrate this point, we show in Figure 4.40 the average recorded charge for two event energies, 25 and 50 MeV, as a function of the distance of closest approach to the surface of the PMTs. The variation is fitted to a second order polynomial, and when this correction is applied to the total visible charge, energy resolution is improved throughout the energy range considered in this study, as shown in Figure 4.39. At 50 MeV the energy resolution becomes 5.9%, a 7% improvement over the uncorrected result. We anticipate that when using a maximum likelihood fit to determine the strength of the light source (as it is currently done in MiniBooNE), the energy resolution will be improved further.

Several GEANT simulations have also been performed for the homogeneous detector with water as active medium. Preliminary analysis shows that the expected light levels in water are similar to those expected in pure mineral oil, as illustrated in Figure 4.41. The average amount of recorded light is approximately 27 PE/MeV. Consequently, the energy resolution is similar to that obtained in mineral oil. Indeed, as illustrated in Figure 4.42, the energy resolution at 50 MeV is 6.5%, when calculated simply from the total visible charge, without corrections for the event location.

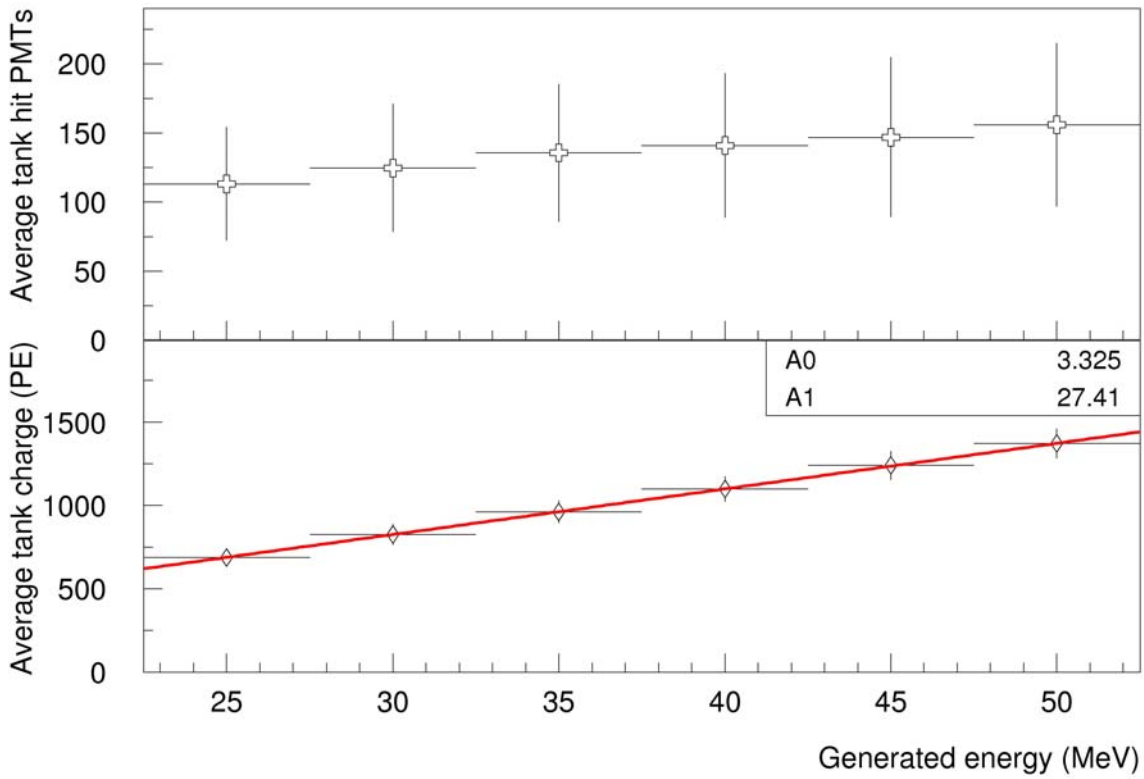

Figure 4.41 Average hit multiplicity and visible charge as a function of the generated energy for electrons in water. Only events generated in the $d > 25$ cm fiducial volume have been considered in this study.

The simulations used in the above studies show that the standard PMT distribution (uniform coverage and PMT orientation normal to the detector inner surfaces) is not ideal for light collection. This is shown explicitly in Figure 4.43, in which we illustrate the relative light collection for the PMTs on one of the detector sides for uniform illumination of the detector volume (as will be the case for neutrino interactions). The corner PMTs have lower light collection, partially due to small average solid angle, but partially due to non-ideal PMT orientation. Tilting the PMTs to point to the geometrical center of the detector offers a possibility to enhance the overall light collection. We plan to investigate a variety of PMT arrangement schemes (both with respect to distribution and orientation) to maximize not only the light collection efficiency, but also the accuracy of position, direction and energy reconstruction.

Each event will be reconstructed under an electron and under a neutron hypothesis, and the ratio of the two likelihoods will serve as a primary particle identification variable. In addition, variables obtained from the maximum likelihood reconstruction under the two hypotheses can be used as input into more powerful discriminants, such as artificial neural networks or boosted decision trees. At this time neutron simulations have not been performed for the homogeneous detector. However, from experience with LSND and MiniBooNE, we expect to be able to effectively reduce neutron background events by a factor of 10^2-10^3. This reduction is comparable to current expectations for the segmented detector, as detailed in the previous subsection. There it is shown that the reduction is good enough to allow clean neutrino identification starting ~1 μs after the spallation pulse start.

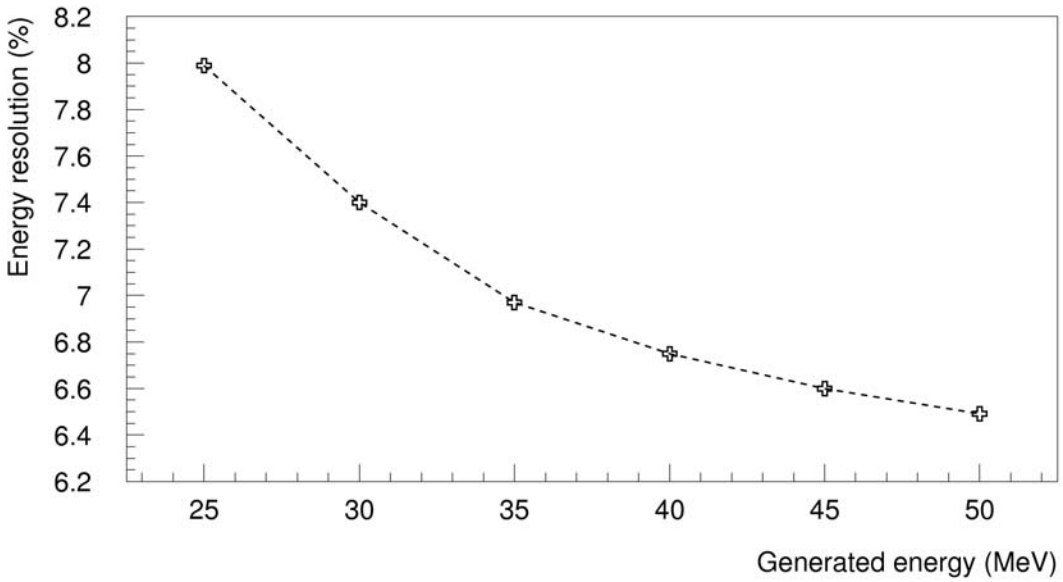

Figure 4.42 Energy resolution as a function of the generated energy for electrons in water. No position-dependent corrections have been applied.

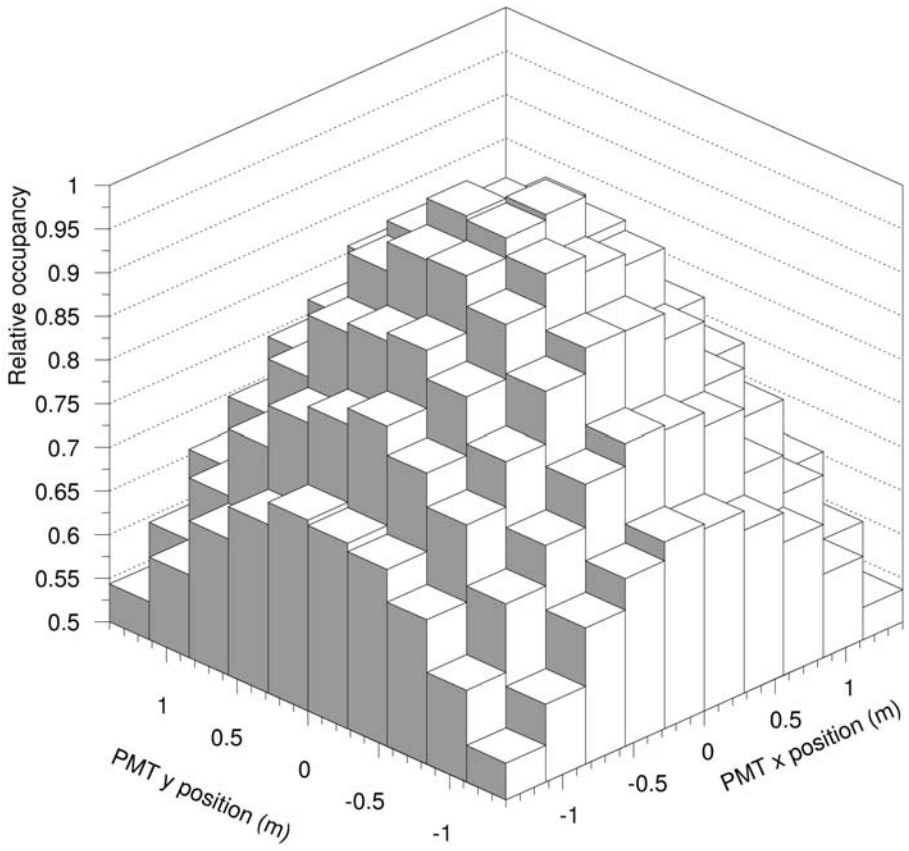

Figure 4.43 Relative PMT light collection as a function of position along one detector face.

Assuming a neutrino flux of 2×10^7 ν/s/cm^2 for each neutrino flavor at the detector location, the event rate for mineral oil, which is mostly C_nH_{2n+2} with $n \approx 20$, yields 180 events/yr/m^3 for the charged-current $\nu_e C$ reaction alone. We have used $\sigma = 9.3 \times 10^{-42}$ cm^2 for transition to the ground state, $\nu_e C \rightarrow e^- N_{gs}$, and $\sigma = 5.1 \times 10^{-42}$ cm^2 for transition to excited states, $\nu_e C \rightarrow e^- N^*$, where both cross sections have been averaged over the incident ν_e decay-at-rest energy spectrum [17]. The mineral oil density was taken to be $\rho = 0.85$ g/cm^3, yielding 3.66×10^{28} carbon atoms per cubic meter of mineral oil. The event rate quoted above contains no corrections for electron detection and identification efficiencies, and assumes that the accelerator runs 200 days per year with 95% live-time. The volume defined by the surface of the PMTs represents 24.4 m^3 out of the total volume of 42.9 m^3. Assuming a fiducial volume that extends to only 20 cm from the PMT faces yields 15.5 m^3, which in turn implies 2,800 $\nu_e C$ events per year before any detection and reconstruction efficiencies are applied. We expect that an efficiency of 40% (including a time cut to eliminate SNS-backgrounds near the spallation pulse and a 10% cosmic-veto deadtime) can be easily achieved with such a detector in the SNS environment, and thus the effective $\nu_e C$ event rate is expected to be about 1,260 events/year. From the above considerations it is obvious that the size of the fiducial volume of the homogeneous detector is an essential factor in obtaining reasonable event rates. Therefore, we shall continue to investigate less intrusive PMTs as well as other compact photosensors as alternatives to the proposed Hamamatsu R5912 phototubes.

4.5.4 Assembly and Construction

Assembly and installation will be similar to well-tested procedures developed in LSND and MiniBooNE. PMTs with attached cables will be pre-tested at the University of Alabama and shipped to the SNS. There they will be installed into holding frames which attach to fixtures welded onto the steel tank. Installation of the tank, HV and plumbing systems will be performed by SNS technicians or qualified subcontractors

4.5.5 Cost Estimate

Our cost estimate for the homogeneous detector is dominated by the cost of the PMTs and electronics, which are based on direct experience with LSND and MiniBooNE. Costs for the tank, plumbing and piping and cables were also based on experience with LSND and MiniBoone. We have also incorporated appropriate contingency.

Costs, (including overheads and contingency) and estimated labor hours are shown in Table 4.6.

Table 4.6 Cost breakdown for the homogeneous detector.

WBS #	Title	Cost w/o Contingency	Contingency	Total	Contingency Fraction	Labor Hours
1.4	**Homogeneous Detector**	**$1,189,080**	**$452,381**	**$1,641,461**	**38%**	**5,680**
1.4.1	**Design HD**	**$56,880**	**$14,789**	**$71,669**	**26%**	**1,680**
	Simulation, prototyping (physicist)	$0	$0	$0	0%	200
	Design drawings	$28,440	$7,394	$35,834	26%	240
	Equipment specs	$18,960	$4,930	$23,890	26%	160
	QC Process	$9,480	$2,465	$11,945	26%	80
	Simulation, prototyping (grad. student)	$0	$0	$0	0%	1,000
1.4.2	**Procure HD**	**$1,023,000**	**$409,200**	**$1,432,200**	**40%**	**0**
	Steel tank	$30,000	$12,000	$42,000	40%	0
	Non-reflective paint	$5,000	$2,000	$7,000	40%	0
	PMTs, bases, frames	$678,000	$271,200	$949,200	40%	0
	HV System	$50,000	$20,000	$70,000	40%	0
	Mineral oil, water	$40,000	$16,000	$56,000	40%	0
	Plumbing and pumping systems	$50,000	$20,000	$70,000	40%	0
	Laser calibration system	$30,000	$12,000	$42,000	40%	0
	PMT quality control setup	$10,000	$4,000	$14,000	40%	0
	Optical medium control setup	$10,000	$4,000	$14,000	40%	0
	Electronics	$120,000	$48,000	$168,000	40%	0
1.4.3	**Assemble and Test HD**	**$58,000**	**$15,080**	**$73,080**	**26%**	**3,200**
	Shipping	$20,000	$5,200	$25,200	26%	0
	Supervision (physicist)	$0	$0	$0	0%	800
	PMT testing (undergrads)	$18,000	$4,680	$22,680	26%	1200
	PMT installation (grad. students)	$0	$0	$0	0%	1200
	Travel for mounting	$20,000	$5,200	$25,200	26%	0

WBS #	Title	Cost w/o Contingency	Contingency	Total	Contingency Fraction	Labor Hours
1.4.4	**Install HD**	**$51,200**	**$13,312**	**$64,512**	**26%**	**800**
	Supervision Scientist	$0	$0	$0	0%	160
	Steel Tank Installation	$12,800	$3,328	$16,128	26%	160
	Plumbing System Installation	$12,800	$3,328	$16,128	26%	160
	HV System Installation	$25,600	$6,656	$32,256	26%	320

4.6 Common Data Acquisition System

The **ν-SNS** data acquisition system (DAQ), shown schematically in Figure 4.44, collects and assembles data from the segmented detector, the homogeneous detector, and the cosmic veto detector. It provides the detector front-end electronics with a beam pulse timer and global clocks and is responsible for collecting various slow controls information from *e.g.*, detector configuration registers, power supplies, gas and temperature sensors, and SNS status feedback systems. The DAQ needs to have some expansion capability in order to allow incorporation of information from other detectors (*e.g.*, supernova neutrino detector prototypes) that may take data as a part of the **ν-SNS** scientific program.

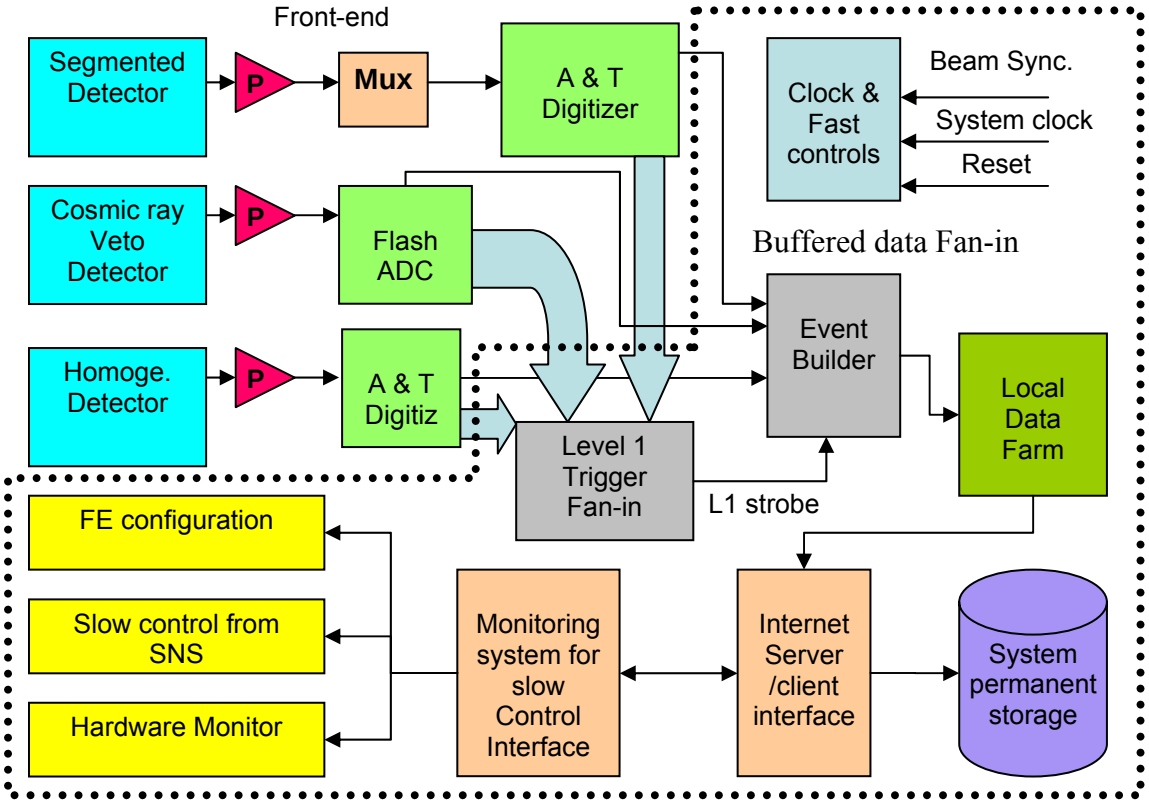

Figure 4.44 Block diagram of the **ν-SNS** front-end electronics (outside the dotted region) and common DAQ (inside the dotted box).

The expected data rates are relatively low, so we anticipate that a few PC-class processors will be sufficient to organize control of the DAQ functions. In addition, we anticipate one electronics rack (environmentally controlled) with several crates housing general function NIM, CAMAC and VME modules for implementation of the level-1 trigger and for data I/O (both event data and slow controls and monitoring). We anticipate a simple trigger algorithm based on hit multiplicity. Several Terabytes of RAID storage provide sufficient disk space to hold all **ν-SNS** data for ten years.

The physical location of the DAQ hardware should be relatively close to the detector to minimize cable lengths. Presently we are considering locations on the roof of the bunker, and on the SNS mezzanine which spans the outer perimeter of the SNS target building at the height of

the roof bunker locations on the floor of the target building. However, the DAQ also has an internet server so operations personnel will be able to monitor the experiment from remote locations.

The DAQ will be designed by physicists, so the project cost is dominated by the cost of the system hardware. The number of modules required is not based on a detailed design, but rather on previous experience. The contingency reflects this, and we feel this is unlikely to be an underestimate. The front-end electronics for detectors (up to and including digitization) are included in the detector cost estimates are not included here.

Costs, (including overheads and contingency) and estimated labor hours are shown in Table 4.7.

Table 4.7 Cost breakdown for the common data acquisition system.

WBS #	Title	Cost w/o Contingency	Contingency	Total	Contingency Fraction	Labor Hours
1.4	**Common DAQ**	**$258,000**	**$64,500**	**$322,500**	**25%**	**3,840**
1.4.1	**Design DAQ**	**$0**	**$0**	**$0**	**0%**	**1,280**
	Design DAQ - Physicist	$0	$0	$0	0%	640
	Design DAQ - Grad. Student	$0	$0	$0	0%	640
1.4.2	**Procure DAQ**	**$258,000**	**$64,500**	**$247,500**	**25%**	**0**
	Rack	$10,000	$2,500	$12,500	25%	0
	VME Crates	$18,000	$4,500	$22,500	25%	0
	I/O registers, memory other VME modules	$135,000	$33,750	$168,750	25%	0
	NIM/CAMAC modules	$30,000	$7,500	$37,500	25%	
	Cables, connectors	$30,000	$7,500	$37,500	25%	
	Computers	$15,000	$3,750	$18,750	25%	0
	3 TB Raid Storage	$20,000	$5,000	$25,000	25%	0
1.4.3	**Assemble and Test DAQ**	**$0**	**$0**	**$0**	**0%**	**2,560**
	Physicist	$0	$0	$0	0%	1,280
	Grad. Student	$0	$0	$0	0%	1,280

4.7 Measurement Precision

In order to make *precise* neutrino-nucleus cross section measurements both statistical and systematic errors must be minimized. As described in the previous subsections the combination of SNS time structure, passive shielding and active veto allows us to make measurements that are largely background free. As a result the statistical accuracy is well-defined by the number of signal counts. Table 4.8 shows the expected statistical significance for several targets for one year of operation at full SNS power.

Table 4.8 Expected statistical significance for charged-current measurements in possible **ν-SNS** targets in one year of operation at full SNS power (neutrino flux = 0.8×10^7 ν/cm^2/s).

Target	Assumed Cross Section (10^{-40} cm^2)		# Target Nuclei	Raw Counts	Assumed Efficiency	Statistical Significance
Segmented Detector (10 ton fiducial mass)						
Iron	2.5	[17]	1.1×10^{29}	3,200	35%	3.0%
Lead	41.0	[20]	2.9×10^{28}	14,000	35%	<1.4%
Aluminum	1.12	[21]	2.2×10^{29}	3,100	35%	3.0%
Homogeneous Detector (15.5 m^3 fiducial volume)						
Carbon	0.144	[17]	5.6×10^{29}	1,000	40%	5.0%
Oxygen	0.08	[22]	4.6×10^{29}	450	40%	7.4%

In order to determine cross sections we also need to determine the efficiency of our detectors and the incoming neutrino flux (which we cannot measure directly, but which is determined by the incoming proton flux and by pion production in a thick mercury target). We will have an abundant source of Michel electrons from decays of stopped muons which we can easily tag with the veto system and detector information. These electrons have an energy range which closely matches the energy range of leptons from neutrino interactions and we will collect enough of them to determine our efficiency arbitrarily well. The proton flux will be measured by the SNS to significantly better than 10%. We therefore expect our systematic errors to be dominated by our incomplete knowledge of stopped pion production in a thick target.

Measurements by the HARP experiment [23], of pion production with a proton beam near 1 GeV incident on high-*Z* targets, will help. But some of the pions in the thick SNS target will be produced by beam-fragment/target interactions over a full spectrum of fragment energies and species, so a measurement with 1 GeV protons is not sufficient. Another important thick-target affect is the re-absorption of the produced pions by the target before they stop and decay. Pion production measurements inside a thick target would also help, but indirectly since the pions we are interested in will stop in the target and not be detected. Therefore our calculation of the neutrino production based on the measured proton current will not be model-independent. We can also compare the cross section we obtain for carbon, to the theoretical value, which is well understood [24-31], and to the previously measured experimental value [32-35], which was found to be in agreement with the theoretical value. We expect the resulting systematic errors to be well under 10%.

Section 4 References:

1. MCNPX Team, "MCNPX, Version 2.4.0", LA-UR-02-5253, Los Alamos National Laboratory, August 2002.
2. F.X. Gallmeier and R.E. Pevey, "Creation of a Set of Interface Utilities to allow Coupled Monte Carlo/Discrete Ordinates Shielding Analyses," Third International Topical Meeting on Nuclear Applications of Accelerator Technology, American Nuclear Society, Long Beach, November 14-18, 1999.
3. W.A. Rhoades and R.L. Childs, *Nucl. Sci. & Engr.*, **99**, 88-89, 1988.
4. T. Miller, "Two-Dimensional Shielding Analysis of the SNS Target Station Shutters, Shutter Beam Stops, Un-instrumented Neutron Beamlines, and Biological Shielding Monolith," SNS-106100200-DA0001-R00, March 2001.
5. R.A. Lillie *et al*., "HILO2k: A coupled Neutron-Photon Transport Cross Section Library for Neutron Energies up to 2000 MeV," Fourth International Topical Meeting on Nuclear Applications of Accelerator Technology, American Nuclear Society, Washington D.C., November 12-15, 2000.
6. **ν-SNS** Collaboration, Neutrino Program at the Spallation Neutron Source, Study Report, March 2004.
7. *Eur. Phys. J. C*, **3**, 1, 1998.
8. F. Ashton, H.J. Edwards and G.N. Kelly, *J. Phys. A* **4**, 1971.
9. F. Ashton, H.J. Edwards and G.N. Kelly, *Phys. Lett. B* **29**, 249, 1969.
10. B. Bodemann *et al*., *Nucl. Instrum. Meth. A* **286**, 214, 1990.
11. http://home.fnal.gov/~asousa/shield/ShieldDocumentation/vetoshield_roy.pdf#search='veto%20performance%20minos'
12. J. Kane, College of William and Mary, Private Communication, 2004.
13. http://phyweb.lbl.gov/~ianh/nlc/talks/morgunov_july16_hcal.pdf#search='hcal%20tile%20readout'
14. V. Golovin and V. Saveliev, *Nucl. Instrum. Meth. A* **518**, 560, 2004.
15. W.W.M. Allison *et al.*, *Nucl. Instrum. Meth. A* **381**, 385, 1996.
16. Yu.V. Efremenko, F.T. Avignone and A. Mezzacappa, p. 248, "Carolina Symposium on Neutrino Physics in Honor of Frank Avignone", Columbia, South Carolina, March 10-12, 2000. Published in *Columbia 2000, Neutrino Physics*.
17. R. Maschuw, *Prog. Part. Phys.* **40**, 183, 1998.
18. E. Kolbe, K. Langanke, *Phys. Rev. C* **63**, 025802, 2001.
19. J. Toivanen *et al*., *Nucl. Phys. A* **694**, 395, 2001.
20. G.C. McLaughlin, *Phys. Rev. C* **70**, 045804, 2004.
21. M. Sajjad Athar, Shakeb Ahmad, S.K.Singh, nucl-th/0506046
22. W.C. Haxton, *Phys. Rev. D* **36**, 2283, 1987 (taken from cross section for supernova neutrino spectrum at T=7.5 MeV to match the SNS spectrum).
23. J.J. Gomez-Cadenas *et al*., *Nucl. Phys. Proc. Suppl.* **143**, 291, 2005.

24. T.W. Donnelly and R.D. Peccei, *Phys Rep.* **50**, 1979
25. T.W. Donnelly, *Phys. Lett. B* **43**, 93, 1973.
26. E. Kolbe, K. Langanke, and S. Krewald, *Phys. Rev. C* **49**, 1122, 1994.
27. E. Kolbe, K. Langanke, and P. Vogel, *Nucl. Phys. A* **652**, 91, 1999.
28. C. Volpe *et al.*, *Phys. Rev. C* **62**, 015501, 2000.
29. A.C. Hayes and I.S. Towner, *Phys. Rev. C* **61**, 044603, 2000.
30. N. Auerbach, N.Van Giai, and O.K. Vorov, *Phys. Rev. C* **56**, R2368, 1997.
31. S.K. Singh, N.C. Mukhopadhyay, and E. Oset, *Phys. Rev. C* **57**, 2687, 1998.
32. J. Kleinfeller *et al.*, in Neutrino '96, edited by K. Enquist, H. Huitu, and J. Maalampi (World Scientific, Singapore, 1997).
33. B.E. Bodmann *et al.*, *Phys. Lett. B* **332**, 251, 1994.
34. B. Zeitnitz, *Prog. Part. Nucl. Phys.* **32**, 351, 1994.
35. C. Athanassopoulos *et al.*, *Phys. Rev. C* **55**, 2078, 1997.

5 COST AND SCHEDULE

5.1 Work Breakdown Structure

The construction of the **ν-SNS** facility will be carried out using conventional project management techniques and project management tools. We have followed the standard practice of preparing a work breakdown structure (WBS) with each major component of the project broken down into lower-level activities. Sections 4.2-4.6 of this proposal provide details on the cost estimates for individual WBS elements.

5.2 Contingency Analysis

The proposed budget includes a calculated contingency. We calculate the overall project contingency by estimating the contingency contribution from each WBS element. We base each contribution on an assessment of the technical, cost, and schedule risk with a weight that reflects the type of cost (labor or material). These individual contributions are summed to give the project contingency.

Base cost: The base cost is the estimated amount of money to do things correctly the first time, unless from past experience it is fairly certain that it will take more than one try. In other words, contingency is not included in the base cost.

Cost contingency: Cost contingency is the estimated amount of additional money, above and beyond the base cost, that may be required to ensure the project's success. Contingency is to be used only for omissions and unexpected difficulties that may arise. While contingency is calculated on an element-by-element basis, this is only a procedure to determine the total project contingency. Contingency is held entirely by project management and not by individual work-package managers.

The procedure for estimating cost contingency is to:

1. Compare the conceptual state of the element with Table 5.1 to determine risk factors.
2. Compare the potential risk within an element with Table 5.2 to determine the appropriate weighting factors.
3. Multiply the individual risk factors by the corresponding weighting factors, and then sum them to determine the composite contingency percentage.
4. Do this for each element at the chosen level of the WBS.
5. Calculate the dollar amount of contingency for an element by multiplying the base cost by the calculated contingency.
6. Sum the calculated contingencies of all WBS elements to determine the total project contingency.

Table 5.1 Technical, cost, and schedule risk factors.

Technical	Cost	Schedule	Risk factor
Existing design and off-the-shelf hardware	Off-the-shelf or catalog item		1%
Minor modifications to an existing design	Vendor quote from established drawings	No schedule impact on any other item	2%
Extensive modifications to an existing design	Vendor quote with some design sketches		3%
New design, nothing exotic	In-house estimate based on previous similar experience	Delays completion of noncritical path subsystem item	4%
New design, different from established designs or existing technology	In-house estimate for item with minimal experience but related to existing capabilities		6%
New design, requires some R&D but does not advance the state-of-the-art	In-house estimate for item with minimal experience and minimal in-house capability	Delays completion of critical path subsystem item	8%
New design, development of new technology which advances state-of-the-art	Top-down estimate from analogous programs		10%
New design, way beyond the current state-of-the-art	Engineering judgment		15%

Table 5.2 Technical, cost, and schedule risk weights.

Technical	Cost	Schedule	Risk weight
	Material cost OR labor rate	Same for all	1
Design OR manufacturing	Material cost AND labor rate		2
Design AND manufacturing			4

Example: Machining Bunker Steel Plates

The cost estimate to machine the bunker steel plates is $707,800K. The calculation used to obtain the total contingency estimate is shown below to illustrate the process used for each WBS element. The technical risk assessment is based on the fact that we anticipate the machined plates we need are "New Design, nothing exotic." The cost risk assessment is based on the fact that our cost estimate is "Engineering Judgment" of the cost of machined steel plates at the time of procurement. The schedule risk assessment is based on the fact that we do not anticipate the steel procurement to be on the critical path.

Technical		
New design, different from established designs or existing technology	4%	
Design OR Manufacturing	× 2	= 8%
Cost		
Vendor quote with some design sketches	15%	
Material Cost OR labor rate	× 1	= 15%
Schedule		
No schedule impact on any other item	2%	
Same for all	× 1	= 2%
Total Contingency		**= 25%**

5.3 Cost Estimate

Table 5.3 shows the unescalated cost and contingency at level three of the WBS in FY05 dollars. These sum to $6,553 with a contingency of $2,022 (31%), for a total of $8,575. We estimate an additional $440K in Other Project Costs (preparation of a conceptual design report, R&D and pre-ops).

5.4 Total Project Cost, Budget Profile and Schedule

In order to calculate the Total Project Cost (TPC) we must develop a profile to calculate escalation. We have not performed a resource-loaded schedule analysis, but we believe it is technically feasible to complete the **ν-SNS** construction project in three years. Our goal is to begin operations as soon as possible after the SNS reaches full power while satisfying requirements set by DOE Order 413.3. The profile shown in Table 5.4 is our attempt to satisfy these varying requirements. The resulting TPC is $9,934K. (Note: pre-conceptual R&D costs are shown, but not included in the TPC.)

We note that although the bunker, safety system, veto, data acquisition system, and one detector and associated target are necessary to start the scientific program the second detector/target could be funded as a separate project. Table 5.5 shows the budget profile assuming the segmented detector is funded separately. In this case the TPC is $8,086K.

The critical decision schedule corresponding to this profile is shown in Table 5.6.

Table 5.3 ν-SNS cost breakdown to WBS level three. Costs (including overheads) are given in FY05 dollars and have not been escalated to account for inflation.

WBS #	Title	Cost w/o Contingency	Contingency	Total	Contingency Fraction
1.1	**Bunker**	**$2,255,487**	**$563,872**	**$2,819,359**	**25%**
1.1.1	Design Bunker	$276,787	$69,197	$345,984	25%
1.1.2	Procure Bunker	$1,231,800	$307,950	$1,539,750	25%
1.1.3	Install Bunker	$746,900	$186,725	$933,625	25%
1.2	**Veto**	**$1,058,835**	**$376,961**	**$1,435,796**	**36%**
1.2.1	Design Veto	$76,785	$19,964	$96,749	26%
1.2.2	Procure Veto	$647,170	$258,868	$906,038	40%
1.2.3	Assemble & Test Veto	$224,280	$58,313	$282,593	26%
1.2.4	Install Veto	$110,600	$39,816	$150,416	36%
1.3	**Segmented Detector**	**$1,154,859**	**$426,785**	**$1,581,644**	**37%**
1.3.1	Design SD	$106,775	$27,762	$134,537	26%
1.3.2	Procure SD	$882,584	$353,034	$1,235,618	40%
1.3.3	Assemble & Test SD	$135,900	$35,334	$171,234	26%
1.3.4	Install SD	$29,600	$10,656	$40,256	36%
1.4	**Homogeneous Detector**	**$1,189,080**	**$452,381**	**$1,641,461**	**38%**
1.4.1	Design HD	$56,880	$14,789	$71,669	26%
1.4.2	Procure HD	$1,023,000	$409,200	$1,432,200	40%
1.4.3	Assemble & Test HD	$58,000	$15,080	$73,080	26%
1.4.4	Install HD	$51,200	$13,312	$64,512	26%
1.5	**Utilities**	**$229,433**	**$61,947**	**$291,380**	**27%**
1.5.1	Design	$51,558	$13,921	$65,479	27%
1.5.2	Procure	$84,600	$22,842	$107,442	27%
1.5.3	Install	$93,275	$25,184	$118,459	27%
1.6	**Safety System**	**$63,242**	**$17,075**	**$80,317**	**27%**
1.6.1	Design	$12,890	$3,480	$16,370	27%
1.6.2	Procure	$30,000	$8,100	$38,100	27%
1.6.3	Install	$20,352	$5,495	$25,847	27%
1.7	**DAQ**	**$258,000**	**$64,500**	**$322,500**	**25%**
1.7.1	Design	$0	$0	$0	0%
1.7.2	Procure	$258,000	$64,500	$322,500	25%
1.7.3	Install	$0	$0	$0	0%
1.8	**Project Management**	**$344,002**	**$58,680**	**$402,682**	**17%**
1.8.1	Project Manager	$108,000	$16,200	$124,200	15%
1.8.2	Project Controls	$61,992	$11,159	$73,151	18%
1.8.3	Project Engineer	$174,010	$31,322	$205,331	18%
	Total	**$6,552,938**	**$2,022,201**	**$8,575,139**	**31%**

Table 5.4 Proposed **ν-SNS** budget profile.

	FY06	FY07	FY08	FY09	FY10	FY11	FY12	Total
Pre-conceptual R&D	**140**							**140**
OPC		**246**					**233**	**480**
R&D		144						144
CDR		103						103
Pre-ops							233	233
TEC			**770**	**2,781**	**3,324**	**2,580**		**9,455**
PED			770					770
Construction				2,781	3,324	2,580		8,685
TPC		**246**	**770**	**2,781**	**3,324**	**2,580**	**233**	**9,934**
Total Funding	**140**	**246**	**770**	**2,781**	**3,324**	**2,580**	**233**	**10,074**

Table 5.5 Proposed **ν-SNS** budget profile with the segmented detector funded separately.

	FY06	FY07	FY08	FY09	FY10	FY11	FY12	Total
Pre-conceptual R&D	**90**							**90**
OPC		**174**					**187**	**361**
R&D		92						92
CDR		82						82
Pre-ops							187	187
TEC			**627**	**1,971**	**2,770**	**2,356**		**7,725**
PED			627					627
Construction				1,971	2,770	2,356		7,097
TPC		**174**	**627**	**1,971**	**2,770**	**2,356**	**187**	**8,086**
Total Funding	**90**	**174**	**627**	**1,971**	**2,770**	**2,356**	**187**	**8,176**

Table 5.6 Proposed **ν-SNS** critical decision schedule.

CD0	CD1	CD2	CD3	CD4
Sep-06	**Sep-07**	**Apr-08**	**Sep-08**	**Sep-12**

6 MANAGEMENT PLAN AND PROJECT CONTROLS

This section describes our proposed approach to the management of the **ν-SNS** construction project (including descriptions of the roles and responsibilities of key individuals and organizations), and discusses the management of the scientific program after operations begin.

6.1 ν-SNS Project Organization

The organization and management of the proposed effort must satisfy a number of requirements. Some of these, such as clear roles and responsibilities and sound project organization, are familiar, and are similar to those of many other projects of this scale. Other proposed organizational features include responsiveness to SNS requirements and to the special nature of this field of research. The management plan also takes cognizance of the fiscal and line reporting responsibilities consistent with our anticipated funding scenario.

In brief, the organization and management of the proposed work will:

- Be consistent with SNS guidelines for construction and operation of beamlines that are outside of the scope of the SNS construction project.
- Be consistent with fiscal and line reporting channels, required by funding sources and recipients (DOE Division of Nuclear Physics (DOE-NP) and the ORNL Physics Division).
- Efficiently accommodate the special character of neutrino research.
- Establish clear fiscal, line, and safety management accountability.
- Provide an effective project organization with clear roles and responsibilities.
- Create an open peer-review process for the allocation **ν-SNS** facility access.
- Ensure oversight and review that are responsive to the SNS, to the ORNL Directorate of Physical Sciences, and to the user community at large.

The overall proposed management structure is given in Figure 6.1.

6.2 ν-SNS Instrument Development Team

The **ν-SNS** facility will serve a broadly based national and international community interested in medium energy neutrino science that can be uniquely pursued at the SNS. In response to the process developed by the SNS for instrument construction, we have formed an Instrument Development Team (IDT) to represent potential **ν-SNS** users. See Appendix 1 for a full collaboration list. Such IDTs are expected to secure the required funding and lead the design, construction, and commissioning scientific instruments at the SNS. In return for providing a working facility IDTs are allocated a specific fraction of the operation time on the instrument. Unallocated time is made available to the general user community through a proposal and review process.

Organization Chart

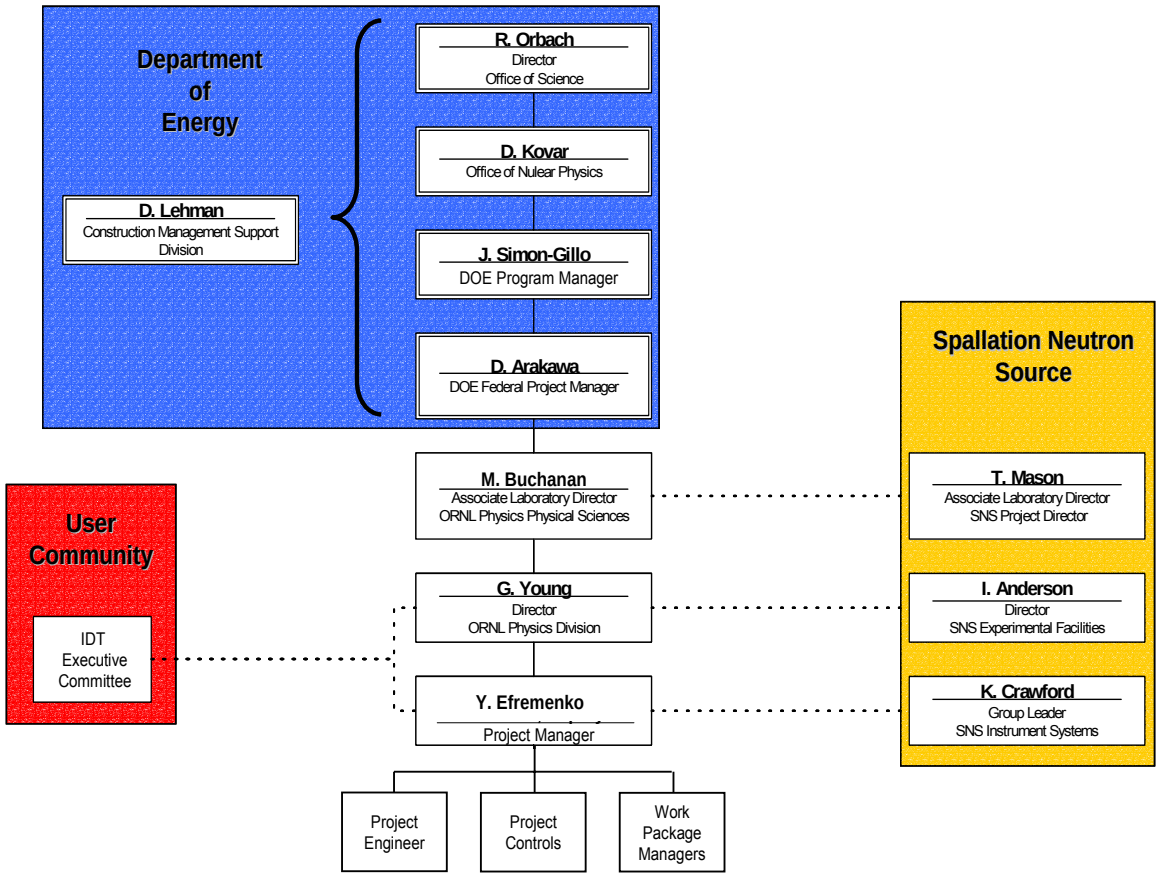

Fig. 6.1 ν-SNS organization chart.

The character of the work proposed here, including both the construction of the beamline and the execution of the user program, differs in many important ways from typical activities at an instrument used for studies in materials science. Some of the characteristics of our proposed work include the following:

- Each individual experiment (beyond the proposed initial set of target materials) will typically be funded as an independent project following proposal submission and review.
- Experiments will typically take data for periods of many months, or possibly years.
- A significant portion of the community is already engaged in this project, making it difficult to establish a clear distinction between the membership of our IDT and the general prospective user population.
- The scientific and technical aspects of the experiments envisioned for **ν-SNS** are not in the realm of expertise currently represented in anticipated SNS program advisory committees.

We respond to these special characteristics by providing for unrestricted IDT membership. This will ensure continued intellectual vitality of the IDT as scientific priorities change and also recognizes that much of the current user community is already engaged in this enterprise.

We elect to subject all proposals to a common peer review process in order to ensure the best science program and in recognition of the major beam time commitment required for each experiment. The details of the peer review and scheduling process will be worked out with the SNS, but we anticipate that a program advisory committee will provide independent advice regarding the scientific program to both the SNS and the ORNL Physics Division. Proposals that originate from within the IDT will be treated no differently from those that originate outside it.

6.3 IDT Executive Committee

General oversight and direction of the activities of the IDT will be the function of the IDT Executive Committee (EC). The committee is expected to consist of ~4-8 individuals. The IDT EC will have the responsibility to represent the overall scientific community interested in **ν-SNS**.

The IDT EC will:

- Act as an advocacy group for the IDT by presenting the scientific goals of the IDT and the benefits of **ν-SNS** to a broad scientific community, to funding agencies, and to laboratory management.
- Provide advice and guidance to the Project Manager concerning **ν-SNS** design and construction.
- Advise the Project Manager regarding change control activities leading to the authorization of appropriate modifications to the scope, cost, or schedule.
- Provide advice and guidance to the Physics Division Director concerning **ν-SNS** operations, as well as concerning the proposal, approval, and scheduling processes for individual experiments.
- Advise, as appropriate, ORNL management on personnel, financial, and management issues related to **ν-SNS**.

The EC is expected to include representation from experimental collaborations that are seriously interested in carrying out experiments at **ν-SNS**. Membership in the EC is expected to be a long-term, though not permanent, commitment. The initial EC membership consists of:

Y. Efremenko (*ex-officio*)	University of Tennessee / ORNL
F.E. Bertrand	ORNL / University of Tennessee
J. Blackmon	ORNL
V. Cianciolo	ORNL
T.A. Gabriel	Spallation Neutron Source
U. Greife	Colorado School of Mines
W.R. Hix	ORNL
E. Hungerford	University of Houston
G. McLaughlin	North Carolina State University

6.4 ORNL Physics Division Fiscal and Management Responsibilities

Because we anticipate that funding for this effort will be directed through the ORNL Physics Division, ORNL line management will have ultimate fiscal and management responsibility for **ν-SNS** construction and its subsequent operation. The ORNL Physics Division will also have the responsibility for supporting user activities, though not necessarily for the construction of individual experiments (for instance, calibration of a proposed supernova neutrino detector).

6.4.1 ORNL Physics Division Director

The ORNL Physics Division Director will have the responsibility for all DOE funding that is allocated to ORNL and will have overall fiscal responsibility for the project.

6.4.2 ν-SNS Project Manager

The **ν-SNS** Project Manager (PM) will have the responsibility for the fiscal and construction management of the project. This involves appropriate planning, budgeting, and reporting. The PM will report to the ORNL Physics Division Director. The PM will act as the technical point of contact for the negotiation of agreements and subcontracts with the SNS and with universities and other laboratories for activities related to this project.

The PM will:

- Have direct line and fiscal responsibility for **ν-SNS** design, construction, and commissioning.
- Ensure that all activities are carried out safely and in a manner consistent with SNS and ORNL guidelines and regulations.
- Coordinate preparation of project reviews and reports as required by the SNS and by other organizations and agencies.
- Monitor progress of all project deliverables and identify emerging cost or schedule issues.
- Release project contingency funds, as appropriate, following the change control process and/or evaluations of unexpected situations.
- Provide the IDT EC with timely information concerning project and user program status.

6.4.3 ORNL Physics Division and SNS Staff

It is anticipated that ORNL Physics Division and SNS staff will carry out a significant portion of the work associated with **ν-SNS** construction under standard ORNL management practices.

6.4.4 Subcontractors

Many activities related to this project will be most efficiently, and/or cost effectively, performed by IDT members at universities. Such work will be carried out using subcontracts or other appropriate instruments and agreements such as MoUs. The subcontracts will specify deliverables and will include provisions for reports on progress and expenditures. They will be established in accordance with standard DOE and ORNL procedures.

6.5 Quality Assurance and Control

The application of national codes, standards, and UT-Battelle procedures will assure appropriate quality control for the construction and operation of the project. A quality assurance evaluation will be performed, and if any portion of the project is determined to be Q-Category II, additional QA requirements will be established to ensure that the design will meet the functional and operational requirements. All other portions of the project will be Q-Category III.

6.6 Procurement and Fabrication

Fabrication of equipment, construction and other services performed by subcontractors will be obtained through ORNL and/or SNS Procurement.

6.7 Cost, Schedule, and Performance Controls

Cost, schedule, and performance baselines will be established for each element at the appropriate WBS level, and performance against baseline will be monitored and evaluated on a periodic basis. Corrective action will be taken as appropriate. The cost, schedule, and performance control system will be in compliance with DOE Order 413.3 and applicable UT-Battelle procedures.

6.8 Environment, Safety, and Health

The principles of the Integrated Safety Management System (ISMS) and the Environmental Management System (EMS) at ORNL/SNS will be incorporated into the project planning, design, construction, and operation of **ν-SNS**. This work will be done on the SNS site and will be overseen and regularly reviewed by the SNS EPO/ECR and the resident head of ES&H at the SNS. Initial consultations have been conducted with the ES&H staff and Fire Protection Engineering (FPE) to analyze the hazards and develop plans for the principle hazard controls. The main hazards that are expected involve confined spaces, flammable materials, compressed gases, high voltage electricity, and other chemical hazards. Controls for these hazards have been evaluated and estimates are included in the WBS for the bunker and detectors.

The first target in the homogeneous detector will be liquid scintillator, implying that over 40,000 liters of flammable liquid will be contained in the detector. This requires special controls, and initial consultations with FPE have resulted in a preliminary plan that involves four areas. First, the bunker will be constructed to serve as an acceptable secondary containment structure. Second, backup storage for the scintillator will be located outside the SNS target hall in an approved above-ground flammable storage tank. All plumbing and systems will have double containment and will be approved for use with flammable liquids. Third, an acceptable scintillator with the highest possible flash point will be used. Fourth, special local fire suppression as designed by FPE will be installed around the **ν-SNS** bunker and integrated with the target hall fire protection systems. The flammability of the plastic scintillator used in the cosmic ray veto is also a hazard that must be controlled. The local fire suppression system will be designed with this hazard in mind. The scintillator panels will also be enclosed in aluminum to suppress ignition from external sources. We will work closely with FPE at all stages of the project to refine and implement these controls.

The gases to be used in the segmented detector may pose a fire hazard. To help mitigate this hazard we expect to operate at approximately atmospheric pressure and we will investigate the

appropriateness of non-flammable gas mixtures. In addition, although a rather large volume of compressed gas may be kept on site for the segmented detector, the gases will be piped into the detector from a compressed gas storage area outside the SNS target hall. The only other significant hazard that may be presented by the segmented detector gas is a suffocation hazard since the gases to be used are likely to be heavier than air and the detector is to be located in a pit area about 2 m below the main SNS instrument hall level. However, an analysis indicates that a significant suffocation hazard is only possible for personnel working inside the **ν-SNS** bunker or in the immediate area around the bunker due to the small volume of gas relative to the pit area. This hazard will be controlled by means such as an oxygen-deficiency alarm system installed inside the **ν-SNS** bunker and in the pit area just around the bunker. Special administrative controls may also apply to workers inside the **ν-SNS** bunker.

Construction, testing, and operation of the **ν-SNS** detectors will involve work with high voltage circuits and chemicals that are common to work with nuclear instrumentation. This work will be conducted following Research Safety Summaries and Work Plans that are developed under the guidance of the SBMS subject areas of Chemical Safety and Electrical Work. The homogeneous detector vessel will likely fall under regulation as a confined space. If so, permit requirements will be established, regularly reviewed, and followed as dictated by the SBMS Confined Space subject area for any work that is to be conducted inside the homogeneous detector vessel.

Special attention will be devoted to pollution prevention and environmental impacts. Gas used for the segmented detector will be inventoried to ensure compliance with air emission regulations, although estimates indicate that these emissions should be quite low, well within regulatory limits. The largest potential waste stream will result from interchange of the target material. We will work with the SNS EPO/ECR to develop a plan to reuse or recycle of the target material.

The initial environmental impacts associated with the construction of this detector system were evaluated in the Final Environmental Impact Statement, Construction, and Operation of the Spallation Neutron Source, DOE/EIS-0247, April 1999. A Record of Decision for the SNS was signed by the Secretary of Energy on June 18, 1999.

6.9 Change Control

The cost, schedule, and performance baselines will be set and controlled at an appropriate level by a Configuration Control Board (CCB). The CCB will include in its membership the PM, the Chairman of the IDT EC, and the ORNL Physics Division Director (or designee), and a representative of the SNS Experimental Facilities Division. Before the baseline is presented to the CCB for approval, it will be reviewed by the IDT EC. Baseline changes and contingency adjustments that significantly impact the project will be reviewed and approved or disapproved by the CCB. The change control system will be in compliance with DOE Order 413.3 and applicable UT-Battelle procedures.

6.10 Risk Analysis

This project consists of well-understood technologies: steel shielding, a fire safety system, standard nuclear/particle physics detectors and a data acquisition system. Some modest R&D is needed to optimize detector design for cost, performance, and simplicity of target replacement,

see Appendix 5 for details. The largest single cost driver is the price of steel for the bunker shielding. Steel prices have risen significantly over the last few years and future prices are quite uncertain. We are exploring possible strategies for mitigating exposure to this risk, such as the use of low-activity recycled steel (Duratek, Inc.). There is some risk that the SNS will not meet its power goals, but if they get anywhere near these goals the proposed measurements will still be possible in an acceptable length of time. There is some amount of uncertainty in the calculations of the dominant source of backgrounds: high energy neutrons associated with the SNS. However, we are confident that even if this background turns out to be significantly worse than expected we will be able to eliminate it, with only a small compromise to the measurement, by slightly extending the time cut eliminating events that occur too close in time to the spallation pulse.

6.11 Communication and Reporting

We are requesting funding for this project from DOE-NP. For projects of this scale, it is customary for DOE to hold regular project reviews to assess progress. We will cooperate fully with such formal reviews while also providing DOE-NP with regular updates and informal briefings. In a similar vein, we expect that the SNS will establish a formal review process for IDT instrument development. Insofar as possible, we will encourage the participation of the SNS in any DOE-mandated reviews and vice versa and we will encourage the DOE-NP and SNS project management to coordinate their reviews to reduce duplication of effort.

Communication with the IDT will be coordinated through the IDT EC. We intend to have regular teleconferences as well as an annual meeting of the entire IDT (most likely coincident with appropriate national conferences). The IDT EC is also expected to participate in all DOE or SNS formal reviews.

6.12 General User Support

After construction is complete and **ν-SNS** is fully operational it will be operated in a mode similar to other nuclear/particle physics facilities. This implies that a suitable level of user support will be provided by the facility. Since this nuclear physics facility is located at a BES materials science facility, we do not expect such user support to be forthcoming from the SNS. As a result, the ORNL Physics Division will be making an explicit request for a modest amount of user support from DOE-NP. Such support will include ORNL scientific staff to act as facility mentors, technical support, SNS crafts support, and some level of materials and supplies. It should be noted that, similar to other SNS IDTs, **ν-SNS** will be free of space charges, will not be charged for beam time, and will only be charged for exceptional utilities.

6.13 Transition to Operations

Final details of the subsequent management of **ν-SNS** operations will be determined and documented via a memorandum of understanding (MoU) between the SNS, the ORNL Physics Division, the IDT, and other interested parties. However, it is our intention that the science program at **ν-SNS** will be operated on a proposal-driven basis with all beam time allocations subject to independent peer review for scientific merit, experimental feasibility, and operational readiness.

We expect the IDT to work with the ORNL Physics Division and SNS management to establish a Program Advisory Committee (PAC) and to develop a process for the approval and scheduling of experiments. The PAC will consist of knowledgeable individuals who are not directly engaged in experimental activities that currently anticipate using **ν-SNS**. The PAC will provide an independent peer review of the theoretical importance, experimental feasibility, engineering details, and staffing of each proposed experiment. In addition it will provide guidance on the relative priorities for the scheduling of experiments and provide an overall assessment of the quality of the **ν-SNS** scientific program. Representatives of the SNS, as well as of the DOE, will be invited to participate as observers in all PAC meetings.

APPENDIX 1 ν-SNS INSTRUMENT DEVELOPMENT TEAM MEMBERS

University of Aarhus
K. Langanke

University of Alabama
I. Stancu

Argonne National Laboratory
R.L. Talaga

University of Basel
E. Kolbe

California Institute of Technology
P. Vogel

University of California - San Diego
G.M. Fuller

Clemson University
B.S. Meyer

Colorado School of Mines
U. Greife, F. Sarazin

Florida State University
J. Piekarewicz

University of Houston
E. Hungerford, K.J. Lan

Kharkov Institute of Physics & Technology
O. Glamazdin, R. Pomatsalyuk

Los Alamos National Laboratory
R.L. Burman, W.C. Louis, G. Mills, R. Van de Water

North Carolina State University
G.C. McLaughlin

North Carolina Central University
D. Markoff

Oak Ridge National Laboratory
D.W. Bardayan, J.C. Blackmon, F.E. Bertrand, V. Cianciolo, D.J. Dean, A.M. Mezzacappa, P.E. Mueller, M.S. Smith, G.R. Young, W.R. Hix

Ohio State University
J.F. Beacom

University of South Carolina
F.T. Avignone, V. Gudkov

Spallation Neutron Source
G.W. Dodson, T.A. Gabriel

University of Tennessee
W.M. Bugg, Y.V. Efremenko

University of Wisconsin
A.B. Balantekin

APPENDIX 2 CURRICULUM VITAE OF ν-SNS EXECUTIVE COMMITTEE MEMBERS

Vitae of the members of the IDT Executive Committee are on the following pages.

Professional Vitae Summary

Fred E. Bertrand

Education:

Ph.D., Physics, Louisiana State University (1968)
M.S., Physics, Louisiana State University (1962)
B.S., Physics, Southwestern at Memphis, (1960)

Professional Experience:

7/2002-Present: Research Professor, University of Tennessee
7/2002-Present: Retired, Oak Ridge National Laboratory
3/94-7/2002: Director, Physics Division, Oak Ridge National Laboratory
10/93-3/94: Associate Director, Physics Division, Oak Ridge National Laboratory
9/87-3/94: Section Head, Nuclear Structure Section, Physics Division, ORNL
9/78-9/87: Group Leader, ORIC Research Section, Physics Division, ORNL
11/75-9/78: Deputy Director, Nuclear Data Project, Oak Ridge National Laboratory
3/70-11/75: Research Staff Member, Nuclear Data Project, ORNL
9/68-3/70: Research Associate, University of Southern California

Areas of Research Interest:
Giant Multipole Resonances
Direct Reactions at Medium Energy
Meson Scattering
Neutrino Physics
Continuum Excitations

Fellow American Physical Society

Publications:
Over 250 publications as author or co-author. Over 50 invited presentations at scientific meetings.

JEFF C. BLACKMON
blackmon@ornl.gov
(865) 574-7834

Physics Division, Oak Ridge National Laboratory
P.O. Box 2008
Oak Ridge, TN 37831

A. PROFESSIONAL PREPARATION

University of North Carolina at Chapel Hill	**Physics**	**Ph.D.**	**1994**
University of North Carolina at Chapel Hill	**Physics**	**M.S.**	**1994**
Guilford College	**Physics**	**B.S.**	**1989**

B. APPOINTMENTS

Research Staff Member, Oak Ridge National Laboratory **1997-present**

Research in experimental nuclear astrophysics and the structure of exotic nuclei.
Recipient 2002 Presidential Early Career Award for Scientists and Engineers
Recipient 2000 ORNL Author of the Year Award

Postdoctoral Research Associate, ORNL & University of North Carolina 1995-1997
Lecturer, Guilford College 1994-1995

C. PUBLICATIONS

1. "Experimental approaches to hot and explosive burning," J. C. Blackmon, C. Angulo, and A. C. Shotter, Nucl. Phys. A, in press.
2. "First Study of the Level Structure of the r-Process Nucleus ^{83}Ge," J. S. Thomas, D. W. Bardayan, J. C. Blackmon, J. A. Cizewski, U. Greife, C. J. Gross, M. S. Johnson, K. L. Jones, R. L. Kozub, J. F. Liang, R. J. Livesay, Z. Ma, B. H. Moazen, C. D. Nesaraja, D. Shapira, and M. S. Smith, Phys. Rev. C 71, 021302 (2005).
3. "Study of the ^{124}Sn(d,p) reaction in inverse kinematics close to the Coulomb barrier," K. L. Jones, R. L. Kozub, C. Baktash, D. W. Bardayan, J. C. Blackmon, W. N. Catford, J. A. Cizewski, R. P. Fitzgerald, M. S. Johnson, R. J. Livesay, Z. Ma, C. D. Nesaraja, D. Shapira, M. S. Smith, J. S. Thomas, and D. W. Visser, Phys. Rev. C 70, 067602 (2004).
4. "Investigation of the ^{23}Na(p,γ)^{24}Mg and ^{23}Na(p,α)^{20}Ne reactions via (^{3}He,d) spectroscopy," S. E. Hale, A. E. Champagne, C. Iliadis, V. Y. Hansper, D. C. Powell, and J. C. Blackmon, Phys. Rev. C 70, 045802 (2004).
5. "Search for astrophysically important ^{19}Ne levels with a thick-target ^{18}F(p,p)^{18}F measurement," D. W. Bardayan, J. C. Blackmon, J. Gómez del Campo, R. L. Kozub, J. F. Liang, Z. Ma, L. Sahin, D. Shapira, and M. S. Smith, Phys. Rev. C 70, 015804 (2004).
6. "Strength of the ^{18}F(p,α)^{15}O Resonance at $E_{c.m.}$ = 330 keV," D. W. Bardayan, J. C. Batchelder, J. C. Blackmon, A. E. Champagne, T. Davinson, R. Fitzgerald, W. R. Hix, C. Iliadis, R. L. Kozub, Z. Ma, S. Parete-Koon, P. D. Parker, N. Shu, M. S. Smith, and P. J. Woods, Phys. Rev. Lett. 89, 262501 (2002).
7. "Thermal-neutron capture by ^{208}Pb," J. C. Blackmon, S. Raman, J. K. Dickens, R. M. Lindstrom, R. L. Paul, and J. E. Lynn Phys. Rev. C 65, 045801 (2002).
8. "Astrophysically important ^{26}Si states studied with the ^{28}Si(p,t)^{26}Si reaction," D.W. Bardayan, J. C. Blackmon, A. E. Champagne, A. K. Dummer, T. Davinson, U. Greife, D. Hill, C. Iliadis, B. A. Johnson, R. L. Kozub, C. S. Lee, M. S. Smith, and P. J. Woods, Phys. Rev. C 65, 032801 (2002).
9. "Stellar Reactions with Short-Lived Nuclei: ^{17}F(p,α)^{14}O," B. Harss, J. P. Greene, D. Henderson, R. V. F. Janssens, C. L. Jiang, J. Nolen, R. C. Pardo, K. E. Rehm, J. P. Schiffer, R. H. Siemssen, A. A. Sonzogni, J. Uusitalo, I. Wiedenhöver, M. Paul, T. F. Wang, F. Borasi, R. E. Segel, J. C. Blackmon, M. S. Smith, A. Chen, and P. Parker, Phys. Rev. Lett. **82**, 3964 (1999).

10. "Measurement of the $^{17}O(p,\alpha)^{14}N$ Cross Section at Stellar Energies," J. C. Blackmon, A. E. Champagne, M. A. Hofstee, M. S. Smith, R. G. Downing, and G. P. Lamaze, Phys. Rev. Lett. 74, 2642 (1995).

D. SYNERGYSTIC ACTIVITIES

- HRIBF Physics Advisory Council, 1994-present
- APS Division of Nuclear Physics Program Committee, 2003-2004
- Co-Organizer (with D. J. Dean), 2003 National Nuclear Physics Summer School

E. COLLABORATORS AND OTHER AFFILIATIONS

Oak Ridge National Laboratory, Oak Ridge, TN
D. W. Bardayan, C. Baktash, J. C. Batchelder, V. Cianciolo, Yu. Efremenko, J. Gómez del Campo, J. K. Dickens, C. J. Gross, W. R. Hix, M. S. Johnson, J. F. Liang, C. D. Nesaraja, S. Raman (deceased), D. Radford, D. Shapira, M. S. Smith, G. R. Young, C.-H. Yu
University of Alabama, Tuscaloosa, AL
I. Stancu
Colorado School of Mines, Golden, CO
U. Greife, F. Sarazin
University of Edinburgh, Edinburgh, UK
T. Davinson, P. J. Woods
University of Houston, Houston ,TX
E. Hungerford, A. Lan
University of North Carolina, Chapel Hill, NC
A. E. Champagne, C. Iliadis
Rutgers University, New Brunswick, NJ
J. A. Cizewski
University of Surrey, Guildford, UK
W. A. Catford,
Tennessee Technological University, Cookeville, TN
R. L. Kozub
Texas A&M University, College Station, TX
C. Gagliardi, A. M. Mukhamedzhanov, L. Trache, R. Tribble
TRIUMF, Vancouver, BC
A. C. Shotter
Yale University, New Haven, CT
P. D. Parker

Graduate advisor: Art Champagne (University of North Carolina)

Postdoctoral advisors: Michael Smith (ORNL), Art Champagne (University of North Carolina)

Thesis and Postdoctoral advisees: D. W. Bardayan, R. P. Fitzgerald, V. Y. Hansper, M. S. Johnson, K. L. Jones, S. D. Pain, B. C. Rasco, L. Sahin, J. S. Thomas, D. W. Visser.

Vince Cianciolo
cianciolotv@ornl.gov
(865) 574-4712

Physics Division, Oak Ridge National Laboratory
P.O. Box 2008
Oak Ridge, TN 37831-6356

A. PROFESSIONAL PREPARATION

Massachusetts Institute of Technology **Physics Ph.D.** **1994**

Thesis: "*Bose-Einstein Correlations of Kaons in 14.6 A·GeV Si+Au Collisions*"

University of Michigan, Ann Arbor **Physics B.S., Honors** **1988**

Thesis: "β *Decay of* ^{187}*Re*"

B. APPOINTMENTS

Group Leader, Oak Ridge National Laboratory **2002-present**

Research Staff Member, Oak Ridge National Laboratory **1997-present**

Research in heavy ion physics
Recipient 2001 Presidential Early Career Award for Scientists and Engineers
Recipient 1999 Lockheed Martin Technical Achievement Award

Postdoctoral Research Associate, Lawrence Livermore National Lab 1995-1996
Postdoctoral Research Associate, Massachusetts Institute of Technology 1995

C. PUBLICATIONS

1. "Impurity Effects on Adhesive Energies," J. R. Smith and T. V. Cianciolo, Surf. Sci. Lett. **210**, L229-36 (1989).
2. "Bose-Einstein Correlations of Kaons in Si+Au Collisions at 14.6 A·GeV," Y. Akiba *et al*. (E802 Collaboration), including V. Cianciolo, Phys. Rev. Lett. **70**, 1057-60 (1993).
3. "Two-Particle Rapidity Correlations From The Bose-Einstein Effect in Central ^{28}Si + Au Collisions at 14.6 A·GeV/c and Intermittency," Y. Akiba *et al*. (E802 Collaboration), including V. Cianciolo, Phys. Rev. C **56**, 1544-52 (1997).
4. "Status of Experiments Leading to a Small Recirculator," T.C. Sangster *et al*., including V. Cianciolo, Nucl. Inst. Meth. A **415**, 310-4 (1998).
5. "Measuring Centrality with Slow Protons in Proton Nucleus Collisions at the AGS," I. Chemkin *et al*. (E910 Collaboration), including V. Cianciolo, Phys. Rev. C **60**, 024902 (1999).
6. "Measurements of Single Electrons and Implications for Charm Production in Au+Au Collisons at $\sqrt{s_{NN}}$ = 130 GeV," K. Adcox *et al*. (PHENIX Collaboration), including V. Cianciolo, Phys. Rev. Lett. **88**, 192303 (2002).
7. "Centrality Dependence of π+/-, K+/-, p and p(bar) Production from $\sqrt{s_{NN}}$ = 130 GeV Au+Au Collisons at RHIC," K. Adcox *et al*. (PHENIX Collaboration), including V. Cianciolo, Phys. Rev. Lett. **88**, 242301 (2002).
8. "PHENIX Muon Arms," H. Akikawa *et al*., including V. Cianciolo, Nucl. Instrum. A **499,** 537 (2003).
9. "Formation of dense partonic matter in relativistic nucleus-nucleus collisions at RHIC: Experimental evaluation by the PHENIX collaboration. Status of our program to create, detect and characterize

quark-gluon plasma," K. Adcox *et al*. (PHENIX Collaboration), including V. Cianciolo, nucl-ex/0410003 (2003).

10. "Centrality Dependence of Charm Production from Single Electrons in Au+Au Collisions at $\sqrt{s_{NN}}$ = 200 GeV," S.S. Adler *et al*. (PHENIX Collaboration), including V. Cianciolo, Phys. Rev. Lett. **94**, 082301 (2005).
11. "J/Ψ production from Proton-Proton Collisions at $\sqrt{s}$ = 200 GeV," S.S. Adler *et al*. (PHENIX Collaboration), including V. Cianciolo, Phys. Rev. Lett. **92**, 051802 (2004).

D. SYNERGYSTIC ACTIVITIES

Co-organizer RHIC Heavy Flavor Workshop (2004)
Memberships:

- American Physical Society , Division of Nuclear Physics
- ΣΠΣ
- Society of Physics Students
    - Vice-President, University of Michigan Chapter, 1987-88.

Referee for:

- Department of Energy
- National Science Foundation
- Physical Review Letters
- Physical Review, C
- IEEE, Transactions on Nuclear Science

E. COLLABORATORS AND OTHER AFFILIATIONS

- Collaborating Scientist on SNS Fundamental Neutron Beamline IDT
    - Member, Executive Committee
- Collaborating Scientist on **ν-SNS** Collaboration
    - Member, Executive Committee
- Collaborating Scientist on PHENIX experiment
    - Member, Executive Council (2004-present)
    - Member Speaker's Bureau (2004-present)
    - Convenor, Heavy Flavor Physics Working Group (2002-2004)
    - Muon Identifier Front-End Electronics Subsystem Manager
    - Muon Identifier Mechanics Coordinating Physicist
- Collaborating Scientist on Experiment BNL E910
- Collaborating Scientist on Experiment BNL E866
- Collaborating Scientist on Experiment BNL E859

Graduate advisor: George S.F. Stephans (MIT)

Postdoctoral advisors: Wit Busza (MIT), Jim Thomas (Lawrence Livermore National Lab)

Thesis and Postdoctoral advisees:
University of Tennessee**:** R.J. Newby, A. Glenn, D. Hornback
Oak Ridge National Lab: D. Silvermyr, S. Batsouli, C. Zhang

Biographical Sketch

YURI EFREMENKO
efremenk@unix.utk.edu
(865) 574-4706

University of Tennessee, Department of Physics and Astronomy
Nielsen 401
Knoxville, TN 37996

A. PROFESSIONAL PREPARATION

Institute for Theoretic and Experimental Physics (Moscow)	**Physics**	**Ph.D.**	**1989**
Moscow Engineering-Physics University	**Physics**	**M.S.**	**1982**
Moscow Engineering-Physics University	**Physics**	**B.S.**	**1981**

B. APPOINTMENTS

Associate Professor (Joint Faculty Member, University of Tennessee, ORNL)	2002-present
Research Associate Professor at the University of Tennessee	1992-2002
Guest Scientist at CEBAF (now TJNF)	1991-1992
Senior Scientist at Institute for Theoretic and Experimental Physics	1989-1991
Scientist at Institute for Theoretic and Experimental Physics	1985-1989
Engineer-Scientist at Institute for Theoretic and Experimental Physics	1982-1985

C. Selected list of publications during last 2 years:

1)A FACILITY FOR NEUTRINO NUCLEUS CROSS-SECTION MEASUREMENTS AT THE SPALLATION NEUTRON SOURCE. By Yu. Efremenko (Oak Ridge),. 2005. 4pp. Published in Nucl.Phys.Proc.Suppl.138:343-346,2005 Also in *Seattle 2003, Topics in astroparticle and underground physics* 343-346

2) SEARCHES FOR NEUTRINO OSCILLATIONS AT INTENSE SPALLATION SOURCES.
By F.T. Avignone, Yu. Efremenko (South Carolina U. & Oak Ridge & Tennessee U.),. 2003. 11pp.
Published in J.Phys.G29:2665-2675,2003

3) NEUTRINO NUCLEUS CROSS-SECTION MEASUREMENTS AT INTENSE, PULSED SPALLATION SOURCES.
By F.T. Avignone, Yu.V. Efremenko (South Carolina U. & Oak Ridge & Tennessee U.),. 2003. 14pp.
Published in J.Phys.G29:2615-2628,2003

4) THE MAJORANA ZERO NEUTRINO DOUBLE BETA DECAY EXPERIMENT.
By Majorana Collaboration (Richard Gaitskell *et al.*). LA-UR-2003-7709, PNNL-14420, Nov 2003. 138pp.
White paper.
e-Print Archive: nucl-ex/0311013

5) PI- ABSORPTION IN WATER AN LIGHT MATERIAL.
By T. Numao, T. Awes, S. Berridge, W. Bugg, V. Cianciolo, Y. Davydov, Y. Efremenko, R. Gearhart, Y. Kamyshkov, S. Ovchinnikov, J.M. Poutissou, G. Young (TRIUMF & Oak Ridge & Tennessee U.)
Published in Nucl.Phys.A721:491-494,2003

6) A HIGH SENSITIVITY SEARCH FOR ANTI-NU(E)'S FROM THE SUN AND OTHER SOURCES AT KAMLAND.
By KamLAND Collaboration (K. Eguchi *et al.*).
Published in Phys.Rev.Lett.92:071301,2004

7) FIRST RESULTS FROM KAMLAND: EVIDENCE FOR REACTOR ANTI-NEUTRINO DISAPPEARANCE.
By KamLAND Collaboration (K. Eguchi *et al.*).
Published in Phys.Rev.Lett.90:021802,2003

D. SYNERGYSTIC ACTIVITIES

- **ν-SNS** project coordinator
- Co-chair of PANIC05 Neutrino Satellite Meeting
- Co-spokesmen of E-930 experiment at TRIUMF
- DOE reviewer
- Co-Organizer of "Workshop on Neutrino Studies at the SNS", 2003

E. COLLABORATORS AND OTHER AFFILIATIONS

KamLAND experiment
PHENIX experiment
ν-SNS - proposal
Majorana – proposal
Dchooze - proposal

Graduate advisor: V.Gavrilov (Institute for Theoretic and Experimental Physics)

Curriculum Vitae

TONY A. GABRIEL

Experimental Facilities Division
Spallation Neutron Source Project
Oak Ridge National Laboratory

Oak Ridge National Laboratory
One Bethel Valley Road
Bldg. 8600, MS-6474
Oak Ridge, Tennessee 37830

Telephone: 865-574-6082 office
865-382-8975 cell

Facsimile: 865-241-1033
E-Mail: tag@ornl.gov

Education:

Ph.D., Physics, University of Tennessee (1969)
BA, Physics and Mathematics, Pfeiffer College (1964)

Areas of Expertise:

Large-scale project management background associated with high-powered accelerator and target systems; high-powered, short-pulsed spallation target system development; high- and low-energy radiation transport code development; particle-nucleus collision model development; application analysis using the transport codes (energy deposition, particle fluxes, activation, etc.); integral shielding experiments for radiation shielding applications; nuclear and high-energy cross section development; radiation detectors and high-energy particle calorimeters; radiation damage mechanisms; applied physics; and fusion reactor neutronics. Tied to these broad-based areas of expertise are strong leadership abilities in organizing, coordinating, and integrating research and development programs and teams.

Professional Experience:

1/05 – present **ORNL Lead for the Rare Isotope Accelerator Project.** Responsible for directing the research and development for the ISOL and Fragmentation target areas at ORNL.

1/05 – present **Senior Consultant to the Experimental Facilities Division (XFD) within the Spallation Neutron Source.** Provide guidance to the Division as it moves from a construction division into an operating division.

3/95 – 12/04 **Senior Team Leader for the Target Systems' part of the SNS Project.** Responsible for directing research and design activities including coordinating neutronic, thermal-hydraulic, and material damage analyses, experimental test facilities, and methods and data development activities associated with the target, moderators, reflectors, and neutron guide systems. Including R&D, the total funding under management was $135M.

3/01 – 6/02 **Acting Division Director, Experimental Facilities Division**: Responsible for the Target Systems, Instruments, Target Building Operations and Users Program for the Spallation Neutron Source Project.

10/93 – 6/96 **Group Leader, Applied Physics Group, Computational Physics and Engineering Division.** Responsible for directing research and development activities supporting DOE high-energy physics programs including accelerator shielding and physics detectors for the Superconducting Super Collider (SSC) Project, Fermilab, and the Stanford Linear Accelerator. Also responsible for other projects managed within the group, including the Radiation Environments Program sponsored by the Defense Nuclear Agency and the Medical Applications Program.

1/90 – 1/94 **Director, Oak Ridge Detector Center (ORDC).** Responsible for directing research, development, and engineering activities associated with accelerator shielding and physics detectors for the Superconducting Super Collider (SSC) Project. Also, coordinated SSC and general physics activities between ORNL and the Southeastern Association of High-Energy Physics (SAHEP) partners. The total potential funding to be managed would have exceeded $100M had the SSC continued.

1/80 – 1/86 **Assignment (intermittent) to the Karlsruhe Research Center, FRG.** Assisted in the initial development of the Target Systems' part of the ISIS Spallation Neutron Source and the proposed German Spallation Neutron Source, SNQ. Shared responsibility for coordinating the research and development of the KARMEN neutrino detector and bunker, which is currently operating at the ISIS Spallation Neutron Source facility at Rutherford-Appleton Laboratory, U.K.

12/68 – 1/90 **Senior Research Staff Member, Oak Ridge National Laboratory.** Performed accelerator shielding analyses, developed and applied methods for the design of high-energy particle calorimeter systems, and developed computational models of material damage mechanisms. Co-developed the internationally used CALOR2000 code system for high-energy particle cascade and transport simulation.

Recent Professional Activities and Honors:

- Corporate Fellow, UTB/ORNL.
- Fellow, American Physical Society.
- Adjunct Professor of Physics at the University of Tennessee.
- Adjunct Professor of Nuclear Engineering at the University of Tennessee.
- Technical Excellence Award, 1985, Radiation Protection and Shielding Division of the American Nuclear Society (ANS).
- Member of the Local Organizing Committee for The Twelfth International Symposium on Reactor Dosimetry, May 8–13, 2005 in Gatlinburg, Tennessee, USA.
- Member of the International Advisory Committee for the Nuclear Applications of Accelerator Technology Meeting (AccApp05) to be held from August 28–September 1, 2005 in Venice, Italy.
- Executive Board Member of the International Collaboration on the Development of High-Powered Targets.
- Executive Board Member for the Rare Isotope Accelerator Project.
- Member, Organizing Committee for the 2004 Shielding Aspects of Accelerator, Targets, and Irradiation Facilities (SATIF-7).
- Past Member, External Review Committee for the Accelerator Production of Tritium Project.
- Past Member, External Radiation Review Committee for the Light Source at Thomas Jefferson National Accelerator Facility (TJNAF).
- Past Member, Executive Board of the Southeastern Association for High-Energy Physics (SAHEP).
- Past Member, Institutional Board of the BaBar Detector Collaboration.
- Past Member, Executive Committee of the ANS Accelerator Application Division.
- Past Chairman, Technical Program Committee of the ANS Accelerator Application Division.

- Past Member, Organizing Committee for the Users Workshop on Instrumentation Needs and Performance Metrics for the Next Generation Spallation Neutron Source, October 31–November 1, 1996.
- Past Member, Organizing Committee for the 1997–2000 Simulating Accelerator Radiation Environments Symposiums (SARE).
- Past Member, Organizing Committee for the 1997–2003 Shielding Aspects of Accelerator, Targets, and Irradiation Facilities (SATIF).
- Past Member, Technical Program Committee, AccApp'99, ’00, ’01.
- Past Member, Technical Program Committee, Monte Carlo 2000.
- Past Program Chair, AccApp’98.
- Past Member, Technical Program Committee for the ICRS-9 Ninth International Conference on Radiation Shielding, October 17–22, 1999.
- Past Organizer, Mini-Workshop on the Utilization of the High-Powered, Short-Pulsed SNS Facility for Low-Energy Neutrino Research, September 26–27, 1996.

Publications:

Dr. Gabriel has authored or helped author over 300 publications. His citations during 1973–2004 have totaled over 1000.

Dr. rer. nat. Uwe Greife, Associate Professor
Department of Physics, Colorado School of Mines, Golden, CO 80401
Email: ugreife@mines.edu, Phone: (303) 273 3618

Curriculum vitae

Higher education and professional experience:

Since April 2003

Associate Professor (tenured), Department of Physics, Colorado School of Mines, Golden, Colorado teaching: Nuclear physics, Radiation Detection and Measurement, Field Session; research: continuation of projects below, RIA R&D, neutrinos at the SNS (member of the executive committee);

August 1999 – April 2003

Assistant Professor (tenure-track), Department of Physics, Colorado School of Mines, Golden, Colorado; teaching: Nuclear physics, Modern Physics, Advanced Laboratory, PH 100, PH 200 recitation, Radiation Detection and Measurement and Field Session; research: Applied Nuclear Physics and Nuclear Astrophysics at ORNL (member of the users executive committee, spokesperson for two experiments), TRIUMF (spokesperson for two experiments), LANL (spokesperson for one experiment) and Colorado School of Mines;

February 1997 – August 1999

'Wissenschaftlicher Assistent' (~ non tenure-track Assistant Professor) of the faculty for physics and astronomy at the University of Bochum; radiation safety officer (open and closed radioactive sources, particle accelerators); teaching: Introduction to Nuclear Astrophysics, advanced physics laboratories and accelerator laboratory; research: nuclear astrophysics at ORNL, TRIUMF, Gran Sasso, Naples and Bochum;

May 1994 - January 1997

"Wissenschaftlicher Mitarbeiter" (research associate and instructor) at the University of Bochum in several projects in the field of nuclear astrophysics; teaching: laboratories for students of physics, medicine, geology, biology and engineering;

May 1994

Ph.D. in physics (Dr. rer. nat.); title: Fusion reactions: On the way to thermal energies; RUB Bochum; Germany

December 1989 - May 1994

Graduate student (Ph.D.) at the University of Bochum (supervisor Prof. C. Rolfs); teaching: laboratories (beginners and advanced);

November 1989

Diploma (M.S. with thesis) in physics; WWU Muenster, Germany

Referee Duties:

Phys. Rev. Lett., Phys. Rev. C, Phys. Essays, Nuclear Instruments and Methods A, European Journal of Physics, Choice Reviews, National Science Foundation, Department of Energy, Research Corporation

Publications in Journals and Refereed Conference Proceedings: 6 selected out of over 80

1. "Laboratory for Underground Nuclear Astrophysics (LUNA)"

U. Greife, C. Arpesella, C.A. Barnes, F. Bartolucci, E. Bellotti, C. Broggini, P. Corvisiero, G. Fiorentini, A. Fubini, G. Gervino, F. Gorris, C. Gustavino, M. Junker, R.W. Kavanagh, A. Lanza, G. Mezzorani, P. Prati, P. Quarati, W.S. Rodney, C. Rolfs, W.H. Schulte, H.P. Trautvetter and D. Zahnow
Nucl. Instrum. Methods A 350 (1994) 326-337

2. "Nuclear Reaction Rates"

U. Greife and C. Rolfs
Encyclopedia of Astronomy and Astrophysics, IOP Publishing and Macmillan , London (2001) 1879-1884

3. "Off-line production of a ^{7}Be radioactive ion beam"

L. Gialanella, U. Greife, N. De Cesare, A. D'Onofrio, M. Romano, L. Campajola , A. Formicola, Z. Fulop, G. Gyurky, G. Imbriani, C. Lubritto, A. Ordine, V. Roca, D. Rogalla, C. Rolfs, M. Russo, C. Sabbarese, E. Somorjai, F. Strieder, F. Terrasi and H.P. Trautvetter
Nucl. Instr. Meth. B 197 (2002) 150-154

4. "The DRAGON facility for Nuclear Astrophysics at TRIUMF-ISAC: Design, Construction and Operation"

D.A. Hutcheon, S. Bishop, L. Buchmann, M.L. Chatterjee, A.A. Chen, J.M. D'Auria, S. Engel, D. Gigliotti, U. Greife, D. Hunter, A. Hussein, C.C. Jewett, . N. Khan, M. Lamey, A.M. Laird, W. Liu, A. Olin, D. Ottewell, J.G. Rogers, G. Roy, H. Sprenger and C. Wrede
Nucl. Instrum. Meth. A 498 (2003) 190-210

5. "Energy loss around the stopping power maximum of Ne, Mg and Na ions in hydrogen"

U. Greife, S. Bishop, L. Buchmann, M.L. Chatterjee, A.A. Chen, J.M. D'Auria, S. Engel, D. Gigliotti, D.A. Hutcheon, D. Hunter, A. Hussein, C.C. Jewett, M. Lamey, A.M. Laird, W. Liu, A. Olin, D. Ottewell, J.G. Rogers and C. Wrede
Nucl. Instrum. Meth. B 217 (2004) 1-6

6. "Background identification and suppression for the measurement of (n,γ) reactions with the DANCE detector at LANSCE"

R. Reifarth, T.A. Bredeweg, A. Alpizar-Vicente, J.C. Browne, E.I. Esch, U. Greife, R.C. Haight, R. Hatarik, A. Kronenberg, J.M. McDonnell, R.S. Rundberg, J.L. Ullmann, D.J. Vieira, J.B. Wilhelmy and J.M. Wouters
Nucl. Instrum. Meth. A 531 (2004) 528-541

Invited Talks and Seminars: 27

List of close collaborators (past 4 years):

Jeff Blackmon (ORNL), Michael Smith (ORNL); Dan Bardayan (ORNL); Ray Kozub (TN Tech); John D'Auria (SFU); Lothar Buchmann (TRIUMF); Alan Chen (McMaster); Peter Parker (Yale); Art Champagne (UNC); Rene Reifarth (LANL); John Ullmann (LANL); Dave Vieira (LANL); Bob Haigth (LANL); Yuri Efremenko (ORNL/University of Tennessee)

Biographical Sketch for William Raphael Hix

Physics Division
Oak Ridge National Laboratory
Oak Ridge, TN 37831-6374
raph@ornl.gov
Voice: (865) 574-4716

Department of Physics and Astronomy
University of Tennessee
Knoxville, TN 37919-1200
raph@utk.edu
FAX: (865) 576-8746

Research Interests:

Nucleosynthesis, Nuclear Astrophysics, Supernovae, Novae, X-ray and γ-ray bursts, Stellar Structure and Evolution

Professional Experience and Education:

Oak Ridge National Laboratory
Research Staff (2004-present)
Member, Theoretical Astrophysics Group/Task**,** 1997-present

University of Tennessee at Knoxville
Adjunct Assistant Professor (2004-present)
Research Assistant Professor (2001-2004)
Postdoctoral Research Associate (1997-2001)

University of Texas at Austin
Postdoctoral Fellow, Department of Astronomy (1995-1997)

Harvard University
Ph.D. in Astronomy (1995), A.M. in Astronomy (1991)
NASA Graduate Student Researchers Program Fellow, NASA Office of Space Science and Department of Astronomy (1990-94)

University of Maryland
B.S. in Physics (with honors) and Astronomy, and B.S. in Mathematics, (1989), *summa cum laude*

Synergistic Experience:

Principal Investigator, PHY-0244783, NSF Nuclear Theory and Stellar Astronomy and Astrophysics Programs (2003-2006)
Co-Investigator, Terascale Supernova Initiative, DoE Scientific Discovery through Advanced Computing Program, (2003-2006)
Collaborator, NAG5-9263, NASA Astrophysics Theory Program (2000-2003)

Recent Relevant Publications

Neutral-current neutrino-nucleus cross-sections in the mass A~55 region, A. Juodagalvis, K. Langanke, G. Martínez-Pinedo, W.R. Hix, D.J. Dean & J.M. Sampaio 2005, *Nuclear Physics A,* 747, 87.
The Consequences of Nuclear Electron Capture in Core Collapse Supernovae, W. R. Hix, O. E. B. Messer, A. Mezzacappa, M. Liebendörfer, J. Sampaio, K. Langanke, D.J. Dean & G. Martínez-Pinedo 2003, *Physical Review Letters* **91** 201102.
Supernova Science at Spallation Neutron Sources, W. R. Hix, A. Mezzacappa, O. E. B. Messer & S.W. Bruenn 2003, *Journal of Physics G* **29**, 2523.
Electron capture rates on nuclei and implications for stellar core collapse, K. Langanke, G. Martínez-Pinedo, J.M. Sampaio, D.J. Dean, W.R. Hix, O.E.B. Messer, A. Mezzacappa, M. Liebendörfer, H.-Th. Janka & M. Rampp 2003, *Physical Review Letters* **90**, 241102.

Probing the Gravitational Well: No Supernova with Boltzmann Neutrino Transport and General Relativity, M. Liebendörfer, A. Mezzacappa, F.-K. Thielemann, O.E.B. Messer, W.R. Hix & S.W. Bruenn 2001, *Physical Review* D **63**, 103004.
Simulation of the Spherically Symmetric Stellar Core Collapse, Bounce, and Postbounce Evolution of a 13 Solar Mass Star with Boltzmann Neutrino Transport, and Its Implications for the Supernova Mechanism, A. Mezzacappa, M. Liebendörfer, O.E.B. Messer, W.R. Hix, F.-K. Thielemann & S.W. Bruenn 2001, *Physical Review Letters* **86**, 1935.
The Role of Electron Capture in Chandrasekhar Mass models for Type Ia Supernovae, F. Brachwitz, D.J. Dean, W.R. Hix, K. Iwamoto, K. Langanke, G. Martínez-Pinedo, K. Nomoto, M. R. Strayer & F.-K. Thielemann 2000, *Astrophysical Journal* **536**, 934-947.

Graduate and Postgraduate Advisors:

Friedrich-Karl Thielemann (U. Basel), Anthony Mezzacappa (ORNL), J. Craig Wheeler (U. Texas)

Thesis and Postgraduate Advisees:

Suzanne Parete-Koon (U. Tenn.), Luc Dessieux (U. Tenn.), Eric Lingerfelt (U. Tenn.), Ching-Tsai Lee (U. Tenn.), O.E. Bronson Messer (U. Tenn.), Rachel Lewis (Yale U., with P.D. Parker), Zhanwen Ma (U. Tenn., with M.S. Smith), Christian Freiburghaus, (U. Basel, with F.-K. Thielemann)

Other Collaborators and Co-authors:

Donink Argast (U. Basel), Daniel W. Bardayan (ORNL), John C. Batchelder (ORAU), Jeffery C. Blackmon (ORNL), John M. Blondin (NC State U.), Franziska Brachwitz (U. Basel), Eduardo Bravo (U. Catalunya), Stephen W. Bruenn (Fl. Atl. U.), Arthur E. Champagne (U. North Carolina), David J. Dean (ORNL), Jacob A. Fisker (Notre Dame), R. Fitzgerald (U. North Carolina), Carla Frohlich (U. Basel), Ortwin E. Gerhard (U. Basel), Michael W. Guidry (U. Tenn.), Masaaki Hashimoto (U. Kyushu), Peter A. Höflich (U. Texas), Christian Iliadis (U. North Carolina), Koichi Iwamoto (Nihon U.), H.-Thomas Janka (Max Planck Inst., Garching), A. Juodagalvis (FAIR), Nobuhiro Kishimoto (U. Tokyo), Edwin Kolbe (NAGRA), Raymond Kozub (Tenn. Tech.), Karl-Ludwig Kratz (U. Mainz), Karlheinz Langanke (FAIR), Matthias Liebendörfer (CITA), Gabriel Martinez-Pinedo (IEEC/ICRA), Gail McLauglin (NC State U.), Bradley S. Meyer (Clemson U.), Richard A. Meyer (RAME Inc.), Takayoshi Nakamura (U. Tokyo), Caroline D. Nesaraja (ORNL), Ken'ichi Nomoto (U. Tokyo), Peter D. Parker (Yale U.), Bernd Pfeiffer (U. Mainz), Markus Rampp (Max Planck Inst., Garching), Thomas Rauscher (U. Basel), Felix Rembges (U. Basel), Stefan Rosswog (U. Leicester), Markus Samland (U. Basel), Jorge M. Sampaio (U. Lisbon), Heinrich Schatz (Mich. State U.), Nengchuan Shu (ORNL), Edward M. Sion (Villanova), Donald L. Smith (Argonne Nat'l Lab.), Michael S. Smith (ORNL), Warren M. Sparks (Los Alamos Nat'l Lab.), Sumner Starrfield (Ariz. State U.), Rebecca Surman (Union C.), Frank X. Timmes (Los Alamos Nat'l Lab.), Hideyuki Umeda (U. Tokyo), H.A.T. Vanhala (Challenger Center for Space Science Education), Michael Wiescher (Notre Dame)

Biographical Sketch

Gail C. McLaughlin
Gail_McLaughlin@ncsu.edu
(919) 513-0516

Department of Physics
North Carolina State University
Raleigh, NC 27608

A. PROFESSIONAL PREPARATION

University of California, San Diego	Physics	Ph.D.	1996
University of California, San Diego	Physics	M.S.	1992
Princeton University	Physics	B.S.	1991

B. APPOINTMENTS

Assistant Professor, North Carolina State University 2001-present
Research in theoretical neutrino and nuclear astrophysics
Recipient 2002 DOE Outstanding Junior Investigator Award
Research Scientist, SUNY Stony Brook 2000-2001
Postdoctoral Research Associate, TRIUMF 1998-2000
Postdoctoral Research Associate, Institute for Nuclear Theory, UW 1996-1998

C. PUBLICATIONS

1. Neutrino scattering, absorption and annihilation above the accretion disks of gamma ray bursts", J. Kneller, G. McLaughlin and R. Surman, MNRAS submitted (2004)
2. "Prospects for obtaining and r-process in gamma ray burst disk winds", G. McLaughlin and R. Surman, Nucl. Phys A in press (2005)
3. "Neutrino Interactions in the outflow from Gamma Ray Burst accretion Disks", R. Surman and G. C. McLaughlin, ApJ 618, 397 (2005)
4. "Neutrino-Nucleus Cross Section Measurements using Stopped Pions and Low Energy Beta Beams", G. McLaughlin, Phys Rev C70, 045804 (2004)
5. "The effect of Bound Dineutrons upon BBN", J. Kneller, G McLaughlin, Phys Rev D70, 043512, (2004)
6. "Prospects for Detecting a Neutrino Magnetic Moment with a Tritium Source and Beta Beams", Phys. Lett B591, 229 (2004)
7. "On the Contribution of Gamma Ray Bursts to the Galactic Inventory of Some Intermediate Mass Nuclei", J. Pruet, R. Surman, and G. McLaughlin, ApJ 602 L101 (2004)
8. "Neutrinos and Nucleosynthesis in Gamma Ray Burst Accretion Disks", ApJ 603, 611 (2004)
9. "What can be learned with a lead-based Supernova Neutrino Detector?", J. Engel, C.Volpe and G. McLaughlin, Phys. Rev. D67, 013005 (2003)
10. "BBN and Lambda QCD", J. Kneller and G McLaughlin, Phys. Rev D68, 103508 (2003).

D. SYNERGYSTIC ACTIVITIES

- APS Division of Nuclear Physics Executive Committee 2004-2005
- APS Division of Nuclear Physics Program Committee, 2002-2003
- APS Division of Astrophysics Nominating Committee, 2004
- NSAC theory subcommittee, 2003
- NSAC subcommittee, 2005
- APS – DNP neutrino workshop organizer for DNP 2005

E. COLLABORATORS AND OTHER AFFILIATIONS

North Carolina State University
J. Kneller
University of North Carolina
J. Engel
IPN Orsay
C. Volpe
Union college
R. Surman
UC San Diego
G. Fuller
University of Wisconsin
A. B. Balantekin
SUNY Stony Brook
G. Brown
Astronomical Institute "Anton Pannekoek", Amsterdam
R. A. M. J. Wijers

Graduate advisor: G. Fuller (UC San Diego)

Postdoctoral advisors: W. Haxon (Institute for Nuclear Theory, UW), J. N. Ng (TRIUMF) G. Brown (Stony Brook)

Thesis and Postdoctoral advisees: J. Kneller, J. Beun

ION STANCU
Department of Physics and Astronomy
Box 870324, The University of Alabama, Tuscaloosa, AL 35487

Tel. (205) 348-7777, -5050
E-mail: ion.stancu@ua.edu

Education:

Rice University, Houston, TX (1987--1990)
Doctor of Philosophy, April 1990
Master of Arts, February 1988

University of Dusseldorf, Germany (1981--1987)
Diplom-Physiker, September 1987

Experience:

Assistant Professor of Physics (August 2000 -- present)
Department of Physics and Astronomy, University of Alabama, Tuscaloosa, AL.

Associate Research Physicist (July 1999 -- July 2000)
Assistant Research Physicist (January 1996 -- June 1999)
Postdoctoral Research Physicist (March 1993 -- December 1995)
Physics Department, University of California, Riverside, CA.

Senior Research Associate (April 1991 -- February 1993)
Research Associate (April 1990 -- April 1991)
T.W. Bonner Nuclear Laboratory, Rice University, Houston, TX.

Publications:

1. R. Kree and I. Stancu, *"Critical Dynamics of Long-range Random-field Models in a 1/N Expansion"*, J. Phys. C: Solid State Physics **21**, L15--L18 (1988).

2. I. Stancu and P.M. Stevenson, *"Second-order Corrections to the Gaussian Effective Potential of $\lambda\phi^4$ Theory"*, Phys. Rev. **D42**, 2710-2725 (1990).

3. I. Stancu, *"The Post-Gaussian Effective Potential in Scalar and Scalar-Fermion Theories"*, Phys. Rev. **D43**, 1283-1299 (1991).

4. U. Ritschel, I. Stancu and P.M. Stevenson, *"Unconventional Large-N Limit of the Gaussian Effective Potential and the Phase Transition in $\lambda\phi^4$ Theory"*, Z. Phys. **C54**, 627-634 (1992).

5. M.Albert, *et al.* (LSND Collaboration), *"Measurement of the Reaction $^{12}C(\nu_\mu,\mu^-)X$ Near Threshold"*, Phys. Rev. **C51**, R1065-R1069 (1995).

6. C. Athanassopoulos *et. al*. (LSND Collaboration), *"Candidate Events in a Search for ν_μ-bar to ν_μ-bar Oscillations"*, Phys. Rev. Lett. **75**, 2650-2653 (1995).

7. R.Ibanez-Meier, I. Stancu and P. M. Stevenson, *"Gaussian Effective Potential for the U(1) Higgs Model"*, Z. Phys. **C70**, 307-320 (1996).

8. C. Athanassopoulos *et. al.* (LSND Collaboration), *"Evidence for ν_μ-bar to ν_e-bar Oscillations from the LSND Experiment at the Los Alamos Meson Physics Facility"*, Phys. Rev. Lett. **77**, 3082-3085 (1996).

9. C. Athanassopoulos *et al.* (LSND Collaboration), "*Evidence for Neutrino Oscillations from Muon Decay at Rest"*, Phys. Rev. **C54**, 2685-2708 (1996).

10. C. Athanassopoulos *et al.* (LSND Collaboration), *"The Liquid Scintillator Neutrino Detector and LAMPF Neutrino Source"*, Nucl. Inst. Methods **A388**, 149-172 (1997).

11. C. Athanassopoulos *et al.* (LSND Collaboration), *"Measurements of the Reactions $^{12}C(\nu_e,e^-)^{12}N_{gs}$ and $^{12}C(\nu_e,e^-)^{12}N^*$"*, Phys. Rev. **C55**, 2078-2091 (1997).

12. C. Athanassopoulos *et al.* (LSND Collaboration), *"Measurements of the Reactions $^{12}C(\nu_\mu,\mu^-)^{12}N_{gs}$ and $^{12}C(\nu_\mu,\mu^-)^{12}N$"*, Phys. Rev. **C56**, 2806-2819 (1997).

13 C. Athanassopoulos *et al.* (LSND Collaboration), *"Results on ν_μ to ν_e Oscillations from the LSND Experiment"*, Phys. Rev. Lett. **81**, 1774-1777 (1998).

14. C. Athanassopoulos *et al.* (LSND Collaboration), "*Results on ν_μ to ν_e Oscillations from Pion Decay in Flight Neutrinos"*, Phys. Rev. **C58**, 2489-2511 (1998).

15. I. Stancu, *"Can the Super-Kamiokande Atmospheric Data Predict the Solar Neutrino Deficit?"*, Mod. Phys. Lett. **A14**, 689-700 (1999).

16. I. Stancu and D.V.Ahluwalia, *"L/E Flatness of the Electron-Like Event Ratio in Super-Kamiokande and a Degeneracy in Neutrino Masses"*, Phys. Lett. **B460**, 431-436 (1999).

17. E. Ma, G. Rajasekaran and I. Stancu, *"Hierarchical Four-Neutrino Oscillations with a Decay Option"*, Phys. Rev. **D61**, 071302-1:5 (2000).

18. L.B. Auerbach *et al*. (LSND Collaboration), *"Measurement of Electron-Neutrino Electron Elastic Scattering"*, Phys. Rev. **D63**, 112001-1:11 (2001).

19. A. Aguilar *et al.* (LSND Collaboration), *"Evidence for Neutrino Oscillations from the Observation of Electron Antineutrino Appearance in a Muon Antineutrino Beam"*, Phys. Rev. **D64**, 112007-1:22 (2001).

20. L.B. Auerbach *et al.* (LSND Collaboration), *"Measurements of Charged Current Reactions of ν_e on ^{12}C"*, Phys. Rev. **C64**, 065501-1:12 (2001).

21. D.V. Ahluwalia, Y. Liu and I. Stancu, *"CP-Violation in Neutrino Oscillations and L/E Flatness of the E-like Event Ratio at Super-Kamiokande"*, Mod. Phys. Lett. **A17**, 13-21 (2002).

22. L.B. Auerbach *et al.* (LSND Collaboration), *"Measurements of Charged Current Reactions of* ν_μ *on* ^{12}C*"*, Phys. Rev. **C66**, 015501-1:12 (2002).

23. L.B. Auerbach *et al.* (LSND Collaboration), "Search for π^0 to ν_μ-bar, ν_μ Decay in LSND", Phys. Rev. Lett. **92**, 091801-1:4 (2004).

24. B.P. Roe *et al*., *"Boosted Decision Trees, an Alternative to Artificial Neural Networks"*, to be published in the Nuclear Instrumentations and Methods.

Collaborations:

Liquid Scintillator Neutrino Detector (LSND) LANL, 1993--1998.
Booster Neutrino Experiment (MiniBooNE) FNAL, 2000--present.
NuSNS.
DoubleChooz.

APPENDIX 3 SNS REVIEW RESULTS

In Summer, 2004 the IDT submitted a Letter of Intent along with the study report "Neutrino Program at the Spallation Neutron Source, **ν-SNS**" to SNS management who subsequently sent the information to two external reviewers. Following the favorable review results the IDT was allocated floor space in the SNS target hall and advised to submit a full proposal.

The following pages contain the review reports on the study report and their transmittal letter from the SNS director, Thom Mason.

OAK RIDGE NATIONAL LABORATORY
MANAGED BY UT-BATTELLE FOR THE U.S. DEPARTMENT OF ENERGY

SNS

Bethel Valley Road
Building 8600
Oak Ridge, TN 37831-6477
Phone: (865) 241-1498
Fax: (865) 576-3041
E-mail: masont@sns.gov

Associate Laboratory Director
for the Spallation Neutron Source

Date: August 27, 2004

To: Professor Yuri Efremenko

c: I. S. Anderson, J. B. Roberto, G. R. Young

From: Thomas E. Mason, 8600, MS-6477 (241-1499) Thomas Mason

Subject: **Neutrino Program at the Spallation Neutron Source**

Following receipt of your Letter of Intent to establish a Neutrino Program at the Spallation Neutron Source (SNS), we have conducted a review of the submission, enlisting external expertise to supplement our own appraisal of the feasibility of this proposal as well as discussions with our Advisory Committees. I am attaching two referee reports that informed our assessment of the scientific promise of this proposal. Both referees felt that it would be appropriate to proceed with a full proposal. In addition, our own review of the impact of the program indicates that it can be accommodated at SNS provided the footprint and floor loading are coordinated with the Experimental Facilities Division to insure there is no unacceptable compromise of access to neighboring instruments. Based on this input there is sufficient merit to the Letter of Intent and the scientific program it describes to warrant proceeding with a full proposal. The full proposal should document in a more detailed way the design of the proposed instrumentation, its scientific capability, and how its makes effective use of the special characteristics of the SNS and benchmarking its performance against the scientific goals of the proposal. Once you have submitted a full proposal we will convene an expert review committee to inform a final decision on accommodating the Neutrino Program at SNS. We look forward to working with you as you develop the proposal. I would encourage you to continue to coordinate your plans with the Instrument group to insure compatibility of the neutrino detector with the Target Building space utilization plans.

TEM:kfr

Attachments

Report on the Letter of Intent for a

Neutrino Program at the Spallation Neutron Source

(ν-SNS)

The Spallation Neutron Source (SNS) under construction at the Oak Ridge National Laboratory is, as an inevitable byproduct, also a powerful source of neutrinos with energies of some tens of MeV through the usual pion decay chain $\pi \rightarrow \mu\nu \rightarrow e\nu\nu\nu$. The large power and pulsed time structure of the produced neutrino radiation allows one to measure neutrino-nucleus cross sections with high accuracy in an energy range where surprisingly few data exist. At the same time, this energy range is of crucial importance for supernova physics where neutrino-nucleus interactions play a key role both for the supernova explosion mechanism and for the astrophysical nucleosynthesis in an environment that is dominated by neutrinos. In addition, one could extract unprecedented nuclear structure information.

From my perspective as a theorist, I can not judge the practical feasibility of the proposed experimental setup, although the detailed presentation in the Letter of Intent sounds eminently plausible.

Without reservation I am enthusiastic about the scientific case presented in the Letter. Core-collapse supernovae are intruiging phenomena where hydrodynamics, nuclear physics andneutrino physics interface in a unique way. The supernova phenomenon is so complicated that to this day it is not yet fully understood, yet it appears to be simple enough that it can be understood from first principles if the required microphysical input parameters, notably the neutrino-nuclear interactions, are correctly included. The recent advance in neutrino physics implies that large neutrino detectors will be operative for the foreseeable future. Therefore, it is quite possible that a high-statistics neutrino signal from the next galactic supernova will eventually be observed. Nuclear cross sections in the energy range of some tens of MeV will be crucial for the interpretation of the measured signal. Even without observing a galactic supernova, the neutrino-nuclear cross sections are crucial for understanding the explosion mechanism and particularly the nucleosynthesis processes that are believed to occur in the neutrino-driven wind of the newly formed neutron star.

As neutrino physics enters a “precision phase,” it has become clear that the

poorly known neutrino-nucleus cross sections in the MeV–GeV energy range have become a serious limitation. The proposed facility will address part of this deficiency and will thus contribute to the progress of neutrino and nuclear physics in a unique way.

ORNL is home to one of the world's leading groups in the area of numerical astrophysics and particularly numerical supernova simulations as well as a nuclear theory group. The presence of a strong theory group in connection with an experimental facility has often proven to be of great significance for the success oft he experimental program. The proposed facility has the great advantage that fruitful synergy with ORNL's supernova and nuclear theory groups is guaranteed. ORNL will be a unique center of excellence for both theoretical and experimental supernova and nuclear structure research.

The ν-SNS collaboration is an impressive collection of world-class nuclear scientists, experimentalists, astrophysicists, and neutrino experts, testifying to the importance of the proposed research and to the interest taken by the communities that will benefit from it.

According to the Letter of Intent, a preliminary agreement has been reached about a possible location for the proposed experiment that allows for the required target mass, detector installation, and shielding material without interfering with the normal operation of the SNS.

Given the outstanding scientific case and the apparent absence of any serious practical obstacles, I endorse the ν-SNS proposal in the strongest possible terms. I urge ORNL to take advantage of this unique opportunity to create a true world-class facility for research at the interface between neutrino-, nuclear-, and astrophysics.

"This proposal appears to be appropriate to proceed to the full proposal phase. It appears to address interesting physics in a way that is otherwise not available internationally. It also appears to be a fairly low cost for such a measurement. The proponents are reputable and experienced experimental and theoretical scientists in this field."

APPENDIX 4 SNS TARGET HALL FLOOR LOADING ANALYSIS

The following pages contain an analysis of the floor loading limits in the SNS target hall performed by **m+w zander** in 2004.

m+w zander

total facility solutions

DEPARTMENT OF ENERGY

NEUTRINOS AT THE SPALLATION NEUTRON SOURCE (ν-SNS)
OAK RIDGE NATIONAL LABORATORY

OAK RIDGE, TENNESSEE

FLOOR LOADING REPORT

Subcontract Number: 4000029836
Project Number: 10241

MARCH 17, 2004

JENOPTIK Group.

m+w zander
total facility solutions

M+W Zander U.S. Operations, Inc.
549 West Randolph Street
Chicago, Illinois 60661
USA
Phone +312-577-3200
Fax +312-577-3525

March 17, 2004

Vince Cianciolo
MS 6356
Oak Ridge National Laboratory
Oak Ridge, TN 37831-6356

Dear Vince:

M+W Zander has completed the floor loading review for the proposed Neutrino enclosure to be located in the SNS Target Building. This study has been undertaken due to the desire to place a Neutrino Detector and Shielding in an area of the Target Building that has an allowable load criteria of 1500 psf. Calculations have been prepared to review the floor and foundation load capacities and to determine the feasibility of increasing the allowable loads. The allowable load for the Neutrino Detector and Shielding and a description of the load assumptions is given below. The calculations are on the following pages.

Case 1 – 395 Tons
Load is assumed to be applied to the footprint of the enclosure. There is no reduction in the live load of 1,500 psf outside the enclosure.

Case 2 – 470 Tons
Half of the 5' width surrounding the enclosure is maintained as a "keep clear" area. Load capacity is reduced in that width to 100 psf with the remaining load capacity assigned to the Neutrino Detector. The area beyond 2.5 feet has a floor load of 1,500 psf.

Case 3 – 545 Tons
The entire 5' width surrounding the enclosure is maintained as a "keep clear" area, load capacity is reduced in that width to 100 psf and all of the remaining load capacity is assigned to the Neutrino Detector. The area beyond 5 feet has a floor load of 1,500 psf.

If either Case 2 or Case 3 is used for designing the Neutrino Detector, we recommend that the "keep clear" area be striped and marked. If Case 3 is used, the Beamline 18 group should be informed that the Neutrino Detector has claimed all of the load for the "keep clear" area.

m+w zander

total facility solutions

If you have questions, please do not hesitate to contact us.

Very truly yours,

M+W ZANDER U.S. OPERATIONS, INC.

John J. Busch, SE, PE
Senior Project Manager

G. P. Reddy, SE
Structural Project Engineer

JENOPTIK Group.

m+w zander

total facility solutions

1. Introduction

The proposed location of the Neutrino enclosure is on the pit floor of Instrument No. 18, along column line G between column lines 1 and 2.5. This area is adjacent to the RTBT enclosure. See attached sketch SK-1 for layout. Location and size of the enclosure has been provided by Vince Cianciolo of ORNL. The proposed enclosure is constructed of solid steel plates and for purposes of analysis, 355 tons is used for the weight of the enclosure. Inside the enclosure are two neutrino detectors, each weighing 20 tons.

The equivalent uniform floor load is calculated as follows:

Weight of steel plate enclosure: 355 tons = ... 710,000. lbs
Weight of two neutrino detectors: 2 x 20 tons = 40 tons = ... 80,000. lbs.
Total weight of Neutrino enclosure =..... 790,000. lbs. = 395 tons
Floor area of enclosure is 219 sq. ft.
Equivalent uniform floor load equals = 790,000 / 219 = 3,607 psf
USE 3,600 psf

2. Pile Capacities

The existing pit floor consists of an 18 inch thick reinforced concrete slab, supported on a compacted layer of stone, 12.5 feet thick, which is supported on a 5 ft thick reinforced concrete mat. The mat is supported on grouted steel pipe piles, which bear on bedrock. The design pile load capacity is 400 kips with a factor of safety of 2. See sketch SK-2 for layout of piles.

The piles under the Target Building are designed for vertical gravity dead and live loads as well as seismic vertical and lateral loads. The design live load for this area is 1,500 psf. The Neutrino load of 790,000 lbs. is distributed at a 2 vertical to 1 horizontal slope to the foundation piles. Two load cases are considered to determine the vertical pile loads: 1.) Total Static Load = Dead Load + Live Load + Neutrino Load and 2.) Total Dynamic Load = Dead Load + Seismic Live Load + Neutrino Load + Earthquake. The attached spreadsheet shows the existing pile loads and the additional loads from the Neutrino detector enclosure.

The maximum vertical pile load for the two load cases are as follows:

Total Static Load = 421 kips ~.400 x 1.05 = 420 kips – Okay.
Factor of safety is 2.0 for pile foundation, but a load increase of 5 % (1.05) is acceptable.

Total Dynamic Load = 502 kips < 400 x 1.33 = 532 kips – Okay. 1.33 is allowable load increase for seismic.

3. "Keep Clear" Area

The "keep clear" area is designated as an open area, 5 feet wide, in which the floor live load is 100 psf. See sketch SK-1. The reduction of live load of 1,400 psf (1,500 – 100) multiplied by the "keep clear" area (216 sq. ft.) is 300,000 lbs or 150 tons. This portion of the live load can be added to the weight of the Neutrino enclosure. Case 1 - No "keep clear" area. The total weight of the Neutrino enclosure is 395 tons. Case 2 - One half "keep clear" area. The total weight of the Neutrino enclosure is 470 tons. Case 3 - Entire "keep clear" area: The total weight of the Neutrino enclosure is 545 tons. In our opinion, the pile load from Cases 2 and 3 are within the allowable factor of safety and further analysis is not needed. Although, the Neutrino enclosure load of 3,600 psf is much greater than the design load of 1,500 psf, the increased load is spread over a larger tributary area (enclosure of 219 sf vs. 734 sf for piles), which results in smaller loads being added to the piles, which have additional capacity.

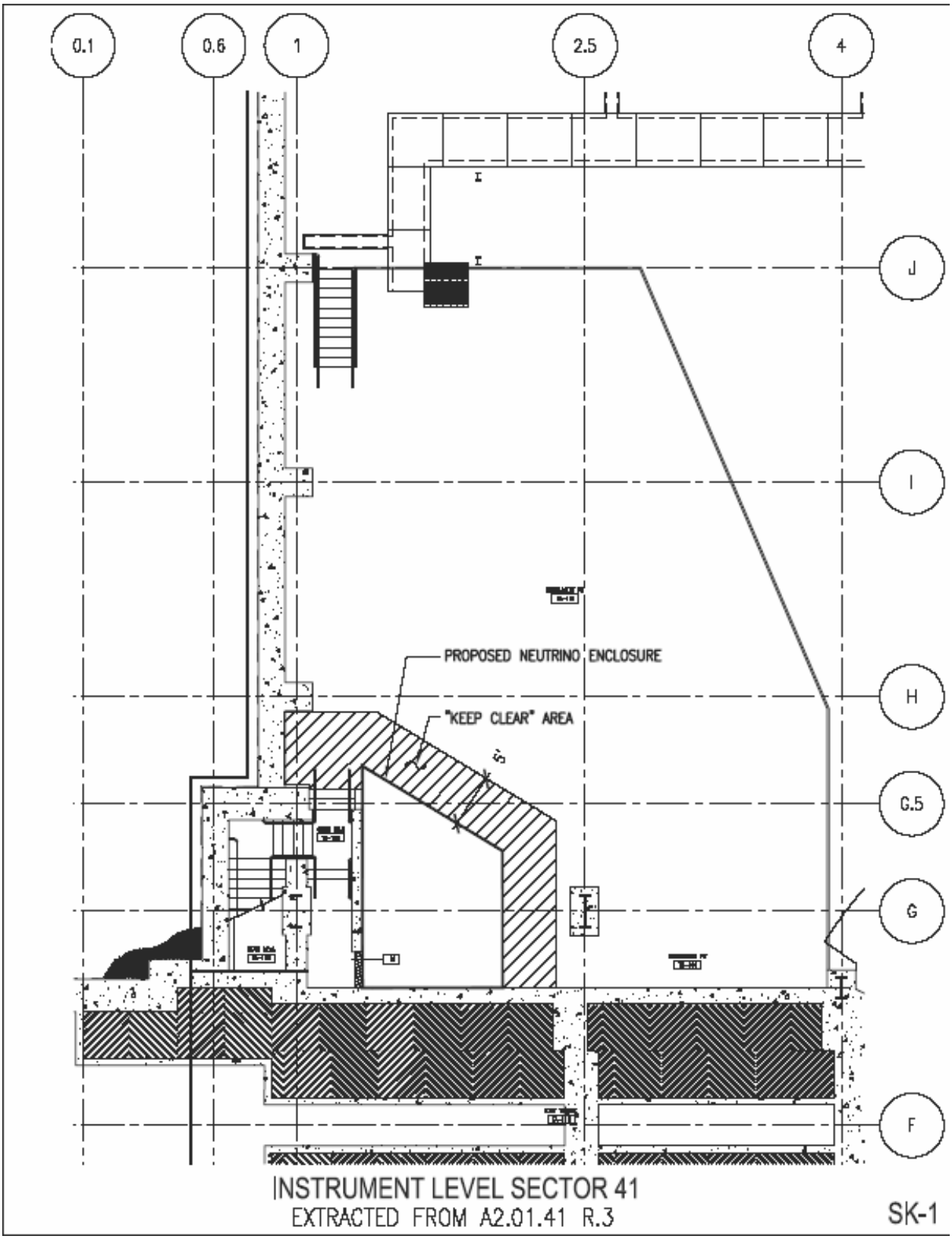
0.1
0.6
1
2.5
4
J
I
H
G.5
G
F
PROPOSED NEUTRINO ENCLOSURE
"KEEP CLEAR" AREA
5'
INSTRUMENT LEVEL SECTOR 41
EXTRACTED FROM A2.01.41 R.3
SK-1

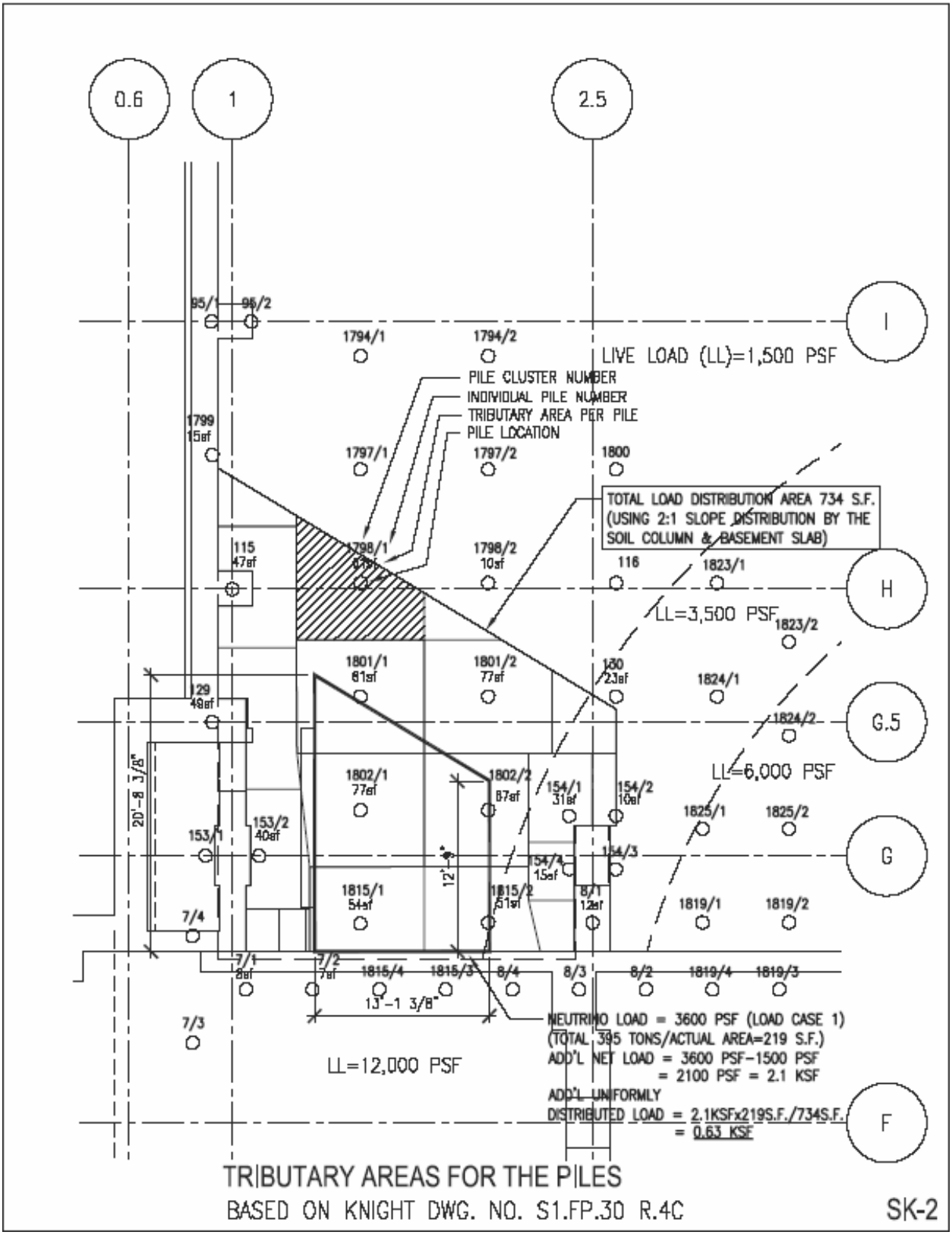

TRIBUTARY AREAS FOR THE PILES

BASED ON KNIGHT DWG. NO. S1.FP.30 R.4C

SK-2

SNS NEUTRINO PILE LOAD TABLE (See Next Page for Notes)

Cluster Node a	No. of Piles b	Individual Piles c	Loads per SDE-00-09-28-C-007 (App.F&G) DL + LL Total Vertical Load (k) d	DL + LL Vertical Load per Pile (k) e=d/b	DL + SLL + EQ Vertical Load per Pile (k) f	Additional Loads from "Neutrino" Uniform DL + LL Load (ksf) g	Area per Pile (sf) h	Add'l Load DL + LL per Pile (k) i=gh	Total Static DL + LL + Neutrino per Pile (k) j=e+i	Add'l Load From Vertical Seismic .24xNeutrino per Pile (k) k=0.24i	Total Seismic DL + SLL + EQ + Neutrino per Pile (k) l=f+l+k
7	4		1502								
		7/1		375	447	0.63	8	5	380	1	453
		7/2		375	447	0.63	7	4	380	1	452
8	4		1587								
		8/1		397	460	0.63	12	8	404	2	469
		8/2		397	460	0.63	0	0	397	0	460
		8/3		397	460	0.63	0	0	397	0	460
		8/4		397	460	0.63	0	0	397	0	460
115	1		377	377	458	0.63	47	30	406	7	495
116	1		391	391	452	0.63	0	0	391	0	452
129	1		376	376	453	0.63	49	31	407	7	491
130	1		386	386	449	0.63	23	14	401	3	467
153	2		749								
		153/1		374	448	0.63	0	0	374	0	448
		153/2		374	448	0.63	40	25	400	6	479
154	4		1555								
		154/1		389	453	0.63	31	20	408	5	477
		154/2		389	453	0.63	10	6	395	2	461
		154/3		389	453	0.63	0	0	389	0	453
		154/4		389	453	0.63	15	9	398	2	465
1798	2		736								
		1798/1		368	430	0.63	61	38	407	9	478
		1798/2		368	430	0.63	10	6	375	2	438
1799	1		372	372	459	0.63	15	9	381	2	471
1801	2		735								
		1801/1		367	432	0.63	81	51	418	12	495
		1801/2		367	432	0.63	77	49	416	12	492
1802	2		746								
		1802/1		373	442	0.63	77	49	421	12	502
		1802/2		373	442	0.63	67	42	415	10	494
1815	4		1544								
		1815/1		386	453	0.63	54	34	420	8	495
		1815/2		386	453	0.63	51	32	418	8	493
		1815/3		386	453	0.63	0	0	386	0	453
		1815/4		386	453	0.63	0	0	386	0	453

SNS NEUTRINO LOAD TABLE NOTES:

- Dead loads (DL) consist of the weight of all construction material.
- Live loads (LL) are produced by the use and occupancy of the building.
- Seismic live load (SLL) is the portion of the live load used for seismic (earthquake) analysis.
- Earthquake (EQ) load is the seismic lateral load due to the motion of the building in the north/south or east/west direction.
- Kip (k) equals 1,000 lbs.
- Kip per square foot (ksf)
- Calculation No. SDE-00-09-28-C-007, Revision 3, May 21, 2002, "Seismic Evaluation of Spallation Neutron Source Target Building – Pile Loads from Gravity and Seismic Motion". Appendix F – Pile Loads from Individual Load Cases. Appendix G – Pile Load Combination Tables.

- Column "a" – Pile cluster node number.
- Column "b" – Number of piles in cluster.
- Column "c" – Individual pile number. See SK-2 for location.
- Column "d" – Total vertical load on pile cluster. 1,500 psf LL is included.
- Column "e" – Total vertical load on individual pile. DL + LL
- Column "f" – Total vertical load on individual pile. DL + SLL + EQ
- Column "g" – Neutrino Uniform DL + LL for Case 1. Load has been distributed at a 2 vertical to 1 horizontal slope and is applied to the piles based on tributary area to each pile. The distribution occurs in the 19 foot thickness of concrete and earth construction, which separates the floor of the enclosure and the top of the piles.
- Column "h" – Tributary area for each pile. See SK-2.
- Column "i" – Load contribution per pile from Neutrino enclosure.
- Column "j" – Total static (vertical) load per pile for DL + LL + Neutrino load
- Column "k" – Additional vertical seismic load per pile from vertical acceleration of the Neutrino enclosure.
- Column "l" – Total vertical seismic load per pile from DL + SLL + EQ + Neutrino Enclosure.

APPENDIX 5 ν-SNS R&D PROGRAM

Detectors similar to those proposed for **ν-SNS** have been deployed in nuclear and particle physics experiments, so R&D for new technology development is not required. However, a modest, focused two-year R&D program prior to the construction project would allow optimization of the shielding and detector designs for cost, performance, and simplicity of installation and target changes. The key R&D areas are:

- **Backgrounds**: We propose to measure the background levels at the SNS after the start of operations. We will use this information to benchmark model calculations which can then be used to optimize our shielding package and provide feedback to the SNS on background source reduction.
- **Cosmic-ray Veto**: Our current design satisfies our criteria for cosmic-ray muon efficiency and low-energy neutron inefficiency. However, R&D is necessary to verify detector simulations and may lead to optimizations that reduce price, improve performance and simplify assembly.
- **Segmented Detector**: This detector must be designed in such a way that it can be easily taken apart and rebuilt with a new target material. In addition, it must be designed to optimize timing and energy resolution. The large number of channels requires adaptation of custom-made readout electronics that will be developed for the MECO experiment and any necessary modifications need to be identified, tested and incorporated into the chosen solution.
- **Homogeneous Detector**: The primary question for this detector is whether use of a flat photosensor would be possible. This development would be important since it would significantly increase the detector's fiducial volume.

The R&D funding would be distributed among the institutions having responsibility for major components of the **ν-SNS** project:

Shielding: ORNL
Active Cosmic-Ray Veto System: Colorado School of Mines
Segmented Detector Mechanics: University of Tennessee
Segmented Detector Electronics: University of Houston
Homogeneous Detector: University of Alabama

Brief descriptions of the proposed activities follow.

Shielding

Due to floor loading limitations, the shielding mass is limited to ~500 tons. It is thus extremely important to optimize the shielding to most efficiently use the available mass. We propose to study neutron backgrounds and how to reduce them both by continuing Monte Carlo simulations of the neutron fluxes, and by measurement inside a mini-bunker. This mini-bunker will be assembled out of several Duratech (junk steel) blocks placed inside the target building in the place allocated for the neutrino bunker. Several scintillator detectors will be placed inside and outside the shielding to measure the neutrons flux and time profile. The SNS will start low-intensity operations in 2006 that will be more than adequate for these background studies, which will allow us to optimize the bunker and veto design.

Estimated cost: $60K
Principal Investigator: Vince Cianciolo, ORNL.

Active Cosmic-Ray Veto System

We propose to investigate the cost efficiency of different options for building an active cosmic-ray veto system for the **ν-SNS** facility. The proposed veto system is based on plastic scintillator that will be required to operate in a neutron rich environment. In such an environment too many false hits will be produced even in a 1 inch-thick scintillator due to neutron capture in structural material near the veto system. The approach chosen by the KARMEN collaboration, very thick (2 inch), high quality scintillator panels, is very expensive. An alternative approach is to use several scintillator layers with a coincidence requirement for muon identification. Because cast plastic scintillator of good quality is too expensive, we are currently looking into the use of extruded scintillator bars, as used previously by the MINOS collaboration. The readout has to be done via wavelength shifting (WLS) fiber attached to a photosensor. Optimization of the fiber diameter and length, including the possible benefits of transitioning to a clear fiber, will be investigated. The standard photosensor technology is a multi-anode PMT. However, flat photosensors, such as APDs or SiPMs, may have significant advantages, including the possibility of reading out both ends of the scintillator layers (a possibility excluded for PMTs due to space considerations), and will be investigated. Optimization of material and thickness for absorber layers in between the scintillator layers will be investigated. Since we require ~99% efficiency for tagging cosmic-ray muons, geometric efficiency is critical. We will investigate different mounting schemes to optimize hermiticity and the ease of installation of these very heavy objects in an area of limited crane access.

Estimated cost: $70K
Principal Investigator: Uwe Greife, Colorado School of Mines

Segmented Detector Mechanics

The segmented detector will contain ~15,000 channels and will be challenging to assemble. It will be installed in an area with limited crane coverage and we anticipate disassembling and reassembling the detector annually in order to make measurements on different solid targets. Another consideration in the design of the segmented detector is the SNS time structure. Electron neutrinos and muon antineutrino (both resulting from muon decays) are emitted several microseconds after the beam spill, whereas muon neutrinos (resulting from pion decays) dominate during the beam spill. This makes it possible to separately study neutrino interactions for neutral- and charged-currents. However, according to our estimates the maximum background of energetic neutrons from the SNS occurs during the second half of the beam spill and up to 1100 nanoseconds later. To study this dangerous background, and exclude it during data analysis, timing resolution of better then 50 ns is desirable. This is challenging since with a typical gas the drift time distribution in our nominal cell size is 150 ns. However, possibilities to improve the timing resolution include pulse shape analysis, gas selection, and a multi-wire strawtube design.

We propose to build a small prototype of the segmented detector, assembled out of 300 strawtubes, each 1 m long and 15 mm in diameter. This will allow us to optimize the design for cost, performance, and ease of assembly, installation, and target changes. It will also allow us to develop reconstruction algorithms and verify performance with cosmic-ray muons which can stop and decay into a Michel electron, which gives a signal nearly identical to a that from a neutrino interaction.

Estimated cost: $40K
Principal Investigator: Yuri Efremenko, University of Tennessee

Segmented Detector Electronics

The segmented detector will consist of ~15,000 strawtubes with analog readout (ADC and TDC) from both ends. This large channel count rules out use of commercial electronics. However, the relatively modest scale of the project makes it cost prohibitive to develop a completely new electronics design.

There are many similar features between the MECO tracker readout electronics (designed by the Houston group) and the requirements for readout of the segmented detector. We propose to adapt the electronics readout for MECO for use in the segmented detector and build a prototype of such electronics to be used to readout the prototype detector described above.

Estimated cost: $60K
Principal Investigator: Ed Hungerford, University of Houston

Homogeneous Detector

The nominal design for the homogeneous detector, using an array of 8 inch PMTs as the photosensors, is essentially risk-free, having been deployed in several large-scale experiments. R&D tasks for the homogeneous detector include PMT selection, performing simulations to determine the effect of PMT tilting, and finalizing the required photocathode coverage. The relatively small volume available at **ν-SNS** makes the nominal design somewhat inefficient because of the large volume required by the PMTs. Therefore, the feasibility of different flat-profile photosensors, such as Avalanche Photodiodes and Silicon Photomultipliers will be investigated. We will also study the design and deployment of the calibration scheme.

Estimated cost: $50K
Principal investigator: Ion Stancu, University of Alabama